SCALING LAWS FOR DENSITY CORRELATIONS AND FLUCTUATIONS IN MULTIPARTICLE DYNAMICS

E.A. De WOLF[a], I.M. DREMIN[b], W. KITTEL[c]

[a] *Department of Physics, Universitaire Instelling Antwerp, B-2610 Wilrijk and Inter-University Institute for High Energies, Universities of Brussels, B-1050 Brussels, Belgium*
[b] *P.N. Lebedev Institute of Physics, Academy of Sciences of the Russia 117924, Moscow, Russia*
[c] *High Energy Physics Institute Nÿmegen (HEFIN), University of Nijmegen/NIKHEF, NL-6525 ED Nijmegen, The Netherlands*

ELSEVIER

AMSTERDAM – LAUSANNE – NEW YORK – OXFORD – SHANNON – TOKYO

ELSEVIER

Physics Reports 270 (1996) 1–141

PHYSICS REPORTS

Scaling laws for density correlations and fluctuations in multiparticle dynamics

E.A. De Wolf[a], I.M. Dremin[b], W. Kittel[c]

[a] *Department of Physics, Universitaire Instelling Antwerp, B-2610 Wilrijk and Inter-University Institute for High Energies, Universities of Brussels, B-1050 Brussels, Belgium*

[b] *P.N. Lebedev Institute of Physics, Academy of Sciences of the Russia 117 924, Moscow, Russia*

[c] *High Energy Physics Institute Nÿmegen (HEFIN), University of Nijmegen/NIKHEF, NL-6525 ED Nijmegen, The Netherlands*

Received July 1995; editor: R. Slansky

Contents

Abstract

Experimental data on particle correlations and fluctuations in various high-energy multiparticle collisions are presented, with special emphasis on evidence for scaling-law evolution in small phase-space domains. The notions of intermittency and fractality as related to the above findings are described. Phenomenological and theoretical work on the subject is reviewed.

SSDI 0370-1573(95)00069-0

Of the achieved triumph pangs and tricks
Are just tightly stretched bow-strings.

B. Pasternak

1. Introduction

Recent years have witnessed a remarkably intense experimental and theoretical activity in search of scale invariance and fractality in multihadron production processes, for short also called "intermittency". These investigations cover all types of reactions ranging from e^+e^- annihilation to nucleus–nucleus collisions, up to the highest attainable energies. The creation of soft hadrons in these processes, a major fraction of the total cross section, relates to the strong-coupling long-distance regime of Quantum Chromodynamics (QCD), at present one of the least explored sectors in the whole of high-energy particle physics.

A primary motivation is the expectation that scale invariance or self-similarity, analogous to that often encountered in complex non-linear systems, might open new avenues ultimately leading towards deeper insight into long-distance properties of QCD and the unsolved problem of colour confinement.

History shows that studies of fluctuations have often triggered significant advances in physics. In the present context, it was the observation of "unusually large" particle density fluctuations, reminiscent of intermittency spikes in spatio-temporal turbulence, which prompted the pioneering suggestion to investigate the pattern of multiplicity fluctuations in multihadron events for ever decreasing domains of phase space. Scale-invariance or fractality would manifest itself in power-law behaviour for scaled factorial moments of the multiplicity distribution in such domains. It is important to stress here that, in practice, one deals with the problem of evolution of particle number distributions for ever smaller bins and intermittent behaviour implies that, for small phase-space bins, the distributions become wider in a specific way. The same problem can be stated as an increasing role of correlations within a small phase-space volume.

Through a multitude of increasingly sophisticated experimental studies of factorial moments, much new information has been gathered in a surprisingly short time. This work indeed confirms approximate power behaviour down to the experimentally possible resolution, especially when carried out in two- and three-dimensional phase space.

The proposal to look for intermittency also has triggered a thorough revival of interest in the old subject of particle correlations, by experimentalists and theorists alike. The need for greater sensitivity in measurements of correlation functions has directly inspired important work on refined analysis techniques. A promising and long overdue systematic approach to correlation phenomena of various sorts, including Bose–Einstein interferometry, is finally emerging.

The large body of experimental observations now available is calling for satisfactory explanation and, indeed, theoretical ideas of all sorts abound.

The level of theoretical understanding is quite different for the various types of collision processes. In e^+e^- annihilation, parton cascade models based on leading-log QCD have met considerable success and good overall description of multiplicity fluctuations is claimed. Closer inspection, nevertheless, reveals potentially serious deviations from the data, thus requiring further study.

For other processes, in particular hadron initiated collisions, models are faced with large and partly unexpected obstacles. This may be a reflection of insufficient knowledge of the reaction dynamics, although present evidence points to hadronization as the main culprit.

Within the framework of perturbative QCD, results of considerable interest on the emergence of power behaviour and multifractality have been obtained. However, these are asymptotic in nature and most likely quite unrelated to present-day experiment. Being related to the mechanism of confinement, not surprisingly, the role of hadronization remains unclear.

Random self-similar multiplicative branching models have inspired much of the original work on intermittency. Among many scale-invariant physical systems, the cascade process is a particularly natural candidate for the description of strong fluctuations self-similar over a wide range of scales. It finds support in the cascade nature, not only of perturbative QCD, but also of the subsequent hadronization. However, further work is needed to help understand the details of the process.

Alternatively, "classic" and extensively studied possibilities are scale-invariant systems at the critical point of a high-order phase transition. This subject has attracted particular attention in view of potential application to quark–gluon plasma formation in heavy-ion collisions.

This paper contains a review of the present status of work on intermittency and correlations as performed over the last years. In Section 2 we introduce the necessary formalism and collect useful results and relations widely scattered in the literature. Section 3 describes experimental data on correlations in various experiments and discusses predictions of popular models. Section 4 is devoted to data and models on the subject of particle fluctuations and the search for power laws. Section 5 gives an overview of the many theoretical ideas related to the problem of multiplicity scaling and fractality. Conclusions are summarized in Section 6.

2. Formalism

2.1. Definitions and notation

In this section, we compile and summarize definitions and various relations among the physical quantities used in the sequel. No originality is claimed in the presentation of this material. It merely serves the purpose of fixing the notation and assembling a number of results scattered throughout the literature.

2.1.1. Exclusive and inclusive densities

We start by considering a collision between particles a and b yielding exactly n particles in a sub-volume Ω of the total phase space Ω_{tot}. Let the single symbol y represent the kinematical variables needed to specify the position of each particle in this space (for example, y can be the c.m. rapidity[1] variable of each particle and Ω an interval of length δy). The distribution of points in

[1] The rapidity y is defined as $y = \frac{1}{2}\ln[(E + p_L)/(E - p_L)]$, with E the energy and p_L the longitudinal component of momentum vector p along a given direction (beam particles, jet axis, etc.); pseudo-rapidity is defined as $\eta = \frac{1}{2}\ln[(p + p_L)/(p - p_L)]$.

Ω can be characterized by continuous probability densities $P_n(y_1, \ldots, y_n)$; $n = 1, 2, \ldots$. For simplicity, we assume all final-state particles to be of the same type. In this case, the *exclusive* distributions $P_n(y_1, \ldots, y_n)$ can be taken fully symmetric in $y_1, \ldots, y_n$; they describe the distribution in Ω when the multiplicity is exactly n.

The corresponding *inclusive* distributions are given for $n = 1, 2, \ldots$ by

$$\rho_n(y_1, \ldots, y_n) = P_n(y_1, \ldots, y_n) + \sum_{m=1}^{\infty} \frac{1}{m!} \int_{\Omega} P_{n+m}(y_1, \ldots, y_n, y'_1, \ldots, y'_m) \prod_{i=1}^{m} \mathrm{d}y'_i \,. \tag{2.1}$$

The inverse formula is

$$P_n(y_1, \ldots, y_n) = \rho_n(y_1, \ldots, y_n) + \sum_{m=1}^{\infty} (-1)^m \frac{1}{m!} \int_{\Omega} \rho_{n+m}(y_1, \ldots, y_n, y'_1, \ldots, y'_m) \prod_{i=1}^{m} \mathrm{d}y'_i \,. \tag{2.2}$$

$\rho_n(y_1, \ldots, y_n)$ is the probability density for n points to be at $y_1, \ldots, y_n$, irrespective of the presence and location of any further points. The probability P_0 of multiplicity zero is given by

$$P_0 = 1 - \sum_{n=1}^{\infty} \frac{1}{n!} \int_{\Omega} \rho_n(y_1, \ldots, y_n) \prod_{i=1}^{n} \mathrm{d}y_i. \tag{2.3}$$

This suggests to define $\rho_0 = 1$ in (2.1). It is often convenient to summarize the above results with the help of the generating functional[2]

$$\mathscr{G}^{\mathrm{excl}}[z(y)] \equiv P_0 + \sum_{n=1}^{\infty} \frac{1}{n!} \int_{\Omega} P_n(y_1, \ldots, y_n)\, z(y_1) \cdots z(y_n) \prod_{i=1}^{n} \mathrm{d}y_i \,, \tag{2.4}$$

where $z(y)$ is an arbitrary function of y in Ω. The substitution

$$z(y) = 1 + u(y) \tag{2.5}$$

gives through (2.1) the alternative expansion

$$\mathscr{G}^{\mathrm{incl}}[u(y)] = 1 + \sum_{n=1}^{\infty} \frac{1}{n!} \int_{\Omega} \rho_n(y_1, \ldots, y_n)\, u(y_1) \cdots u(y_n) \prod_{i=1}^{n} \mathrm{d}y_i \tag{2.6}$$

and the relation

$$\mathscr{G}^{\mathrm{incl}}[z(y)] = \mathscr{G}^{\mathrm{excl}}[z(y) + 1] \,. \tag{2.7}$$

From (2.4) and (2.7) one recovers by functional differentiation:

$$P_n(y_1, \ldots, y_n) = \partial^n \mathscr{G}^{\mathrm{excl}}[z(y)] / \partial z(y_1) \cdots \partial z(y_n)|_{z=0} \,, \tag{2.8}$$

$$\rho_n(y_1, \ldots, y_n) = \partial^n \mathscr{G}^{\mathrm{incl}}[u(y)] / \partial u(y_1) \cdots \partial u(y_n)|_{u=0} \,. \tag{2.9}$$

---

[2] The technique of generating functions has been known since Euler's time and was used for functionals by N.N. Bogoliubov in statistical mechanics already in 1946 [1]; see also [2].

To the set of inclusive number densities ρ_n corresponds a sequence of inclusive differential cross sections:

$$\frac{1}{\sigma_{\text{inel}}}\,\mathrm{d}\sigma = \rho_1(y)\,\mathrm{d}y\,, \tag{2.10}$$

$$\frac{1}{\sigma_{\text{inel}}}\,\mathrm{d}^2\sigma = \rho_2(y_1, y_2)\,\mathrm{d}y_1\,\mathrm{d}y_2\,. \tag{2.11}$$

Integration over an interval Ω in y yields

$$\begin{aligned}
&\int_\Omega \rho_1(y)\mathrm{d}y = \langle n\rangle,\\
&\int_\Omega\int_\Omega \rho_2(y_1, y_2)\mathrm{d}y_1\,\mathrm{d}y_2 = \langle n(n-1)\rangle\,,\\
&\int_\Omega \mathrm{d}y_1 \cdots \int_\Omega \mathrm{d}y_q\,\rho_q(y_1, \ldots, y_q) = \langle n(n-1)\cdots(n-q+1)\rangle\,,
\end{aligned} \tag{2.12}$$

where the angular brackets imply the average over the event ensemble.

2.1.2. Cumulant correlation functions

The inclusive q-particle densities $\rho_q(y_1, \ldots, y_q)$ in general contain "trivial" contributions from lower-order densities. Under certain conditions, it is, therefore, advantageous to consider a new sequence of functions $C_q(y_1, \ldots, y_q)$ as those statistical quantities which vanish whenever one of their arguments becomes statistically independent of the others. It is well-known that the quantities with such properties are the correlation functions – also called (factorial) cumulant functions – or, in integrated form, Thiele's semi-invariants [3]. A formal proof of this property was given by Kubo [4] (see also [5]). The cumulant correlation functions are defined as in the cluster expansion familiar from statistical mechanics via the sequence [6–8]:

$$\rho_1(1) = C_1(1)\,, \tag{2.13}$$

$$\rho_2(1,2) = C_1(1)\,C_1(2) + C_2(1,2)\,, \tag{2.14}$$

$$\begin{aligned}
\rho_3(1,2,3) = {}& C_1(1)\,C_1(2)\,C_1(3) + C_1(1)\,C_2(2,3) + C_1(2)C_2(1,3) + C_1(3)\,C_2(1,2)\\
&+ C_3(1,2,3);
\end{aligned} \tag{2.15}$$

and, in general, by

$$\begin{aligned}
\rho_m(1, \ldots, m) = \sum_{\{l_i\}_m}\sum_{\text{perm.}} & \underbrace{[C_1(\,)\cdots C_1(\,)]}_{l_1\text{ factors}}\,\underbrace{[C_2(\,,\,)\cdots C_2(\,,\,)]}_{l_2\text{ factors}}\cdots\\
&\cdots\underbrace{[C_m(,\ldots,)\cdots C_m(,\ldots,)]}_{l_m\text{ factors}}.
\end{aligned} \tag{2.16}$$

Here, l_i is either zero or a positive integer and the sets of integers $\{l_i\}_m$ satisfy the condition

$$\sum_{i=1}^{m} i\, l_i = m\ . \tag{2.17}$$

The arguments in the C_i functions are to be filled by the m possible momenta in any order. The sum over permutations is a sum over all distinct ways of filling these arguments. For any given factor product there are precisely [7]

$$m!/[(1!)^{l_1}(2!)^{l_2}\cdots(m!)^{l_m}]\, l_1!l_2!\cdots l_m! \tag{2.18}$$

terms. The complete set of relations is contained in the functional identity:

$$\mathscr{G}^{\mathrm{incl}}[u(y)] = \exp\{g[u(y)]\}\ , \tag{2.19}$$

where

$$g[u(y)] = \int \rho_1(y)u(y)\mathrm{d}y + \sum_{q=2}^{\infty}\frac{1}{q!}\int_{\Omega} C_q(y_1,\ldots,y_q)\,u(y_1)\cdots u(y_q)\prod_{i=1}^{m}\mathrm{d}y_i. \tag{2.20}$$

It follows that

$$C_q(y_1,\ldots,y_q) = \partial^q g[u(y)]/\partial u(y_1)\cdots\partial u(y_n)|_{u=0}\ . \tag{2.21}$$

The relations (2.16) may be inverted with the result:

$$C_2(1,2) = \rho_2(1,2) - \rho_1(1)\rho_1(2)\ ,$$

$$C_3(1,2,3) = \rho_3(1,2,3) - \sum_{(3)}\rho_1(1)\rho_2(2,3) + 2\rho_1(1)\rho_1(2)\rho_1(3)\ ,$$

$$C_4(1,2,3,4) = \rho_4(1,2,3,4) - \sum_{(4)}\rho_1(1)\rho_3(1,2,3) - \sum_{(3)}\rho_2(1,2)\rho_2(3,4)$$

$$+ 2\sum_{(6)}\rho_1(1)\rho_1(2)\rho_2(3,4) - 6\rho_1(1)\rho_1(2)\rho_1(3)\rho_1(4)\ . \tag{2.22}$$

In the above relations we have abbreviated $C_q(y_1,\ldots,y_q)$ to $C_q(1,2,\ldots,q)$; the summations indicate that all possible permutations have to be taken (the number under the summation sign indicates the number of terms). Expressions for higher orders can be derived from the related formulae given in [9].

It is often convenient to divide the functions ρ_q and C_q by the product of one-particle densities. This leads to the definition of the normalized inclusive densities and correlations:

$$r_q(y_1,\ldots,y_q) = \rho_q(y_1,\ldots,y_q)/\rho_1(y_1)\cdots\rho_1(y_q)\ , \tag{2.23}$$

$$K_q(y_1,\ldots,y_q) = C_q(y_1,\ldots,y_q)/\rho_1(y_1)\cdots\rho_1(y_q)\ . \tag{2.24}$$

From expression (2.19) it can be deduced that, at finite energy, an infinite number of C_q will be non-vanishing: The densities ρ_q vanish for $q > N$, where N is the maximal number of particles in Ω allowed e.g. by energy–momentum conservation. As a consequence, the functional $\mathscr{G}$ is a

"polynomial" in $u(y)$. This in turn requires the exponent in (2.19) to be an "infinite series" in $u(y)$. In other words, the higher-order correlation functions must cancel the lower-order ones that contribute to a vanishing density function. Phenomenologically, this implies that it is meaningful to use correlation functions C_q only if the number of correlated particles in the considered phase-space domain Ω is considerably smaller than the average multiplicity in that region [2]. These conditions are not always fulfilled in present-day experiments for very small phase-space cells, with the exception of perhaps AA collisions.

2.1.3. Correlations for particles of different species

The generating functional technique of Section 2.1.1 can be extended to the general situation where several different species of particles are distinguished. This will not be pursued here and we refer to the literature for details [2, 10–12]. Considering two particle species a and b, the two-particle rapidity correlation function is of the form:

$$C_2^{ab}(y_1, y_2) = \rho_2^{ab}(y_1, y_2) - f\rho_1^a(y_1)\rho_1^b(y_2)\,, \tag{2.25}$$

with

$$\rho_1^a(y_1) = \frac{1}{\sigma_{inel}}\frac{d\sigma^a}{dy_1}\,; \quad \rho_2^{ab}(y_1, y_2) = \frac{1}{\sigma_{inel}}\frac{d\sigma^{ab}}{dy_1\,dy_2}. \tag{2.26}$$

Here, y_1 and y_2 are the c.m. rapidities, σ_{inel} the inelastic cross section and a, b represent particle properties, e.g. charge.

The normalization conditions are

$$\int \rho_1^a(y_1)dy_1 = \langle n_a\rangle; \quad \int\int \rho_2^{ab}(y_1, y_2)dy_1\,dy_2 = \langle n_a(n_b - \delta^{ab})\rangle\,, \tag{2.27}$$

$$\int\int C_2^{ab}(y_1, y_2)dy_1\,dy_2 = \langle n_a(n_b - \delta^{ab})\rangle - f\langle n_a\rangle\langle n_b\rangle\,, \tag{2.28}$$

where $\delta^{ab} = 0$ for the case when a and b are particles of different species and $\delta^{ab} = 1$ for identical particles, and n_a and n_b are the corresponding particle multiplicities.

Most experiments use

$$f = 1\,, \tag{2.29}$$

so that the integral over the correlation function (equal to the ratio $\bar{n}^2/k$ of the negative binomial parameters [13]) vanishes for the case of a Poissonian multiplicity distribution. Other experiments use

$$f = \langle n_a(n_b - \delta^{ab})\rangle/\langle n_a\rangle\langle n_b\rangle \tag{2.30}$$

to obtain a vanishing integral also for a non-Poissonian multiplicity distribution.

To be able to compare the various experiments, we use both definitions and denote the correlation function $C_2^{ab}(y_1, y_2)$ when following definition (2.29) and $C_2'^{ab}(y_1, y_2)$ when following definition (2.30). We, furthermore, use a reduced form of definition (2.30),

$$\tilde{C}_2^{ab}(y_1, y_2) = C_2'^{ab}(y_1, y_2)/\langle n_a(n_b - \delta^{ab})\rangle\,. \tag{2.31}$$

The corresponding normalized correlation functions

$$K_2^{ab}(y_1, y_2) = C_2^{ab}(y_1, y_2)/f\rho_1^a(y_1)\rho_1^b(y_2) \tag{2.32}$$

follow the relations

$$K_2' = (1/f)(K_2 + 1) - 1\,, \tag{2.33}$$

and $\tilde{K}_2$ is defined as $\tilde{K}_2 = K_2'$. These are more appropriate than C_2 when comparisons have to be performed at different average multiplicity and are less sensitive to acceptance problems.

The correlation functions defined by expressions (2.25)–(2.33), contain a pseudo-correlation due to the summation of events with different charge multiplicity n and different semi-inclusive single-particle densities $\rho_1^{(n)}$.

The relation between inclusive and semi-inclusive correlation functions has been carefully analysed in [14]. Let σ_n be the topological cross section and

$$P_n = \sigma_n/\sum\sigma_n. \tag{2.34}$$

The semi-inclusive rapidity single- and two-particle densities for particles a and b are defined as

$$\rho_1^{(n)}(y) = \frac{1}{\sigma_n}\frac{d\sigma_n^a}{dy} \quad \text{and} \quad \rho_2^{(n)}(y_1, y_2) = \frac{1}{\sigma_n}\frac{d\sigma_n^{ab}}{dy_1\,dy_2}\,. \tag{2.35}$$

The inclusive correlation function $C_2(y_1, y_2)$ can then be written as

$$C_2(y_1, y_2) = C_S(y_1, y_2) + C_L(y_1, y_2)\,, \tag{2.36}$$

where

$$C_S(y_1, y_2) = \sum P_n C_2^{(n)}(y_1, y_2)\,, \tag{2.37}$$

$$C_L(y_1, y_2) = \sum P_n \Delta\rho^{(n)}(y_1)\Delta\rho^{(n)}(y_2) \tag{2.38}$$

with $C_2^{(n)}(y_1, y_2) = \rho_2^{(n)}(y_1, y_2) - \rho_1^{(n)}(y_1)\rho_1^{(n)}(y_2)$ and $\Delta\rho^{(n)}(y) = \rho_1^{(n)}(y) - \rho_1(y)$. In (2.37) C_S is the average of the semi-inclusive correlation functions (often misleadingly denoted as "short-range") and is more sensitive to dynamical correlations. The term C_L (misleadingly called "long-range") arises from mixing different topological single-particle densities.

A normalized form of C_S can be defined as

$$K_S(y_1, y_2) = \frac{C_S(y_1, y_2)}{\sum_n P_n\rho_1^{(n)}(y_1)\rho_1^{(n)}(y_2)} = \frac{\sum_n P_n\rho_2^{(n)}(y_1, y_2)}{\sum_n P_n\rho_1^{(n)}(y_1)\rho_1^{(n)}(y_2)} - 1\,. \tag{2.39}$$

C_S' and $\tilde{C}_S$ and their normalized forms K_S' and $\tilde{K}_S$ are defined accordingly, with the averages $\langle n\rangle$ and $\langle n_a(n_b - \delta^{ab})\rangle$ replaced by n and $n_a(n_b - \delta^{ab})$, respectively.

Analogous expressions may be derived for three-particle correlations. They are discussed in Section 3.4.

2.1.4. Factorial and cumulant moments

When the parametric function $z(y)$ is replaced by a constant z, the generating functionals reduce to the generating function for the multiplicity distribution. Indeed, the probability P_n for producing

n particles is given by

$$P_n = \sigma_n^{\text{excl}}/\sigma_{\text{inel}} \tag{2.40}$$

and we have

$$G(z) = \sum_{n=0}^{\infty} P_n(1+z)^n = \mathscr{G}^{\text{excl}}[z+1] = \mathscr{G}^{\text{incl}}[z] \tag{2.41}$$

$$= 1 + \sum_{q=1}^{\infty} \frac{z^q}{q!} \int_{\Omega} \rho_q(y_1, \ldots, y_q)\mathrm{d}y_1 \ldots \mathrm{d}y_q \tag{2.42}$$

$$= 1 + \sum_{q=1}^{\infty} \frac{z^q}{q!} \tilde{F}_q . \tag{2.43}$$

The $\tilde{F}_q$ are the unnormalized factorial (or binomial) moments

$$\tilde{F}_q \equiv \langle n^{[q]} \rangle \equiv \langle n(n-1)\cdots(n-q+1) \rangle$$

$$= \int_{\Omega} \mathrm{d}y_1 \ldots \int_{\Omega} \mathrm{d}y_q \, \rho_q(y_1, \ldots, y_q)$$

$$= \sum_n P_n n(n-1)\cdots(n-q+1) . \tag{2.44}$$

This relation can (formally) be inverted. If $P_n = 0$ for $n > N$ then an approximation for P_n is given by

$$P_n = \frac{1}{n!} \sum_{j=0}^{N-n} (-1)^j \frac{\tilde{F}_{j+n}}{j!} \quad (n = 0, 1, \ldots N) , \tag{2.45}$$

and P_n is included between any two successive values obtained by terminating the sum at $j = s$ and $j = s+1$, respectively.

In (2.44) n denotes the multiplicity in Ω and the average is taken over the ensemble of events. All the integrals are taken over the same volume Ω such that $y_i \in \Omega \ \forall i \in \{1, \ldots, q\}$. Using the correlation-function cluster decomposition, one further has

$$\log G(z) = \langle n \rangle z + \sum_{q=2}^{\infty} \frac{z^q}{q!} f_q . \tag{2.46}$$

The f_q are the unnormalized factorial cumulants, also known as Mueller moments [8]

$$f_q = \int_{\Omega} \mathrm{d}y_1 \ldots \int_{\Omega} \mathrm{d}y_q \, C_q(y_1, \ldots, y_q) , \tag{2.47}$$

the integrations being performed as in (2.44). The quantities $\tilde{F}_q$ and f_q are easily found if $G(z)$ is known:

$$\tilde{F}_q = \mathrm{d}^q G(z)/\mathrm{d}z^q|_{z=0} , \tag{2.48}$$

$$f_q = \mathrm{d}^q \log G(z)/\mathrm{d}z^q|_{z=0} \tag{2.49}$$

$$P_q = (1/q!)\, \mathrm{d}^q\, G(z)/\mathrm{d}z^q|_{z=-1} \tag{2.50}$$

Using Cauchy's theorem, this can also be written as

$$P_n = \frac{1}{2\pi i} \oint \frac{G(z)}{(1+z)^{n+1}} dz \,, \tag{2.51}$$

where the integral is on a circle enclosing $z = -1$. Eq. (2.51) is sometimes useful in deriving asymptotic expressions for P_n in terms of factorial moments or cumulants [15, 8].

As a simple example, we consider the Poisson distribution

$$P_n = e^{-\langle n \rangle} \langle n \rangle^n / n! \,,$$

for which

$$G(z) = \sum_0^\infty P_n (1+z)^n = \exp\{\langle n \rangle z\} \,, \tag{2.52}$$

showing that $f_q \equiv 0$ for $q > 1$. In that case one has

$$\tilde{F}_q = \langle n(n-1) \cdots (n-q+1) \rangle = \langle n \rangle^q . \tag{2.53}$$

The expressions of density functions in terms of cumulant correlation functions, and the reverse relations, are duplicated for their integrated counterparts. They follow directly from the equations:

$$1 + \sum_{q=1}^\infty \frac{z^q}{q!} \tilde{F}_q = \exp\left\{ \langle n \rangle z + \sum_{q=2}^\infty \frac{z^q}{q!} f_q \right\} \tag{2.54}$$

or

$$\log\left(1 + \sum_{q=1}^\infty \frac{z^q}{q!} \tilde{F}_q \right) = \langle n \rangle z + \sum_{q=2}^\infty \frac{z^q}{q!} f_q \tag{2.55}$$

by expanding either the exponential in (2.54) or the logarithm in (2.55) and equating the coefficients of the same power of z. One finds [9]:

$$\begin{aligned}
\tilde{F}_1 &= f_1 \,, \\
\tilde{F}_2 &= f_2 + f_1^2 \,, \\
\tilde{F}_3 &= f_3 + 3 f_2 f_1 + f_1^3 \,, \\
\tilde{F}_4 &= f_4 + 4 f_3 f_1 + 3 f_2^2 + 6 f_2 f_1^2 + f_1^4 \,, \\
\tilde{F}_5 &= f_5 + 5 f_4 f_1 + 10 f_3 f_2 + 10 f_3 f_1^2 + 15 f_2^2 f_1 + 10 f_2 f_1^3 + f_1^5 \,;
\end{aligned} \tag{2.56}$$

and in general

$$\tilde{F}_q = q! \sum_{\{l_j\}} \prod_{j=1}^q \left(\frac{f_j}{j!} \right)^{l_j} \frac{1}{l_j!} \,, \tag{2.57}$$

with the summation as in (2.16) and $\sum_{i=1}^q i l_i = q$.

The latter formula can also be written as

$$\tilde{F}_q = \sum_{l=0}^{q-1} \binom{q-1}{l} f_{q-l} \tilde{F}_l \,, \tag{2.58}$$

(with $\tilde{F}_0 \equiv 1$, $f_0 \equiv 0$) and is well-suited for computer calculation. An equivalent relation was derived in [8]. The (ordinary) moments

$$\mu_q = \langle n^q \rangle = \sum_{n=0}^{\infty} n^q P_n \,, \tag{2.59}$$

may be derived from the moment generating function

$$M(z) = \sum_{n=0}^{\infty} n^{nz} P_n \,, \tag{2.60}$$

since

$$\mu_q = \mathrm{d}^q M(z)/\mathrm{d}z^q|_{z=0} \,. \tag{2.61}$$

We note the useful relations

$$M(z) = G(\mathrm{e}^z - 1) \,, \tag{2.62}$$

$$G(z) = M(\log(1+z)) \,. \tag{2.63}$$

Moments and factorial moments are related to each other by series expansions. From the identities [16]:

$$n(n-1)\cdots(n-q+1) = \sum_{m=0}^{q} S_q^{(m)} n^m \,, \tag{2.64}$$

$$n^q = \sum_{m=0}^{q} \mathscr{S}_q^{(m)} n(n-1)\cdots(n-m+1) \,, \tag{2.65}$$

where $S_q^{(m)}$ and $\mathscr{S}_q^{(m)}$ are Stirling numbers of the first and second kind, respectively, follows directly:

$$\tilde{F}_q = \sum_{m=0}^{q} S_q^{(m)} \mu_m \,, \tag{2.66}$$

$$\mu_q = \sum_{m=0}^{q} \mathscr{S}_q^{(m)} \tilde{F}_m \,. \tag{2.67}$$

Cumulants κ_q can be defined in terms of the moments μ_q in the standard way [17, 9]. They obey relations identical to (2.56). The cumulants are integrals of the type (2.47) of differential quantities known as density moments. These are discussed in [18, 19]. Relations expressing central moments in terms of factorial moments via non-central Stirling numbers are derived in [20].

2.1.5. Cell-averaged factorial moments and cumulants; generalized moments

In practical work, with limited statistics, it is almost always necessary to perform averages over more than a single phase-space cell. Let Ω_m be such a cell (e.g. a single rapidity interval of size δy) and divide the phase-space volume into M non-overlapping cells Ω_m of size $\delta\Omega$, independent of m. Let n_m be the number of particles in cell Ω_m. Different cell-averaged moments may be considered, depending on the type of averaging.

Normalized factorial moments [21, 22], which have become known as *vertical moments*, are defined as[3]

$$F_q^{\mathrm{V}}(\delta y) \equiv \frac{1}{M}\sum_{m=1}^{M}\frac{\langle n_m(n_m-1)\cdots(n_m-q+1)\rangle}{\langle n_m\rangle^q} \tag{2.68}$$

$$\equiv \frac{1}{M}\sum_{m=1}^{M}\frac{\int_{\delta y}\rho_q(y_1,\ldots,y_q)\prod_{i=1}^{q}\mathrm{d}y_i}{(\int_{\delta y}\rho(y)\mathrm{d}y)^q},$$

$$= \frac{1}{M(\delta y)^q}\sum_{m=1}^{M}\int_{\delta y}\frac{\rho_q(y_1,\ldots,y_q)\prod_{i=1}^{q}\mathrm{d}y_i}{(\bar{\rho}_m)^q}. \tag{2.69}$$

The full rapidity interval ΔY is divided into M equal bins: $\Delta Y = M\,\delta y$; each y_i is within the δy range and $\langle n_m\rangle \equiv \bar{\rho}_m\,\delta y \equiv \int_{\delta y}\rho_1(q)\mathrm{d}y$.

One may also define normalized *horizontal moments* by

$$F_q^{\mathrm{H}}(\delta y) \equiv \frac{1}{M}\sum_{m=1}^{M}\frac{\langle n_m(n_m-1)\cdots(n_m-q+1)\rangle}{\langle \bar{n}_m\rangle^q}. \tag{2.70}$$

with $\bar{n}_m = \sum_m n_m/M$; $\langle\bar{n}_m\rangle = \langle n\rangle/M$; $n = \sum_m n_m$.

Horizontal and vertical moments are equal if $M = 1$. Vertical moments are normalized locally and thus sensitive only to fluctuations within each cell but not to the overall shape of the single-particle density. Horizontal moments are sensitive to the shape of the single- particle density in y and further depend on the correlations between cells. To eliminate the effect of a non-flat rapidity distribution, it was suggested to either introduce correction factors [23] or use "cumulative" variables which transform an arbitrary distribution into a uniform one [24, 25].

Likewise, cell-averaged normalized factorial cumulant moments may be defined as

$$K_q(\delta y) = \frac{1}{M(\delta y)^q}\sum_{m=1}^{M}\int_{\delta y}\prod_i \mathrm{d}y_i\,\frac{C_q(y_1,\ldots,y_q)}{(\bar{\rho}_m)^q}. \tag{2.71}$$

They are related [26] to the factorial moments by[4]

$$F_2 = 1 + K_2,$$

$$F_3 = 1 + 3K_2 + K_3,$$

$$F_4 = 1 + 6K_2 + 3\overline{K_2^2} + 4K_3 + K_4. \tag{2.72}$$

In F_4 and higher-order moments, "bar averages" appear. They are defined as $\overline{AB} \equiv \sum_m A_m B_m/M$.

Besides factorial and cumulant moments, other measures of multiplicity fluctuations have been proposed. In particular, G moments [27] – known in statistics as frequency moments [9] – were

---

[3] Here and in the following we consider rapidity space for definiteness.

[4] The higher-order relations can be found in [26].

extensively used to investigate whether multiparticle processes possess (multi)fractal properties [28, 29]. G moments are defined as

$$G_q = \sum_{m=1}^{M}{}' p_m^q , \qquad p_m = n_m/n , \qquad n = \sum_{m=1}^{M} n_m . \tag{2.73}$$

Also here, n_m is the number of particles in bin m, the absolute frequency; n is the total multiplicity in an initial interval and M is the number of bins at "resolution" M. Bins with zero content ("empty bins") are excluded in the sum, so that q can cover the whole spectrum of real numbers. For q negative, G_q is sensitive to "holes" in the rapidity distribution of a single event. Note that p_m in (2.73) is not a probability but a relative frequency or "empirical measure" in modern terminology. For small n, G moments are very sensitive to statistical fluctuations ("noise"), especially for large M. This seriously limits their potential. In attempts to reduce this noise sensitivity, modified definitions have been proposed in [30].

2.1.6. Multivariate distributions

The univariate factorial moments $\tilde{F}_q$ characterize multiplicity fluctuations in a single phase-space cell and thus reflect only local properties. More information is contained in the correlations between fluctuations (within the same event) in two or more cells. This has led to consider multivariate factorial moments. For non-overlapping cells, the two-fold factorial moments, also called *correlators*, are defined as:

$$\tilde{F}_{pq} = \langle n_m^{[p]} n_{m'}^{[q]} \rangle , \tag{2.74}$$

where n_m ($n_{m'}$) is the number of particles in cell m (cell m'). A normalized version of the two-fold correlator is discussed in [21] and defined as:

$$F_{pq} = \langle n_m^{[p]} n_{m'}^{[q]} \rangle / \tilde{F}_p \tilde{F}_q . \tag{2.75}$$

For reasons of statistics, these quantities are usually averaged over many pairs of cells, keeping the "distance" (D) between the cells constant.[5] This averaging procedure requires the same precautions regarding stationarity of single particle densities as for their single-cell equivalents.

Multifold factorial moments are a familiar tool in radiophysics and radar physics and in quantum optics [31]. There, they relate to simultaneous measurement of photo-electron counts detected in, say M, time-intervals, or in M space points, leading to a joint probability distribution $P_M(n_1, n_2, \ldots, n_M)$. The importance of multifold moments derives from the fact that e.g. in the simplest case of two cells, $\tilde{F}_{11} = \langle n_m n_{m'} \rangle$ is directly related to the auto-correlation function of the radiation field and obeys, for small cells, the Siegert relation [31], whatever the statistical properties of the field. The higher-order moments are sensitive to higher-order correlations and to the phase of the field.

---

[5] In one-dimensional rapidity space, D is defined as the distance between the centres of two rapidity intervals; in multidimensional phase space a proper metric must first be defined.

Factorial moments and factorial correlators are intimately related quantities. In terms of inclusive densities one has

$$\tilde{F}_{pq} = \int_{\Omega_1} \mathrm{d}y_1 \ldots \mathrm{d}y_p \int_{\Omega_2} \mathrm{d}y_{p+1} \ldots \mathrm{d}y_{p+q}\, \rho_{p+q}(y_1, \ldots, y_p; y_{p+1}, \ldots, y_{p+q}) , \tag{2.76}$$

where ρ_{p+q} is the inclusive density of order $p+q$. The integrations are performed over two arbitrary (possibly overlapping) phase-space cells Ω_1 and Ω_2, separated by a "distance" D.

It should be noted that the definition (2.76) is more general than (2.74). For $\Omega_1 = \Omega_2$ or $D = 0$, (2.76) reduces to the correct definition of $\tilde{F}_2$ whereas (2.74) is, in this case, equal to $\langle n^2 \rangle$ and misses the so-called "shot-noise" term $-\langle n \rangle$.

Factorial moments and factorial correlators of the same order are thus seen to differ only in the choice of the integration domains. Note that for $p \neq q$, definition (2.76) is not symmetric in p and q and a symmetrized version is often used in experimental work:

$$\tilde{F}^{(s)}_{pq} = (\tilde{F}_{pq} + \tilde{F}_{qp})/2 . \tag{2.77}$$

From (2.76) follows that F_{11} is directly derivable from measured two-particle correlation functions or from appropriate analytical parametrizations. Higher-order correlators involve higher-order density functions which, in general, are unknown.

We now turn to a discussion of multivariate factorial cumulants. For M non-overlapping cells, we introduce the M-variate multiplicity distribution $P_M(n_1, \ldots, n_M)$ and the corresponding moment- and factorial-moment generating functions:

$$M(z_1, \ldots, z_M) = \sum_{n_1=0}^{\infty} \sum_{n_2=0}^{\infty} \cdots \sum_{n_M=0}^{\infty} \mathrm{e}^{z_1 n_1 + \cdots + z_M n_M} P_M(n_1, \ldots, n_M) , \tag{2.78}$$

$$G(z_1, \ldots, z_M) = \sum_{n_1=0}^{\infty} \sum_{n_2=0}^{\infty} \cdots \sum_{n_M=0}^{\infty} (1+z_1)^{n_1} \cdots (1+z_M)^{n_M} P_M(n_1, \ldots, n_M) , \tag{2.79}$$

from which the M-variate moments are easily obtained by differentiation:

$$\mu_{q_1 \cdots q_M} = \langle n_1^{q_1} \cdots n_M^{q_M} \rangle = \left(\frac{\partial}{\partial z_1}\right)^{q_1} \cdots \left(\frac{\partial}{\partial z_M}\right)^{q_M} M(z_1, \ldots, z_M)\Big|_{z_1 = \cdots = z_M = 0} , \tag{2.80}$$

$$\tilde{F}_{q_1 \cdots q_M} = \langle n_1^{q_1} \cdots n_M^{[q_M]} \rangle = \left(\frac{\partial}{\partial z_1}\right)^{q_1} \cdots \left(\frac{\partial}{\partial z_M}\right)^{q_M} G(z_1, \ldots, z_M)\Big|_{z_1 = \cdots = z_M = 0} . \tag{2.81}$$

The multivariate (ordinary) cumulants $\kappa_{q_1 \cdots q_M}$ and multivariate factorial cumulants $f_{q_1 \cdots q_M}$ are likewise obtained by replacing $M(\cdot)$ and $G(\cdot)$ in (2.80) and (2.81) by their respective natural logarithms [32]. The same expressions serve to extend the relations between univariate moments and cumulants to their multivariate counterparts.

For $M = 2$ and non-overlapping cells, one has the identity [cf. (2.54)]:

$$\sum_{l=0}^{\infty} \sum_{m=0}^{\infty} \frac{(z_1)^l (z_2)^m}{l!\, m!} \tilde{F}_{lm} = \exp\left(\sum_{l=0}^{\infty} \sum_{m=0}^{\infty} \frac{(z_1)^l (z_2)^m}{l!\, m!} f_{lm} \right) , \tag{2.82}$$

where $\tilde{F}_{00} \equiv 1$ and f_{00} is defined equal to zero. It follows that[6]

$$\tilde{F}_{11} = f_{11} + f_{01}f_{10}\,, \tag{2.83}$$

$$\tilde{F}_{12} = f_{12} + f_{01}f_{20} + 2f_{10}f_{11} + f_{01}f_{10}^2\,, \tag{2.84}$$

$$\tilde{F}_{13} = f_{13} + f_{01}f_{30} + 3f_{11}f_{20} + 3f_{01}f_{10}f_{20} + 3f_{10}f_{12} + 3f_{10}^2f_{11} + f_{01}f_{10}^3\,, \tag{2.85}$$

$$\tilde{F}_{22} = f_{22} + 2f_{10}f_{21} + f_{02}f_{20} + f_{01}^2f_{20} + 2f_{01}f_{12} + 2f_{11}^2 + 4f_{01}f_{10}f_{11} + f_{02}f_{10}^2 + f_{01}^2f_{10}^2\,. \tag{2.86}$$

Similarly, expanding the logarithm in

$$\sum_{l=0}^{\infty}\sum_{m=0}^{\infty}\frac{(-z_1)^l(-z_2)^m}{l!\,m!}f_{lm} = \log\left(\sum_{l=0}^{\infty}\sum_{m=0}^{\infty}\frac{(-z_1)^l(-z_2)^m}{l!\,m!}\tilde{F}_{lm}\right), \tag{2.87}$$

in powers of s and t and identifying coefficients, the reverse relations follow:

$$f_{11} = \tilde{F}_{11} - \tilde{F}_{01}\tilde{F}_{10}\,, \tag{2.88}$$

$$f_{12} = \tilde{F}_{12} - \tilde{F}_{01}\tilde{F}_{20} - 2\tilde{F}_{10}\tilde{F}_{11} + 2\tilde{F}_{01}\tilde{F}_{10}^2\,, \tag{2.89}$$

$$f_{13} = \tilde{F}_{13} - \tilde{F}_{01}\tilde{F}_{30} - 3\tilde{F}_{11}\tilde{F}_{20} + 6\tilde{F}_{01}\tilde{F}_{10}\tilde{F}_{20} - 3\tilde{F}_{10}\tilde{F}_{12} + 6\tilde{F}_{10}^2\tilde{F}_{11} - 6\tilde{F}_{01}\tilde{F}_{10}^3\,, \tag{2.90}$$

$$f_{22} = \tilde{F}_{22} - 2\tilde{F}_{10}\tilde{F}_{21} - \tilde{F}_{02}\tilde{F}_{20} + 2\tilde{F}_{01}^2\tilde{F}_{20} - 2\tilde{F}_{01}\tilde{F}_{12} - 2\tilde{F}_{11}^2 + 8\tilde{F}_{01}\tilde{F}_{10}\tilde{F}_{11} + 2\tilde{F}_{02}\tilde{F}_{10}^2 - 6\tilde{F}_{01}^2\tilde{F}_{10}^2\,. \tag{2.91}$$

The quantities $\tilde{F}_{0i}$, $\tilde{F}_{i0}$, and f_{0i}, f_{i0} are equal to the single-cell factorial moments and factorial cumulants, respectively. Expressions for $\tilde{F}_{ji}$ (f_{ji}) are obtained from the corresponding expression for $\tilde{F}_{ij}$ (f_{ij}) by permutation of the subscripts. By definition, $f_{01} = \tilde{F}_{01}$ and f_{01} is equal to the average multiplicity in cell 2.

It may be noted that the bivariate relations reduce to the univariate ones (2.56) by simply amalgamating the indices. For example, from

$$\tilde{F}_{12} = f_{12} + f_{01}f_{20} + 2f_{10}f_{11} + f_{01}f_{10}^2\,, \tag{2.92}$$

one recovers, by summing the indices

$$\tilde{F}_3 = f_3 + 3f_1f_2 + f_1^3\,. \tag{2.93}$$

It is shown in [9] (Section 13.12) that the above relations, while seemingly complex, have in fact a surprisingly elegant structure, rooted in simple algebraic properties of completely symmetric functions. Further discussion on this point and other useful properties may be found in [32].

Extensions to more than two cells is straightforward, in principle, but involves tedious algebra.

2.2. *Poisson-noise suppression*

To detect dynamical fluctuations in the density of particles produced in a high-energy collision, a way has to be devised to eliminate, or to reduce as much as possible, the statistical fluctuations

[6] See also [33].

– noise – due to the finiteness of the number of particles in the counting cell(s). This requirement can to a large extent be satisfied by studying factorial moments and their multivariate counterparts. It forms the basis of the factorial moment technique, known in optics, but rediscovered in multihadron physics in [21, 22]. The method rests on the conjecture that the multicell multiplicity distribution $P_M(n_1, \ldots, n_M)$ can be written as

$$P_M(n_1, \ldots, n_M) = \int \mathrm{d}\rho_1 \ldots \mathrm{d}\rho_M \, P_\rho(\rho_1, \ldots, \rho_M) \prod_{m=1}^{M} \frac{(\rho_m \delta)^{n_m}}{n_m!} \exp(-\rho_m \delta) \,. \tag{2.94}$$

The Poisson factors represent uncorrelated fluctuations of n_m around the average $\rho_m \delta = \langle n_m \rangle$ in mth interval; δ is here the size of the interval. This can also be written as

$$P_M(n_1 \ldots n_M) = \left\langle \prod_{m=1}^{M} \frac{\langle n_m \rangle^{n_m}}{n_m!} \exp(-\langle n_m \rangle) \right\rangle_\rho , \tag{2.95}$$

where the outer brackets mean that an average is taken over the probability distribution of the densities ρ_m, which are subject only to dynamical fluctuations. If these are absent, $P_\rho(\rho_1, \ldots, \rho_M)$ is simply a product of δ functions.

The formulae (2.94) and (2.95) are formally identical to the expression for the multi-interval photo-electron counting probability distribution in quantum optics and based on the famous Mandel formula [34, 35]. The latter relates the probability distribution of the *number of detected photo-electrons* to the statistical distribution of the e.m. field.

In optics, ρ_m has the meaning of a space- or time-integrated field intensity. The ensemble average is calculated from the field density matrix which describes its statistical properties.

Eqs. (2.94) and (2.95) express $P_M(n_1, \ldots, n_M)$ as a linear transformation of $P_\rho(\rho_1, \ldots, \rho_M)$ with a "Poisson kernel". This transformation is known as the "Poisson transform" of P_ρ [36].

The Poisson transform of a single-variable function $f(x)$ is the function $\tilde{f}(n)$ (n integer) defined by the linear transformation

$$\tilde{f}(n) = \int_0^\infty \mathrm{d}x f(x) \frac{x^n}{n!} \mathrm{e}^{-x} \,. \tag{2.96}$$

A trivial example is the function $\delta(x - \mu)$ whose transform is the Poisson probability distribution. The Bose–Einstein distribution

$$\tilde{f}(n) = \mu^n/(1 + \mu)^{n+1} \quad (n = 0, 1, \ldots) \,, \tag{2.97}$$

is obtained as the Poisson transform of the exponential function $(1/\mu) \exp(-x/\mu)$.

For suitably behaved functions, the inverse Poisson transform exists. It is closely related to the Laplace-transform of $f(x)$. Several practical methods have been developed to determine the function $f(x)$ from its Poisson-transform. Besides methods based on series expansions, the inversion problem may be reduced to an inverse moment problem. This follows from the equality between the factorial moments of $\tilde{f}(n)$ and the ordinary moments of $f(x)$, as further discussed below.

A table of useful transforms for probability distributions and further mathematical properties can be found in [31].

From the basic Poisson transform equation (2.95) it is easily seen that the multifold factorial moment generating function has the simple form

$$G(z_1, \ldots, z_M) = \left\langle \prod_{j=1}^{M} \exp(z_j \rho_j \delta) \right\rangle_\rho , \tag{2.98}$$

where the statistical average is again taken over the ensemble of densities $\rho_1, \ldots, \rho_M$, as indicated by the subscript.

On the other hand, the (ordinary) moment generating function of the densities is given by:

$$Q(z_1, \ldots, z_M) = \int P_\rho(\rho_1, \ldots, \rho_M) e^{\rho_1 z_1 + \cdots + \rho_M z_M} \, d\rho_1 \cdots d\rho_M \tag{2.99}$$

$$= \left\langle \prod_{j=1}^{M} e^{\rho_j z_j} \right\rangle_\rho . \tag{2.100}$$

Comparing (2.98) and (2.100), it follows that

$$G(z_1, \ldots, z_M) = Q(\delta \rho_1 z_1, \ldots, \rho_M z_M \delta) . \tag{2.101}$$

This equation implies that the normalized multivariate factorial moments of the multiplicity distribution

$$F_{q_1 \cdots q_M} = \tilde{F}_{q_1 \cdots q_M} / \langle n_1 \rangle^{q_1} \cdots \langle n_M \rangle^{q_M} \tag{2.102}$$

are equal to the normalized multivariate (ordinary) moments of the relative density fluctuation $\rho_m / \langle \rho_m \rangle$. This is the "noise-suppression" theorem [21, 22]. It assumes that the noise is Poissonian (cf. (2.94)) and that the number of counts in all intervals (the total multiplicity) is unrestricted.[7]

The property of Poisson-noise suppression has made measurement of factorial moments a standard technique, e.g. in quantum optics, to study the statistical properties of arbitrary electromagnetic fields from photon-counting distributions. Their utility was first explicitly recognized, for the single time-interval case, in [37, 5] and later generalized to the multivariate case in [32]. The authors of [5] further stress the advantages of factorial cumulants compared to factorial moments, since the former measure genuine correlation patterns, whereas the latter contain additional large combinatorial terms which may mask the underlying dynamical correlations (however, see the discussion in Section 2.1.2).

Multivariate factorial cumulants are derived from the (natural) logarithm of the factorial moment generating function. Taking logarithms of both sides of (2.101), one finds that the multivariate normalized factorial cumulants of the counting distribution are equal to the multivariate normalized ordinary cumulants of the densities $[\rho\delta]$. This relation, therefore, extends the noise-suppression theorem to cumulants. This property is exploited in many fields from quantum optics [32] to radar-physics and astrophysics (see e.g. [38]).

---

[7] If the sum over all intervals of the number of counts is fixed, a slightly more complicated relation can be obtained if the noise has a Bernoulli (multinomial) distribution [21].

2.3. Sum rules

In an interesting α-model analysis of factorial correlators [39], scaling relations are derived between single-variate and 2-variate factorial moments which are independent of the dimension of the phase space. The result is stated as follows: if a correlator $F_{11}(D, \delta)$ is effectively independent of δ in a range $\delta < D \leq \delta_0$, then

$$F_{11}(D) = 2F_2(2D) - F_2(D) \,. \tag{2.103}$$

Here, δ is the interval size and D the distance between the intervals.

Similar types of relations – or sum rules – are well-known in optics since the early 1970s. They are exploited in so-called Multi-Cathode and Multiple-Aperture Single-Cathode (MASC) photo-electron counting experiments (see e.g. [40, 41] and references therein).

Consider again the multivariate multiplicity distribution $P_M(n_1, \ldots, n_M)$ giving the joint probability for the occurrence of n_1 particles in a cell Ω_1, $\ldots$, n_M particles in cell Ω_M, with $\Omega_i \cap \Omega_j = 0$, $\forall i, j$ and $i \neq j$. Let n be the number of particles counted in the union of the M cells,

$$n = \sum_{m=1}^{M} n_m \,. \tag{2.104}$$

The probability distribution of n is given by

$$P(n) = \sum_{n_1=0}^{n} \cdots \sum_{n_M=0}^{n} p_M(n_1, \ldots, n_M)\, \delta_{n, n_1 + \cdots + n_M} \,. \tag{2.105}$$

Define the single-variate factorial moment generating function

$$g(z) = \sum_{n=0}^{\infty} (1+z)^n \, P(n) \,. \tag{2.106}$$

The function $g(z)$ can be expressed in terms of the multivariate generating function (2.79) as:

$$g(z) = G_M(z_1, \ldots, z_M)|_{z_1 = z_2 = \cdots = z_M = z} \,. \tag{2.107}$$

Eq. (2.107) allows to express factorial moments of n in terms of the multivariate factorial moments of $\{n_1, \ldots, n_M\}$. Application of the Leibnitz rule

$$\left(\frac{\mathrm{d}}{\mathrm{d}z}\right)^k f(z) = \sum_{\{a_j\}} \frac{k!}{a_1! a_2! \cdots a_k!} \left(\frac{\mathrm{d}}{\mathrm{d}z}\right)^{a_1} f_1(z) \cdots \left(\frac{\mathrm{d}}{\mathrm{d}z}\right)^{a_k} f_M(z)$$

to the function

$$f(z) = f_1(z) \cdots f_M(z)$$

leads immediately to the relation

$$\tilde{F}_q = \sum_{\{a_j\}} \tilde{F}^{(M)}_{a_1 \cdots a_M} \frac{q!}{a_1! \cdots a_M!} \,. \tag{2.108}$$

The summation is over all sets $\{a_j\}$ of non-negative integers such that

$$\sum_{j=1}^{M} a_j = q\,.$$

Formula (2.108) may be looked upon as a generalization of the usual multinomial theorem for factorial moments.[8]

Likewise, taking the natural logarithm of both sides of (2.107), one obtains a relation identical to (2.108) among single-variate and multivariate factorial cumulants.

As an example, for two rapidity bins ($M = 2$) of size δ separated by a distance D, one finds

$$\begin{aligned}
\tilde{F}_2 &= \tilde{F}^{(2)}_{02} + 2\tilde{F}^{(2)}_{11} + \tilde{F}^{(2)}_{20}\,,\\
\tilde{F}_3 &= \tilde{F}^{(2)}_{03} + 3(\tilde{F}^{(2)}_{12} + \tilde{F}^{(2)}_{21}) + \tilde{F}^{(2)}_{30}\,,\\
\tilde{F}_4 &= \tilde{F}^{(2)}_{04} + 4(\tilde{F}^{(2)}_{13} + \tilde{F}^{(2)}_{31}) + 6\tilde{F}^{(2)}_{22} + \tilde{F}^{(2)}_{40}\,,
\end{aligned} \tag{2.109}$$

The factorial moments $\tilde{F}_{0l}$ are determined from the single-cell (marginal) counting distribution, whereas the univariate factorial moments $\tilde{F}_q$ are obtained from the sum of the counts in the two cells.

The relations derived in [39] follow immediately from (2.109) by considering two adjacent cells and normalizing properly. Since the derivation of (2.108) is completely general, it obviously holds irrespective of the dimension of phase space.

The relations (2.109) are trivially extended to more than two cells. They allow to measure high-order correlators by varying the distances between the cells. In optics and radar physics, they are typically used in determining spatial coherence properties of arbitrary e.m. fields.

2.4. Scaling laws

A major part of this paper is devoted to recent experimental and theoretical research on possible manifestations of scale invariance in high-energy multiparticle production processes. This work centres around two basic inter-related notions: intermittency and fractality. A review of the experimental data accumulated over the last years will be given in Section 4. Theoretical work is discussed in Section 5.

In particle physics, intermittency is defined, in a strict sense, as the scale invariance of factorial moments (2.68)–(2.70) with respect to changes in the size of phase-space cells (or bins) say δy, for small enough δy:

$$F_q(\delta y) \propto (\delta y)^{-\phi_q} \quad (\delta y \to 0)\,. \tag{2.110}$$

The power $\phi_q > 0$ is a constant at any given (positive integer) q and called "intermittency index" or "intermittency slope". The form of (2.110) strictly implies that the inclusive densities ρ_q and the connected correlation functions C_q become singular in the limit of infinitesimal separation ($\delta y \to 0$) in momentum space.

---

[8] See also [12].

Inspired by the theory of multifractals, scaling behaviour of the G moments (2.73) has also been looked for in the form

$$G_q(\delta y) \propto (\delta y)^{\tau(q)} \quad (\delta y \to 0) . \tag{2.111}$$

To describe the inter-relation of the two proposals, we briefly discuss the formalism of fractals.

Power-law dependence is typical for fractals [42], i.e. for self-similar objects with a non-integer dimension. These range from purely mathematical ones (the Cantor set, the Koch curve, the Serpinsky gasket, etc.) to real objects of nature (coast-lines, clouds, lungs, polymers, etc). For reviews see [43–45].

The fractal dimension D_F is defined as the exponent which provides a finite limit

$$0 < \lim_{\varepsilon \to 0} N(\varepsilon)\varepsilon^{D_F} < \infty \tag{2.112}$$

for the product of ε^{D_F} and the minimal number of hypercubes $N(\varepsilon)$ of linear size $l = \varepsilon$ (Kolmogorov definition) or $l \leq \varepsilon$ (Hausdorff definition) covering the object when $\varepsilon \to 0$.

To a physicist, the definition becomes more transparent if one considers the relation between the size l of an object and its mass M as a scaling law:

$$M \propto l^{D_F} . \tag{2.113}$$

For usual objects D_F coincides with the topological dimension (for a line $D_F = 1$, for a square $D_F = 2$ and so on). The condition $\varepsilon \to 0$ means in practice that such a law should hold in some interval of "rather small" ε-values.

The probability $p_i(l)$ to be in a hypercube $N_i(l)$ is proportional to l^{D_F} at small l. Therefore, for a fractal the mean value of the qth order (ordinary) moment is given by

$$\langle p_i^q(l) \rangle \propto l^{qD_F} \quad (D_F = \text{const.}) . \tag{2.114}$$

Multifractals generalize the notion of fractals, since for these the following holds:

$$\sum_i p_i^q(l) = \langle p_i^{q-1}(l) \rangle \propto l^{\tau(q)} , \tag{2.115}$$

where

$$\tau(q) = (q-1)D_q . \tag{2.116}$$

The D_q are called the Rényi dimensions [46, 27] and depend on q (generally, for multifractals they are decreasing functions of q).

Sometimes it is more convenient to characterize multifractals by spectral properties, rather than by their dimensions.

Let us group all the boxes with a singularity α ($p_i(l) \sim l^{\alpha}$, $l \to 0$) into a subset $S(\alpha)$, where α is called the local mass dimension. The number of boxes $dN_\alpha(l)$ needed to cover $S(\alpha)$ is

$$dN_\alpha(l) = d\rho(\alpha) l^{-f(\alpha)} , \tag{2.117}$$

where $f(\alpha)$ is the fractal dimension of the set $S(\alpha)$ related to the Rényi dimension. For the sum of moments one obtains

$$\sum_{i=1}^{N_i(l)} p_i^q(l) \propto \int \mathrm{d}\rho(\alpha) l^{\alpha q - f(\alpha)} . \tag{2.118}$$

From (2.118), one gets by the saddle-point method

$$D_q = \frac{1}{q-1} \min_\alpha (\alpha q - f(\alpha)) = \frac{1}{q-1} (\bar{\alpha} q - f(\bar{\alpha})) \tag{2.119}$$

with $\bar{\alpha}$ defined as

$$\mathrm{d}f/\mathrm{d}\alpha|_{(\alpha=\bar{\alpha})} = q(\bar{\alpha}) . \tag{2.120}$$

The notion of Rényi dimensions D_q generalizes the notion of fractal dimension $D_0 = D_F$, information dimension D_1 and correlation dimension $D_2 = \nu$. A Rényi dimension, therefore, is often called a generalized dimension.

The difference between the usual topological dimension D (i.e. the support dimension) and the Rényi dimension is called the anomalous dimension (or codimension)

$$d_q = D - D_q . \tag{2.121}$$

The multifractal method is a widely used tool in many branches of physics and science in general (cf. [43, 44, 47]).

A direct relation may be established between the exponents of factorial and generalized moments at comparatively low values of q, much smaller than effective multiplicities contributing to the sum:

$$\phi_q + \tau(q) = (q-1)D. \tag{2.122}$$

Then the exponents are related to Rényi dimension and to codimension as

$$\tau(q) = (q-1)D_q \tag{2.123}$$

$$\phi_q = (q-1)d_q . \tag{2.124}$$

According to the general theory [48, 49], there exists "a class of multifractals exhibiting universal properties". They are called universal multifractals and are classified by a Lévy index $0 \leq \mu \leq 2$ which allows the codimension to be expressed as

$$d_q = (C_1/\mu - 1)(q^\mu - q/q - 1) \quad (C_1 = \text{const}) . \tag{2.125}$$

The Lévy index μ is also known as the degree of multifractality ($\mu = 0$ for monofractals). Values $\mu < 1$ correspond to so-called "calm" singularities, values $\mu > 1$ correspond to "wild" singularities.

One can proceed further and try to analyse experimental data at two different levels of bin splitting. For that purpose, it was recently suggested [50, 51] to study Double Trace Moments (DTM). The procedure is, first, to sum up νth-order moments of multiplicity distributions at some bin-splitting level Θ within bins belonging to a single bin of one of the previous steps (having bins of size Δ) and then to calculate their qth moments at that level

$$Tr_q^\nu \propto \sum_\Delta \left(\sum_\Theta n_m^\nu \right)^q \propto \Delta^{-K(q,\nu)+q-1} . \tag{2.126}$$

It is claimed [50] that "the DTM-technique provides a robust estimate of μ and C_1'' for universal multifractals. According to the theory of universal multifractals [48, 50], one should observe the following factorizable behaviour of "double" exponents $K(q, v)$:

$$K(q, v) = v^{\mu} K(q, 1) , \tag{2.127}$$

where μ is the same Lévy index as in (2.125).

Experimental results on multifractals and generalized multifractals, as well as some theoretical implications are discussed in Sections 5 and 4.7.7.

2.5. Bunching-parameter approach

A simple mathematical tool alternative to the normalized factorial moments (2.68)–(2.70) is the bunching-parameter approach, suggested for high-energy applications in [52]. In order to reveal spiky structure of the events, it is only necessary to study the behaviour of the probability distribution near the multiplicity $n = q$ by means of the "bunching parameters"

$$\eta_q(\delta y) = (q/(q-1))\,[P_q(\delta y) P_{q-2}(\delta y)/P_{q-1}^2(\delta y)], \quad q > 1 . \tag{2.128}$$

As is the case for the normalized factorial moments, the bunching parameters η_q are independent of δy if there are no dynamical fluctuations. For example, $\eta_q = 1$ for all q for the case of a Poissonian probability distribution.

As the $F_q(\delta y)$, the $P_q(\delta y)$ can be averaged over a number M of bins. Assuming approximate proportionality of $\bar{n}_m$ and δy at $\delta y \to 0$ and $P_0(\delta y) \to 1$ for $\delta y \to 0$, one obtains

$$\begin{aligned} &\eta_2(\delta y) \simeq F_2(\delta y) \\ &\eta_q(\delta y) \simeq F_q(\delta y)\, F_{q-2}(\delta y)/[F_{q-1}(\delta y)]^2, \quad q > 2 \end{aligned} \tag{2.129}$$

or

$$\begin{aligned} &\eta_2(\delta y) \propto (\delta y)^{-\beta_2} \\ &\eta_q(\delta y) \propto (\delta y)^{-\beta_q} \end{aligned} \tag{2.130}$$

with

$$\begin{aligned} &\beta_2 = d_2, \\ &\beta_q = d_q(q-1) + d_{q-2}(q-3) - 2d_{q-1}(q-2) , \quad q > 2 . \end{aligned} \tag{2.131}$$

Expressing d_q in terms of the Lévy-law approximation (2.125),

$$\beta_q = d_2\,[q^{\mu} + (q-2)^{\mu} - 2(q-1)^{\mu}]/(2^{\mu} - 2) . \tag{2.132}$$

In case of monofractal behaviour ($\mu = 0$), $\beta_q = 0$ for $q > 2$. In the limit of the log-normal approximation ($\mu = 2$), on the other hand, $\beta_q = d_2$ and all bunching parameters follow the same power law.

The Lévy-law approximation allows a simple description of multifractal properties of random cascade models using only one free parameter μ. In the bunching-parameter approach, one can

make an approximation of the high-order bunching parameters to obtain a simple *linear* expression for the anomalous fractal dimensions d_q, still maintaining the number of free parameters at one.

Assuming that high-order bunching parameters can be expressed in terms of the second-order one as

$$\eta_q(\delta y) = [\eta_2(\delta y)]^r , \quad q > 2 , \tag{2.133}$$

the linear expression becomes

$$d_q = d_2(1 - r) + d_2 r\, q/2 . \tag{2.134}$$

The use of bunching parameters is interesting, because it gives a general answer to the problem of finding a multiplicity distribution leading to intermittency: according to (2.128), any multiplicity distribution can be expressed as

$$P_q(\delta y) = P_0(\delta y) \frac{[P_1(\delta y)/P_0(\delta y)]^q}{q!} \prod_{l=2}^{q} [\eta_l(\delta y)]^{q+1-l}, \quad q > 1 . \tag{2.135}$$

The possible forms of multiplicity distributions with multifractal behaviour of d_q (2.121) are discussed in [53, 54].

2.6. The wavelet transform

An increase of factorial and cumulant moments with decreasing bin sizes reflects a widening of a multiplicity distribution, i.e. an increase of multiplicity fluctuations in individual events. This phenomenon can be studied by other methods, as well. In particular, the so-called wavelet transform seems to be suited for that purpose.

The wavelet transform is of particular importance in pattern recognition. This is a more general problem than the fluctuation study itself, since it involves the analysis of individual event shapes, not only the event ensemble, and may become of interest in the analysis of very high multiplicity events.

It is shown [55] that, for pattern recognition, the wavelet transform is about two orders of magnitude more efficient than ordinary Fourier analysis.

An application of wavelets to multiparticle production processes has been proposed in [56]. The main principle of the wavelet transform is to study the dependence of fluctuations on the phase-space bin size by the so-called difference method. One considers the difference between the histogram of an individual event at a definite resolution to the corresponding histogram at a (e.g. twice) finer resolution. Proceeding step by step, one is able to restore the whole pattern of fluctuations.

Let us explain how this procedure can be applied to an individual event. We consider the one-dimensional projection of the event onto the rapidity interval ΔY. Any n-particle event can be represented by the histograms of particle densities $\rho = \mathrm{d}n/\mathrm{d}y$ at various resolutions. The simplest information is obtained from the value of the average density $\langle\rho\rangle = n/\Delta Y$. To consider the forward–backward correlations, one splits the rapidity interval ΔY into two equal parts and gets the forward and backward average densities $\langle\rho_{\mathrm{f,b}}\rangle = 2n_{\mathrm{f,b}}/\Delta Y$, where $n_{\mathrm{f,b}}$ are the forward

(backward) multiplicities with $n_f + n_b = n$. Proceeding further to the Jth step, we approximate the event in terms of the histogram with 2^J bins.

Let us construct now the difference of the two histograms described above. Namely, we subtract the average density from the forward–backward histogram and get another histogram with positive ordinate at one side and negative at the other, demonstrating the forward–backward fluctuations in the event.

Splitting the forward and backward regions further into equal halves, one gets the histogram at $J = 2$. Its difference from the forward–backward histogram at $J = 1$ reveals the fluctuations at finer resolution. Iterating to higher values of J, one studies how fluctuations evolve at ever finer resolution. The set of difference histograms is called the wavelet transform of the event. The above procedure corresponds to the so-called Haar-wavelet transform. Those interested in mathematical details are referred to [57].

The wavelet transform provides direct information on the evolution of fluctuations at different scales, i.e. on the dynamics of individual high-multiplicity events revealing their clustering (and sub-clustering) structure. A generalization to factorial (and cumulant) wavelets is possible [56]. The simplest cascade models show such remarkable properties of wavelet transforms [56] as (quasi)-diagonalization of their correlation density matrices, scaling exponents, etc. It is interesting to note that the equations for the generating functions of wavelet transforms [56] look very similar to the "gain–loss" equations (in particular, to QCD equations) discussed at the end of Section 5. All those features are yet to be studied.

The very first application to experimental data is presented in [58], where wavelet spectra of JACEE events are studied.

3. Experimental survey on correlations

In this section, we review experimental results on "classical" correlations, a subject with a long history in particle physics. It was instrumental in establishing fundamental concepts of hadrodynamics, such as short-range order, which are an essential ingredient of all popular Monte-Carlo models of hadronization. With the exception of Bose–Einstein interferometry, the field lay dormant for several years, but was revived with the introduction of generalized concepts. The data cover a variety of multiparticle-production processes ranging from e^+e^- annihilation to nucleus–nucleus collisions.

In Section 4, we shall review material on factorial moments and related quantities, obtained since 1986. At that time, a pioneering suggestion was made to investigate the patterns of particle density fluctuations in multihadronic events: the intermittency idea. Measurement of factorial moments opened a way to establish possible scale invariance and fractal behaviour in hadrodynamics.

Interest in correlation functions received a vigorous boost when their intimate connection with factorial moments was realized (see Section 2). Both are now explored in parallel with novel techniques. These offer promising perspectives towards a long overdue unified approach to correlation phenomena, including Bose–Einstein interferometry.

Another obviously related subject, the phenomenology of multiplicity distributions [59], is not explicitly covered here. Multiplicity distributions inspired many early ideas on scale-invariance and phase-transition analogies in multiparticle production, such as Koba–Nielsen–Olesen scaling [60]

and the Feynman–Wilson liquid picture [61]. However, the major part of the data relate either to full phase space or to sizable portions of it. It remains an interesting task for the future to explain the "large-scale" properties of multiplicity distributions in terms of correlation function behaviour at "small distances", the main subject of this paper. Of course, the factorial moments discussed in Section 4 are just another representation of multiplicity distributions and their increase with decreasing bin size reveals the evolution of the multiplicity distribution.

3.1. Rapidity correlations

The study of correlation effects in particle production processes provides information on hadronic production dynamics beyond that obtained from single-particle inclusive spectra. Correlations in rapidity y, as defined in Section 2.1, have been studied in various experiments on e^+e^-, lepton–nucleon, hadron–hadron, hadron–nucleus and nucleus–nucleus collisions. Strong y correlations have been observed in all experiments in one form or another, depending on the specific form of the correlation function, type of interaction, kind of particles, the kinematic region under consideration, etc. The main conclusions were (for early reviews see [62, 63]):

1. Two-particle correlations are strong at small interparticle rapidity-distances $|y_1 - y_2|$ (see Fig. 3.1).
2. They strongly depend on the two-particle charge combination.

Rapidity correlations are now being studied with renewed attention. One reason is that their structure at very small rapidity distances is directly related to self-similar particle-density fluctuations (intermittency), a topic to be covered in Section 4.

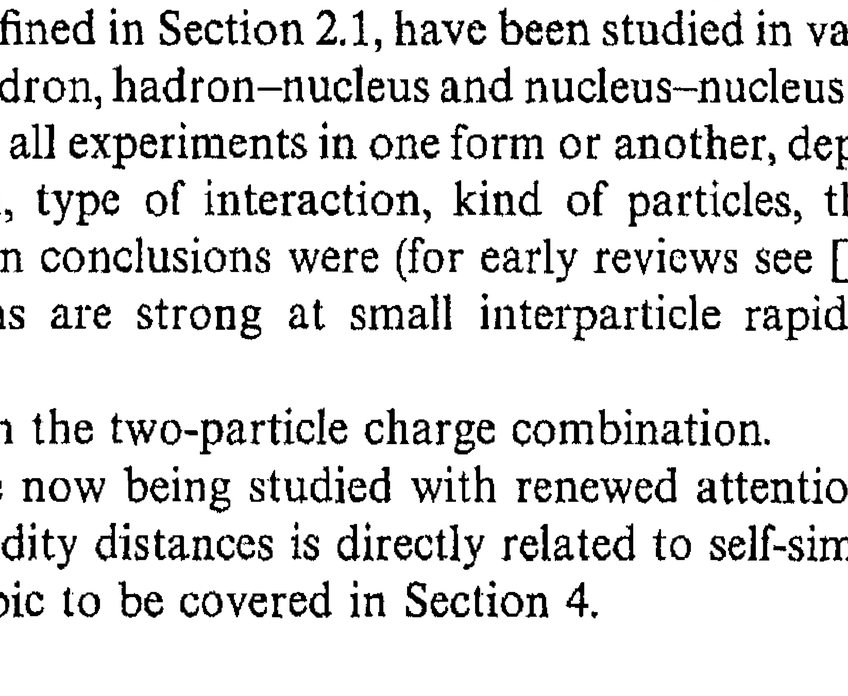

Fig. 3.1. Contours of the two-particle correlation function, $R^{cc}(y_1, y_2)$, from 205 GeV/c pp interactions [64].

3.1.1. Correlations in hadron–hadron collisions

In Fig. 3.2 the pseudo-rapidity correlation function $C_2(\eta_1, \eta_2)$ as defined in (2.25) is given for $\eta_1 = 0$, as a function of $\eta_2 = \eta$, for the energy range between 63 and 900 GeV [65]. Whereas $C_2(0, \eta)$ depends on energy, the short-range correlation C_S defined in (2.36) does not strongly depend on energy and has a full width of about 2 units in pseudo-rapidity. The function C_L is not a two-particle correlation, but derives from the difference in the single-particle distribution function for different multiplicities. As can be seen in Fig. 3.2(b), C_L is considerably wider than C_S and increases with energy (the 63 GeV data are from [66]).

In Fig. 3.3, the semi-inclusive correlation $C_2^{(n)}(\eta_1, \eta_2)$ for $p\bar{p}$ collisions at 900 GeV [67] is compared to the UA5 Cluster Monte Carlo (MC) GENCL [68], as well as to the FRITIOF 2 [69] and PYTHIA [70] Monte Carlos, for charge multiplicity $34 \leqslant n \leqslant 38$. The Cluster MC is designed to fit just these short-range correlations, but also FRITIOF 2 is doing surprisingly well (see however Subsection 4.4.4).

At lower energy, the NA23 Collaboration [71] has studied the short-range correlation of charged particles in pp collisions of $\sqrt{s} = 26$ GeV in terms of $K_2(y_1, y_2)$ defined in (2.32). Only events with charge multiplicity $n > 6$ are used. The positive short-range correlations are in agreement with those found earlier at $\sqrt{s} = 53$ GeV [72].

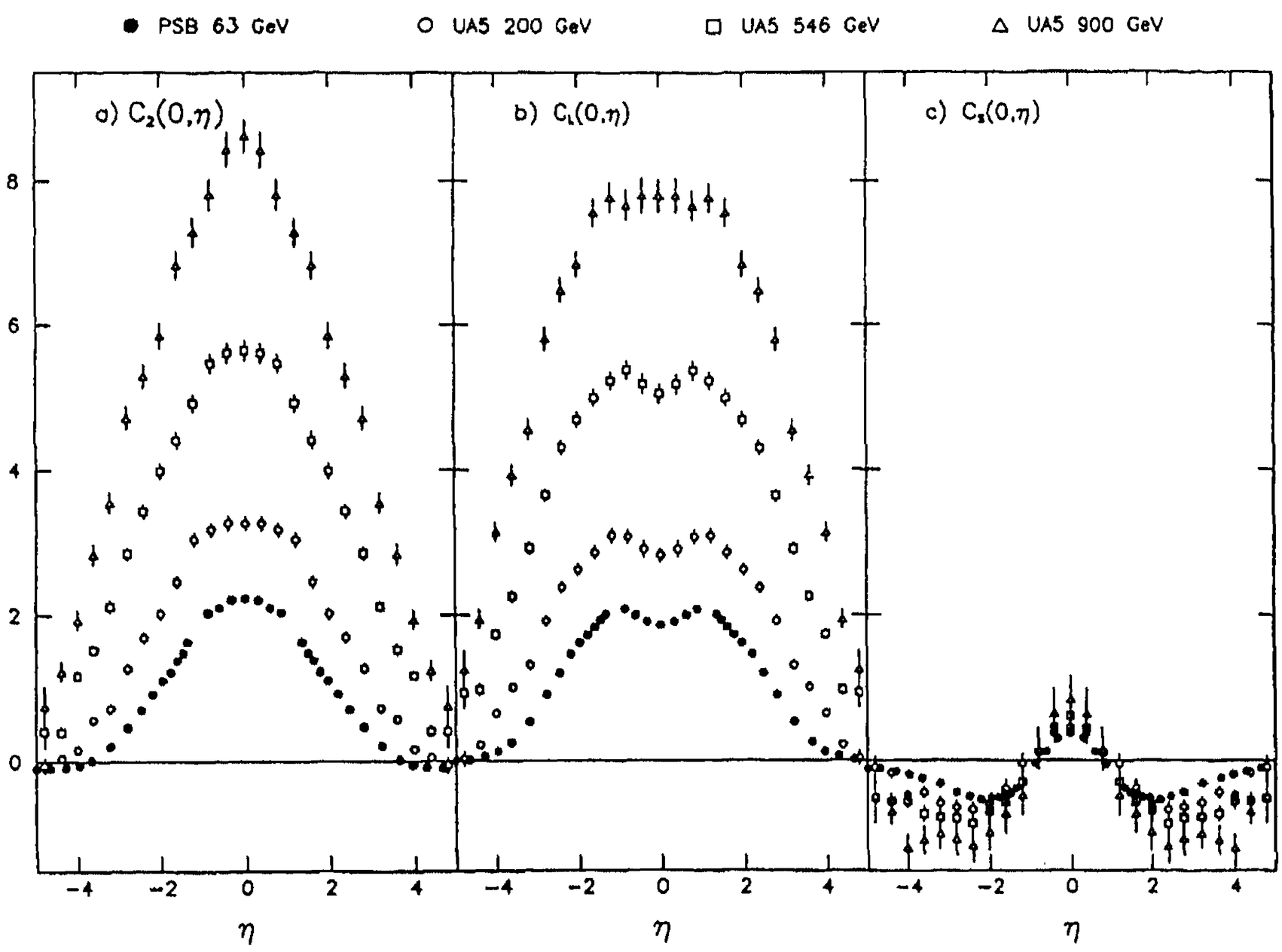

Fig. 3.2. (a) The charge correlation function $C_2(\eta_1, \eta_2)$ plotted for $p\bar{p}$ collisions at fixed $\eta_1 = 0$ versus η_2 at 63, 200, 546 and 900 GeV, (b) the "long-range" contribution C_L and (c) the short-range contribution C_S [65].

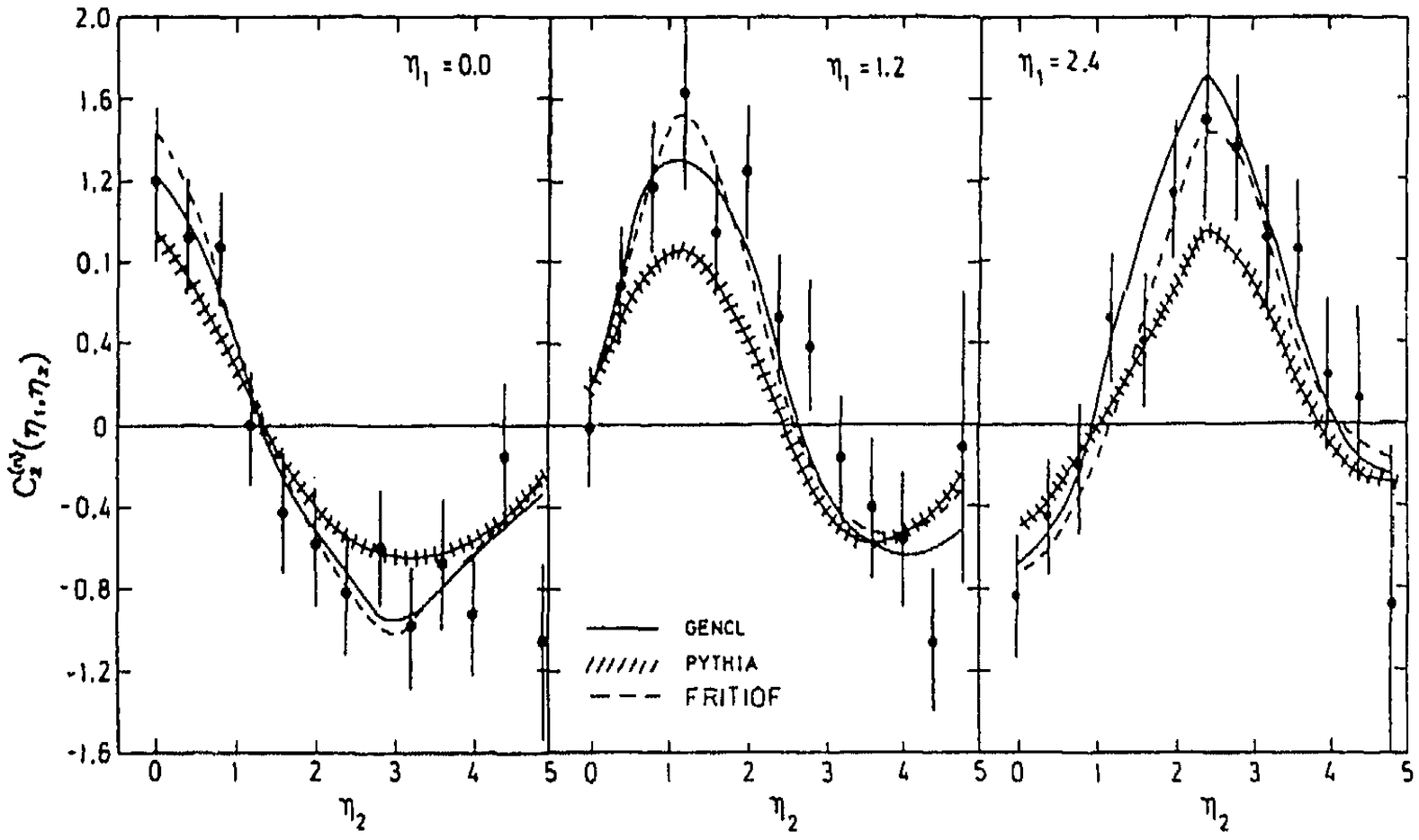

Fig. 3.3. The semi-inclusive correlation function $C_2^{(n)}(\eta_1, \eta_2)$ for $34 \leq n \leq 38$ $p\bar{p}$ collisions at 900 GeV, compared to the UA5 Cluster MC, PYTHIA and FRITIOF 2.0 [67].

The NA23 data are compared to single-string LUND [73] and to a two-chain Dual-Parton Model (DPM) [74] in Fig. 3.4. The one-string model (without gluon radiation) does not at all describe the short-range rapidity correlation in the data. The two-chain model does better, but remains unsatisfactory. Somewhat better but still insufficient agreement is obtained by renormalizing the MC events to the experimental multiplicity distribution (not shown). The effect of Bose–Einstein correlations in the $(++)$ and $(--)$ data is found to be insignificant, as may be expected for data integrated over transverse momentum p_T and azimuthal angle φ. Obviously, more chains, possibly with higher p_T, are needed to explain short-range order with fragmentation models, even below $\sqrt{s} \approx 30$ GeV.

NA22 results for $C_2(0, y_2)$ and $\tilde{C}_2(0, y_2)$ (Eqs. (2.25) and (2.30)) for $\pi^+ p$ and $K^+ p$ collisions at $\sqrt{s} = 22$ GeV [75] are compared with FRITIOF 2, a two-string DPM and QGSM [76] predictions in Fig. 3.5(a) and (b). FRITIOF and two-string DPM largely underestimate the correlation. QGSM reproduces $C_2^{--}(0, y_2)$ very well and even overestimates $C_2^{++}(0, y_2)$ and $C_2^{+-}(0, y_2)$. It has been verified that the differences between QGSM and FRITIOF or DPM are not due to the different treatment of tensor mesons (only included in the latter two).

In Fig. 3.5(c), FRITIOF and QGSM are compared to the NA22 data in terms of the short-range contribution $\tilde{C}_S(0, y_2)$. The $(+-)$ short-range correlation is reproduced reasonably well by these models. For equal charges, however, the strong anti-correlation predicted by FRITIOF is not seen in the data. QGSM contains a small equal-charge correlation due to a cluster component, but still underestimates its size. Similar discrepancies are also observed in semi-inclusive (fixed multiplicity) data for each charge combination (not shown here). They are even larger than in the inclusive data, also in the QGSM model.

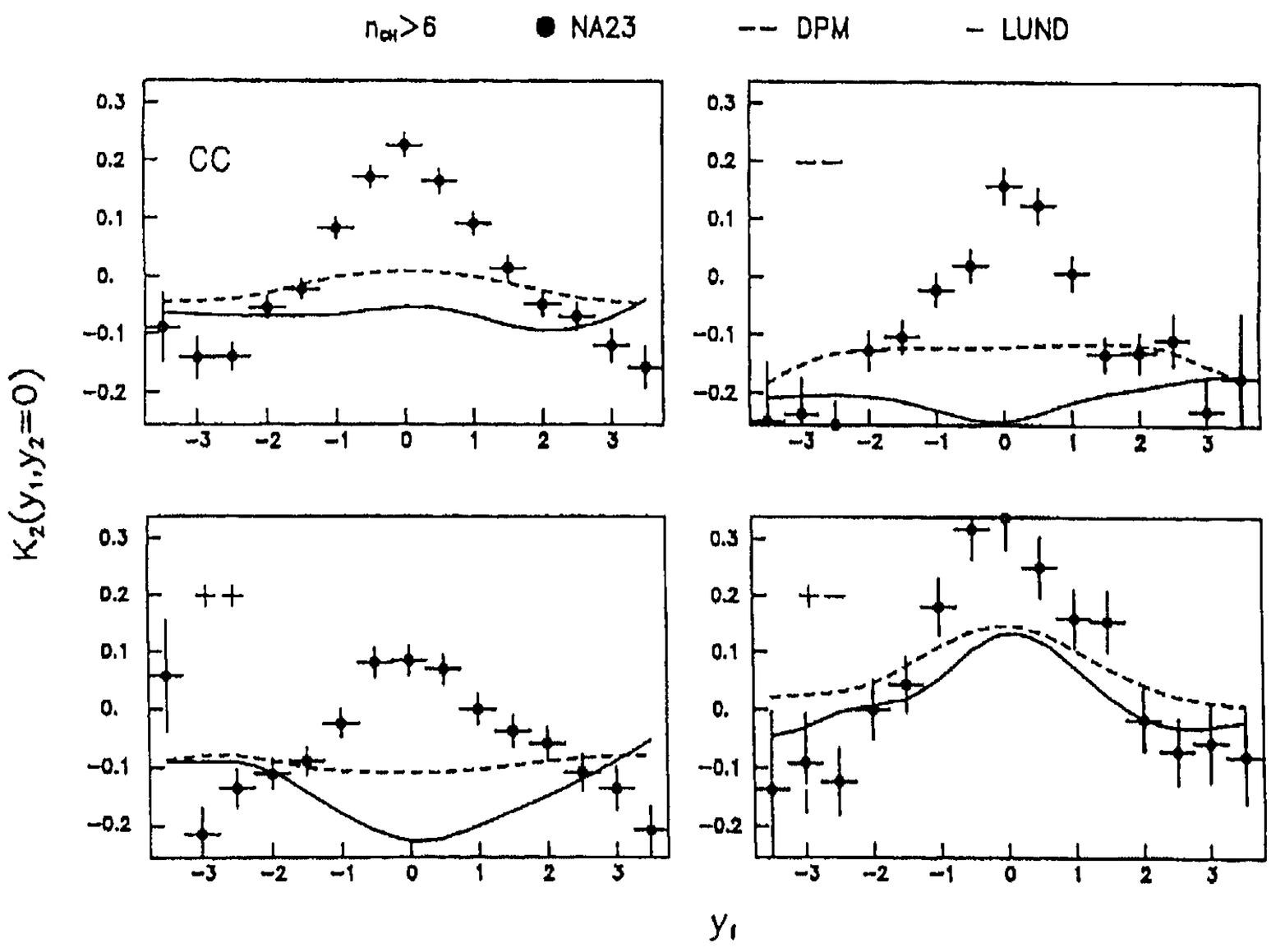

Fig. 3.4. Normalized correlation function $K_2(y_1, y_2 = 0)$ for (CC), $(- -)$, $(+ +)$ and $(+ -)$ combinations in $n > 6$ pp collisions at 360 GeV/c, compared to predictions from single chain LUND and a two-chain DPM [71].

From this brief survey, we conclude that in hadron–hadron collisions two-particle correlations are badly reproduced and generally underestimated in currently used models.

3.1.2. Correlations in e^+e^- *and* μ^+p*-collisions*

Fig. 3.6 shows $K_2^{+-}(y_1, y_2)$ and $K_2^{--}(y_1, y_2)$ for muon–nucleon interactions at 280 GeV/c [77]. A steep peak is seen at $y_1 = y_2 = 0$ for K_2^{+-}, with two shoulders along the diagonal $y_1 = y_2$. On the other hand, K_2^{--} is below 0 for most of the distribution, but we shall see that the most impressive correlation is in fact coming from $y_1 \approx y_2$, just for this case. As in hadron–hadron collisions, correlations are strong and depend on the two-particle charge combination.

Fig. 3.7 shows $K_2(y_1, y_2)$ in μ^+p interactions at 280 GeV/c with $y_1 \in [-0.5, 0.5]$, the hadronic invariant mass W in the interval $13 < W < 20$ GeV and for $n \geq 3$ [78], together with the NA22 non-single-diffractive M^+p sample, $n \geq 2$ [75]. Correlations in μ^+p seem smaller than in NA22, but one has to consider a possible energy dependence. Indeed, extrapolating from the energy dependence of $K_2(0, 0)$ published in [78], one finds quite similar values for μ^+p at 22 GeV and M^+p in NA22.

In Figs. 3.8(a) and (b) we compare the function $\tilde{K}_2(0, y)$ for the NA22 non-single-diffractive M^+p sample (charge multiplicity $n \geq 2$) [75] with that for e^+e^- annihilation at the same energy ($\sqrt{s} = 22$ GeV) [79]. The values of $\tilde{K}_2(0, y)$ are larger for $(+ +)$ pairs than for $(- -)$ in meson–proton (M^+p) reactions; for $(- -)$ and $(+ -)$ pairs they agree with $\tilde{K}_2$ for e^+e^- annihilation in the central region.

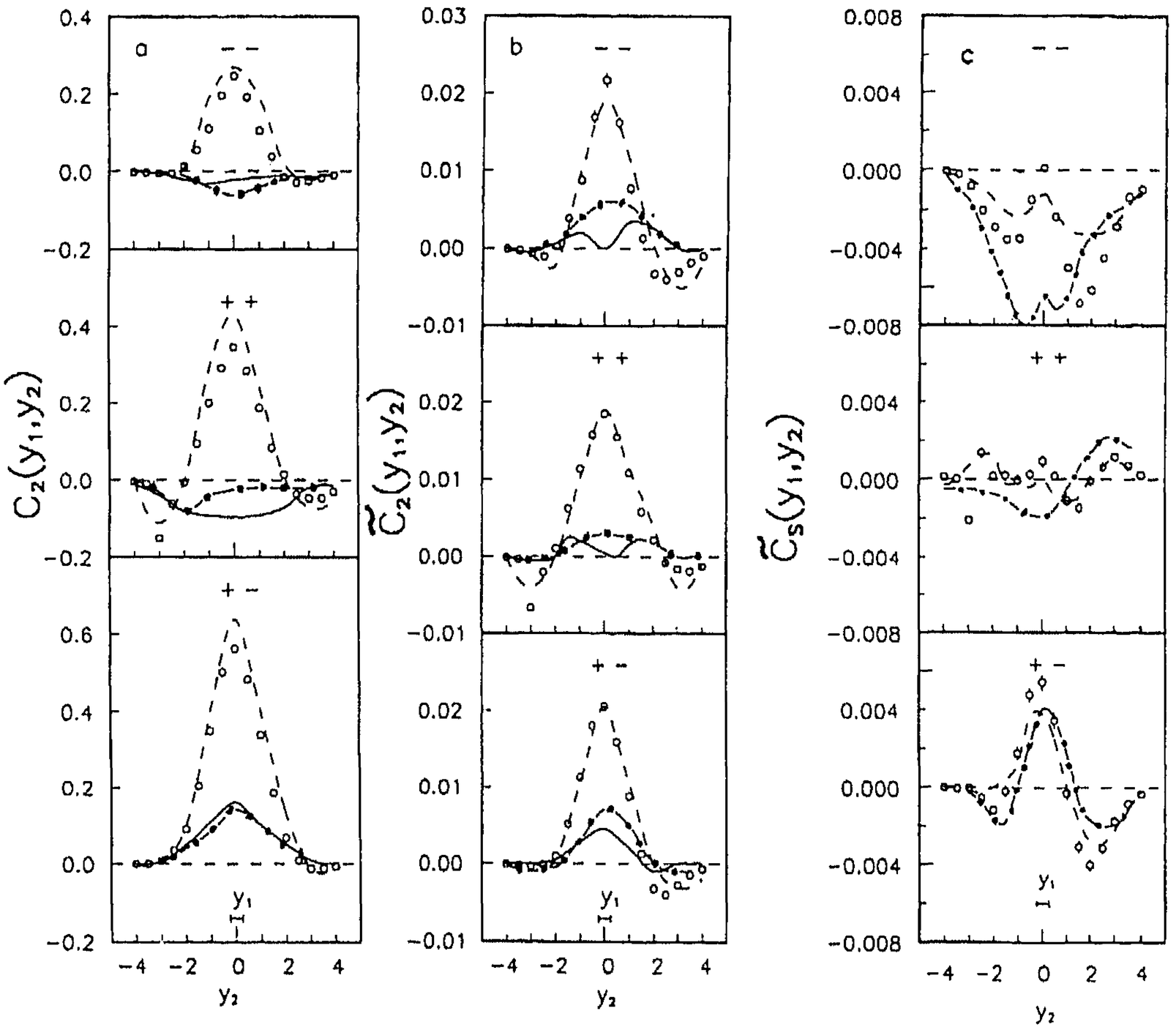

Fig. 3.5. (a, b) Correlation functions $C_2(0, y)$ and $\tilde{C}_2(0, y)$ for M^+p reactions as compared with calculations in FRITIOF (–·–·–), DPM (——) and QGSM (– – –) (non-single-diffractive sample). (c) Correlation functions $\tilde{C}_S(0, y_2)$ for M^+p reactions as compared with FRITIOF (–·–·–) and QGSM (– – –) [75].

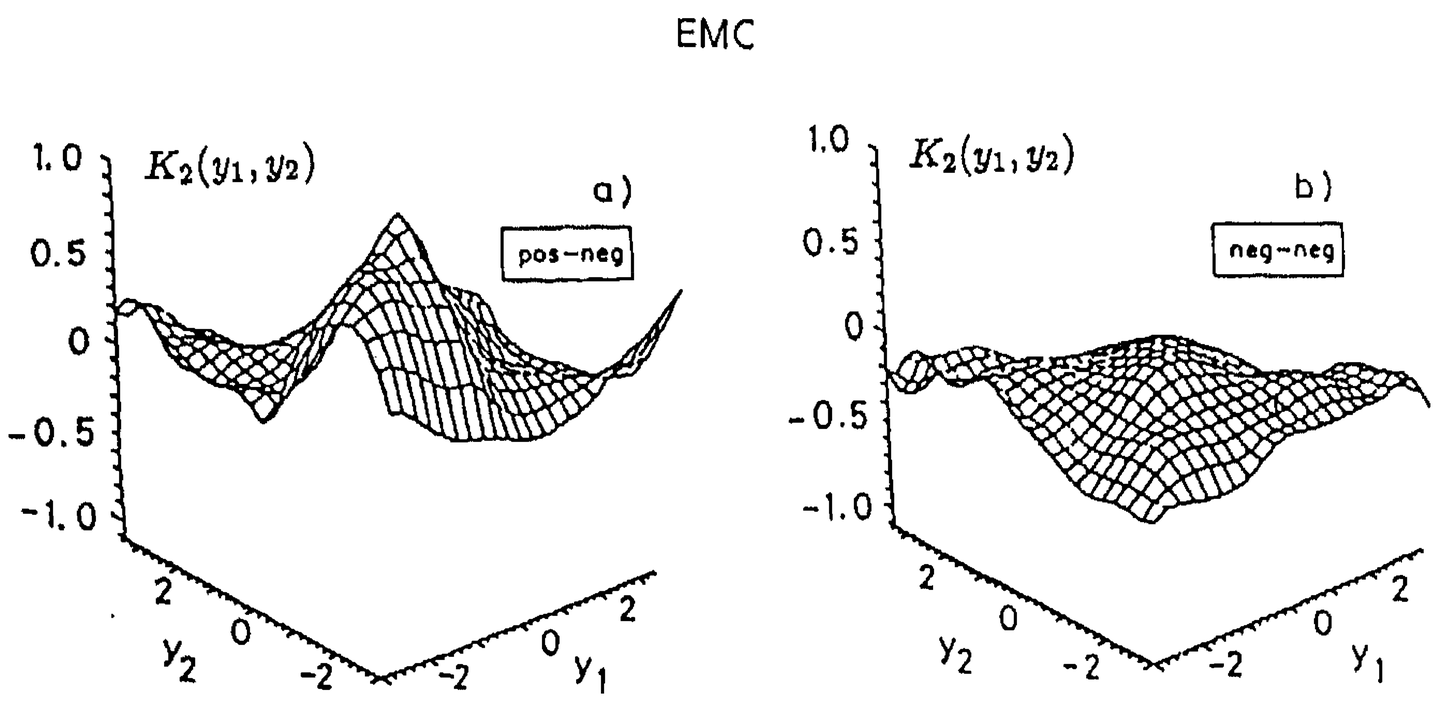

Fig. 3.6. Normalized two-particle correlation function $K_2(y_1, y_2)$ for pairs of (a) oppositely and (b) negatively charged hadrons produced in muon–nucleon scattering at 280 GeV/c [77].

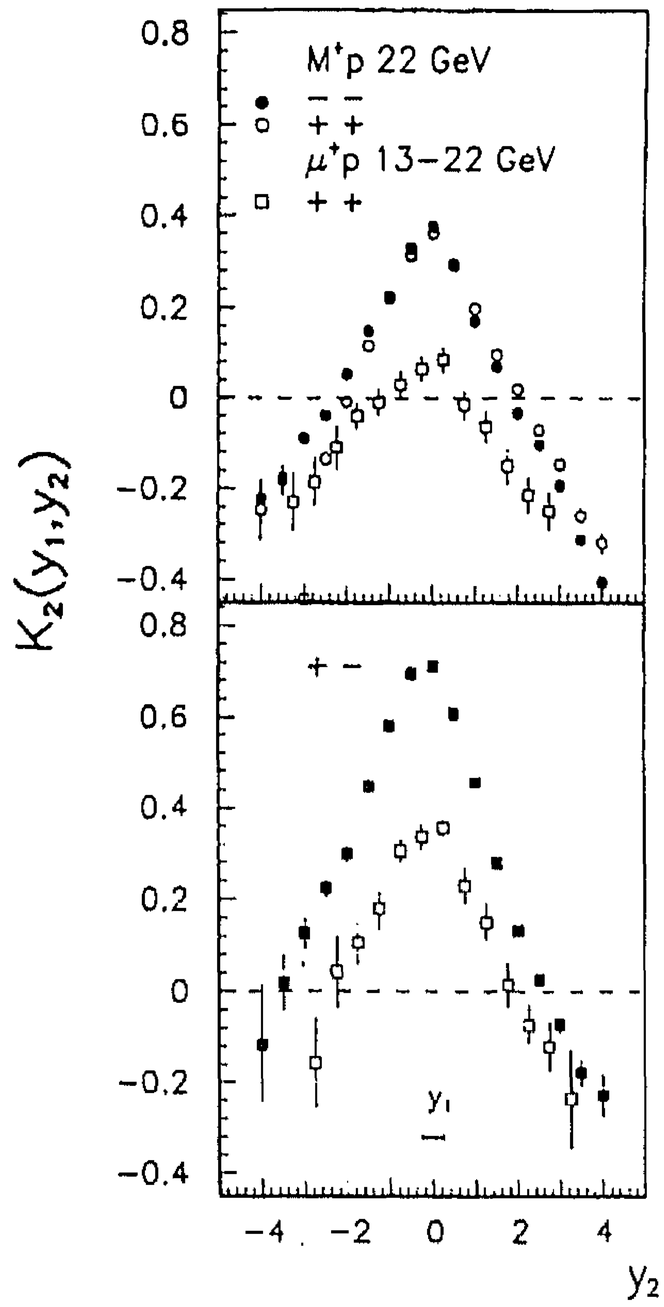

Fig. 3.7. Normalized correlation functions $K_2(0, y)$ for the M^+p non-single-diffraction sample and μ^+p-interactions at 280 GeV/c ($13 < W < 20$ GeV) [78].

A comparison of the correlation functions for e^+e^- annihilation and non-single-diffractive M^+p collisions throughout the full kinematic region with $y_1 \in [-1, 0]$ is shown in Fig. 3.8(c) for charged pairs. The e^+e^- data are given at $\sqrt{s} = 14$ and 44 GeV [79]. At $y_2 = y_1$, the 22 GeV M^+p correlation lies between the e^+e^- results. The shape is, surprisingly, more symmetric than in e^+e^-.

For μ^+p [77, 78] and e^+e^- collisions [79–81], the LUND-type Monte Carlo is reported to reproduce the majority of the experimental distributions. In [71] it is shown that this is mainly due to the inclusion of hard and soft gluon effects. However, important underestimates of $K_2(y_1, y_2)$ are still observable, in particular in the central and current fragmentation regions. For e^+e^- [80], this is shown in Fig. 3.9, where $K_2(y_1, y_2)$ is compared to the LUND model (JETSET 7.2 PS) as a function of $y_1 - y_2$ (dotted line), for the full sample (upper plots) and for a two-jet sample (lower plots). In all cases, the LUND model underestimates the correlation at $y_1 - y_2 = 0$. In general, the disagreement becomes smaller when Bose–Einstein correlations are included (full lines). The main feature to note is that correlations are much weaker in the two-jet sample than in the full sample. Furthermore, correlations are larger for $y \leq 0$ (left plot), i.e. in the hemisphere opposite the most energetic jet, than for $y > 0$ (right plot). These two observations, again, point to hard gluon radiation as the main source of two-particle correlation in e^+e^- collisions.

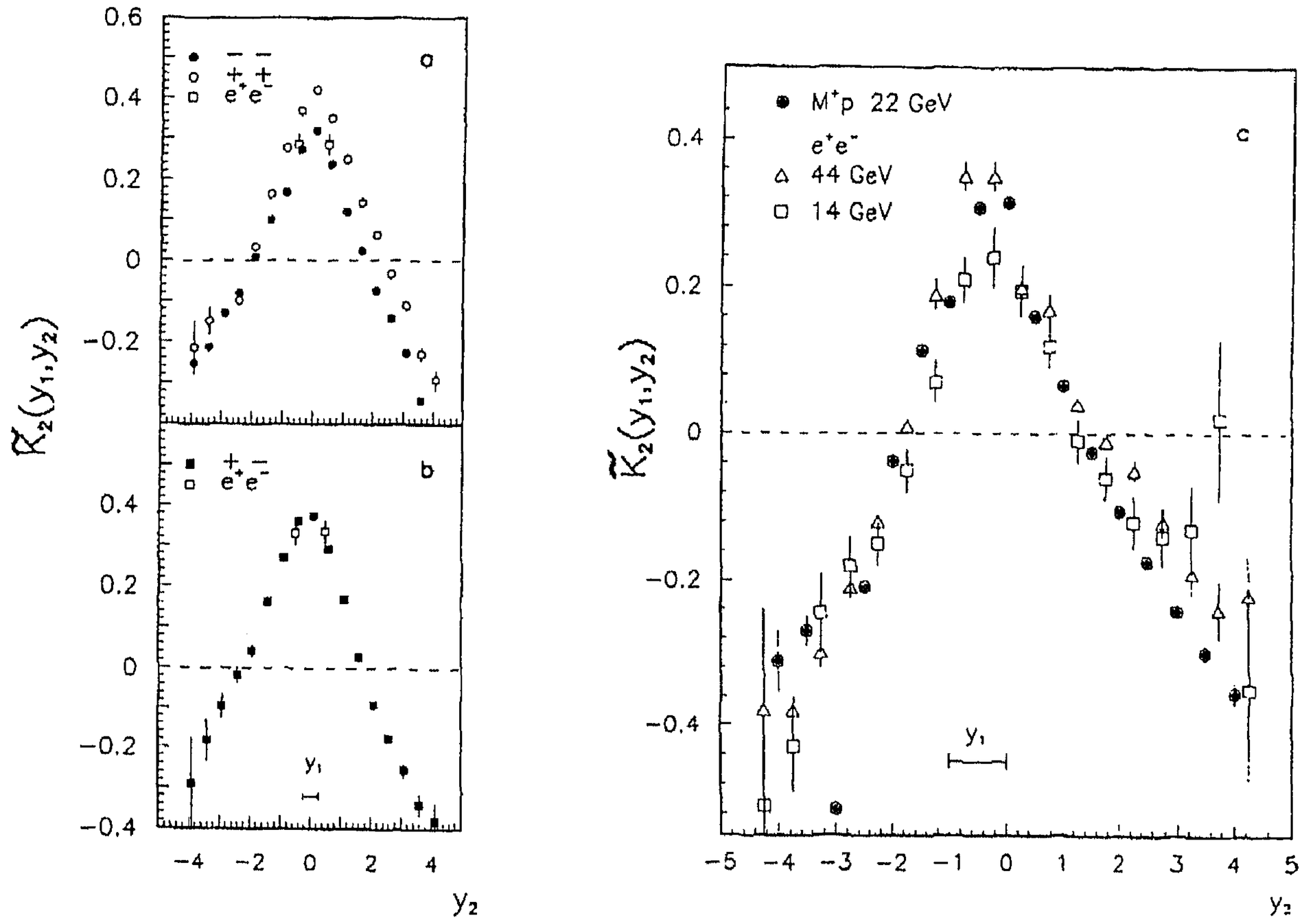

Fig. 3.8. (a, b) Normalized correlation functions $\tilde{K}_2(0, y)$ for the M^+p non-single-diffraction sample and e^+e^--annihilation at $\sqrt{s} = 22$ GeV. (c) Normalized correlation function $\tilde{K}_2^{cc}(y_1, y_2)$ at $y_1 = -1$–0 in the non-single-diffraction M^+p sample at 22 GeV and e^+e^- annihilation at 14 and 44 GeV [75].

A systematic test of analytic QCD calculations and of QCD Monte-Carlo models for two-particle correlations has been performed by OPAL [81]. The authors study the function

$$R(\xi_1, \xi_2) = K_2(\xi_1, \xi_2) + 1 \tag{3.1}$$

with $\xi = \ln(1/x_F)$, $x_F = 2p/E_{cm}$ being the Feynman variable, i.e. the particle momentum p in the cms normalized to half the cms energy E_{cm}. In Fig. 3.10, R is plotted as a function of $(\xi_1 - \xi_2)$ for $(\xi_1 + \xi_2)$ centred at the values 6, 7 and 8, respectively. Fig. 3.10(a) proves that a next-to-leading order calculation [82] (full lines) is better than leading order (dashed), but still overestimates the overall level of the correlation for any reasonable value of Λ. Since the next-to-leading correction is large, still higher-order terms are needed. It is therefore likely that a satisfactory analytical treatment of correlations, even at the parton level, will not be obtained in the very near future.

Higher-order effects are, in an average sense, included in the existing Monte-Carlo models. In Fig. 3.10(b), the same data are compared to the coherent parton shower models JETSET PS [73], HERWIG [83] and ARIADNE [84]. The latter gives an excellent fit to the data, JETSET lies slightly below (within uncertainty of parameters), but HERWIG considerably above. The

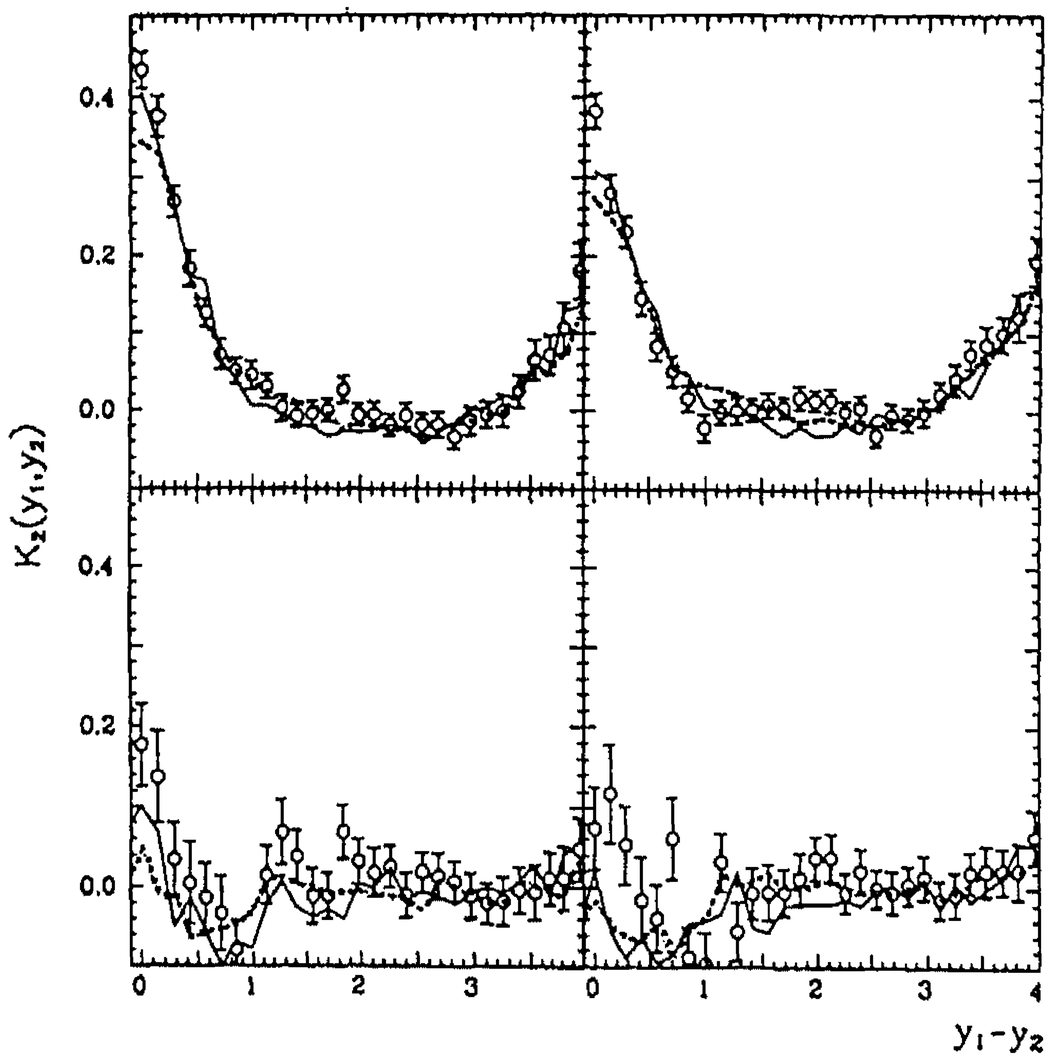

Fig. 3.9. Normalized correlation functions $K_2(y_1, y_2)$ for the entire data sample (upper plots) and for selected two-jet events (lower plots) in e^+e^- annihilation at 35 GeV. The left plots show the average over the region $-1 \leq y_1 + y_2 \leq 0$ and the right plots correspond to the average over $0 \leq y_1 + y_2 \leq 1$. The data (open circles) are compared to the JETSET 7.2 PS model with (solid lines) and without (dotted lines) Bose–Einstein correlations [80].

agreement of JETSET could only slightly be improved by including Bose–Einstein correlations. As far as incoherent parton shower models are concerned, none of the various versions of COJETS [85] gives a particularly good representation of the correlation data.

All the models were tuned on the OPAL data in terms of event shapes and generally describe single-particle distributions. It is clear that correlations allow better and more discriminative tests than more integrated quantities.

We have mentioned the difficulties string-hadronization models experience in predicting like-sign correlations in hadron–hadron collisions. It is important to verify if the otherwise successful e^+e^- models are also able to reproduce correlations between charge-separated systems such as $(+-)$ and $(\pm\pm)$ particle pairs.

3.1.3. Charge dependence

How C_S and $\tilde{C}_S$ depend on the charge of the pairs is shown in Fig. 3.11 for the combinations $(--)$, $(++)$ and $(+-)$ in NA22 [75]. The short-range correlation is significantly larger for $(+-)$ than for $(--)$ and $(++)$ combinations. This is also seen in the EMC data [77]. Resonance production is a likely explanation of this difference. For like charges, a small enhancement is seen near $y_1 \approx y_2 \approx 0$ above a large negative background. This is possibly due to Bose–Einstein interference.

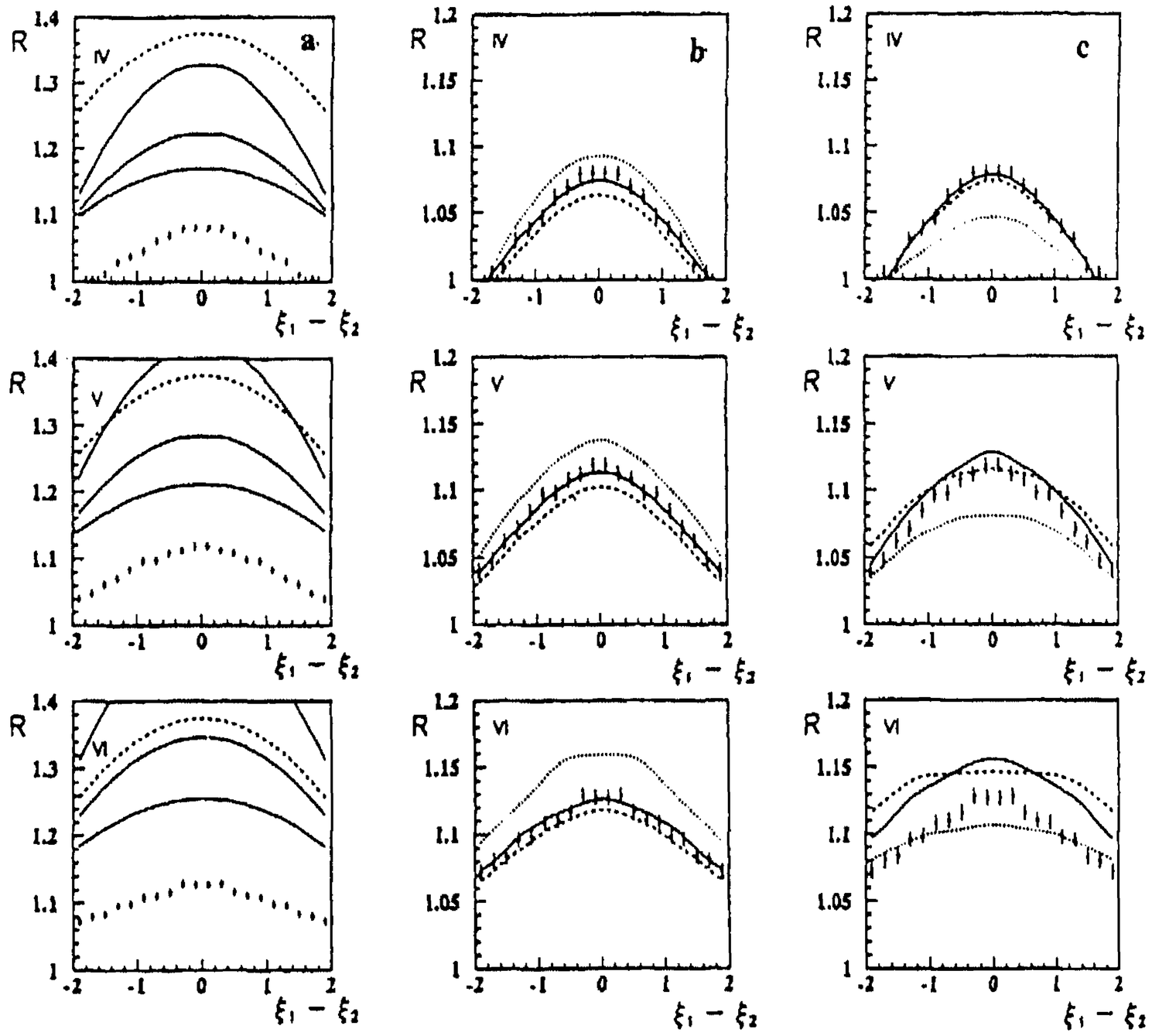

Fig. 3.10. OPAL data on $R(\xi_1, \xi_2)$ as a function of $(\xi_1 - \xi_2)$, for $(\xi_1 + \xi_2)$ between 5.9 and 6.1 (IV), 6.9 and 7.1 (V), 7.9 and 8.1 (VI), respectively, compared to (a) analytic QCD calculations (the dashed curves indicate leading order QCD calculations for $\Lambda = 225$ MeV, the three solid curves represent next-to-leading QCD calculations with, from top to bottom, $\Lambda = 1000$, 255 and 50 MeV, respectively), and (b) coherent parton-shower Monte-Carlo models ARIADNE (solid), JETSET (dashed) and HERWIG (dotted); (c) incoherent parton-shower Monte-Carlo models JETSET (solid) and two versions of COJETS (dashed and dotted) [81].

3.1.4. Charge-multiplicity dependence

The multiplicity dependence of $\tilde{C}_2^{(n)}(0, y)$ for the $(+-)$ combination is shown in Fig. 3.12 [75]. Near the maximum at $y = 0$ the correlation function is approximately Gaussian and narrows with increasing n. In Fig. 3.13(a) are presented the values of $\tilde{C}_2^{(n)}(0, 0)$ as a function of n for three charge combinations. Within errors, $\tilde{C}_2^{(n)}(0, 0)$ is independent of n, but consistently higher for $(+-)$ and $(--)$ than for $(++)$. The reason for the difference between $(--)$ and $(++)$ probably lies in the positive charge of both beam and target.

On the other hand, an increase of $\tilde{C}_2^{(n)}(|\eta_1 - \eta_2|)$ with $1/(n-1)$ is found [86] when averaging over a region $|\eta| < 2$ (Fig. 3.13(b)). Since $\tilde{C}_2$ becomes smaller when moving away from the centre, and that may happen faster for higher than for lower n, this is not necessarily in contradiction with the data in Fig. 3.13(a).

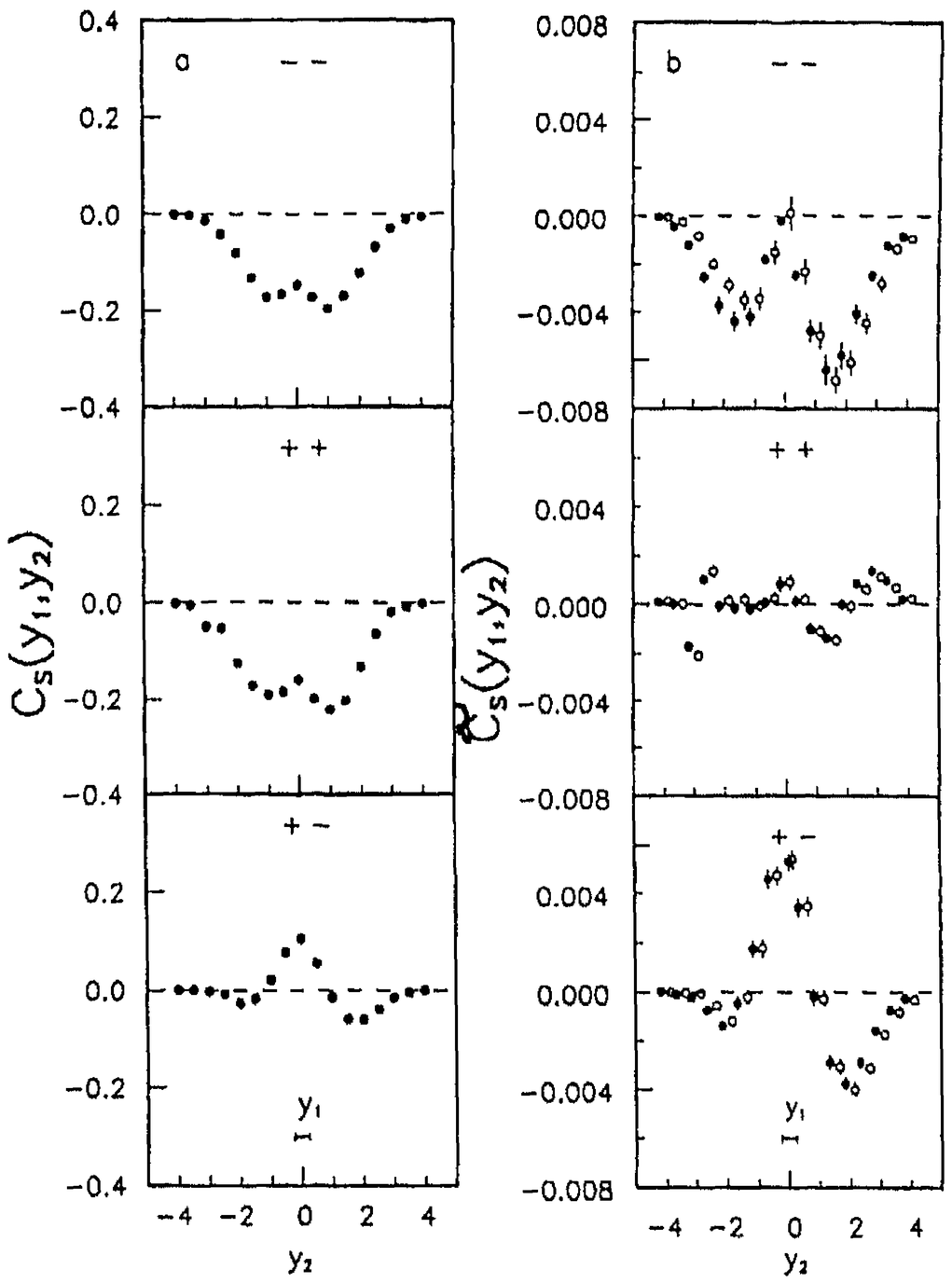

Fig. 3.11. Correlation functions $C_s(0, y)$ (a) $\tilde{C}_s(0, y)$ (b) in M^+p interactions at 250 GeV/c (open circles correspond to non-single-diffractive events and are shifted to the right to avoid overlap) [75].

3.1.5. Transverse momentum dependence

The search for density fluctuations, described in later sections, has revealed the importance of correlations in multidimensional phase space. It is, therefore, of interest to gain insight into the transverse momentum (p_T) dependence of rapidity correlations. Early results on this topic can be found in [87]. Recent data on $K_2(0, y_2)$ [88] for all particles and for particles with p_T smaller or larger than 0.3 GeV/c, plotted in Fig. 3.14, indeed reveal a strong sensitivity to transverse momentum. The correlation function is largest, and stronger peaked, near $y_2 = 0$ for $p_T < 0.3$ GeV/c, in particular for (− −)-pairs. A similar effect was noted already in [87]. The data of Fig. 3.14 were fitted with the functions

$$f_1 = c \exp[-(y - y_0)^2/2\sigma^2] \quad \text{(full line)}, \tag{3.2}$$

$$f_2 = a \exp(-b|y|) \quad \text{(dashed)}, \tag{3.3}$$

with c, y_0, σ, a and b as free parameters. Even though for low p_T the data point at $y_2 = 0$ lies systematically above the curve, $K_2(0, y_2)$ is well fitted by the Gaussian f_1 but not by the exponential f_2, in this one-dimensional projection on rapidity.

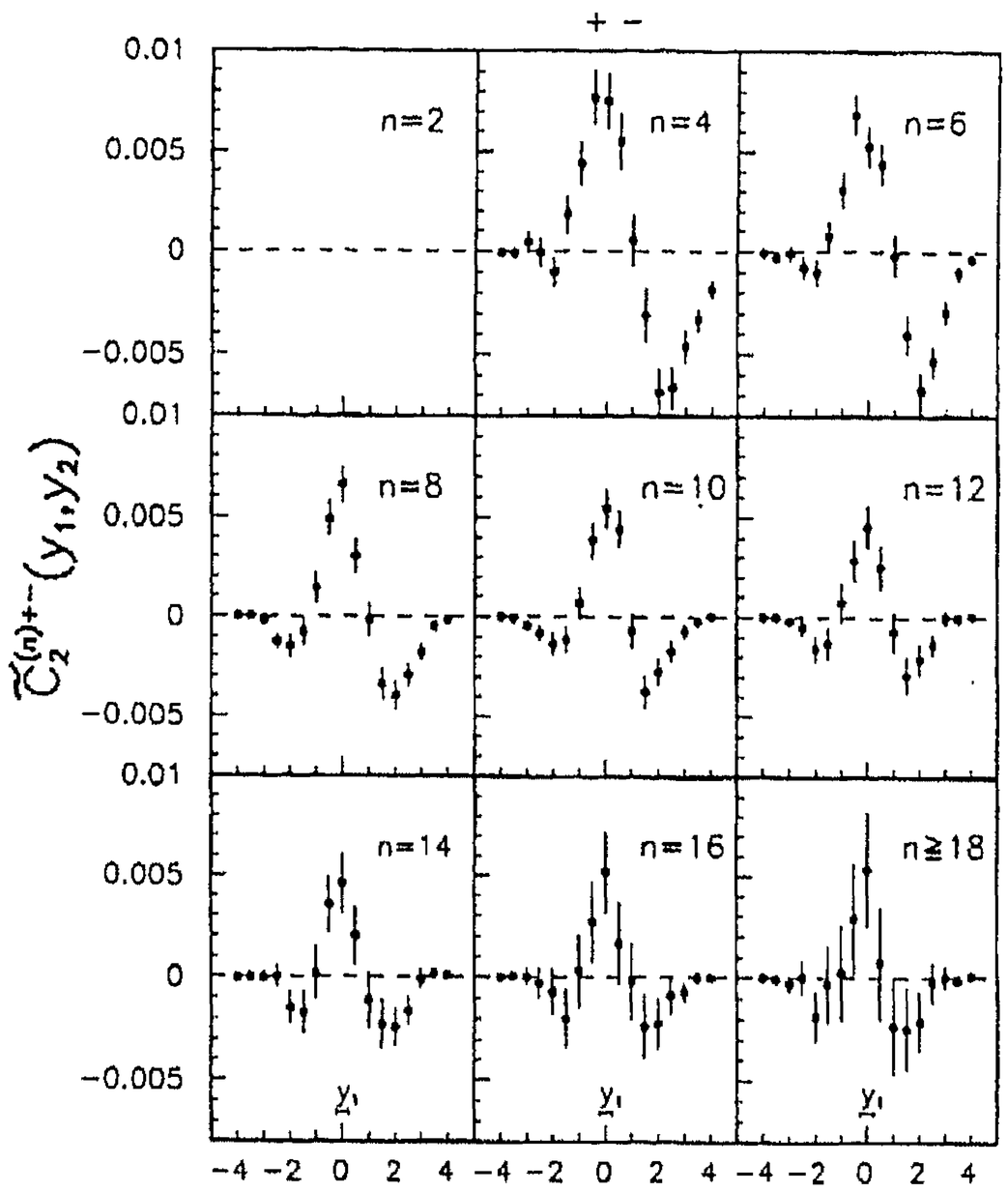

Fig. 3.12. Topological correlation functions $\tilde{C}_2^{(n)}(0, y)$ in M^+p reactions at 250 GeV/c for $(+\ -)$ pairs [75].

Changing to the variables $x_1 = (y_2 + y_1)/2$ and $x_2 = (y_2 - y_1)/2$, a steepening is observed at small x_2 (not shown). For like-charge pairs, this becomes particularly sharp when the bin size is reduced to $\delta x_2 = 0.1$. For the latter, $C_2(x_1, x_2 = 0)$ increases and both a Gaussian and an exponential can fit the correlation function.

3.1.6. Strange particles

In string-fragmentation models, first-rank hadrons are formed from neighbouring quark–anti-quark pairs tunnelling out of the vacuum. The hadronic final states, therefore, show short-range order due to local flavour conservation. Using stable mesons only, this characteristic property is difficult to study experimentally because of the large $q\bar{q}$ combinatorial background. What is needed is a flag identifying the $q\bar{q}$ pairs created together. A suitable choice is strangeness since the number of $s\bar{s}$ pairs per event is small and the combinatorial background strongly reduced.

Good strangeness identification is available for e^+e^- annihilation in the TPC detector at $\sqrt{s} = 29$ GeV [89]. This collaboration observes significant short-range K^+K^- correlations in y, well reproduced by the LUND model and by the Webber QCD model.

In hadron–hadron collisions, strange particle pairs have been studied by the NA23 Collaboration [90]. The distribution in the rapidity difference Δy for two K^0's is given in Fig. 3.15(a), for a K^0

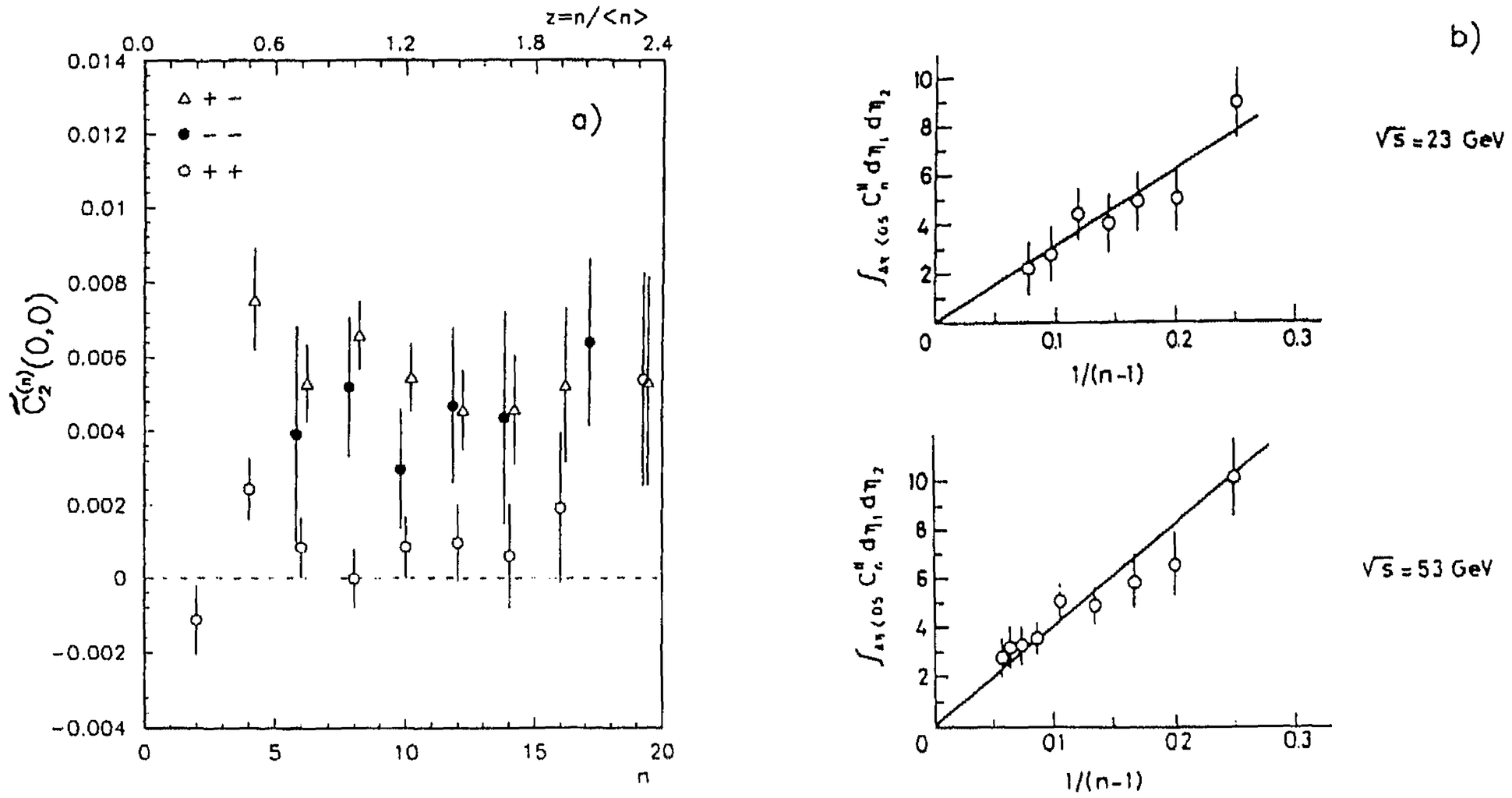

Fig. 3.13. $\tilde{C}_2^{(n)}(0,0)$ dependence on n and $z = n/\langle n\rangle$ for M^+p interactions at 250 GeV/c. The last $(- -)$ point corresponds to $n \geq 16$, the last $(+ -)$ and $(+ +)$ points to $n \geq 18$ [75]. (b) $\tilde{C}_2^{(n)}(|\eta_1 - \eta_2|)$ as a function of $1/(n-1)$ for pp collisions at ISR energies [86].

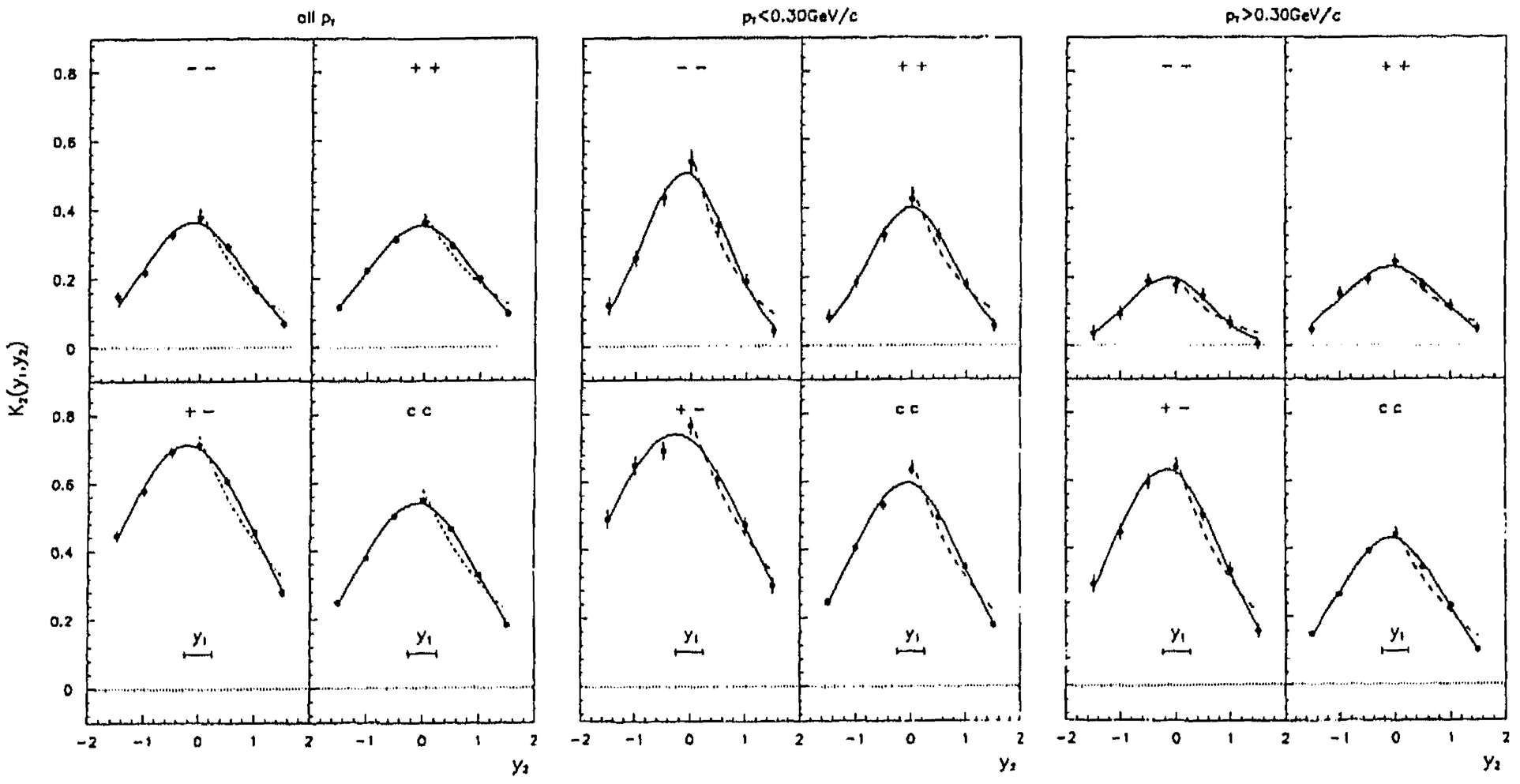

Fig. 3.14. Normalized correlation functions $K_2(0, y)$ for particles with all p_T, $p_T < 0.30$ GeV/c, $p_T > 0.30$ GeV/c as compared to functions (3.2) and (3.3), solid and dot-dashed lines, respectively [75].

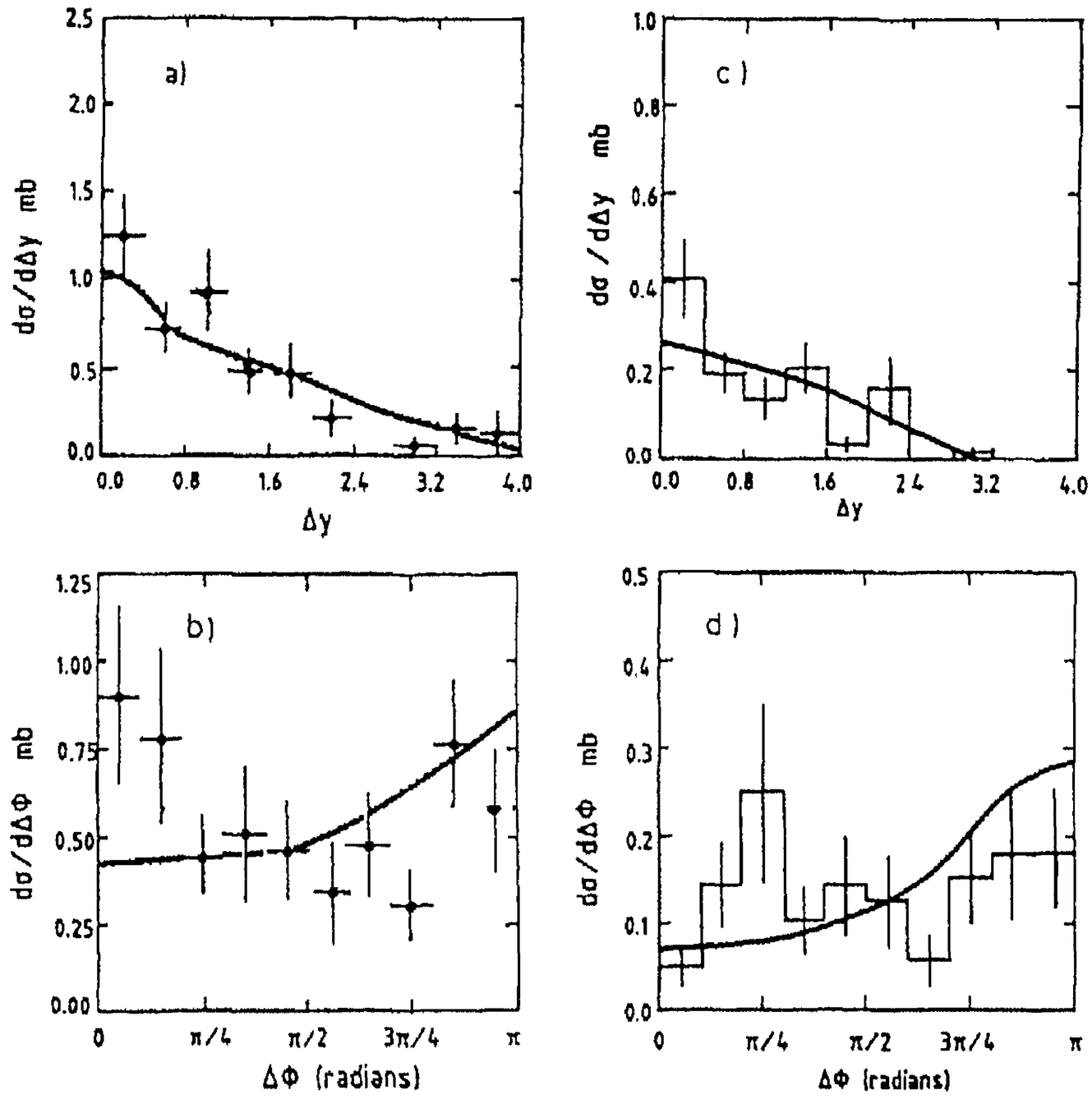

Fig. 3.15. Distribution in (a) the rapidity gap Δy and (b) the azimuthal distance $\Delta\varphi$ for $K^0_S K^0_S$ pairs in pp collisions at 360 GeV/c. (c) and (d) same for $K^0_S\Lambda$ pairs [90]. The lines correspond to LUND.

and a Λ^0 in Fig. 3.15(c). The results are compared to the single-string LUND model. As is the case for non-strange particles, the model slightly underestimates the rapidity correlation.

3.2. Azimuthal correlations

In interactions of unpolarized particles, no distinguished direction exists in the plane transverse to the beam and the distribution in the azimuthal angle φ is uniform. Still, a two-particle correlation exists also in φ and is visible in the distribution $W(\Delta\varphi)$ of $\Delta\varphi = |\varphi_1 - \varphi_2|$, the azimuthal angle between two particles, $\Delta\varphi \in (0, \pi)$. The azimuthal correlation may depend on the charge of the particles in the pair, on the rapidity distance $\Delta y = |y_1 - y_2|$ between these particles and on their transverse momentum.

The first experiments to extensively study two-particle correlations as a function of both rapidity and azimuthal angular separation [86, 91] already showed that the correlation at small rapidity distance is strongest when the two particles are produced in the same or opposite directions in transverse momentum (see Fig. 3.16). The correlation-length in rapidity is larger towards $\Delta\varphi = \pi$

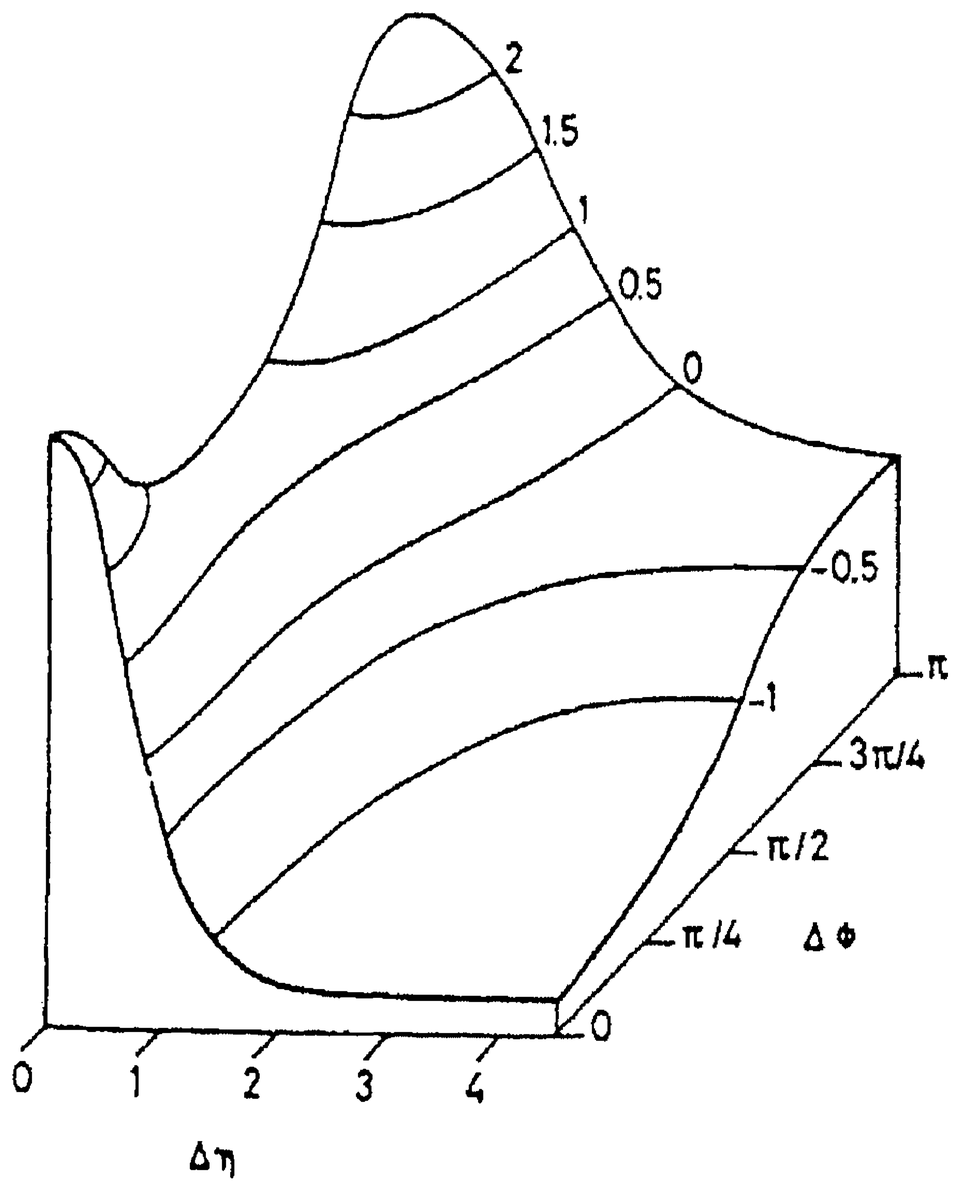

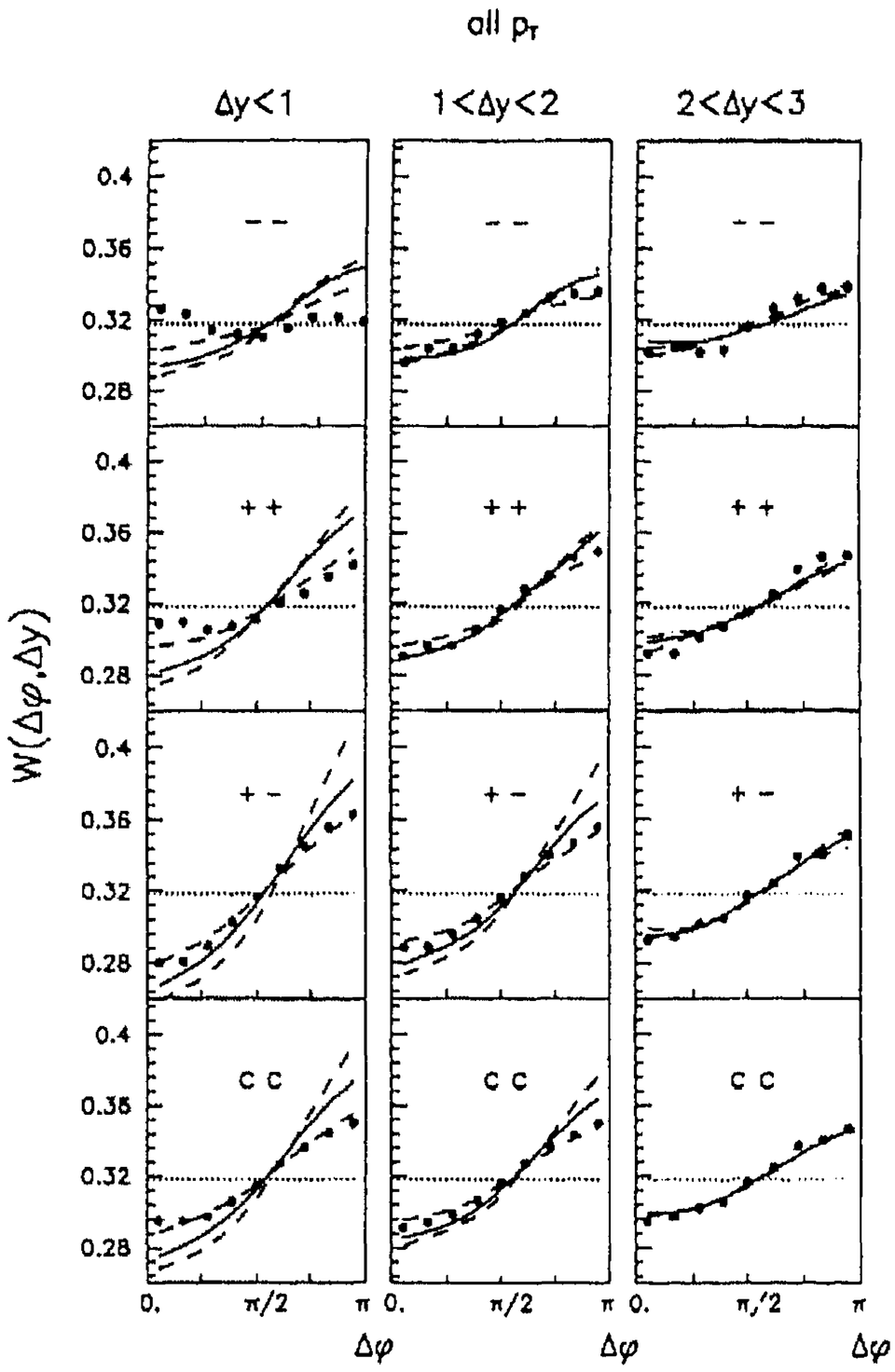

Fig. 3.16. The multiplicity-averaged angular correlation function $\langle (n-1)\tilde{C}_2^{(n)}(\eta_1,\varphi_1;\eta_2,\varphi_2)\rangle$ for CC combinations in units of 10^{-3} [86].

Fig. 3.17. $W(\Delta\varphi,\Delta y)$ for inclusive non-single-diffractive π^+p interactions at 250 GeV/c as compared to FRITIOF2.0 (dot-dashed), DPM (full) and QGSM (dashed) [88].

than towards $\Delta\varphi = 0$. Furthermore, significant differences in the shape of the joint rapidity and azimuthal correlation functions have been observed for pairs of like and unlike pions [91].

In Fig. 3.17, the distribution $W(\Delta\varphi, \Delta y)$, normalized to unity, is shown as a function of $\Delta\varphi$, for all charge combinations, in the intervals $\Delta y < 1$, $1 < \Delta y < 2$ and $2 < \Delta y < 3$ [88]. A horizontal line at the average value $1/\pi$ corresponds to a flat distribution in $\Delta\varphi$. The distribution is influenced by conservation of transverse momentum, by the decay of resonances (mainly for unlike-sign particles) and by Bose–Einstein correlations (for like-sign particles). In all cases, W is larger than $1/\pi$ for $\Delta\varphi > \pi/2$ and has a maximum at $\Delta\varphi = \pi$. Except for $(--)$ pairs at $\Delta y < 1$, the W function is smaller than $1/\pi$ for $\Delta\varphi < \pi/2$. Such a global anti-correlation follows from transverse momentum conservation.

Model predictions are shown in Fig. 3.17 for FRITIOF 2 (dot-dashed), two-string DPM (full) and multistring QGSM (dashed). The comparison with the data shows that it is much easier to

account for azimuthal correlations at large than at small Δy. At small Δy the models differ from each other and from the experimental data. The QGSM shows somewhat better agreement with experiment than the other models. This is a consequence of the multistring structure of QGSM, where strong azimuthal correlations in a single string are destroyed, with the result that the $\Delta\varphi$ dependence is weaker than in two-string models.

Differences between experiment and all models exist at small $\Delta\varphi$ and $\Delta y < 1$, in particular for $(--)$ pairs. Bose–Einstein correlations, not included in the models, may explain this disagreement. The influence of Bose–Einstein correlation can also be observed in the $(++)$ combination, but is smaller because of the influence of the (positive) beam particle.

Azimuthal distributions are shown in Fig. 3.18 for particles with $\Delta y < 1$, for $p_T < 0.30$ GeV/c and for $p_T > 0.30$ GeV/c, together with model calculations. A comparison of these figures reveals that azimuthal correlations have a strong p_T dependence. Large *positive* azimuthal correlations exist at small $\Delta\varphi$ and $\Delta y < 1$ for like-sign particles with small p_T. As the transverse momentum of

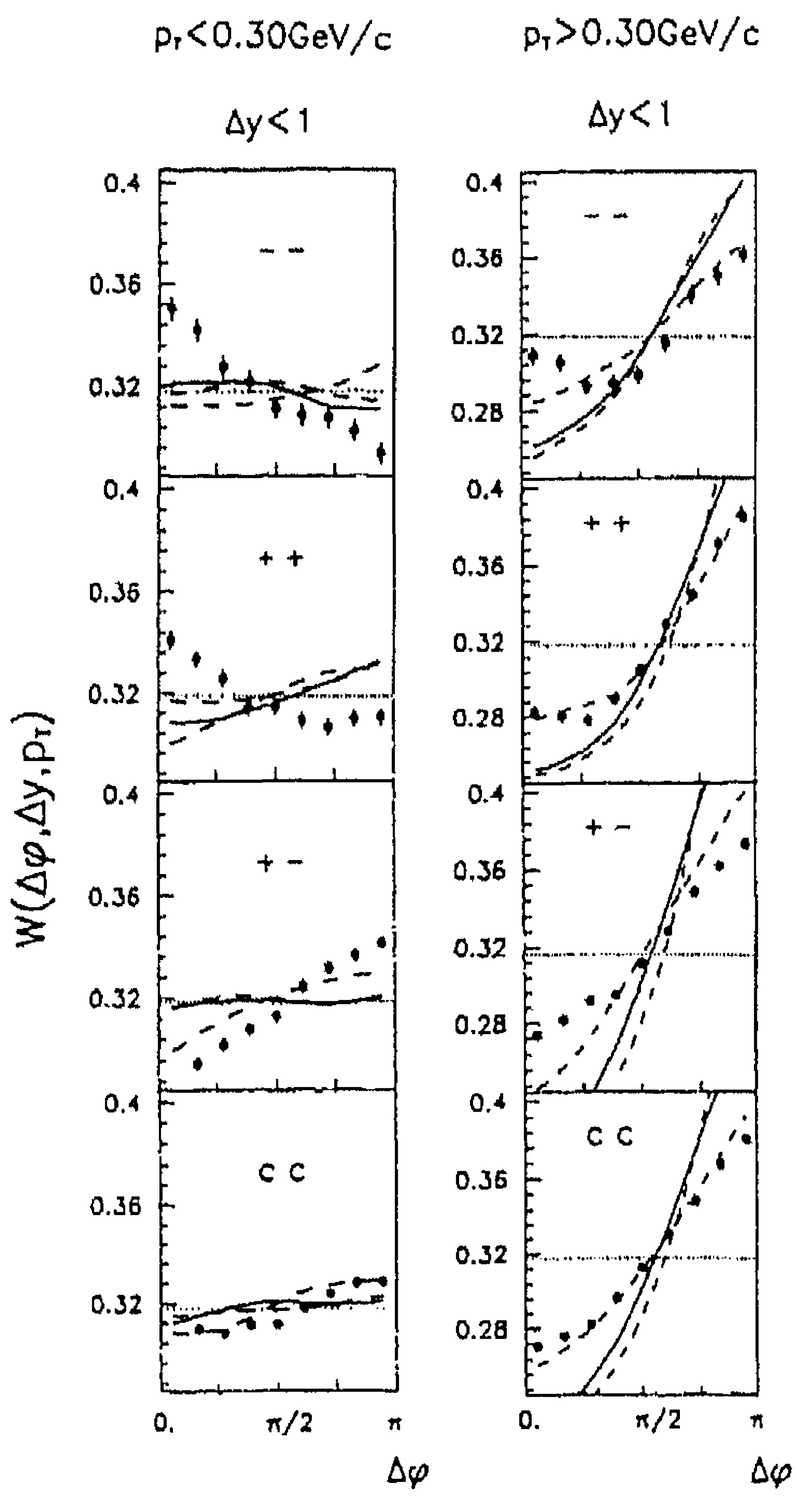

Fig. 3.18. $W(\Delta\varphi, \Delta y, p_T)$ as compared with calculations in FRITIOF2.0 (dot-dashed), DPM (full) and QGSM (dashed) for $\Delta y < 1$ and p_T cuts as indicated [88].

particles increases, the peak at $\Delta\varphi = \pi$ becomes more pronounced. This is reproduced by the models and reflects momentum conservation.

For $\Lambda\bar{\Lambda}$ pairs, an azimuthal correlation has been observed in MARK II at 29 GeV [92]. Similar K^+K^- correlations are seen in the exclusive hh final state $K^-p \to pK^+K^-K^-\pi^+\pi^-$ at 32 GeV/c [93].

Azimuthal correlations between $(+-)$ and $(++, --)$ charge combinations have been studied in μp collisions [77] for $|\Delta y| < 1$ and $|\Delta y| > 1$. The distribution $W(\Delta\varphi)$ is described fairly well by the LUND model including primordial k_T and gluons, except that for $|\Delta y| < 1$ it slightly underestimates the anti-correlation for $(+-)$ and overestimates it for $(++, --)$.

In the azimuthal correlation of K^0 pairs (Fig. 3.15(b)) and of $K^0\Lambda^0$ (Fig. 3.15(d)) studied by NA23 [90], the data tend to show pairs of small $\Delta\varphi$ not present in low-p_T LUND (solid line).

By the same collaboration, the azimuthal correlation is studied [71] in terms of the asymmetry parameter

$$B = [N(\Delta\varphi > \pi/2) - N(\Delta\varphi < \pi/2)]/N_{all} \tag{3.4}$$

for hadron pairs with
(a) opposite charge (h^+h^-),
(b) equal charge ($h^+h^+ + h^-h^-$),
(c) possibly opposite strangeness (Λ^0h^+, $x_\Lambda < -0.2$),
(d) no opposite strangeness (Λ^0h^-, $x_\Lambda < -0.2$),
for $\Delta y < 2$ and for $\Delta y > 2$. No azimuthal correlation is seen for $\Delta y > 2$ in all cases and for $\Delta y < 2$ in case of no common $q\bar{q}$ pairs ($h^+h^+ + h^-h^-$, Λ^0h^-). For h^+h^- and Λ^0h^+, the parameter B is compared to low-p_T LUND and DPM predictions in Table 3.1.

The parameter B is strongly overestimated in single-string low-p_T LUND and still too large in the two-string DPM. Furthermore, B increases with the sum of the transverse momenta (Fig. 3.19) but less strongly than in the models.

The azimuthal correlation has also been studied for $c\bar{c}$ pairs in $D\bar{D}$ production. An asymmetry is indeed observed in π^-p collisions at 360 GeV/c [94]. Also there, the LUND model overestimates the effect.

As shown on π^-N interactions at $\sqrt{s} = 26$ GeV [95], also NLO perturbative QCD calculations overestimate the azimuthal asymmetry for $D\bar{D}$ pairs (Fig. 3.20(a)). Agreement can be obtained with a model [96] where a (Gaussian shaped) transverse component is added to the incoming parton momentum before performing the NLO perturbative QCD calculation (Fig. 3.20(b)).

Table 3.1
Asymmetry parameter B

	Experiment	LUND	DPM
Λ^0h^+ ($\Delta y < 2$)	0.18 ± 0.03	0.30 ± 0.01	0.19 ± 0.01
h^+h^- ($\Delta y < 2$)	0.066 ± 0.003	0.126 ± 0.002	0.106 ± 0.002

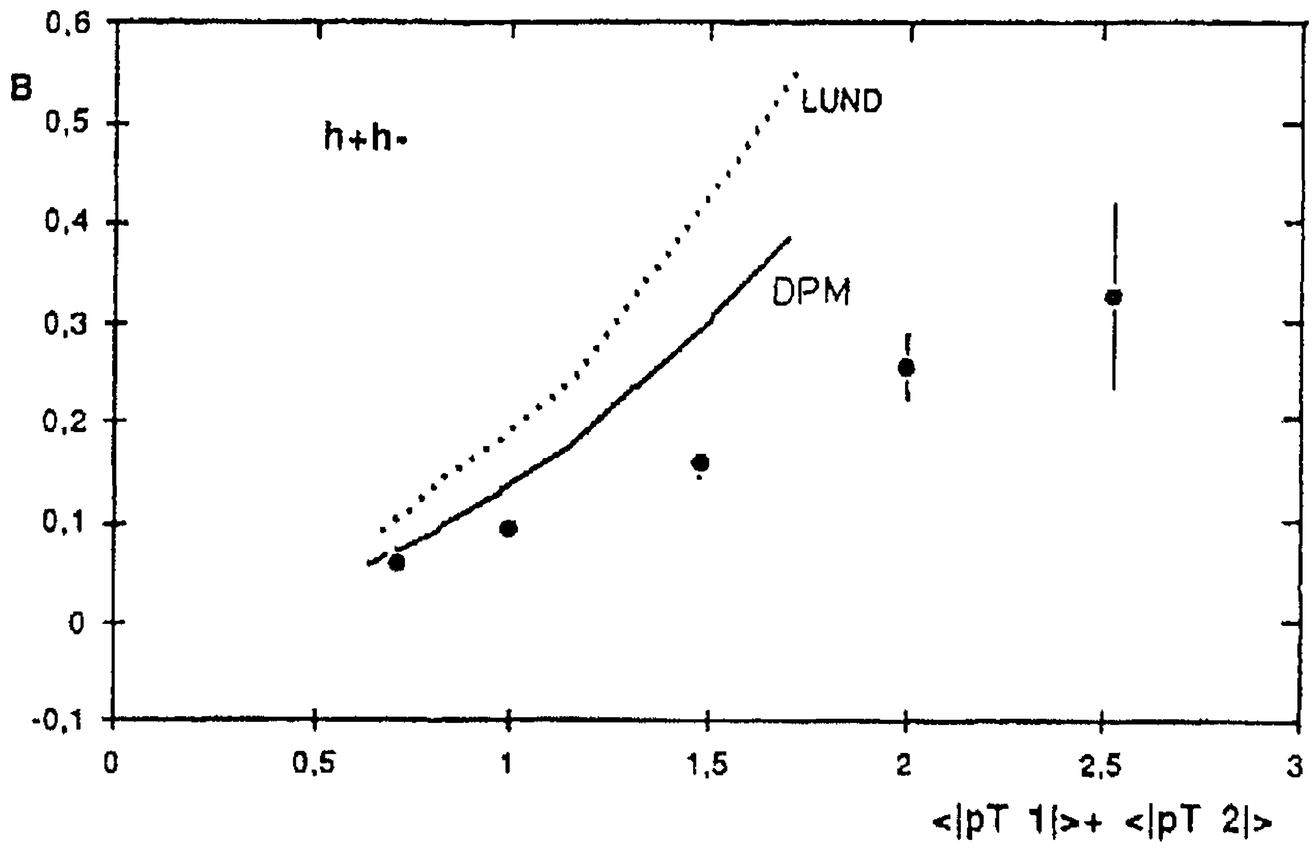

Fig. 3.19. The p_T dependence of the azimuthal correlation parameter B for h^+h^- pairs in pp collisions at 360 GeV/c compared to LUND and DPM [71].

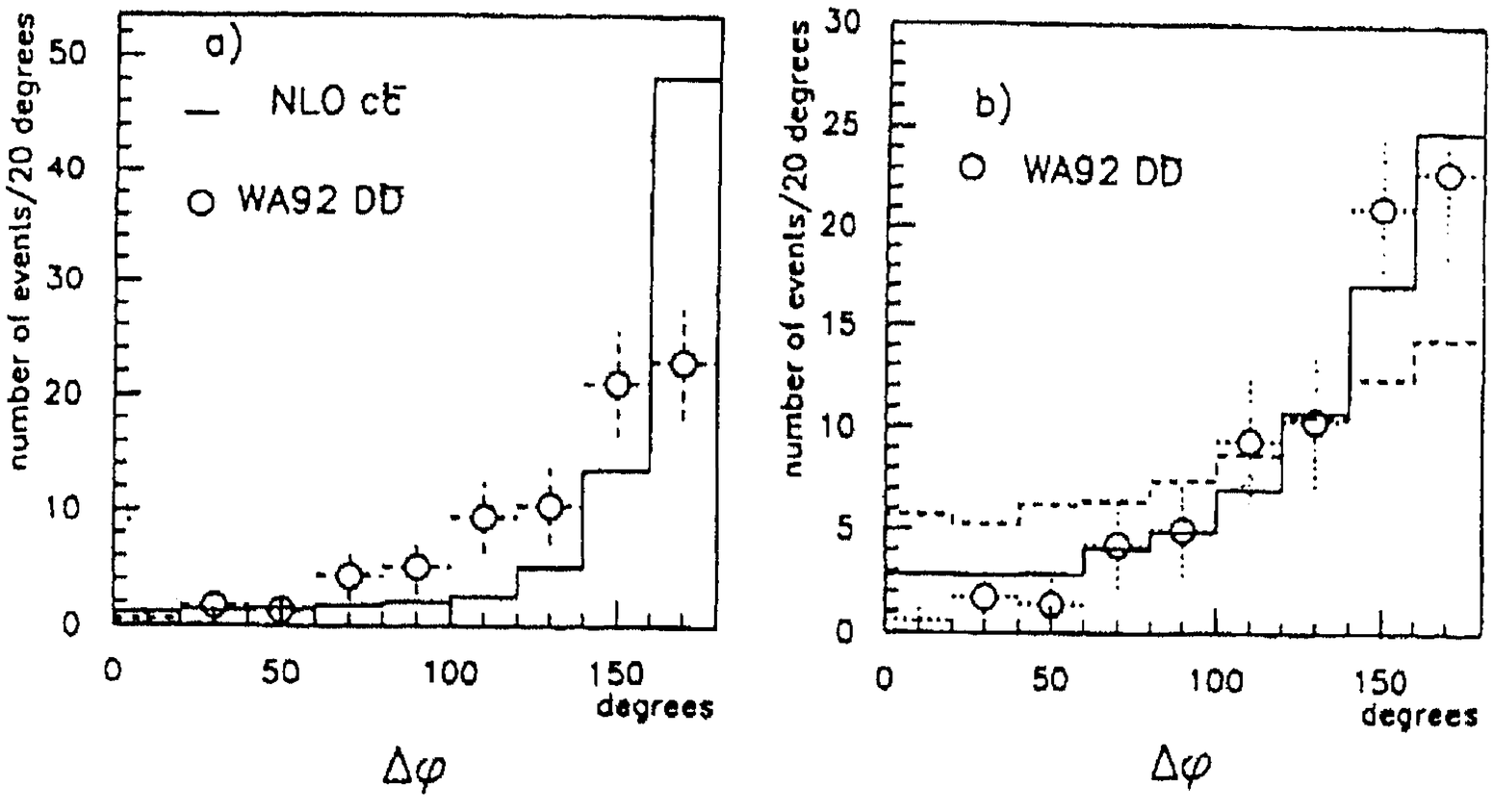

Fig. 3.20. Charmed pair azimuthal correlation: WA92 data are compared with predictions from (a) an NLO perturbative QCD calculation and (b) a model where a parton transverse momentum, p_T, is added to the NLO perturbative QCD predictions (dotted line: $\langle p_T^2 \rangle = 1.0$ (GeV/c)^2, solid line: $\langle p_T^2 \rangle = 0.3$ (GeV/c)^2) [95].

3.3. Correlations on the parton level

The OPAL collaboration [97] has compared hadronic azimuthal correlations to coherent and incoherent shower models (Fig. 3.21). The coherent models JETSET PS with angular ordering [73], HERWIG [83] and ARIADNE [84] describe the azimuthal correlations in hadronic Z^0

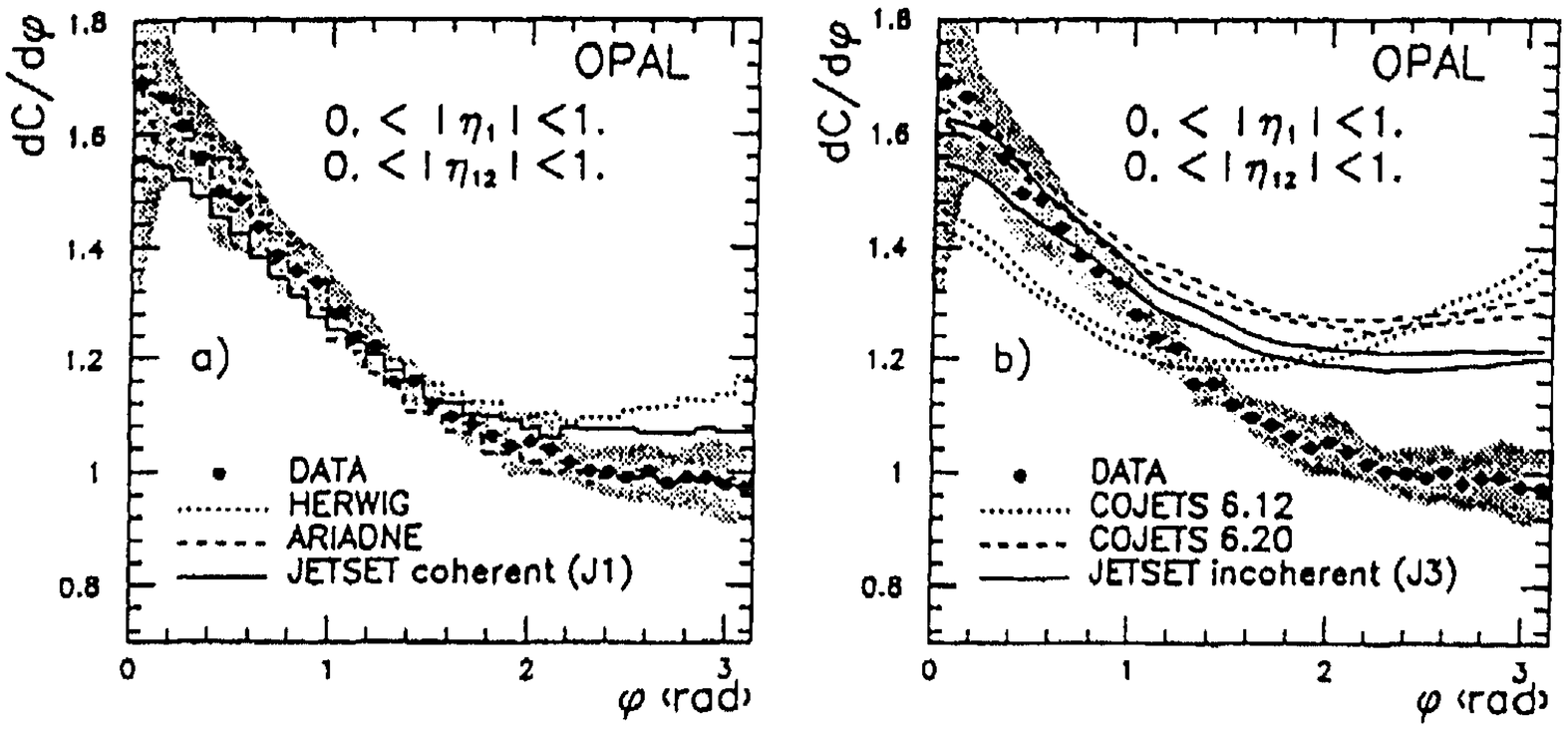

Fig. 3.21. Two-particle azimuthal correlations with respect to the sphericity axis in OPAL [97] compared to coherent and incoherent MC models.

decays, but the incoherent models JETSET PS without angular ordering [73] and COJETS [85] fail for $\varphi \gtrsim \pi/2$.

The hadronization of a quark–antiquark pair at high virtuality is currently thought to proceed via parton showering [98]. QCD implies that this parton showering is coherent. The coherence can be incorporated into Monte-Carlo programs as angular ordering [99], whereby for each successive branching the gluon is emitted at a smaller angle.

Furthermore, the idea of local parton–hadron duality (LPHD) [100] suggests that features at the parton level survive the fragmentation process. We can, therefore, expect that the coherence of the parton radiation will be reflected in angular ordering of the observed particles.

As a method particularly sensitive to angular ordering, particle–particle correlations (PPC) and their asymmetry (PPCA) [101, 102] are examined in a way analogous to the study of energy–energy correlations [103],

$$\mathrm{PPC}(\chi) = \frac{1}{\Delta\chi}\left\langle 2\sum_{i<j}^{n}\frac{1}{n^2}\,\delta_{\mathrm{bin}}(\chi-\chi_{ij})\right\rangle , \tag{3.5}$$

$$\mathrm{PPCA}(\chi) = \mathrm{PPC}(180^\circ-\chi) - \mathrm{PPC}(\chi) , \tag{3.6}$$

where χ_{ij} is the full spatial angle between tracks i and j, $\langle\ \ \rangle$ is the average over all events in the sample, n is the number of charged tracks in an event, and $\Delta\chi$ is the bin width. The function $\delta_{\mathrm{bin}}(\chi-\chi_{ij})$ is 1 if χ_{ij} and χ are in the same bin and 0 otherwise.

At $\sqrt{s} = M_Z$, the fraction of two-jet events is very high. For two-jet events, particles in different jets will in general be separated by an angle χ greater than 90°. The PPC for $\chi > 90^\circ$ can, therefore, serve as an indication of what the PPC *within* a jet ($\chi < 90^\circ$) would be *in the absence* of angular ordering. By forming the asymmetry, these "uninteresting" correlations are effectively subtracted. The effects of angular ordering should, therefore, be more directly observable in the PPCA than in the PPC. Note, however, that the sign convention following [103] leads to a *negative* sign for a *positive* correlation.

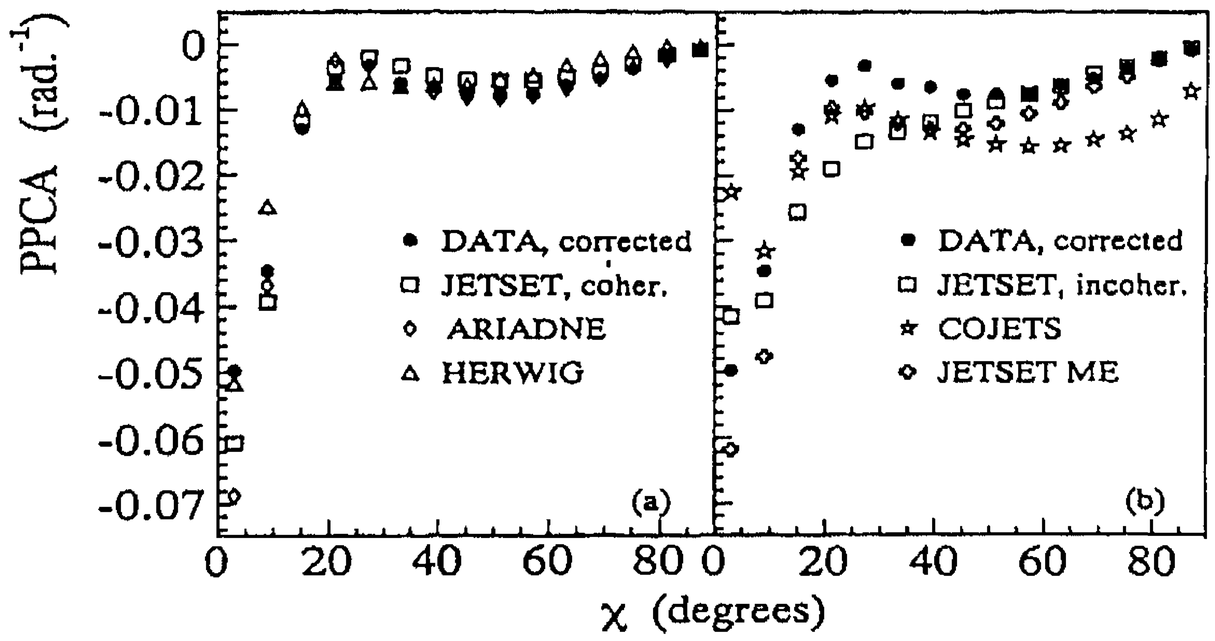

Fig. 3.22. The PPCA distribution for corrected L3 data compared to (a) coherent and (b) incoherent Monte-Carlo models [102].

Figs. 3.22(a) and (b) show the PPCA distribution of L3 data (corrected for detector effects [102]) compared to coherent and incoherent Monte-Carlo models, respectively.

In Fig. 3.22(b) we see that for $\chi \lesssim 60°$ JETSET 7.3 PS without angular ordering (incoherent) disagrees strongly with the data, while being in fair agreement at larger values of χ. COJETS is seen not to reproduce the data over the entire angular range. On the other hand, in Fig. 22(a), the coherent Monte-Carlo models, JETSET with angular ordering, HERWIG, and ARIADNE all reproduce the data reasonably well over the full angular range. Note that the disagreement of the incoherent models cannot be due to the Bose–Einstein effect. Turning this effect off in the non-angular ordered JETSET model does not raise but lower its PPCA points. So, the data from the L3 experiment strongly disfavour the incoherent models.

3.4. Three-particle rapidity correlations

Whether dynamical correlations exist beyond the two-particle correlations discussed so far is of crucial importance for much of the present search for scaling phenomena in multiparticle processes, a subject treated in Section 4. With conventional techniques, this question is not easy to answer and beyond the sensitivity of many experiments.

Nevertheless, three-particle correlations in rapidity have been looked for in a number of experiments [63, 75, 104–106]. The third-order normalized factorial cumulant is defined by [cf. (2.22)]

$$K_3(y_1, y_2, y_3) = C_3(y_1, y_2, y_3) \Big/ \frac{1}{\sigma_{\text{inel}}^3} \frac{\mathrm{d}\sigma}{\mathrm{d}y_1} \frac{\mathrm{d}\sigma}{\mathrm{d}y_2} \frac{\mathrm{d}\sigma}{\mathrm{d}y_3}, \tag{3.7}$$

$$\begin{aligned} C_3(y_1, y_2, y_3) = {} & \frac{1}{\sigma_{\text{inel}}} \frac{\mathrm{d}^3\sigma}{\mathrm{d}y_1 \mathrm{d}y_2 \mathrm{d}y_3} + 2 \frac{1}{\sigma_{\text{inel}}^3} \frac{\mathrm{d}\sigma}{\mathrm{d}y_1} \frac{\mathrm{d}\sigma}{\mathrm{d}y_2} \frac{\mathrm{d}\sigma}{\mathrm{d}y_3} \\ & - \frac{1}{\sigma_{\text{inel}}^2} \frac{\mathrm{d}^2\sigma}{\mathrm{d}y_1 \mathrm{d}y_2} \frac{\mathrm{d}\sigma}{\mathrm{d}y_3} - \frac{1}{\sigma_{\text{inel}}^2} \frac{\mathrm{d}^2\sigma}{\mathrm{d}y_2 \mathrm{d}y_3} \frac{\mathrm{d}\sigma}{\mathrm{d}y_1} - \frac{1}{\sigma_{\text{inel}}^2} \frac{\mathrm{d}^2\sigma}{\mathrm{d}y_1 \mathrm{d}y_3} \frac{\mathrm{d}\sigma}{\mathrm{d}y_2} \end{aligned} \tag{3.8}$$

with

$$\sigma_{\text{inel}} = \sum_{n \geq 8} \sigma_n \,.$$

The $\tilde{C}_S(y_1, y_2, y_3)$ correlation function is determined as a sum of topological correlation functions:

$$\tilde{C}_S(y_1, y_2, y_3) = \sum_{n \geq 8} P_n \tilde{C}_3^{(n)}(y_1, y_2, y_3), \tag{3.9}$$

$$\tilde{C}_3^{(n)}(y_1, y_2, y_3) = \tilde{\rho}_3^{(n)}(y_1, y_2, y_3) - \tilde{A}_3^{(n)}(y_1, y_2, y_3)\,, \tag{3.10}$$

$$\tilde{A}_3^{(n)}(y_1, y_2, y_3) = \tilde{\rho}_2^{(n)}(y_1, y_2)\tilde{\rho}_1^{(n)}(y_3) + \tilde{\rho}_2^{(n)}(y_2, y_3)\tilde{\rho}_1^{(n)}(y_1) + \tilde{\rho}_2^{(n)}(y_1, y_3)\tilde{\rho}_1^{(n)}(y_2) - 2\tilde{\rho}_1^{(n)}(y_1)\tilde{\rho}_1^{(n)}(y_2)\tilde{\rho}_1^{(n)}(y_3)\,,$$

$$\tilde{\rho}_3^{(n)}(y_1, y_2, y_3) = \frac{1}{n(1,2,3)}\frac{1}{\sigma_n}\frac{\mathrm{d}^3\sigma}{\mathrm{d}y_1\mathrm{d}y_2\mathrm{d}y_3}\,, \tag{3.11}$$

where $n(1, 2, 3)$ is the mean number of three-particle combinations in events with charge multiplicity n.

The corresponding normalized function is defined as:

$$\tilde{K}_S(y_1, y_2, y_3) = \tilde{C}_S(y_1, y_2, y_3)/\sum_n P_n \tilde{\rho}_1^{(n)}(y_1)\tilde{\rho}_1^{(n)}(y_2)\tilde{\rho}_1^{(n)}(y_3)\,. \tag{3.12}$$

Because of small statistics, three-particle correlations were not observed in pp interactions at 200 GeV/c at FNAL [63]. In K^-p interactions at 32 GeV/c [104], three-particle correlations were considered using $\tilde{C}_S(y_1, y_2, y_3)$ and $\tilde{K}_S(y_1, y_2, y_3)$. No positive short-range correlation effect was observed. Correlations in the form of K have been observed in the central region by the ISR experiment for $n \geq 8$ [106].

Fig. 3.23 from NA22 shows $K_3(0, 0, y)$ and $\tilde{K}_S(0, 0, y)$ for the combined M^+p sample at 250 GeV/c [75]. Also shown are the values of $K_3(0, 0, y)$ obtained in pp-interactions at $\sqrt{s} = 31$–62 GeV [106] (lines). Inclusive three-particle correlations $K_3(0, 0, y)$ are indeed seen in the NA22 data. They are strongest when a third particle partially compensates the charge of a pair of identical particles. There are, however, no correlation effects visible in the function $\tilde{K}_S(0, 0, y)$. In FRITIOF and QGSM, three-particle rapidity correlations are absent in both $K_3(0, 0, y)$ and $\tilde{K}_S(0, 0, y)$.

Recently, a factorization of the normalized three-particle correlation function has been proposed [107–109] under the form of a "linked-pair" structure:

$$K_3(y_1, y_2, y_3) = K_2(y_1, y_2)K_2(y_2, y_3) + K_2(y_1, y_3)K_2(y_3, y_2)\,. \tag{3.13}$$

The comparison of the prediction of (3.13) to the data is given in Table 3.2, for $n \geq 2$, at a resolution of 0.5 rapidity units. At this resolution, the linked-pair ansatz is in agreement with the measured three-particle correlation within two standard deviations. Note, that y-correlations are much stronger for low-p_T particles and that the linked-pair ansatz continues to hold.

With the accuracy presently attainable for three-particle correlations, it is obvious that studies of still higher-order correlation functions require better methods. The most successful ones will be discussed in Section 4.

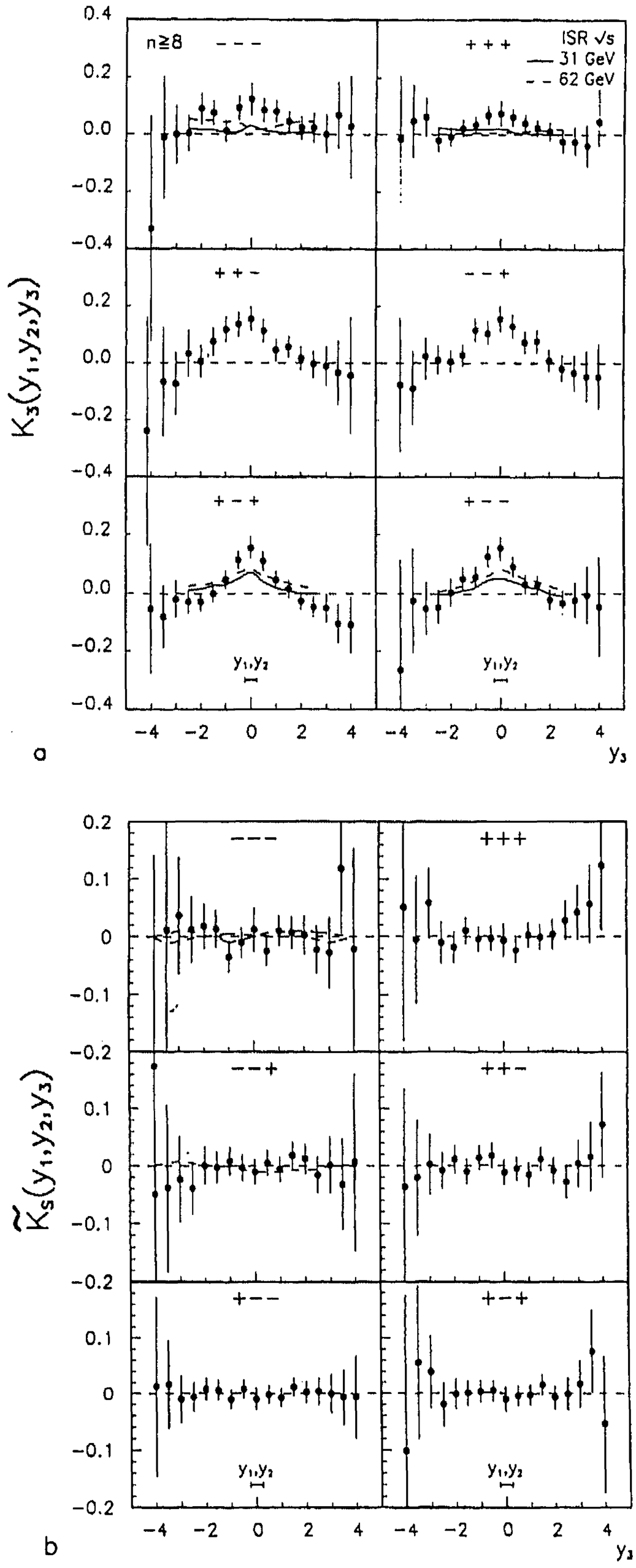
n≥8 − − −
+ + +
ISR √s
31 GeV
62 GeV
+ + −
− − +
+ − +
+ − −
$K_3(y_1,y_2,y_3)$
y_1,y_2
y_3
− − −
+ + +
− − +
+ + −
+ − −
+ − +
$\tilde{K}_5(y_1,y_2,y_3)$
a
b

Table 3.2
The three-particle correlation function compared to the prediction from the linked-pair ansatz, for non-single diffractive data ($n \geq 2$)

	All p_T		$p_T < 0.15$ GeV/c	
	Data	LPA	Data	LPA
$K_3^{---}(0,0,0)$	0.23 ± 0.10	0.30 ± 0.03	2.3 ± 1.7	2.0 ± 0.4
$K_3^{+++}(0,0,0)$	0.14 ± 0.06	0.21 ± 0.02	1.2 ± 0.6	1.0 ± 0.2
$K_3^{\text{ccc}}(0,0,0)$	0.39 ± 0.04	0.53 ± 0.03	1.9 ± 0.5	1.7 ± 0.2

3.5. Summary and conclusions

1. The main contributions to the correlation functions C_2 and C_3 come from the mixing of events with different multiplicity and different single-particle density, but some effect remains in the so-called short-range correlation part.
2. $C_2(0, y_2)$ increases much faster with increasing energy than its short-range contribution.
3. The short-range correlation is significantly larger for $(+-)$ than for the equal-charge combinations, and is positive over a wider rapidity range in $C_2(y_1, y_2 = y_1)$.
4. The correlation functions $\tilde{C}_2^{(n)}(0, y_2)$, contrary to $C_2^{(n)}(0, y_2)$, are similar for different multiplicity n, except that $\tilde{C}_2^{(n)+-}$ becomes narrower with increasing n.
5. In hadron–hadron collisions, the correlation functions depend strongly on transverse momentum and are largest for small-p_T particles. Consequently, correlations are stronger in multidimensional phase space than in a lower-dimensional projection, such as rapidity space. Further implications of this observation will be discussed in Section 4.3.
6. In the central c.m. region, and at comparable energy, the correlation strength observed in M^+p collisions at $\sqrt{s} = 22$ GeV is of similar magnitude as in e^+e^- collisions and as in μp collisions, if the trend of the latter is extrapolated to $W = 22$ GeV. Model predictions for e^+e^- and μp interactions slightly underestimate the correlation strength but give, nonetheless, clear evidence that (hard) gluon effects are the main source of correlations in rapidity space.
7. Combinatorial background can be suppressed by studying the correlation of strange particles. Data are scarce, but support the conclusions drawn from data on non-strange particles.
8. The UA5 cluster Monte Carlo and FRITIOF describe $C_2^{(n)}(\eta_1, \eta_2)$ at CERN-Collider energies, at least in the charge multiplicity range $34 \leq n \leq 38$. At lower energies ($20 \lesssim \sqrt{s} \lesssim 30$ GeV), the single-chain LUND model shows a strong anti-correlation among like-charge particles. The two-string FRITIOF model and DPM predict negative values for $C_2(y_1, y_2)$ or $K_2(y_1, y_2)$ in the central region for like charges. They are positive but far below the data for unlike-charge

Fig. 3.23. Three-particle rapidity correlations (a) $K_3(0, 0, y)$ [the lines correspond to the ISR results at 31 GeV (full) and 62 GeV (dashed) and (b) $K_3(0, 0, y)$ for M^+p interactions at 250 GeV/c [the FRITIOF (dot-dashed) prediction is indicated for the charge combination (−−−), QGSM (dashed) for (−−−) and (−− +)] [75].

pairs. QGSM reproduces $C_2(y_1, y_2)$ and $\tilde{C}_2(y_1, y_2)$ for all charge combinations, but cannot account for the short-range part $\tilde{C}_S(y_1, y_2)$.

9. Positive correlations are observed at large values of the azimuthal angle $\Delta\varphi$, as expected from transverse momentum conservation. The correlations among like-charge particle pairs at small values of $\Delta\varphi$ and Δy, where Bose–Einstein effects should contribute, are significantly larger than predicted by FRITIOF 2, DPM and QGSM. The deviations are stronger for particles with small transverse momentum.
10. In general, short-range correlations in e^+e^- annihilation are reasonably well described by the LUND- and Webber-type models. To the contrary, in models for hh collisions which contain only one or two strings without additional p_T effects or gluons, correlations in rapidity are underestimated, those in azimuthal angle overestimated.
    Models such as LUND and DPM are known to underestimate the height of the "sea-gull" wings (the particle average transverse momentum as a function of Feynman-x) [110], a signal of semi-hard interactions. The models neglect such processes. This may partially explain why the models fail in both instances.
11. The distribution in the interparticle opening angle of e^+e^- collisions at LEP favours models with coherent parton showering.
12. Three-particle correlations are now observed in all charge combinations. They are particularly large for low-p_T particles. Within two standard deviations, they satisfy the linked-pair ansatz. No short-range contribution $\tilde{K}_S$ is observed in three-particle correlations. Other methods are needed to study higher-order correlations.

4. Multiplicity fluctuations and intermittency

4.1. Prelude

The study of fluctuations in particle physics already has a long history going back to early cosmic-ray observations. To our knowledge, Ludlam and Slansky [111] were the first to advocate analysis of event-to-event fluctuations in hadron–hadron collisions. Comparing rapidity distributions of single events with the sample averaged distribution, they put in evidence strong clustering effects in longitudinal phase space, indicating "a remarkably structured phase-space density" [112]. Fluctuations in individual events were also considered in the context of Reggeon theory in the important paper establishing the AGK-cutting rules [113].

Early evidence for large concentrations of the particle number in small rapidity regions for single events were reported in cosmic-ray experiments [114–116] and in pN collisions at 200 GeV beam momentum [117]. A further number of high density "spikes" in rapidity space have been reported during the last decade. Fig. 4.1(a) shows the notorious JACEE event [118] at a pseudo-rapidity resolution (binning) of $\delta\eta = 0.1$. It has local fluctuations up to $dn/\delta\eta \approx 300$ with a signal-to-background ratio about 1:1. The NA22 event [119] of Fig. 4.1(b) contains a "spike" at a rapidity resolution $\delta y = 0.1$ of $dn/dy = 100$, corresponding to 60 times the average density in this experiment. UA5 [120] has reported "spikes" in $dn/d\eta$ up to 30 (10 times average) as early as JACEE, but found these to be in agreement with a short-range cluster Monte Carlo. Also EMU-01 [121] sees events with $dn/d\eta = 140$ satisfactorily explained by FRITIOF.

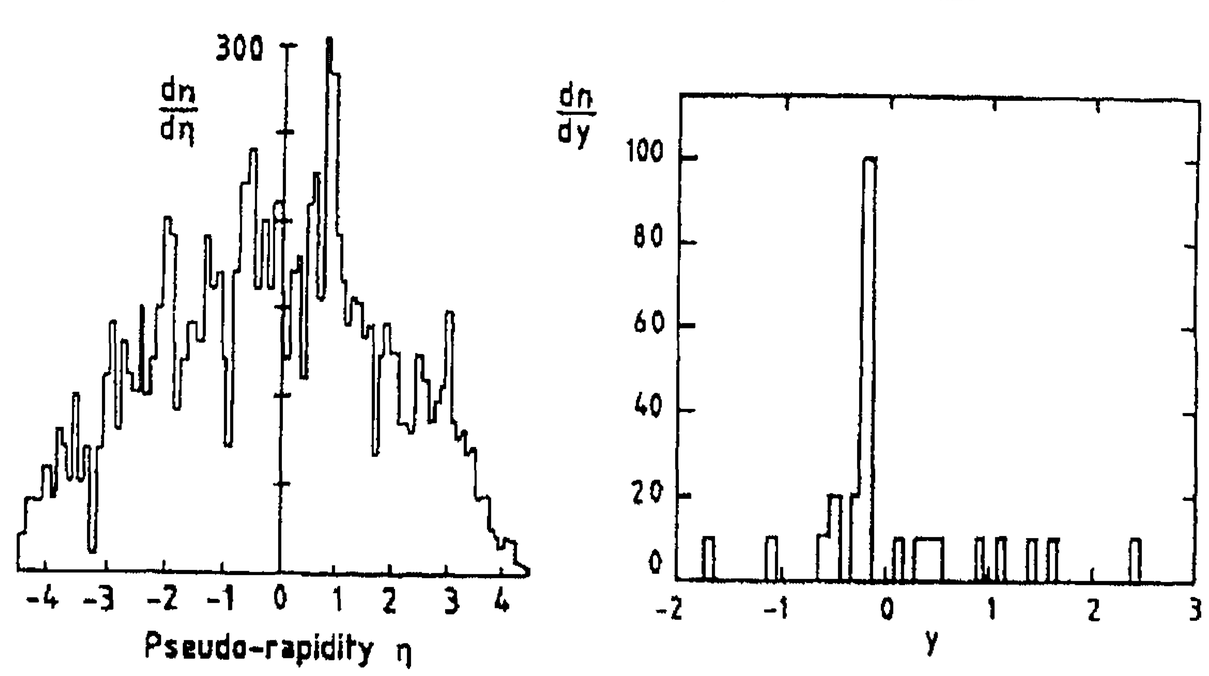

Fig. 4.1. (a) The JACEE event [118]; (b) The NA22 event [119].

From an experimental point of view, there is little doubt that events with large local density fluctuations exist. The real question is whether these are of dynamical or merely statistical origin, whether the underlying probability density is continuous or intermittent.

Early attempts were made to answer the question of non-statistical fluctuations employing transform techniques [122], but these were not followed up. The problem resurfaced in the work of Białas and Peschanski [21,22], who suggested that spikes could be a manifestation in hadron physics of "intermittency", a phenomenon well-known in fluid-dynamics. The authors argued that if intermittency occurs in particle production, large density fluctuations are not only expected, but should also exhibit self-similarity with respect to the size of the phase-space volume.

Ideas on self-similarity and fractals in jet physics had earlier been formulated in [123,124], rephrased in the language of QCD branching processes in [125] and in a simplified form in [126]. For soft hadronic processes, fractals and self-similarity were first considered in [127] and their quantitative measures in [128,129].

In multiparticle experiments, the number of hadrons produced in a single collision is small and subject to considerable "noise". To exploit the techniques employed in complex system theory, a method must be devised to separate fluctuations of purely statistical origin, due to finite particle numbers, from the possibly self-similar fluctuations of the underlying particle densities. The latter are the quantities of physical interest. A solution, already used in optics and suggested for multiparticle production in [21,22], consists in measuring suitably normalized factorial moments of the multiplicity distribution in a given phase-space volume.

4.2. Normalized factorial moments

4.2.1. The method

The method proposed in [21,22] consists in measuring the dependence of the normalized factorial moments $F_q(\delta y)$ defined in (2.68)–(2.70) as a function of the resolution δy. For definiteness,

δy is supposed to be an interval in rapidity, but the method generalizes to arbitrary phase-space dimensions.

In Section 2.2 we have pointed out that the scaled factorial moments enjoy the property of "noise-suppression". It is easily verified that this crucial property does not apply to ordinary moments $\langle n^q\rangle/\langle n\rangle^q$ (cf. Section 4.7 below). High-order moments further act as a filter and resolve the large n_m tail of the multiplicity distribution. They are thus particularly sensitive to large density fluctuations at the various scales δy used in the analysis.

As proven in [21,22], a "smooth" (rapidity) distribution, which does not show any fluctuations except for the statistical ones, has the property that $F_q(\delta y)$ is independent of the resolution δy in the limit $\delta y \to 0$. This follows directly from (2.100), if P_ρ is a product of δ-functions in $\rho_m\,(m = 1, \ldots, M)$ centred around $\langle\rho_m\rangle$. On the other hand, if dynamical fluctuations exist and P_ρ is "intermittent" (i.e. regions of fluctuations exist at all scales of y), the F_q obey the power law (2.110). Eq. (2.110) is a scaling law, since the ratio of the factorial moments at resolutions L and ℓ

$$R = F_q(\ell)/F_q(L) = (L/\ell)^{\phi_q} \tag{4.1}$$

only depends on L/ℓ.

As mentioned in Sections 2.4 and 5.2.2, the "intermittency indices" ϕ_q (slopes in a double-log plot) are related [130,131,28] to the anomalous dimensions $d_q = \phi_q/(q-1)$, a measure for the deviation from an integer dimension.

We noted in Section 3.4 that the experimental study of correlations is difficult already for three particles. The close connection between correlations and factorial moments (Section 2.1.4) offers a possibility to measure higher-order correlations with the factorial moment method at smaller distances than previously feasible. The method further relates possible scaling behaviour of such correlations to the physics of fractal objects. Despite the advantages, it should be remembered that reliable data can only be extracted if factorial moments are averaged over a large domain of phase space. This holds the danger of obscuring important dynamical effects.

The definition of "intermittency" given in (2.110), has its origin in other disciplines.[1] It rests on a loose parallel between the high non-uniformity of the distribution of energy dissipation, for example, in turbulent intermittency and the occurrence of large "spikes" in hadronic multiparticle final states (Section 4.1). In the following we use the term "intermittency" in a weaker sense, referring to the rise of factorial moments with increasing resolution but not necessarily according to a strict power law.

The suggestion that normalized factorial moments of particle distributions might show power-law behaviour has spurred a vigorous experimental search for (more or less) linear dependence of $\ln F_q$ on $-\ln \delta y$. Within a surprisingly short time (one-dimensional) analyses were performed for e^+e^- [133–139], μp [140], νA [141], hh [142–148], hA [149–154] and AA [149,150,155–161] collisions. With respect to the original objective, the early one-dimensional work has remained inconclusive, but valuable information and experience was accumulated. Much more promising insight has come from studies in two- and three-dimensional phase space. This is discussed in Section 4.3. Further extensions of this approach, concentrating on improved integration methods

[1] For a masterly exposé of this subject see [132].

and differential studies in Lorentz-invariant variables have lead to further clarification of the issues involved in intermittency. These very recent developments are presented in Sections 4.8–4.10.

4.2.2. Results on log–log plots (in one dimension)

In this and the next few sections we review experimental results and model predictions obtained from one-dimensional studies. Due to the vast amount of data available, we limit ourselves to an illustration of the major characteristics of factorial moment behaviour in various processes and at various energies.

In Fig. 4.2(a), $\log F_5$ is plotted [21,22] as a function of $-\log \delta\eta$ (η is the pseudorapidity) for the JACEE event. It is compared with an independent emission Monte-Carlo model tuned to reproduce the average η distribution of Fig. 4.1(a) and the global multiplicity distribution, but has no short-range correlations included. While the Monte-Carlo model indeed predicts constant F_5, the JACEE event shows a first indication for a linear increase, i.e. a possible sign of intermittency.

Further examples are given in Fig. 4.2(b) for KLM [149], again showing a roughly linear increase for $\delta\eta < 1$ ($-\ln \delta\eta > 0$) instead of the flat behaviour expected for independent emission, and in Figs. 4.2(c) and (d) for UA1 [143] in terms of $\delta\eta$ and $\delta\phi$, respectively.

Anomalous dimensions d_q fitted over the range $0.1 < \delta y(\delta\eta) < 1.0$ are compiled in Fig. 4.3 [162]. They typically range from 0.01 to 0.1, which means that the fractal (Rényi) dimensions $D_q = 1 - d_q$ are close to one. The d_q are larger and grow faster with increasing order q in μp and e^+e^- (Fig. 4.3(a)) than in hh collisions (Fig. 4.3(b)) and are small and almost independent of q in heavy-ion collisions (Fig. 4.3(c)). For hh collisions, the q-dependence is considerably stronger for NA22 ($\sqrt{s} = 22$ GeV) than for UA1 ($\sqrt{s} = 630$ GeV).

4.2.3. Model predictions

4.2.3.1. Hadron–hadron collisions. A comparison to NA22 data on slopes ϕ_q (Fig. 4.4(a)) shows [142] that intermittency is absent at $\sqrt{s} = 22$ GeV in a two-chain DPM and underestimated by FRITIOF. In Fig. 4.4(b), PYTHIA is seen to stay below the UA1 data [143], even after inclusion of Bose–Einstein interference for identical particles. The UA5 cluster Monte Carlo GENCL, able to reproduce conventional short-range correlations (at least in a certain range of multiplicities cf. Fig. 3.3), follows the data down to a resolution of $\delta\eta \approx 0.3$, but completely fails for smaller $\delta\eta$.

Also, a multichain version of DPM including mini-jet production has been compared to NA22 and UA1 data. The slopes are found to be too small by at least a factor of 2 [163].

With respect to intermittency analysis, the situation may improve with the introduction of ECCO [164], an eikonal cascade model based on geometrical branching, which now can account for strong fluctuations, in particular in higher dimensions (Section 4.3 below). However, the present version of ECCO is still less refined than the more conventional models with respect to other observables.

The above examples show that present models for multiparticle production in hh collisions are unable to reproduce the magnitude and the growth of factorial moments with increasing resolution. From the discussion in Section 3, it is evident that model predictions for correlations in general are quite unreliable. The two-particle correlation function, measured by F_2, also determines to a large extent the higher-order factorial moments (cf. Eq. (2.72)) because of the weakness of

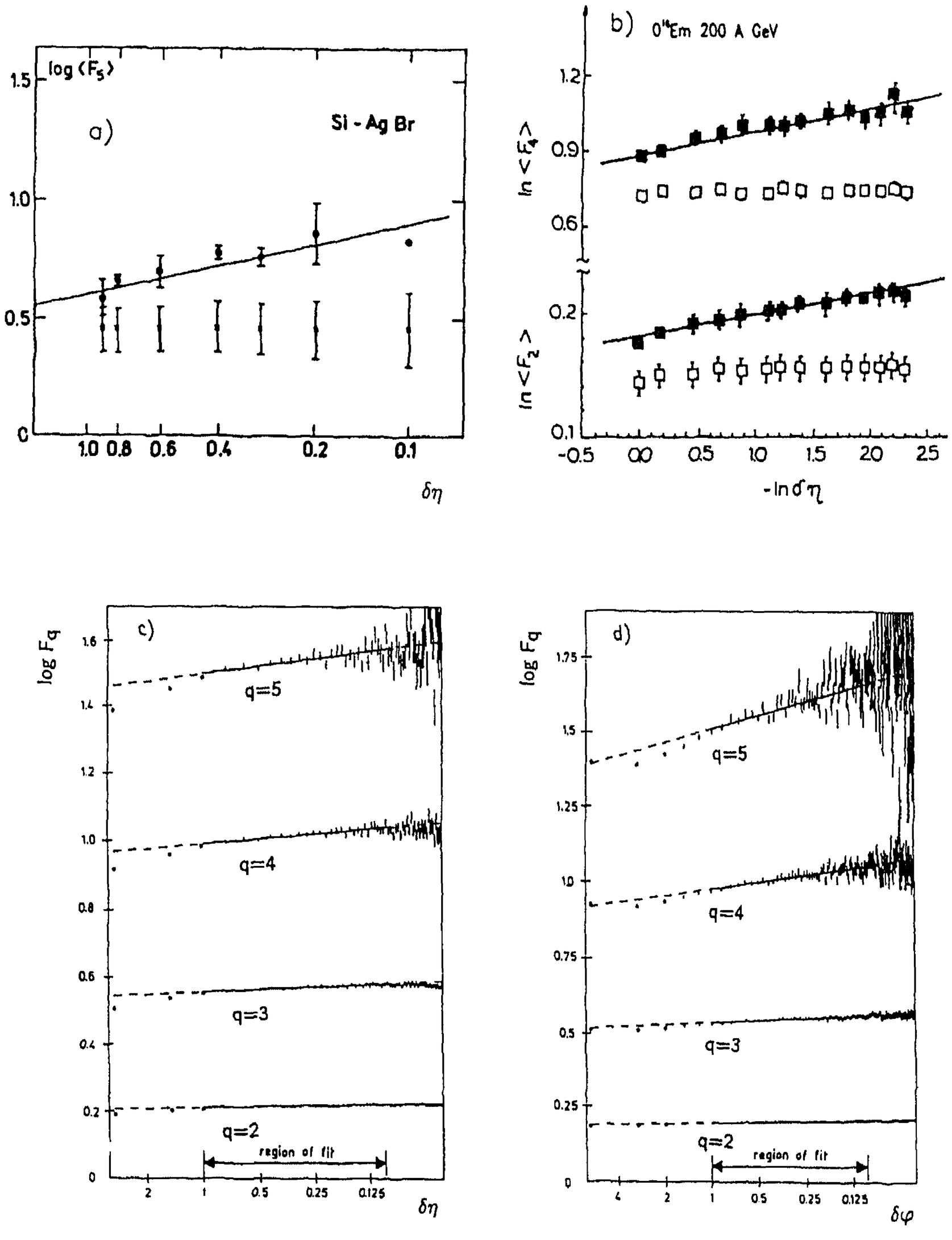

Fig. 4.2. (a) $\log F_5$ as a function of $-\log \delta\eta$ for the JACEE event [21, 22] (full circles) compared to independent emission (small crosses); (b) $\ln F_2$ and $\ln F_4$ as functions of $-\ln \delta\eta$ for O^{16} Em at 200 A GeV (KLM) [149], (c) $\log F_q$ on $_2\log \delta\eta$ and (d) $_2\log \delta\varphi$ at 630 GeV (UA1) [143].

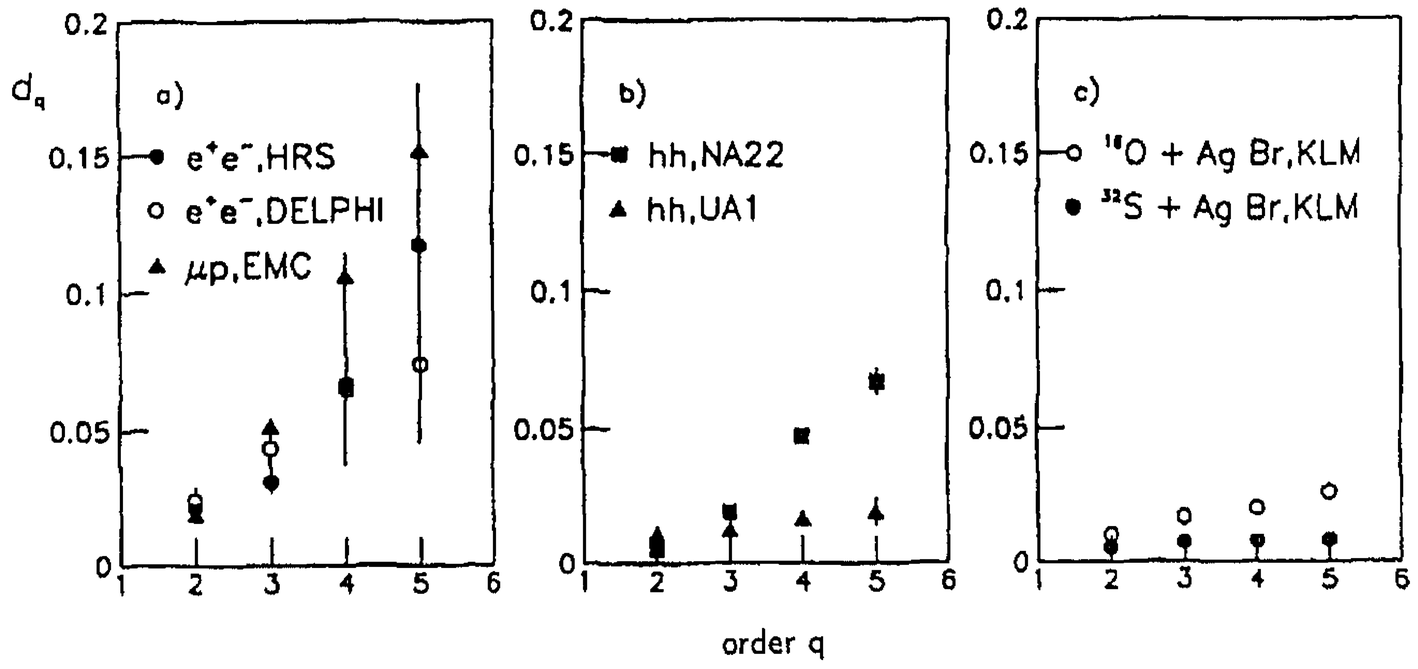

Fig. 4.3. Anomalous dimension d_q as a function of the order q, for (a) μp and e^+e^- collisions, (b) NA22 and UA1, (c) KLM [162].

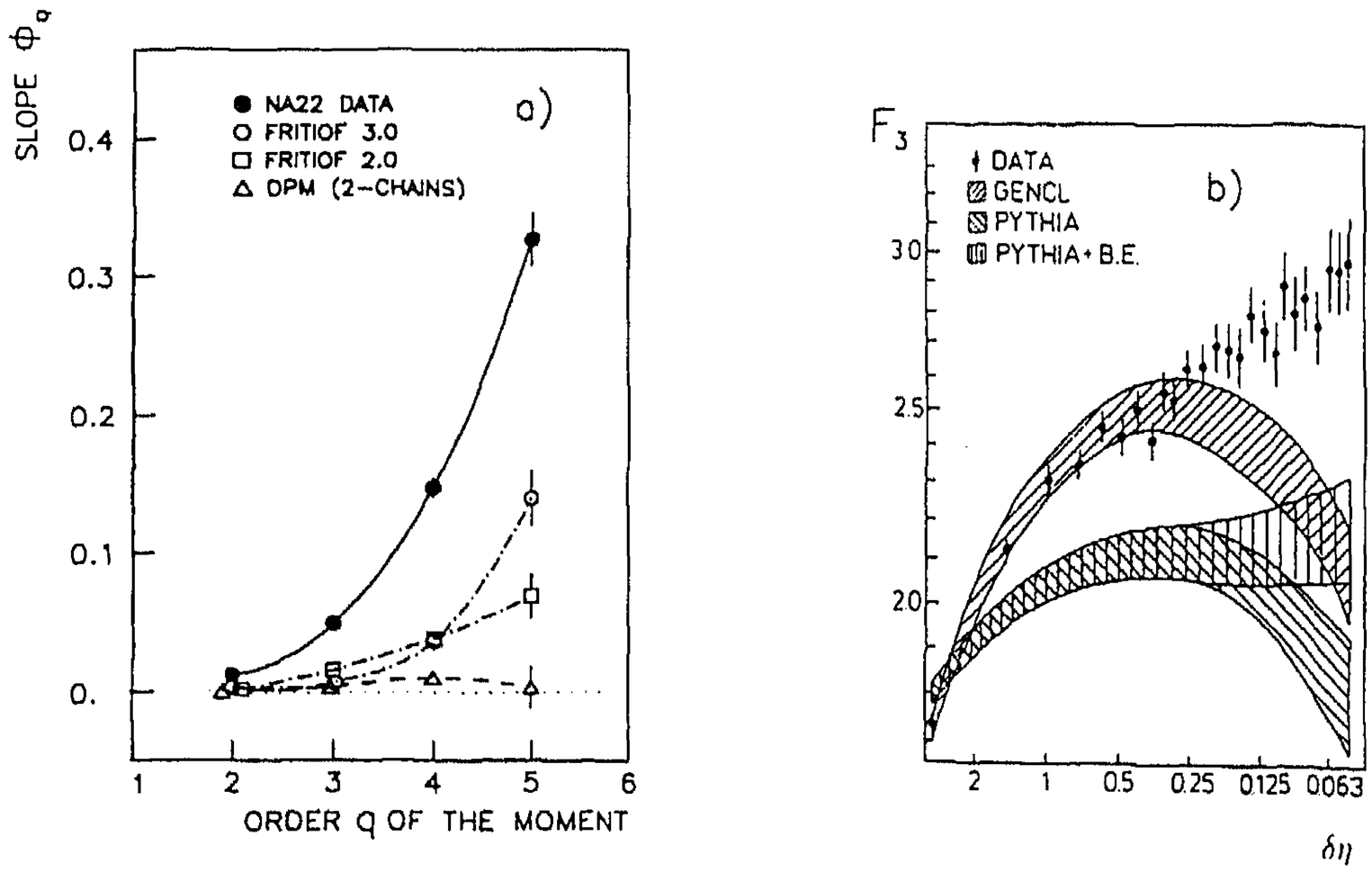

Fig. 4.4. (a) Slope ϕ_q as a function of order q for NA22 [142], two versions of FRITIOF and a two-chain dual parton model, (b) F_3 versus $\delta\eta$ from UA1 [143] compared to GENCL, PYTHIA and PYTHIA + Bose–Einstein Monte Carlos.

genuine high-order correlations. It is, therefore, mandatory to improve the models before evidence for "new physics" at very small (rapidity) separation can be claimed. We return to this important question in later sections.

4.2.3.2. hA *and* AA *collisions.* The intermittency indices are much smaller in hA and AA collisions than in hh collisions, and the event samples are much smaller. Model comparisons are, therefore,

less conclusive than in hh collisions. FRITIOF is found too low in NA22 [151] for π^+/K^+ on Al and Au at 250 GeV/c, in E802 [160] for central ^{15}OAl and ^{16}OCu at 14.6 A GeV/c, in WA80 [161] for SS and Au at 200 A GeV/c, and in NA35 [150] for pAu, OAu, SAu and SS at 200 A GeV/c. In WA80 it is shown that rough agreement can be obtained by renormalization to the leftmost point of FRITIOF on the log–log plot (essentially the shape of the overall multiplicity distribution) to the data. NA35 shows that agreement can be obtained by adding Bose–Einstein interference for like-charged particles (for a detailed analysis of the influence of BE correlations see further below).

4.2.3.3. Lepton–hadron collisions. In Fig. 4.5(a) EMC data [140] are compared to what is expected from an extrapolation of conventional short- and long-range correlations [108]. At small δy, the data are consistently above these expectations. As Fig. 4.5(b) shows, the slopes ϕ_q in the same data are considerably larger than predicted by the Webber and LUND models. Similarly, Fig. 4.5(c) shows too low $\ln F_3$ from LUND, not only for νNe but also for the "simpler" νD_2 interactions [141].

We tentatively conclude that presently used *lepton–hadron* models as such are unable to reproduce the intermittency observed in this process.

4.2.3.4. e^+e^- *annihilation.* The annihilation of e^+e^- into hadrons is by far the best understood of all multihadron reactions. Creation of hadrons is traditionally pictured as a multistep process comprising a "hard" parton evolution phase, described by perturbative QCD – the parton shower – and a non-perturbative colour-confining soft hadronization phase (Fig. 4.6). The former is a cascade process of nearly self-similar type, and is expected to show characteristics typical of a fractal object [123, 124, 126]. In fact, already in 1979, in a discussion of QCD jets, it was stated [124] that "the resulting picture of a jet is formally similar to that of certain mathematical objects, known as fractals, which look more and more irregular and complex as we look at them with a better and better resolution". The expectation is, therefore, that parton showers should exhibit intermittency at the parton level. However, this is not sufficient to guarantee "intermittency" at the hadron level. It is indeed difficult to imagine how the "re-shuffling" of the parton momenta during the hadronization phase with e.g. the formation of hadronic resonances and their subsequent decay would preserve the (supposedly singular) nature of the correlations. A local parton–hadron duality type of explanation is not satisfactory either, since "it is merely a name for a mechanism that is not at all understood" [165].

To describe the hadronization phase, all present Monte-Carlo codes rely in last instance on a large amount of e^+e^- data at different energies and are carefully tuned to these. It came, therefore, as a surprise that a first (indirect) analysis [133] of HRS results, shortly followed by TASSO data [134], revealed deviations from model predictions quite similar to those observed in lh and hh collisions (Figs. 4.7(a) and (b)). More recently, CELLO [135] and, in particular, the LEP experiments [136–138], claim "reasonable" agreement with the parton shower version of the LUND Monte Carlo (Figs. 4.7(c) and (d)). Nevertheless, new DELPHI data now show, with ten times larger statistics, significant deviations even with a "re-tuned" version of the Monte Carlo (Fig. 4.7(d)).

The origin of intermittency in the models is not quite as clear as is often stated. Indeed, comparison of the factorial moments on parton and hadron level in Figs. 4.8(a) and (b) [166],

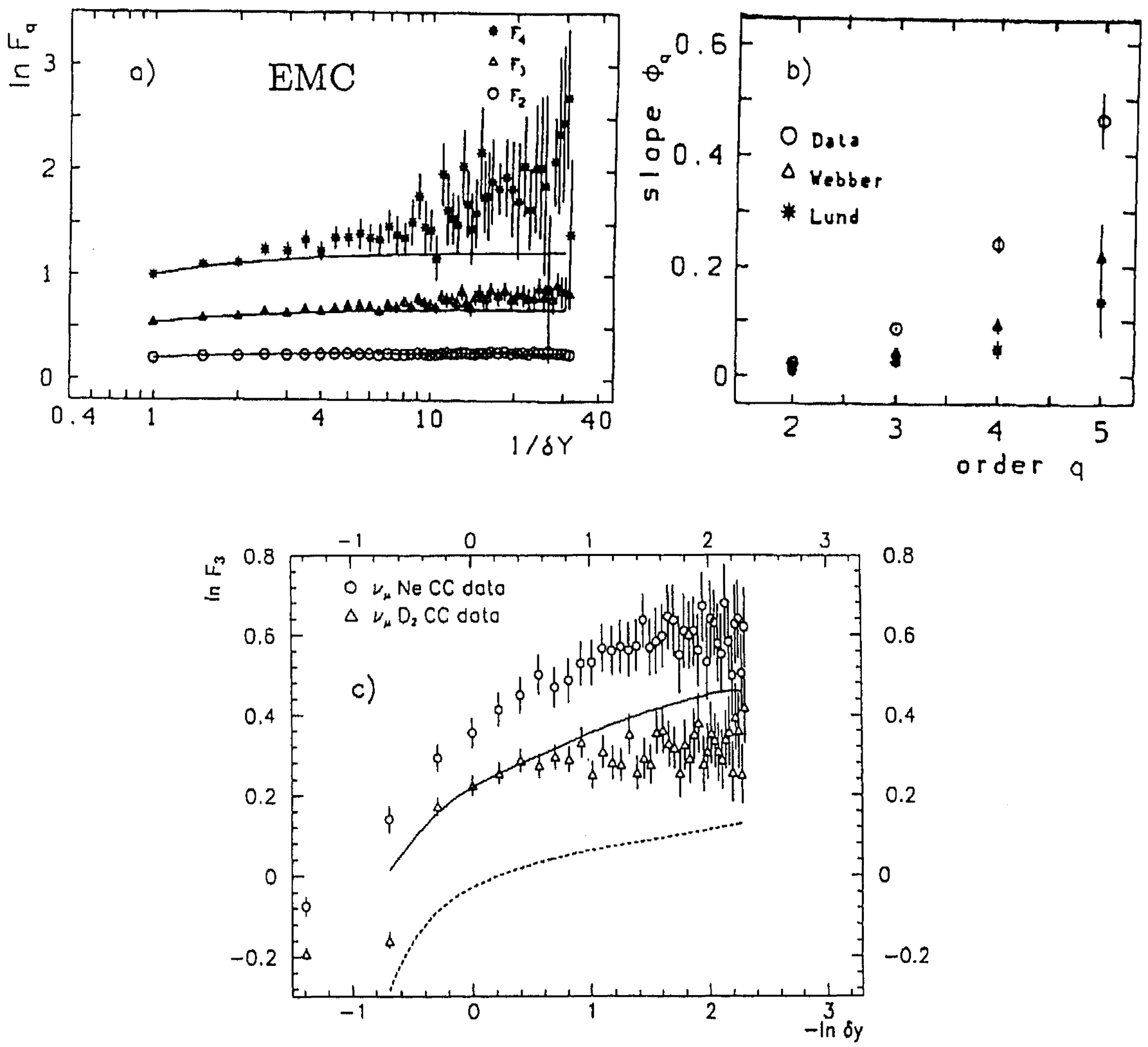

Fig. 4.5. (a) EMC results [140] compared to expectations from [108], (b) slopes ϕ_q for EMC data as well as Webber and LUND models, (c) νA data [141] in comparison to LUND model expectations.

shows that in (standard) JETSET the increase of ln F_q at small δy is not due to the parton shower, but to hadronization! Only if the parton shower is allowed to continue down to very low Q_0^2 values (Fig. 4.8(c) and (d) for $Q_0^2 = 0.4\,\mathrm{GeV}^2$), implying local hadron–parton duality, is intermittency becoming visible also at the parton level. It has been verified that the influence of Q_0^2 is, of course, much less important at 1 TeV.

On the other hand, intermittency seems to be fully developed on the parton level already at 91 GeV in the Webber model, and is in fact smeared out by hadronization [167].

The sensitivity to the cut-off in the perturbative QCD cascade and the role of hard and soft phases has also been discussed in terms of the dipole radiation model [168]. Intermittency

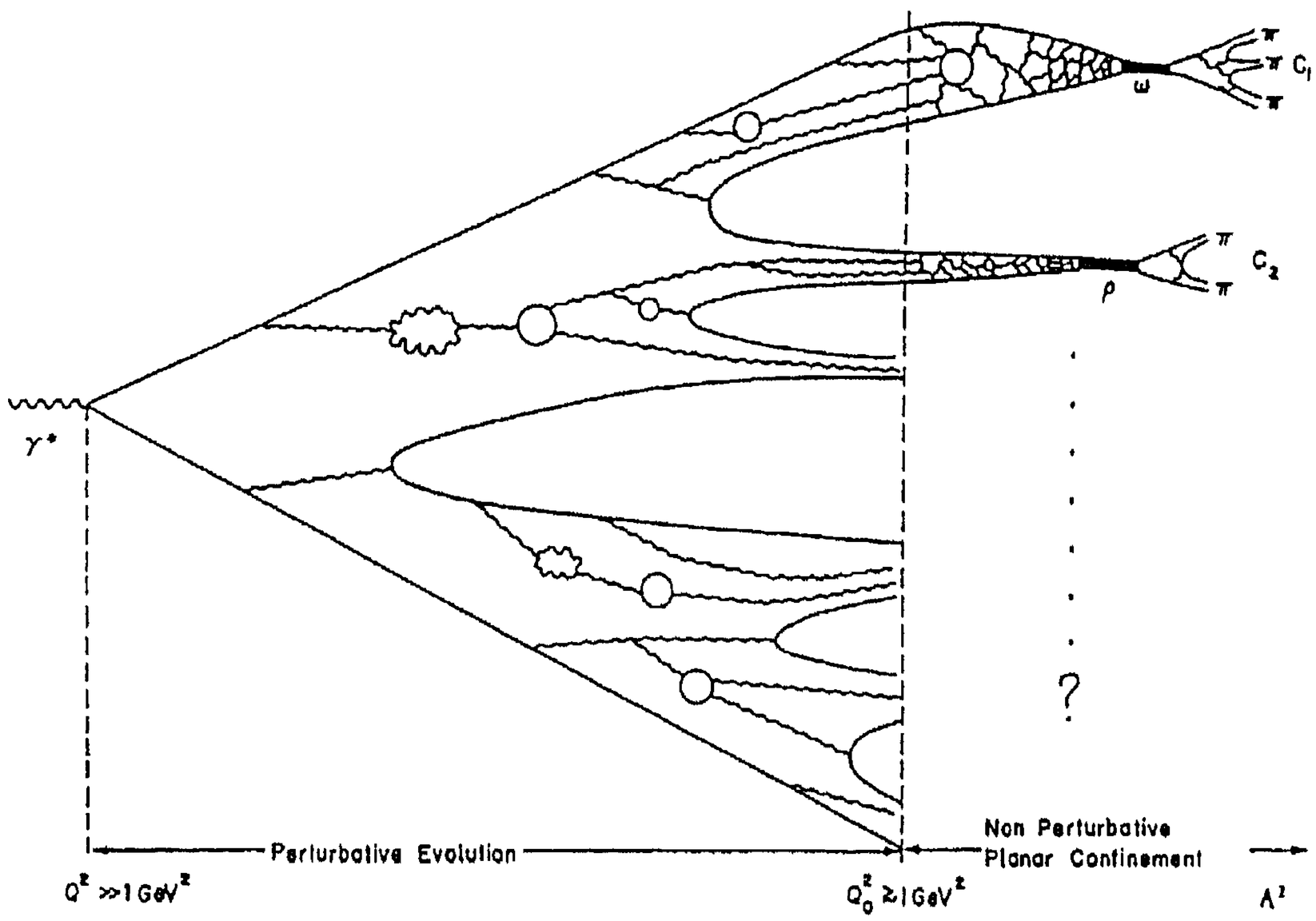

Fig. 4.6. Jet evolution: the self-similarity in the parton cascade derives from the similarity of each step in the evolution [124].

can be increased in the soft phase by an increase of the π/ρ ratio, also required from direct measurements by NA22 [169], EMC [170] and in hA collisions [171]. The direct pions resolve the underlying parton structure better than the more massive resonances. From a tunnelling production mechanism, these pions are expected to have smaller p_T than other particles, a property presently neglected in the MC programs. A Goldstone-like mechanism causing additional soft direct pion production at break-up points has recently been suggested by the LUND group [172].

For further progress, additional studies are needed.

- One should identify the true causes of intermittency in present Monte-Carlo models, preferably on more sensitive distributions, such as those to be discussed below. This should reveal the influence of hard and soft gluon emission at high energies where parton showering is fully developed and dominates over the soft phase.
- Intermittency is also particularly sensitive to the exact treatment of the *soft* phase. This phase can be studied with high statistics at lower energies where parton showering is less important.

4.2.4. *A warning*

Before going into the necessary further detail, we should mention the influence of possible experimental biases. On purpose and by its very definition, the higher factorial moments are

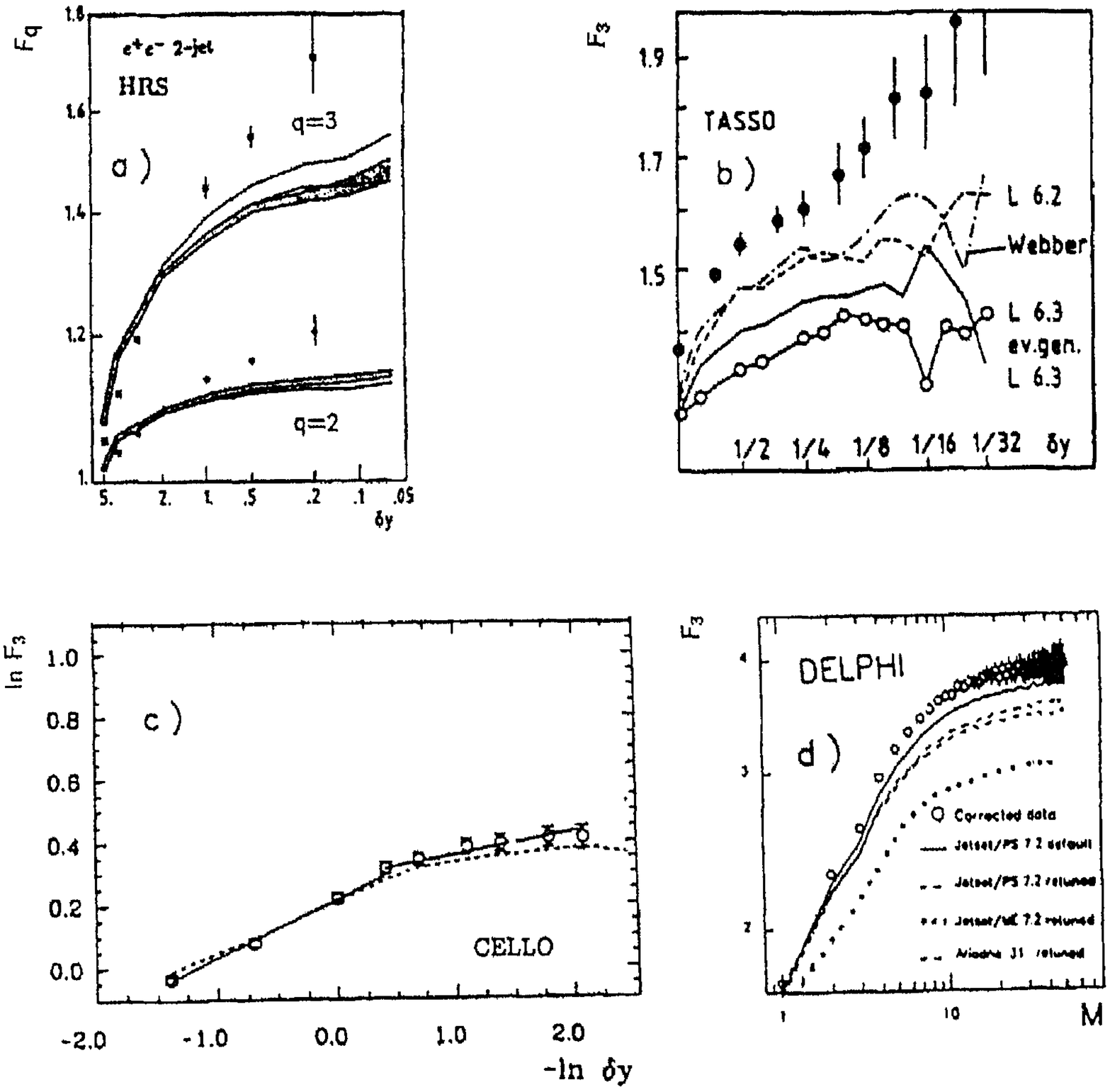

Fig. 4.7. $\ln F_3$ (and $\ln F_2$) as a function of $-\ln \delta y$ (or $\ln M$, $M = \Delta Y/\delta y$) for (a) HRS [133], (b) TASSO [134], (c) CELLO [135] and (d) DELPHI [136] data compared to LUND (and Webber) parton shower models.

sensitive to a small number of events in the tail of the multiplicity distribution in small phase-space bins.

Moments can be *reduced* by limited two-track resolution, by track losses from limited acceptance or bad reconstruction, or simply due to truncation of the multiplicity distribution in a finite event sample.

Moments can be *increased* due to double counting of tracks (track match failures), Dalitz decays and nearby γ conversions or K^0/Λ decays. A dangerous increase comes from the commonly used "horizontal" averaging, where a *constant* average (pseudo-) rapidity distribution is assumed over the range ΔY. Contrary to first belief, this problem is *not* completely solved by the correction method proposed in [23]!

Further influence is to be expected from the choice of the sample e.g. inelastic or non-diffractive, cuts on multiplicity, cuts on p_T, all events or only those with $n \geq n_0$ in ΔY, etc., the size and position of ΔY, the δy region chosen for the fit and the correlation of errors.

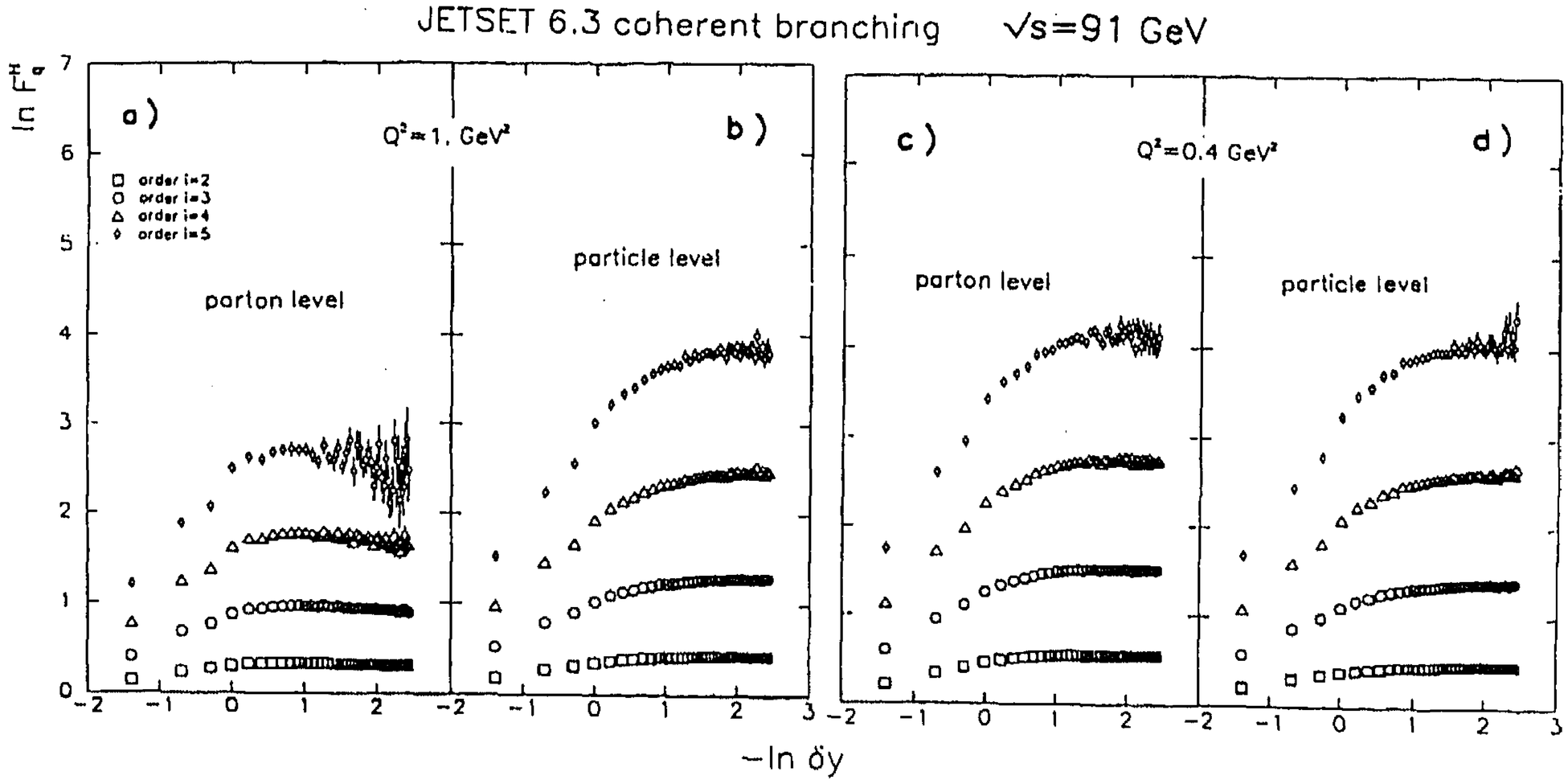

Fig. 4.8. $\ln F_q^H$ as functions of $-\ln \delta y$ for JETSET 6.3 parton shower at $\sqrt{s} = 91$ GeV at the (a) parton, (b) hadron level, both with cut-off $Q_0^2 = 1$ GeV^2, (c), (d) with cut-off $Q_0^2 = 0.4$ GeV^2 [166].

Many of these effects have been studied in a number of experiments and we refer to these and to [173, 174] for more details.

4.3. Higher dimensions

4.3.1. The projection effect

So far, we have discussed factorial moments derived from one-dimensional distributions in rapidity or pseudorapidity. The analysis can evidently be extended to other 1D variables, such as the azimuthal angle φ in the plane perpendicular to the beam or event axis, or the particle transverse momentum (p_T). Given sufficient statistics, distributions can be analysed in two- and three-dimensional phase-space domains. Common choices are $(\Delta y, \Delta\varphi)$, $(\Delta y, \Delta \ln p_T)$, $(\Delta\varphi, \Delta \ln p_T)$ and $(\Delta y, \Delta\varphi, \Delta \ln p_T)$.

Fig. 4.9(a) gives an example of 1D results from UA1 [143] showing that intermittency is also present in φ. The intermittency effect is larger when two-dimensional cells $(\Delta y, \Delta\varphi)$ are studied than in 1D (Fig. 4.9(b) and (c)). This is particularly pronounced in e^+e^- annihilations (Figs. 4.10(a) and (b)), the measured slopes ϕ_q being about six times larger in 2D than in 1D. These observations are now understood to imply that intermittency "lives in 3D" [24, 175]. Projection onto lower-dimensional subspaces dilutes the effect and leads to flattening of the factorial moments. This is most pleasantly demonstrated by the fact that one can enjoy a continuous (two-dimensional) shadow of a tree, in spite of the self-similar branching of this tree in three dimensions.

The projection-effect is convincingly illustrated in Figs. 4.10(a) and (b). The lines in Fig. 4.10(a) are fits by a 2D α model; the curves in Fig. 4.10(b) are the projections onto rapidity-space and show

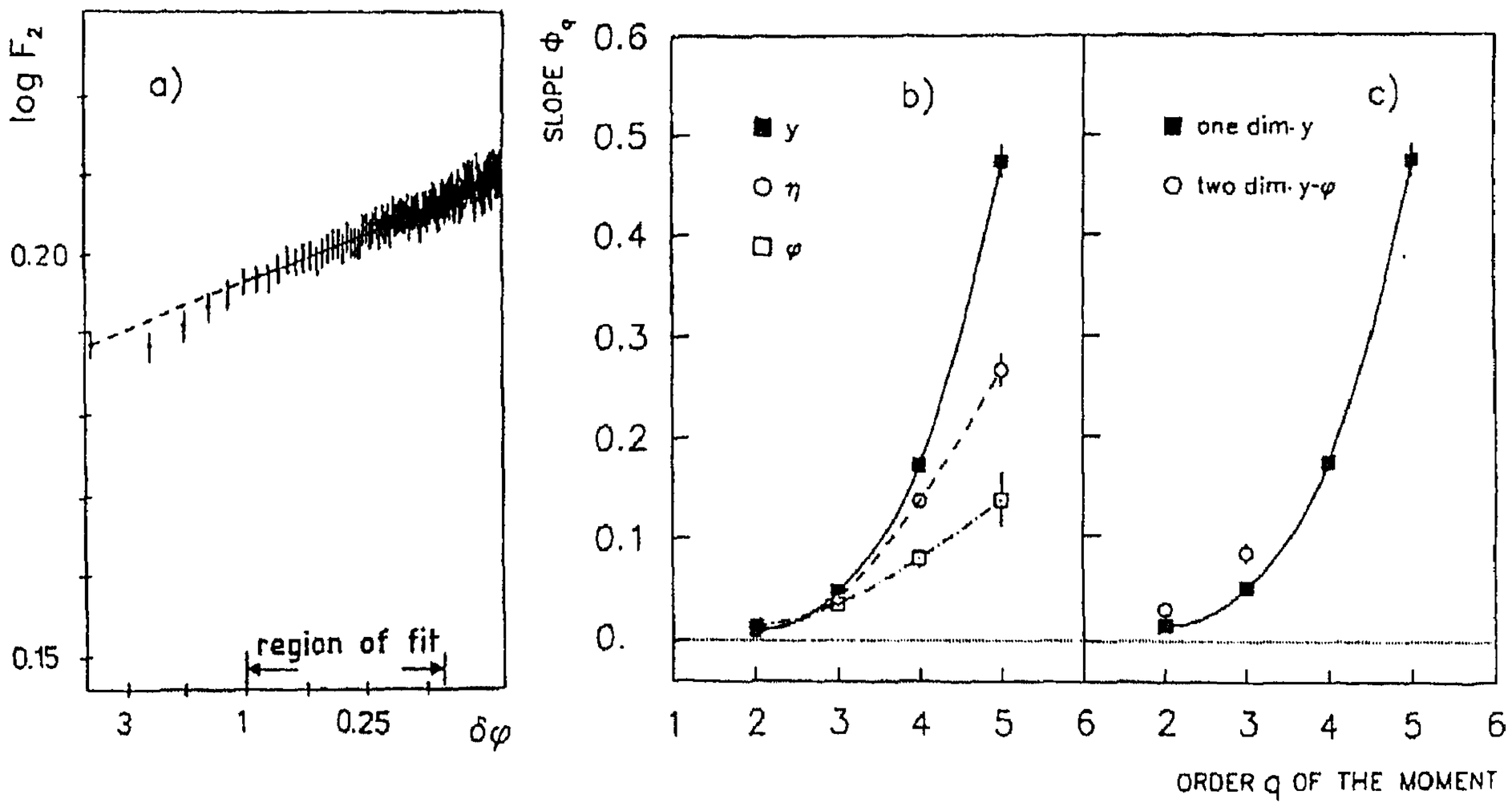

Fig. 4.9. (a) $\log F_2$ as a function of $-\log\delta\varphi$ for UA1 data [143]; (b), (c) slope ϕ_q as a function of order q for y, η, φ or (y and φ) as variables for NA22 [142].

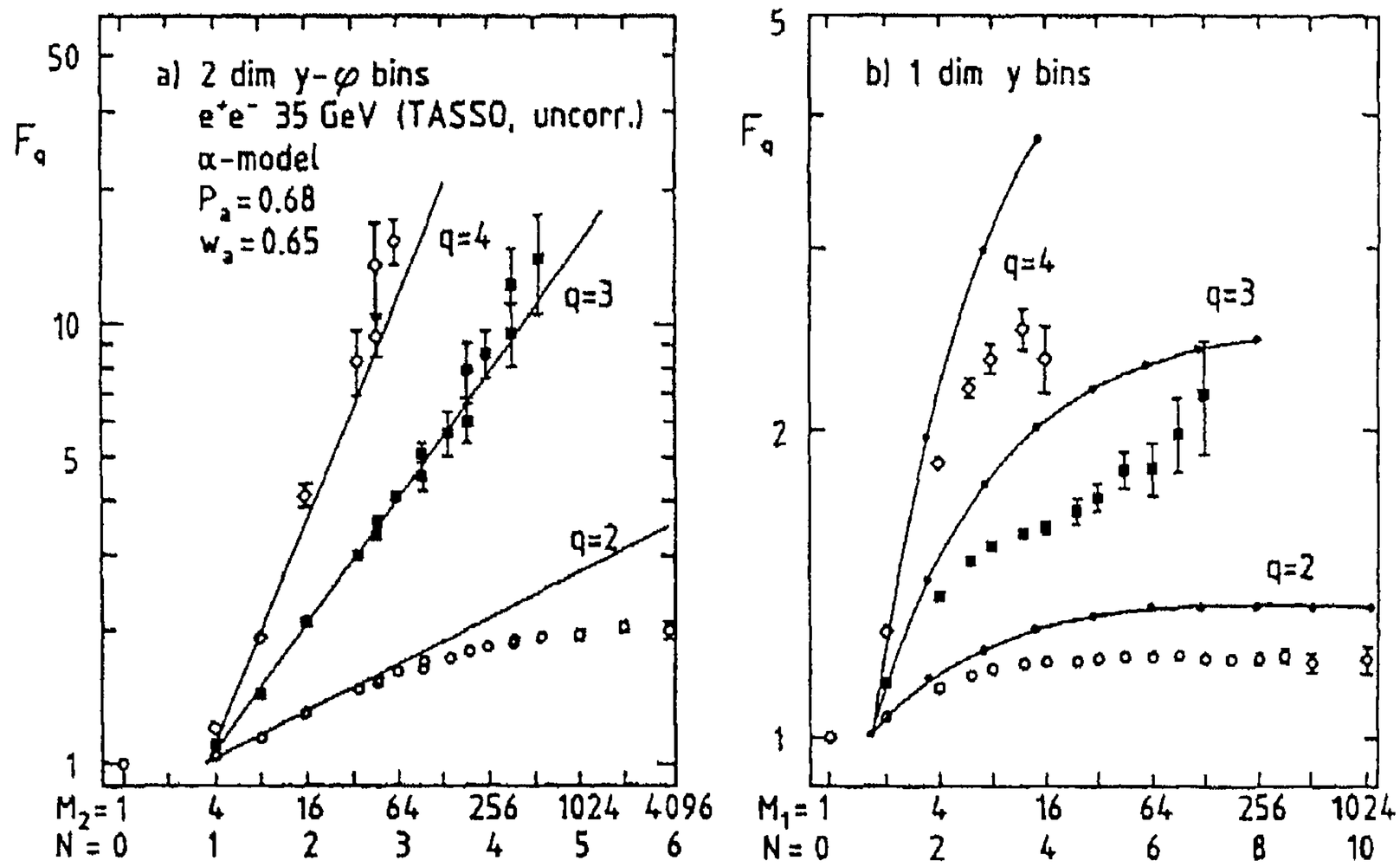

Fig. 4.10. The log–log plot for TASSO data using (a) two-dimensional y–φ bins, (b) one-dimensional y bins, in comparison to a two-dimensional α-model [134, 24].

considerably less increase and even a flattening for $\delta y \to 0$ (note the difference in scale). Nevertheless, Fig. 4.10(a) still shows saturation of F_2 at large M even in 2D, an indication that an analysis in three dimensions may be required.

4.3.2. Transformed momentum space

To study intermittency in three-dimensional phase space, one faces the additional difficulty that the particle density is all but uniform in the usual single-particle variables y, φ and p_T. The distribution in p_T is in fact falling exponentially. Uniformity of the density is, however, an explicit assumption in the derivation of the power law (2.110). Violation of this condition renders an intermittency analysis useless.

To circumvent this problem, the authors of [24, 25] have proposed to use domains in a transformed momentum space with (almost) constant density. This is accomplished by a transformation of the original variables y, φ and $\ln p_T$ to "cumulative" variables. Thus, for a single variable, say y, one defines the new variable $X(y)$ as

$$X(y) = \frac{\int_{y_{min}}^{y} \rho_1(y')\,dy'}{\int_{y_{min}}^{y_{max}} \rho_1(y')\,dy'} . \tag{4.2}$$

For higher dimensions, it is assumed in [24] that the single particle density factorizes as

$$\rho_1(y, \varphi, p_T) = \rho_a(y)\rho_b(\varphi)\rho_c(p_T) . \tag{4.3}$$

Under this rather strong hypothesis, one can transform each of the three variables independently. The method proposed in [25] does not assume factorization but is technically quite involved. In practice, the two techniques give satisfactorily similar results [176].

Data on F_2 in various dimensions are shown in Fig. 4.11 for e^+e^- [136] and hh collisions [142, 143]. In all cases, the data behave more power-like in 2D than in 1D. From Fig. 4.11(a), it is also evident that JETSET PS remains in good agreement with e^+e^- data in higher dimensions.

At variance with power-like behaviour expected from intermittency, NA22 finds that the 3D factorial moments show an upward bending (Fig. 4.11(c)). This effect persists after exclusion of Dalitz decays and γ conversions. A rise faster than power law is also observed in 3D for collisions of various projectiles with Au by NA35 (Fig. 4.12(a)) [150]. Following a suggestion in [177], NA35 finds that the normalized factorial cumulant $K_2 = F_2 - 1$ shows much better linearity in a log–log plot than F_2 itself (Fig. 4.12(b)).

This observation, in fact, furthers considerably our understanding of the intermittency phenomenon. In [177, 178] the author has compared 3D data on F_2 at $\sqrt{s} \simeq 20$ GeV for μp [140], π/Kp [142], pAu, OAu and SAu [150] collisions using the parametrization

$$F_2 = 1 + c(M^3)^{\phi_2} + c' , \tag{4.4}$$

where M^3 is the number of 3D phase-space cells. The second term in (4.4) is equal to K_2. The constant c' accounts for long-range correlations, known to exist in hh collisions.

The comparison of (4.4) to the data is shown in Fig. 4.13; the parameters are given in the figure caption. The parameter c' is negligible for μp and heavy ion collisions, but non-zero for

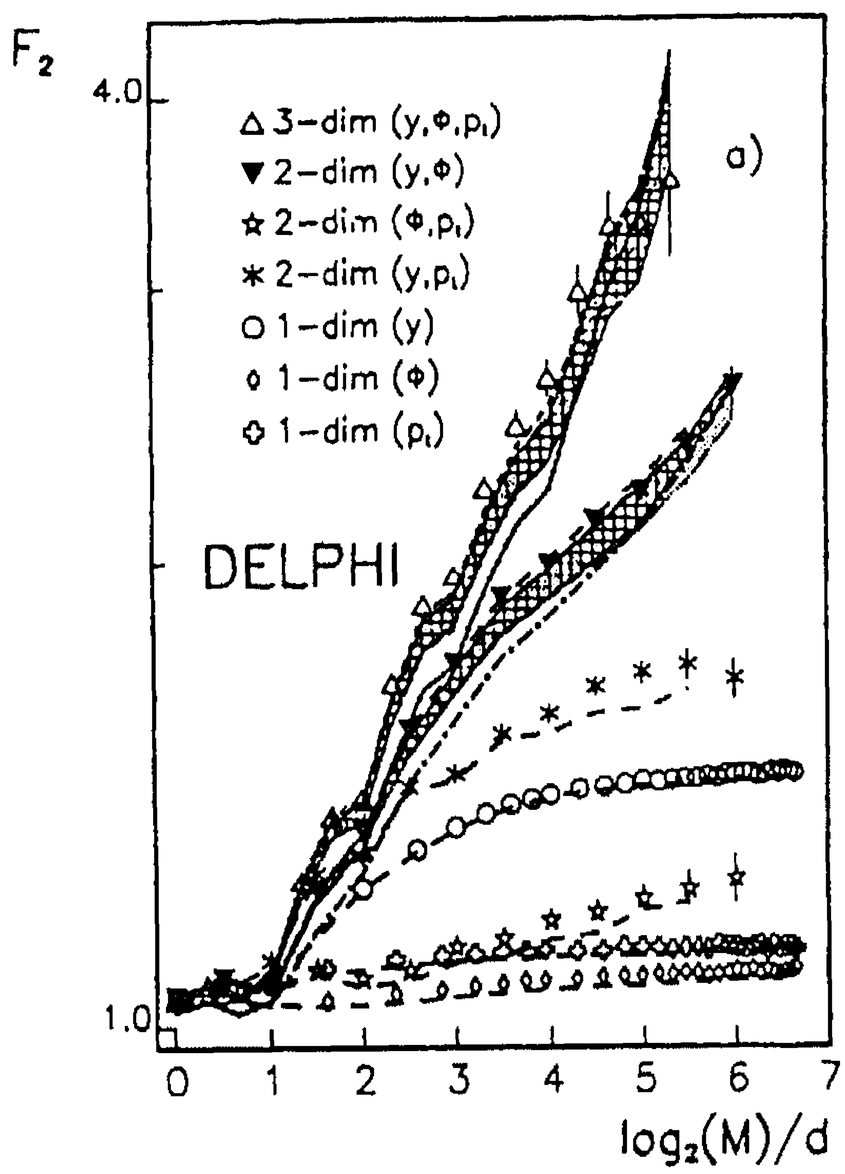

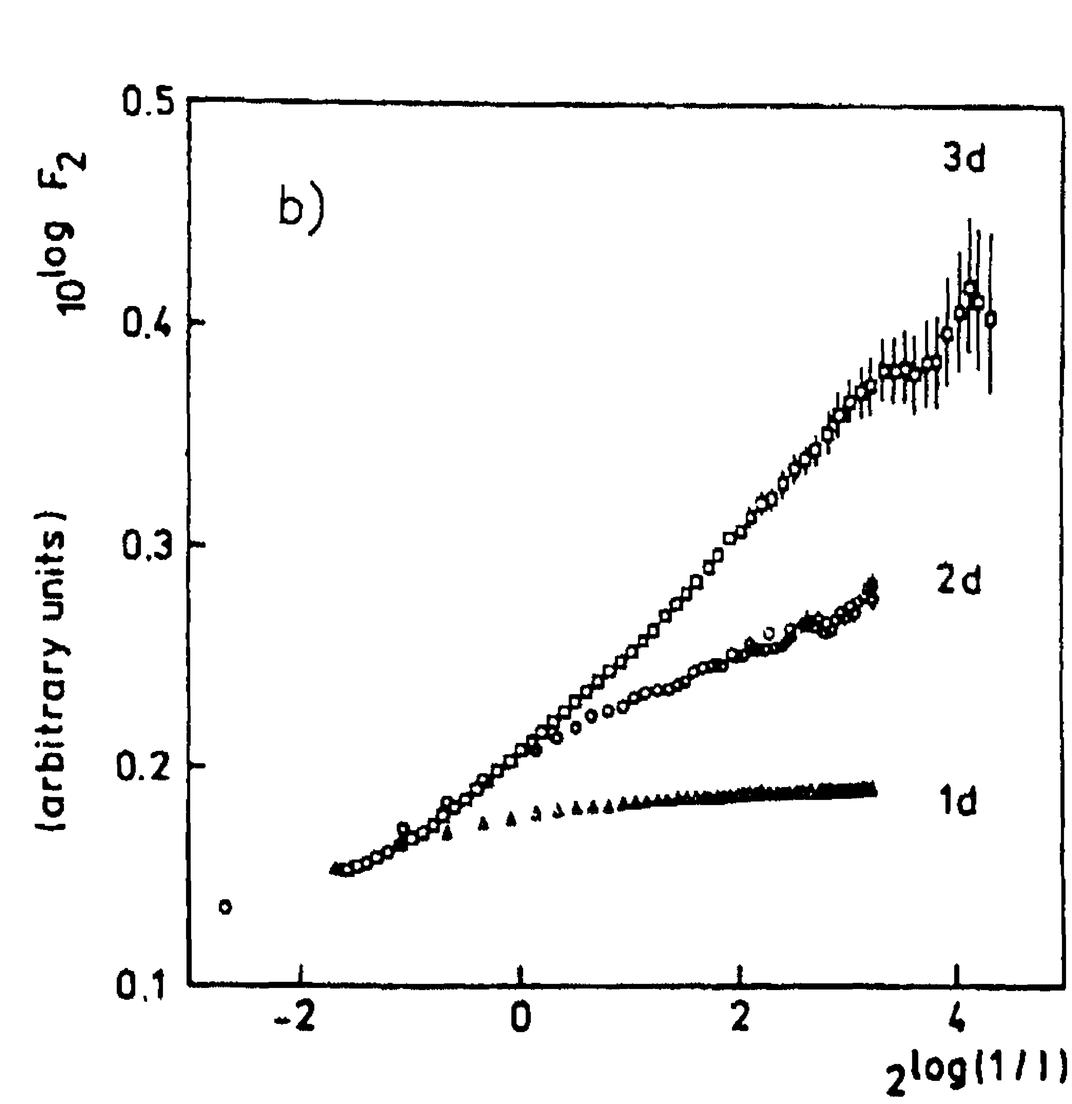

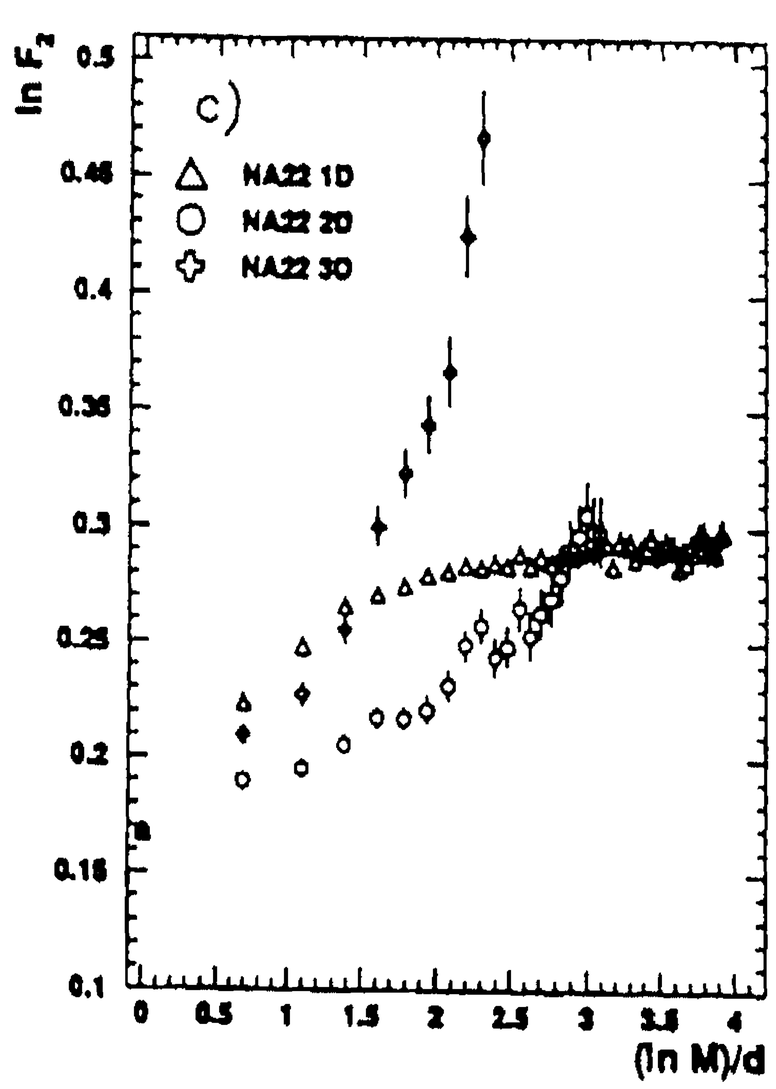

Fig. 4.11. Factorial moment of order $q = 2$ for 1, 2 and 3 dimensional analysis for (a) DELPHI [136], (b) UA1 [143] and (c) NA22 [142] as a function of $(\log_2 M)/d$ and $(\ln M)/d$, respectively, where M denotes the total number of boxes in a d-dimensional analysis.

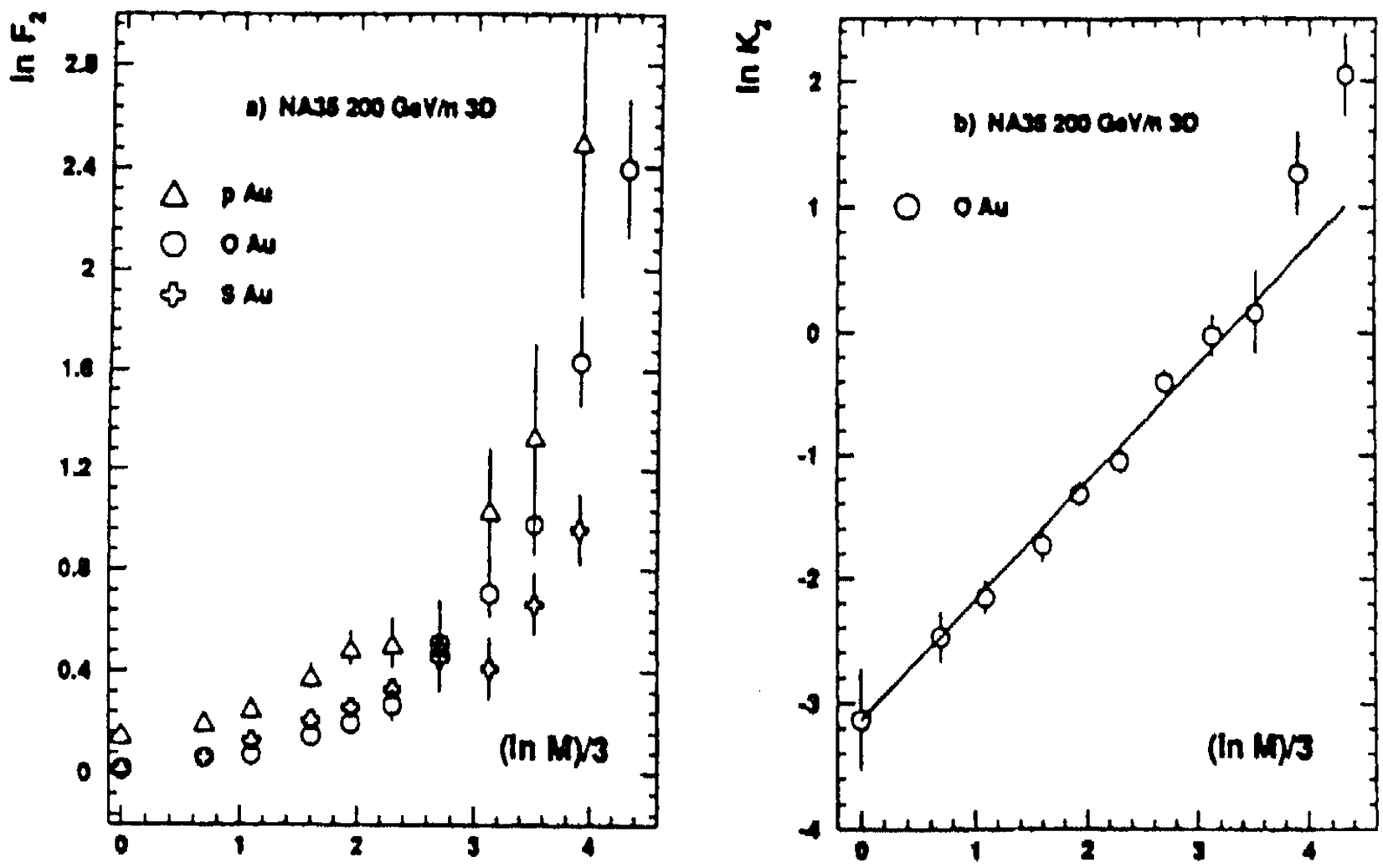

Fig. 4.12. (a) Factorial moment ln F_2 as a function of (ln M)/d from a three-dimensional analysis of negative particles in pAu and central OAu and SAu collisions [150]; (b) Factorial cumulant K_2 from the same analysis in central OAu collisions [150].

meson–proton and pA collisions, in agreement with expectations. The most noteworthy result, however, concerns ϕ_2, which is seen to have a value in the range 0.4–0.5 for all processes. This is remarkable in various respects.

Firstly, if confirmed in further studies, and in particular for e^+e^- annihilation, it strongly suggests that the resolution dependence of F_2 exhibits a high degree of "universality", is independent of specific details of the production process and thus reflects general features of hadronization dynamics.

Secondly, such universality is at variance with the hitherto accepted idea that the factorial moments and the anomalous dimensions become smaller the more complex the collision process, due to an increasing inter-mixing of production sources [131].

Thirdly, if "universality" continues to hold in high energy e^+e^- annihilation, one must revise the commonly expressed opinion that the perturbative parton evolution, and in particular hard-jet emission, is the primary cause of the rise of factorial moments at high resolution. Needless to say, it would be most interesting to verify systematically the universality conjecture in other reactions and for three-particle correlations.

The experimental success of expression (4.4) becomes quite intriguing when one realizes that the volume $\delta \sim M^{-3}$ of a phase-space cell (for sufficiently large M) is in fact related to the invariant mass M_{inv} of the two-particle system or to Q^2, the square of their four-momentum difference. The form (4.4) implies that the two-particle correlation function behaves as a power law in M_{inv} or Q^2. The data, therefore, seem to tell that an intermittency analysis should be performed in

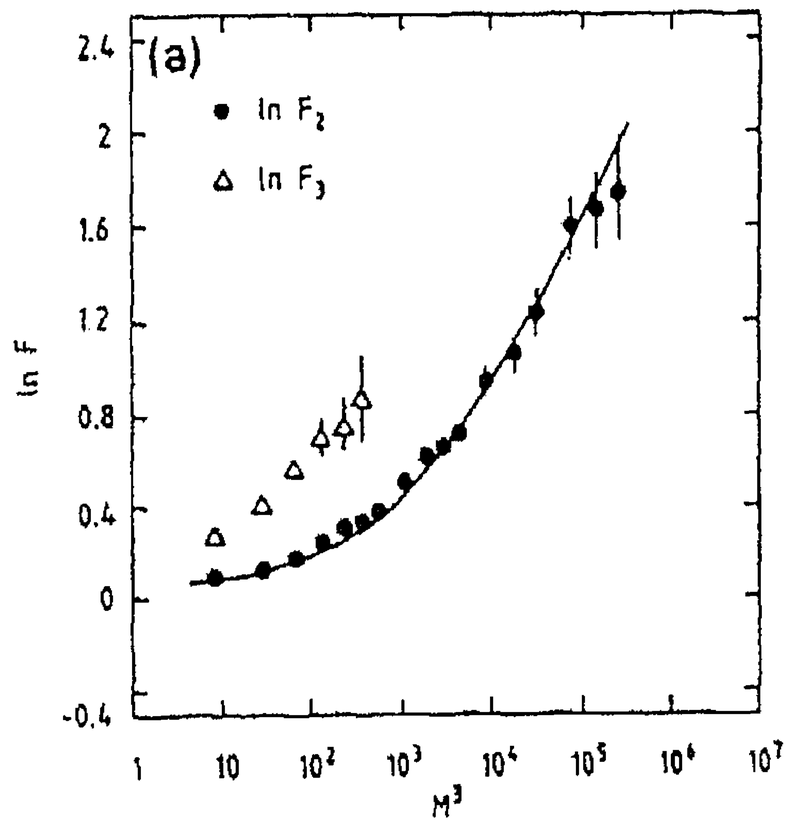

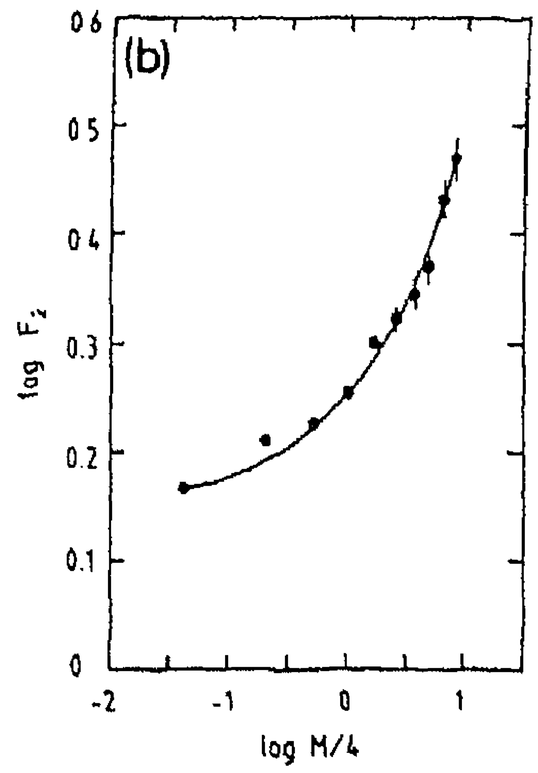

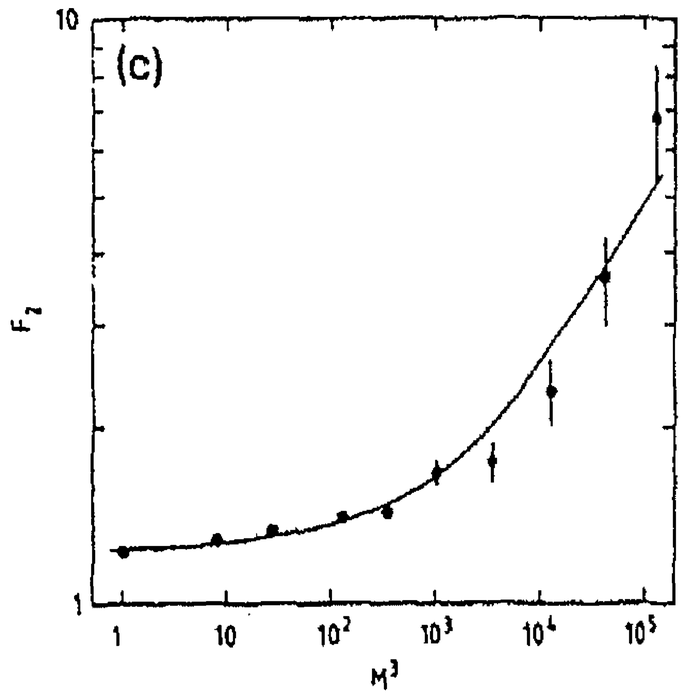

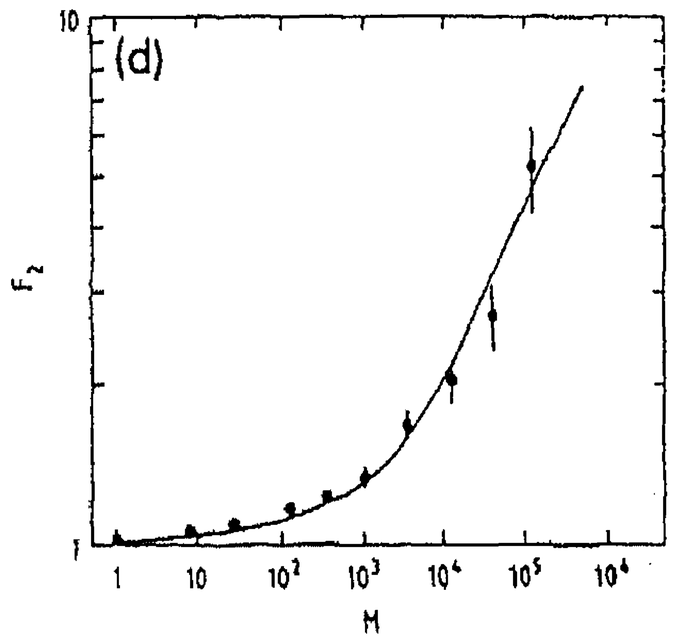

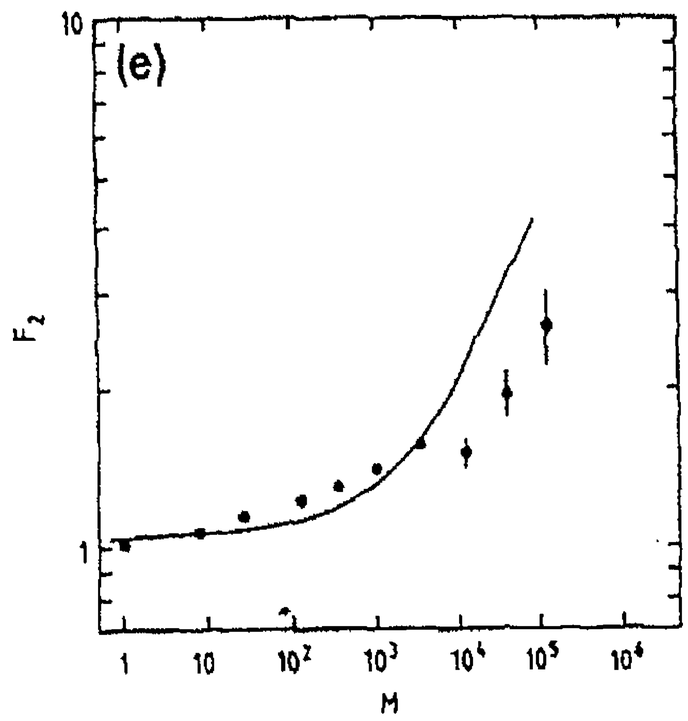

Fig. 4.13. The second scaled factorial moment F_2 as a function of the number of bins M^3 in the log–log scale [177] for (a) μp data [140], (b) π/Kp data [142], (c) pAu, (d) OAu and (e) SAu data [150]. Solid lines represent (4.4) with parameter values: (a) $c = 0.025$, $\phi_2 = 0.45$, $c' = 0$; (b) $c = 0.02$, $\phi_2 = 0.45$, $c' = 0.16$; (c) $c = 0.02$, $\phi_2 = 0.45$, $c' = 0.2$; (d) and (e) $c = 0.01$, $\phi_2 = 0.5$, $c' = 0$.

(Lorentz-invariant) multiparticle variables, rather than single-particle variables. This will be further discussed in Sections 4.8–4.10.

As mentioned in Section 4.2.3 above, ECCO [164] has some success in describing the NA22 data on fluctuations in varying scales of resolution, in particular when the analysis is done in three dimensions (Fig. 4.14). The basis of this model is geometrical branching for soft production at low p_T. The geometrical aspect of hadrons, i.e. the fact that they are extended objects, puts the impact parameter R in a pre-eminent role. The fluctuation in R from event to event leads to fluctuations in p_T and explains the non-vanishing intermittency in $\ln p_T$ reported by NA22. The (stronger) intermittency in rapidity can be generated only with a singular splitting function for branching in rapidity space. Since there is no branching in φ in the model, intermittency is nearly non-existent in this variable. Still, the long-range correlation due to p_T conservation leads to a decrease of F_q at large bin size, a feature also observed by NA22.

4.3.3. A generalized power law

It has been pointed out [179] that the one-dimensional moments follow the generalized power law

$$F_q \propto (g(\delta y))^{\phi_q} , \tag{4.5}$$

in multiplicative cascade models. In (4.5), $g(\delta y)$ is a general function of δy. Expressing g in terms of F_2, one finds the linear relation

$$\ln F_q = c_q + (\phi_q/\phi_2) \ln F_2 , \tag{4.6}$$

from which the ratio of anomalous dimensions is directly obtained. This intriguing relation has successfully been confirmed by experiment, not only in one dimension, but up to 3D [24]. Moreover, the ratios ϕ_q/ϕ_2 are found to be largely independent of the dimension of phase space (Fig. 4.15(a)) and of the type of collision (Fig. 4.15(b)).

The ratio of the anomalous dimensions $d_q(=\phi_q/(q-1))$ and d_2 are shown in Fig. 4.16(b) as a function of q. The q dependence is claimed to be indicative of the mechanism causing intermittent behaviour. For a (multiplicative) cascade mechanism, in the log-normal approximation (long cascades), the moments satisfy the relation [21,22]

$$\frac{d_q}{d_2} = \frac{\phi_q}{\phi_2} \frac{1}{q-1} = \frac{q}{2} . \tag{4.7}$$

However, the use of the Central Limit Theorem for a multiplicative process, such as in the α-model, is a very crude approximation [180] particularly in the tails. As argued in [181], a better description might be obtained if the density probability distribution is assumed to be a log-Lévy-stable distribution, characterized by a Lévy index μ. In that case (4.7) generalizes to

$$\frac{d_q}{d_2} = \frac{1}{2^\mu - 2} \frac{q^\mu - q}{q-1} . \tag{4.8}$$

For $\mu = 2$, the Gaussian case, (4.8) reduces to (4.7).

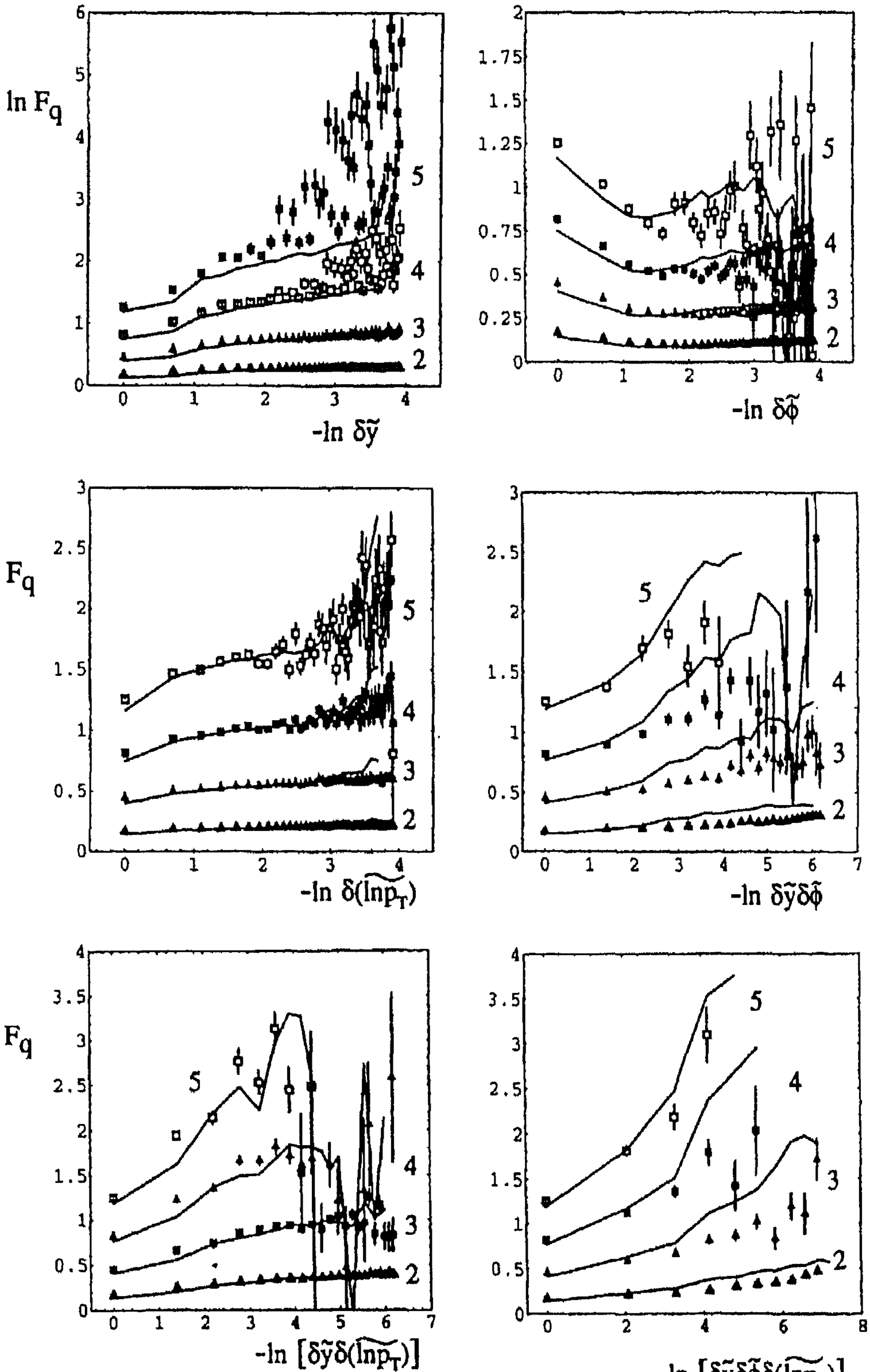

Fig. 4.14. The factorial moments $\ln F_q$ for NA22 [142] in various variables and dimensions indicated, as compared to ECCO [164].

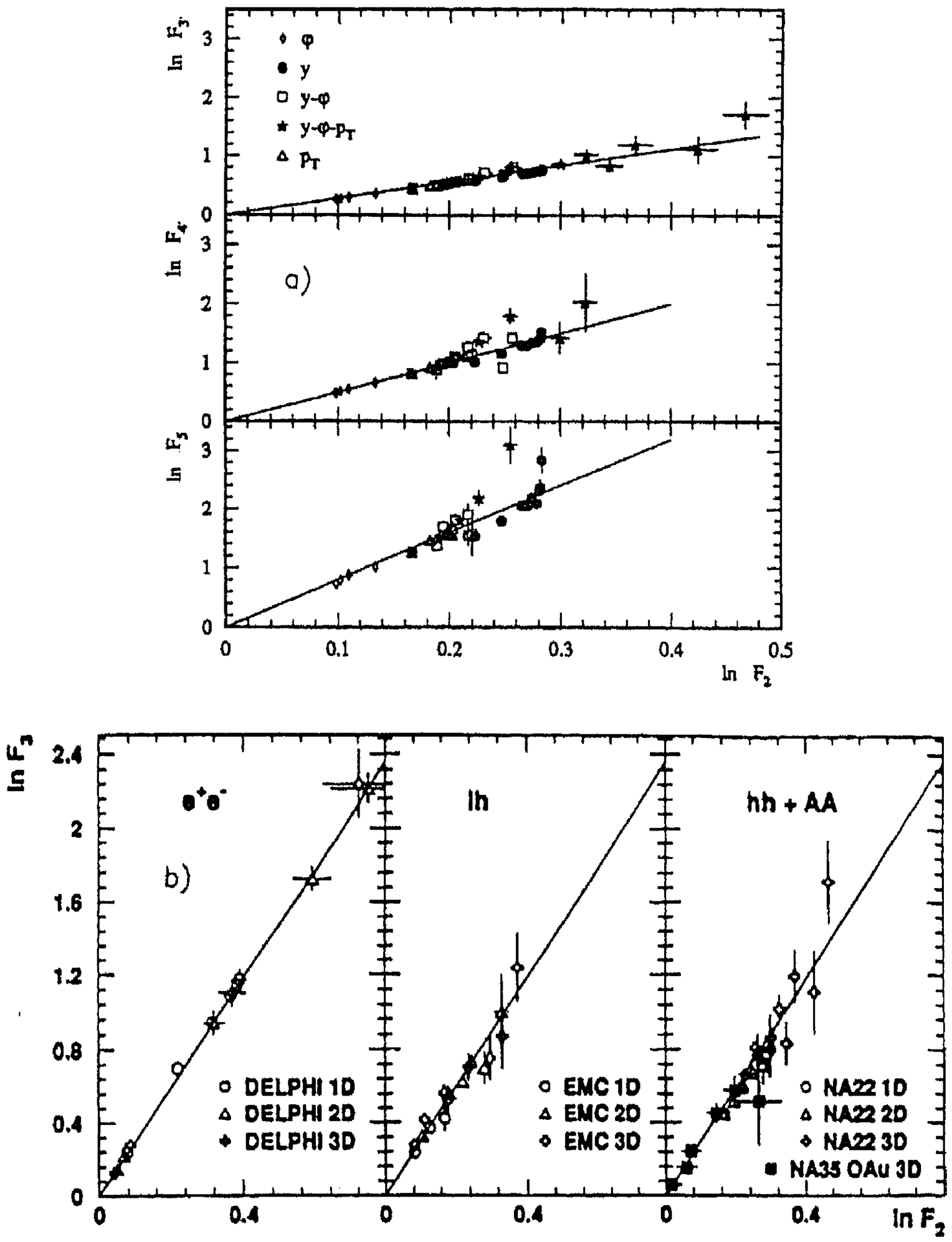

Fig. 4.15. (a) Illustration of the modified power-law behaviour. The lines indicate an "eye-ball" fit to the data. Only the data in bins where F_2 varies strongly are used; (b) Test of the universal scaling law (4.6) for ln F_3 and ln F_2 in e^+e^-, lh, hh and AA collisions as indicated. The straight line is adjusted to the e^+e^- data and reproduced on the other data sets [24].

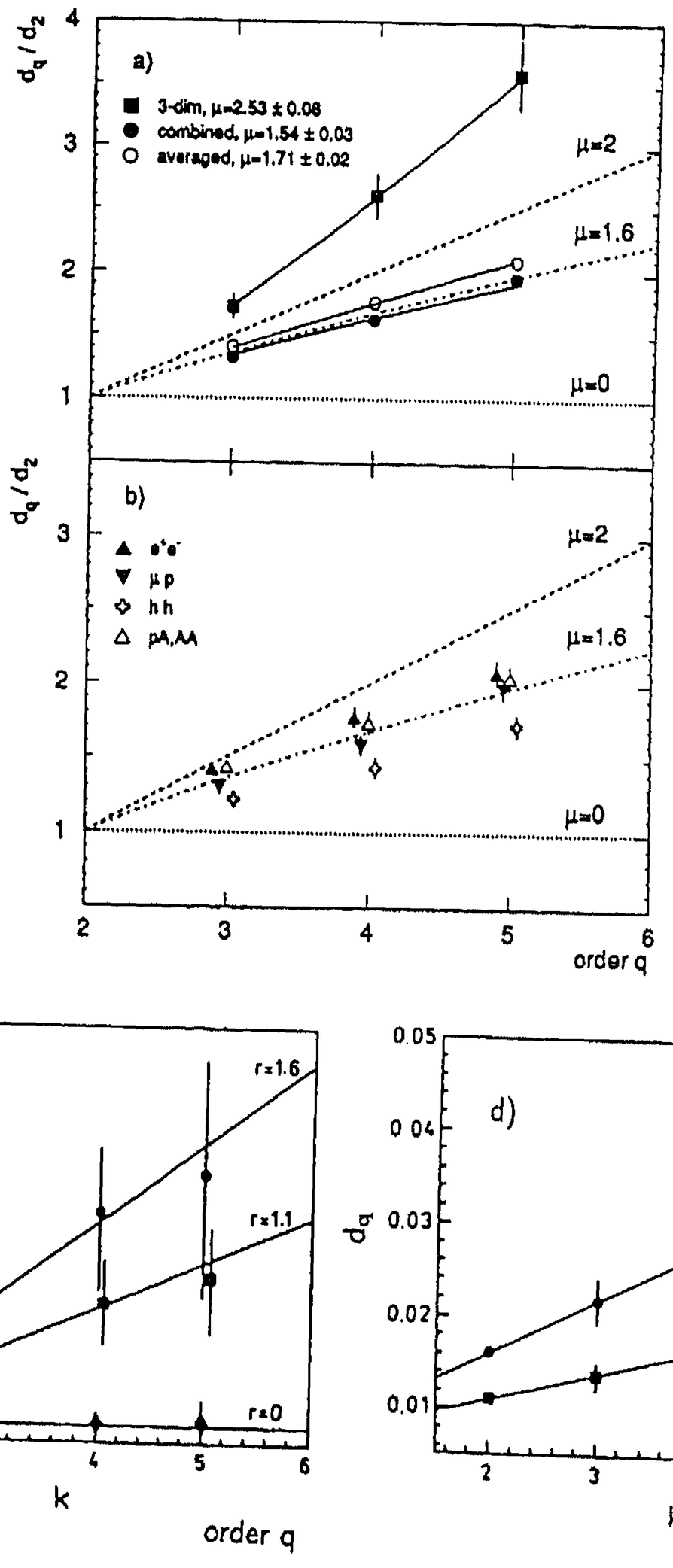

Fig. 4.16. Ratio of anomalous dimensions as a function of the order q for (a) NA22 results [142] and (b) earlier results on all types of collisions [24], (c) and (d) d_q as a function of the order q. Continuous lines in (c) and (d) show the best fits using (2.134) (c) ●– Z^0 decay, DELPHI, $r = 1.6(8)$, ■– p-Ag/Br, KLM, $r = 1.1(5)$, ◆– S-Ag/Br, KLM, $r = 0.0(2)$; (d) ●– O + Ag/Br, KLM, $r = 0.7(2)$, ■– $p\bar{p}$, UA1, $r = 0.5(3)$ [52].

The multifractal behaviour characterized by (4.7) and (4.8) reduces to a monofractal behaviour [182, 183]

$$d_q/d_2 = 1 \tag{4.9}$$

for $\mu = 0$, implying an order-independent anomalous dimension. This would happen if intermittency were be due to a second-order phase transition. Consequently, monofractal behaviour might be a signal for a quark–gluon–plasma phase transition.

The data are best fitted with the Lévy-law solution with $\mu = 1.6$. This value is inconsistent with the Gaussian approximation, and also definitely higher than expected for a second-order phase transition.

The validity of the dimension-independent generalized power behaviour has been questioned in a recent NA22 analysis [142] shown in Fig. 4.16(a). While a fit to the combined data on all variables and dimensions (full circles), as well as a weighted average over all individual fits give μ values in rough agreement with those of [24], the 3D data have $\mu > 2$, not allowed in the sense of Lévy laws.

Even larger values of μ, ranging from 3.2 to 3.5, have been found for μp deep-inelastic scattering in [181]. According to [50, 51], this is evidence that the procedure to obtain the Lévy index is used outside its domain of validity. An allegedly more general method, based on Double Trace Moments (to be discussed in Section 4.7.7) indeed yields μ values within the mathematically allowed boundaries. However, we shall see that the latter method may be criticized on other grounds. A possible way out is self-affinity to be discussed in Section 4.3.5.

The linear d_q/d_2 behaviour in Figs 4.16(a) and (b) gives some justification for (2.134). Figs. 4.16(c) and (d) show [52] the slope r of (2.134) for a number of experiments. All experiments, except perhaps SAg/Br, show multifractal behaviour ($r > 0$).

Despite the confusion, it remains a noteworthy experimental fact that the factorial moments of different orders obey simple hierarchical relations of the type (4.6). This means that correlation functions of different orders are not completely independent but are somehow interconnected. Such situations are commonly encountered in various branches of many-body physics (see e.g. [107, 109, 184]), but a satisfactory link with particle phenomenology, let alone QCD, remains to be established. Nevertheless, on a simple example it was recently shown [185] that a linear relation between $\ln F_3$ and $\ln F_2$ can be obtained if the connected correlation functions are assumed to be of a factorized Mueller–Regge power-law form in two-particle invariant-masses squared s_{ij}, i.e. $C_3(1,2,3) \propto (s_{12})^{1-\alpha_1}(s_{23})^{1-\alpha_2}$ + cycl. perm. Note that this Regge-form has the "linking" structure of (3.13).

4.3.4. Thermal versus non-thermal phase transition

4.3.4.1. Second order phase transition? A simple model that can provide some hint on the nature of a second-order phase transition is the Ising model in 2D [186]. Its intermittency behaviour has been studied both analytically and numerically [182, 187]. The anomalous dimension is found to be $d_q = \frac{1}{8}$, independent of q. Based on that finding, it has been conjectured that intermittency may be monofractal if due to a QCD second-order phase transition [183]. However, as mentioned in Section 4.3.3, all types of interactions, including heavy-ion collisions, show multifractal behaviour.

Of course, the Ising model is very simple and the above conjecture has little basis. In [188], intermittency is, therefore, studied in the framework of the Ginzburg–Landau theory also used to describe the confinement of magnetic fields into fluxoids in a type II superconductor. In the model, the anomalous dimension is not constant, but follows

$$d_q/d_2 = (q-1)^{\nu-1}, \quad \nu = 1.304\,, \tag{4.10}$$

with ν being a universal quantity valid for all systems describable by the GL theory, independent of the underlying dimension or the parameters of the model. This is of particular importance for a QCD phase transition, since neither the transition temperature nor the other important parameters are known there.

In quantum optics, γ production at the threshold of lasing is describable as a second-order phase transition. Indeed, a photo-count experiment [189] has verified (4.10) to high precision. On the other hand, the current NA22 data on particle production in hadronic collisions give $\nu = 1.45 \pm 0.04$ [190], heavy-ion experiments $\nu = 1.55 \pm 0.12$ [188] and $\nu = 1.459 \pm 0.021$ [156].

For a first-order phase transition, all d_q are zero and no intermittency would be observed [183]. However, it has been shown in [191] that in a generalized GL model, a first-order phase transition combined with the quantum optics analogy of lasing at threshold can lead to intermittency behaviour in some regions of the parameters, with approximately the same intermittency indices as a second-order phase transition.

4.3.4.2. Non-thermal phase transition? Of course, the phase transition does not need to be thermal, i.e. the new phase need not be characterized by a thermodynamical behaviour. Such a transition could, e.g. take place during a parton-shower cascade and has been formulated in [192] for a number of "ultra-soft" phenomena, including intermittency. It leads to the co-existence of different phases, in analogy to different phases of the spin-glass systems. The examples of the JACEE event (Fig. 4.1(a)), which contains many "spikes" and "holes", and that of the NA22 event (Fig. 4.1(b)), which consists of just one spike, indicate that such a possibility may be more than just a speculation.

The condition for the existence of such different phases of a self-similar cascade is that the function

$$\lambda_q = (\phi_q + 1)/q \tag{4.11}$$

has a minimum at some value $q = q_c$ (not necessarily an integer) [45, 193–195]. The regions $q < q_c$ and $q > q_c$ are dominated by numerous small fluctuations and rare large fluctuations, respectively. In the terminology of [195], the system resembles a mixture of a "liquid" of many small fluctuations and a "dust" of high density. We see either the liquid or the dust phase, depending on whether we probe the system by a moment of order $q < q_c$ or $q > q_c$, respectively.

In Fig. 4.17(a), λ_q is compiled [195] from KLM, EMC and NA22 as a function of the order q. The low p_T NA22 data [142] ($p_T < 0.15$ GeV/c) indeed show a marked minimum with q_c between 3 and 4, while the uncut data have not saturated at $q \leq 5$. Following [195], the λ_q behaviour has been studied by a number of heavy-ion experiments [153, 154, 156, 159]. While a saturation, but no clear minimum is seen by experiments stopping their analysis at $q = 5$ or 6, a minimum is now observed for $4 < q_c < 5$ in central C–Cu collisions at 4.5 A GeV/c, where the analysis is carried to $q = 8$ [159] (Fig. 4.17(b)).

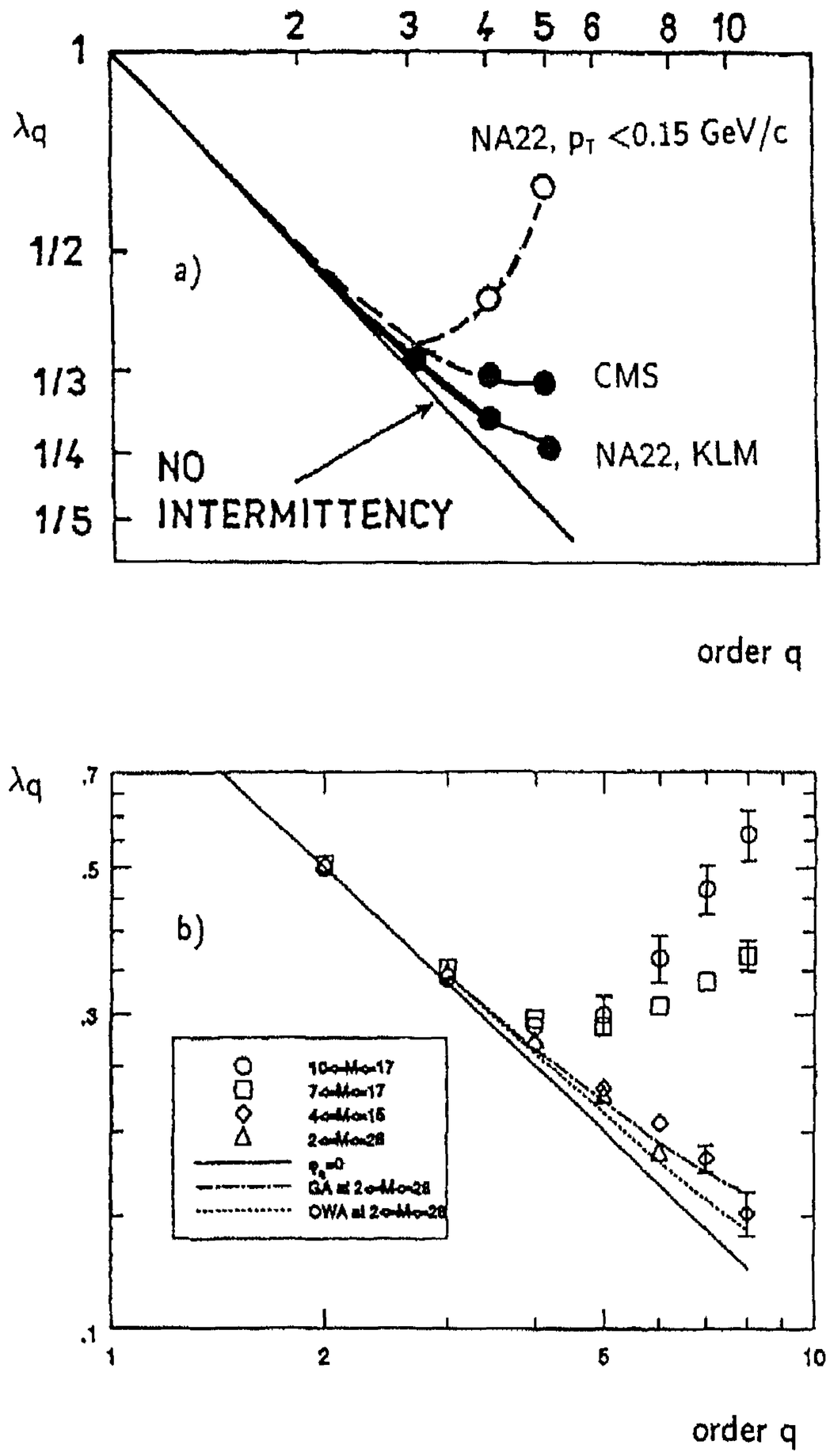

Fig. 4.17. λ_q as a function of q for (a) KLM, CMS and NA22 results [195, 142] and (b) central C–Cu collisions at 4.5 A GeV/c [159].

The observation of a minimum in the λ_q-distribution suggests a phase transition [45, 193, 194], but according to the interpretation [195] it is merely the "apparatus" changing from a sensitivity for the dominating small fluctuations at $q < q_c$ to an insensitivity for those at $q > q_c$. The two phases could coexist without a transition being necessary.

So, phase transition or not, two phases seem to coexist and it will be a challenge to find their physical interpretation in terms of the theory of strong interactions.

4.3.5. *Self-affinity*

Comparing log–log plots for one phase-space dimension, one notices that the $\ln F_q$ saturate, but at different F_q values for different variables y, φ or $\ln p_T$. The saturation in one dimension can be explained as projection effect of a three-dimensional phenomenon. However, also in three-dimensional analysis the power law (2.110) is not exact. In Fig. 4.11(c), the 3D data are seen to bend upward.

It has been shown in [196] (see also [197]) that this can be understood by taking the anisotropy of occupied phase space (longitudinal phase space [198]) into account. In view of this phase space anisotropy, also its partition should be anisotropic. In other words, the density fluctuation in phase space should be *self-affine* rather than *self-similar* [199].

If the phase-space structure is indeed self-affine, it can be characterized by a parameter called roughness or Hurst exponent [199], defined as

$$H_{ij} = \ln \lambda_i / \ln \lambda_j \quad (0 \leq H_{ij} \leq 1) \tag{4.12}$$

with λ_i ($i = 1, 2, 3$; $\lambda_1 \leq \lambda_2 \leq \lambda_3$) being the shrinkage ratios in the self-affine transformations

$$\delta x_i \to \delta x_i / \lambda_i \,, \tag{4.13}$$

of the phase-space variables x_i.

The Hurst exponents can be obtained from the experimentally observed saturation curves of the one-dimensional $\ln F_q(\delta x_i)$ distributions. Using the NA22 curves for y and $\ln p_T$ (Fig. 4.11(c)), a Hurst exponent of $H_{y, p_T} = 0.516 \pm 0.015$ is obtained for these two variables, in agreement with self-affinity ($H < 1$) rather than self-similarity ($H = 1$).

The upward bending for F_q in the three-dimensional self-similar analysis is then easy to understand: performing a self-similar analysis, phase space is not shrunk according to the self-affine dynamical fluctuation. So, the real dynamic fluctuation cannot be fully observed and the corresponding F_q comes out smaller at intermediate scales. At very small bins, however, this difference between self-affine and self-similar space shrinkage disappears and the F_q values obtained approach each other. As a consequence, the slope on the log–log plot has to increase at small bin sizes and the self-similar analysis grants an upward bending if the underlying structure is self-affine (i.e. corresponds to a power law).

On a self-affine Monte-Carlo branching model exactly reproducing the NA22 d_q/d_2 values of Fig. 4.16(a), this upward-bending effect is shown to cause the apparent violation of the Lévy stability $\mu \leq 2$ described in Section 4.3.3 [200].

4.4. *Dependences of the effect*

4.4.1. *Charge dependence*

A mechanism known to cause correlations at small distances in phase space is Bose–Einstein interference between identical particles [108, 201, 202]. For reviews of the present status of this field we refer to [203, 204]. From the outset it must be realized, however, that the conventional

Gaussian- or exponential-type parametrizations of the Bose–Einstein effect lead to a saturation at $\delta y \to 0$ and *not* to the power law (2.110)!

In [202] it is argued that the slopes should be roughly a factor 2 larger for identical particles than for all charges combined. The experimental situation is less than clear, in particular for 1D analyses. Contrary to the prediction, TASSO and DELPHI see less intermittency for identical particles. EMC finds an enhanced effect for positive but not much for negative particles in a one-dimensional analysis, and very similar slopes in a 3D analysis. NA22 observes an enhancement for negatives, but not for positives. UA1 sees no difference, whereas NA35 sees an increase.

CELLO finds Bose–Einstein interference necessary to explain the residual difference between data and JETSET 7.2, but needs an un-physically large strength-parameter λ to obtain agreement. In the DELPHI analysis, Bose–Einstein interference is insufficient to explain the difference between data and models, even with an un-physically large value of the coherence parameter λ.

Following a suggestion in [205], higher-order Bose–Einstein correlations have been studied by UA1 [206], NA22 [207] and DELPHI [208]. In this study, "correlation functions" of order q,

$$R_q(Q^2_{q\pi}) = N_q(Q^2_{q\pi})/N^{BG}_q(Q^2_{q\pi}) \,, \tag{4.14}$$

are defined as ratios of the distribution of like-charged q-tuplets $(q = 2, 3, \ldots, 5) N_q(Q^2_{q\pi})$ and a distribution of reference (background) q-tuplets $N^{BG}_q(Q^2_{q\pi})$ obtained from random event mixing. The variable $Q^2_{q\pi}$ is defined as a sum over all permutations

$$Q^2_{q\pi} = Q^2_{12} + Q^2_{13} + \cdots + Q^2_{(q-1)q} \tag{4.15}$$

of the squared four-momentum difference $Q^2_{ij} = -(p_i - p_j)^2$ of particles i and j. Note that the functions (4.14) are normalized inclusive densities and not correlation functions in the proper sense (cf. Section 4.8).

The UA1 data are shown in Fig. 4.18. A good fit is obtained if in the expansion of $R_q(Q^2_{q\pi})$ suggested in [205], Gaussians (dashed curve) are replaced by exponentials in $Q_{q\pi}$ (solid curve). Since low Q^2_{ij} pairs are lost due to limited two-track resolution in the detector, the data at the smallest Q^2_{ij} have to be regarded as a lower limit. A power law as expected from intermittency cannot be excluded.

UA1 has further studied the distributions R_2 for all-charged-(cc), $(\pm\pm)$- and $(+-)$-pairs as a function of $Q^2 (\equiv Q^2_{2\pi})$ (Fig. 4.19) [143]. These results have important implications. The charge dependence of "intermittency", controversial in single-particle variable analyses (see before), is now quite clear in invariant-mass variables ($Q^2 = M^2_{\text{inv}} - 4m^2_\pi$). The data for $R_2^{\pm\pm}$ (dashed) has a much stronger Q^2-dependence than R_2^{+-} and effectively determines the small-Q^2 behaviour of R_2^{cc}. This is unambiguous evidence that intermittency at small Q^2 is predominantly due to like-sign particle correlations. It does not necessarily imply, however, that Bose–Einstein interference is the sole cause.

In [77] it is shown on EMC data that, especially in 3D, F_2^{--} deviates much more from LUND model predictions than F_2^{+-}. The LUND model version used does not include Bose–Einstein correlations. The deviation from the data is indicative for the importance of this effect.

Bose–Einstein interference must thus play a significant role at least for small Q^2. This seems in contradiction with claimed successes in e^+e^- annihilation of parton shower Monte Carlos which neglect Bose–Einstein interference.

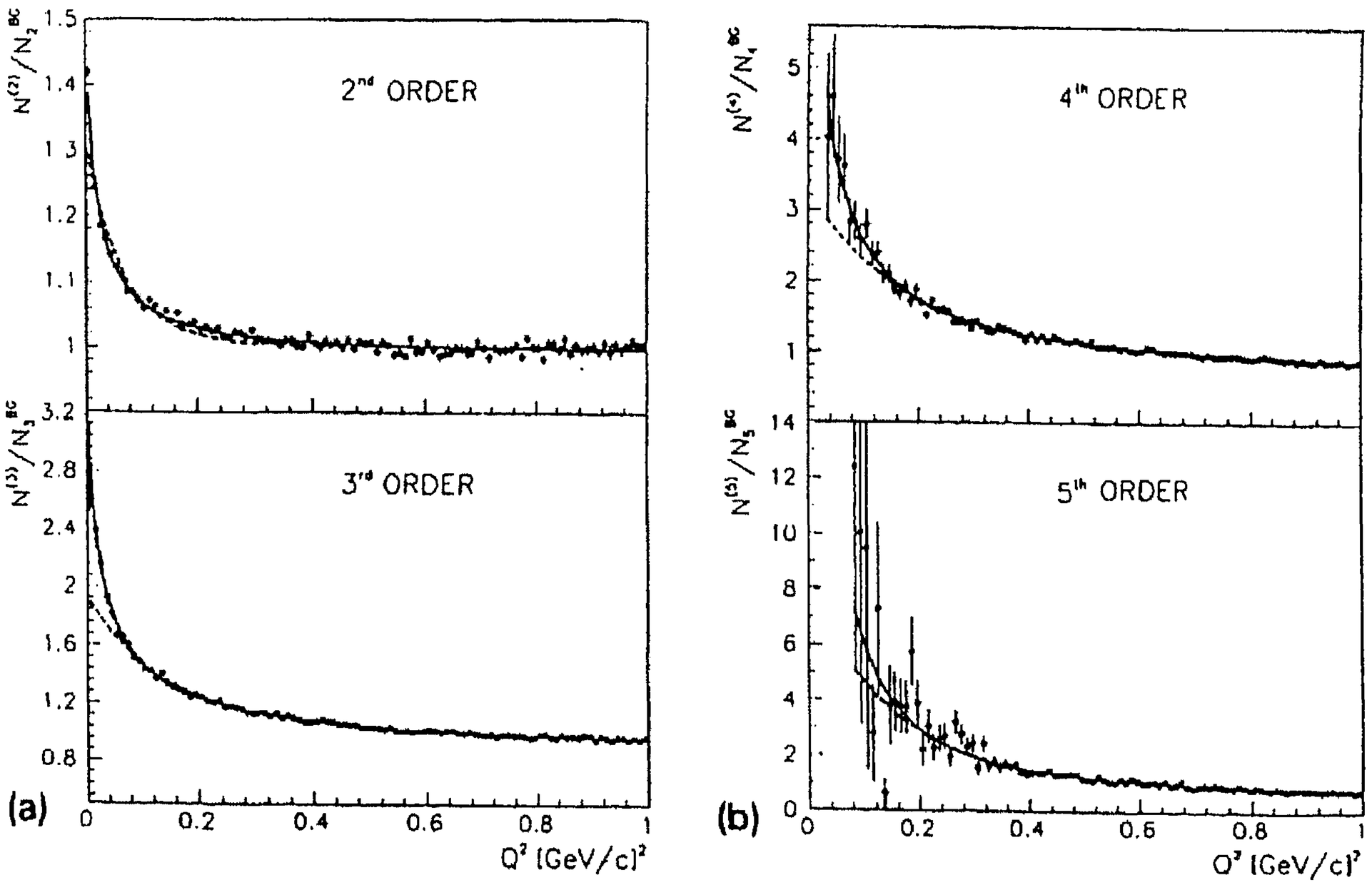

Fig. 4.18. Bose–Einstein correlation of order 2 to 5, as indicated. The dashed lines represent fits by Gaussian terms, the full lines by exponential terms. All data are corrected for Coulomb interaction [206].

Finally, we reiterate our remark that a "conventional" Bose–Einstein effect with exponential or Gaussian Q dependence is incompatible with intermittent power-law behaviour. We return to this point in Section 4.8.4.

4.4.2. Transverse-momentum dependence

An interesting question is whether semi-hard effects [179], observed to play a role in the transverse-momentum behaviour even at NA22 energies [110], or low-p_T effects [192, 209] are at the origin of intermittency. A first indication for the latter comes from the most prominent NA22 "spike" event [119], where 5 out of 10 tracks in the spike have $p_T < 0.15$ GeV/c.

In Fig. 4.20(a), NA22 data on $\ln F_q$ versus $-\ln \delta y$ are given for particles with transverse momentum p_T below and above 0.15 GeV/c, and with p_T below and above 0.3 GeV/c. For particles with p_T below the cut (left), the F_q exhibit a stronger δy dependence than for particles with p_T above the cut (right).

NA22 does not claim straight lines in Fig. 4.20(a), but uses fits as an indicative measure of the increase of $\ln F_q$ over the region $1 > \delta y > 0.1$. In the upper half of Fig. 4.20(b), the fitted anomalous dimensions d_q are compared to those obtained in the full p_T-range. The restriction to particles with $p_T < 0.15$ or 0.30 GeV/c indeed leads to an *increase* of d_q; a *decrease* is observed for $p_T > 0.15$ or 0.30 GeV/c. This observation is confirmed by IHSC [145].

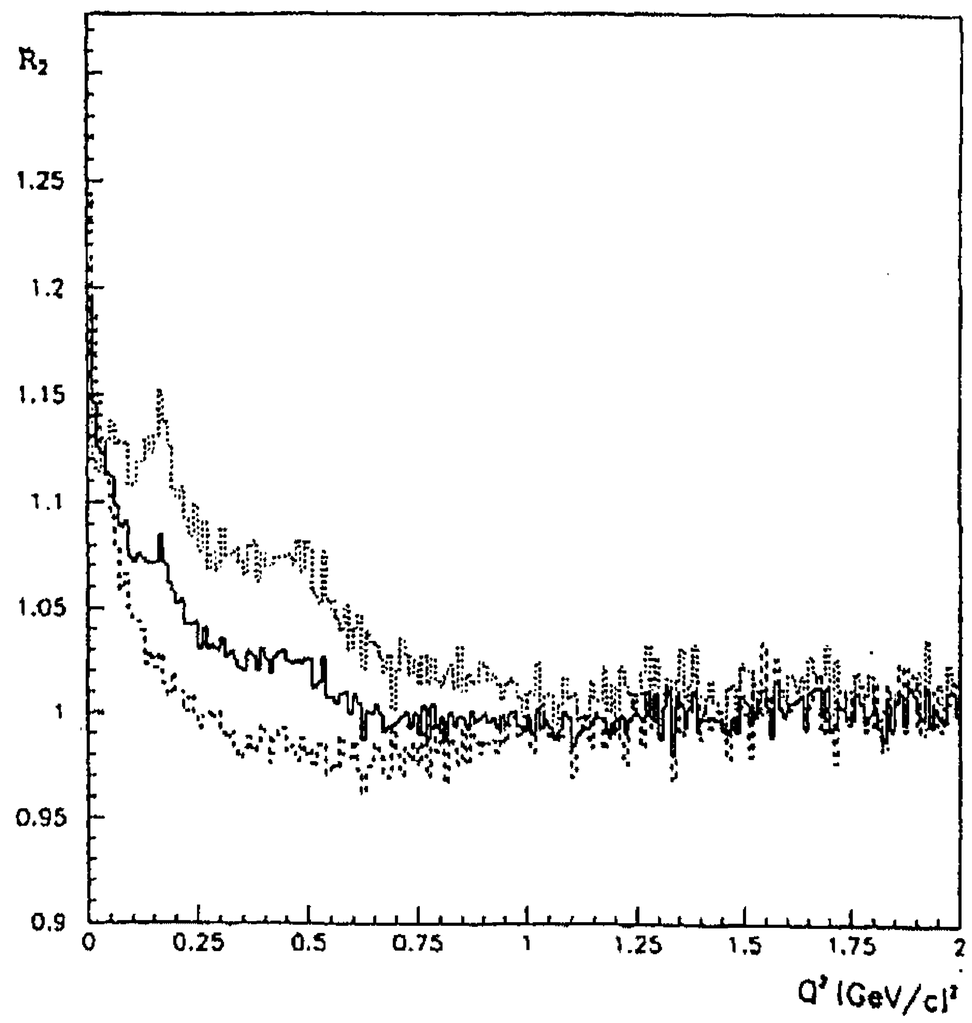

Fig. 4.19. The dependence of $R_2 = N_2/N_2^{BG}$ on $Q^2_{q\pi}$ for all pairs of charged particles (full line), for opposite-charged pairs (dotted) and for same-charged pairs (dashed) [143].

FRITIOF predictions are given in the lower part of Fig. 4.20(b), again for all tracks and for tracks with restricted p_T. It is known [142] that FRITIOF gives too small slopes for factorial moments integrated over p_T. Here, one notices that it also fails to reproduce their p_T dependence.

UA1 has a bias against tracks with $p_T < 0.15$ GeV/c, but gives the dependence of ϕ_2 on the average transverse momentum $\bar{p}_T$ of the event (Fig. 4.20(c)) [210]. The data show a remarkable decrease of ϕ_2 with increasing $\bar{p}_T$ and, after passing through a minimum at $\bar{p}_T \approx 0.5$ GeV/c, a slight increase at higher $\bar{p}_T$ values. Lower $\bar{p}_T$ events correspond to soft processes, while higher $\bar{p}_T$ ones correspond to events with hard jet sub-processes. Both types of events have higher slopes ϕ_2 than their mixture at intermediate $\bar{p}_T$ values. (See further [211] for a possible connection to the multiplicity dependence to be described in Section 4.4.4)

Fig. 4.20(c) also contains the results obtained from Monte-Carlo events generated with PYTHIA 5.6 [70]. At low $\bar{p}_T$ values, the PYTHIA ϕ_2 values are strongly suppressed as compared to those of the data.

We conclude that the intermittency observed in NA22 and UA1 data is enhanced at low transverse momentum and is not dominated by semi-hard effects. Hard effects dominate in high energy e^+e^- and lh collisions. Data on the p_T dependence of factorial moments in these processes should help in clarifying the origin of intermittency. The effect of p_T cuts on e^+e^- data has been studied by DELPHI [136]. One-dimensional data are shown in Fig. 4.21 and provide several important pieces of information:

(i) The log–log plot for low-p_T particles shows less saturation (i.e. stronger intermittency) than for larger-p_T particles. So, intermittency is strongest in the p_T region where hard gluon effects are weakest!

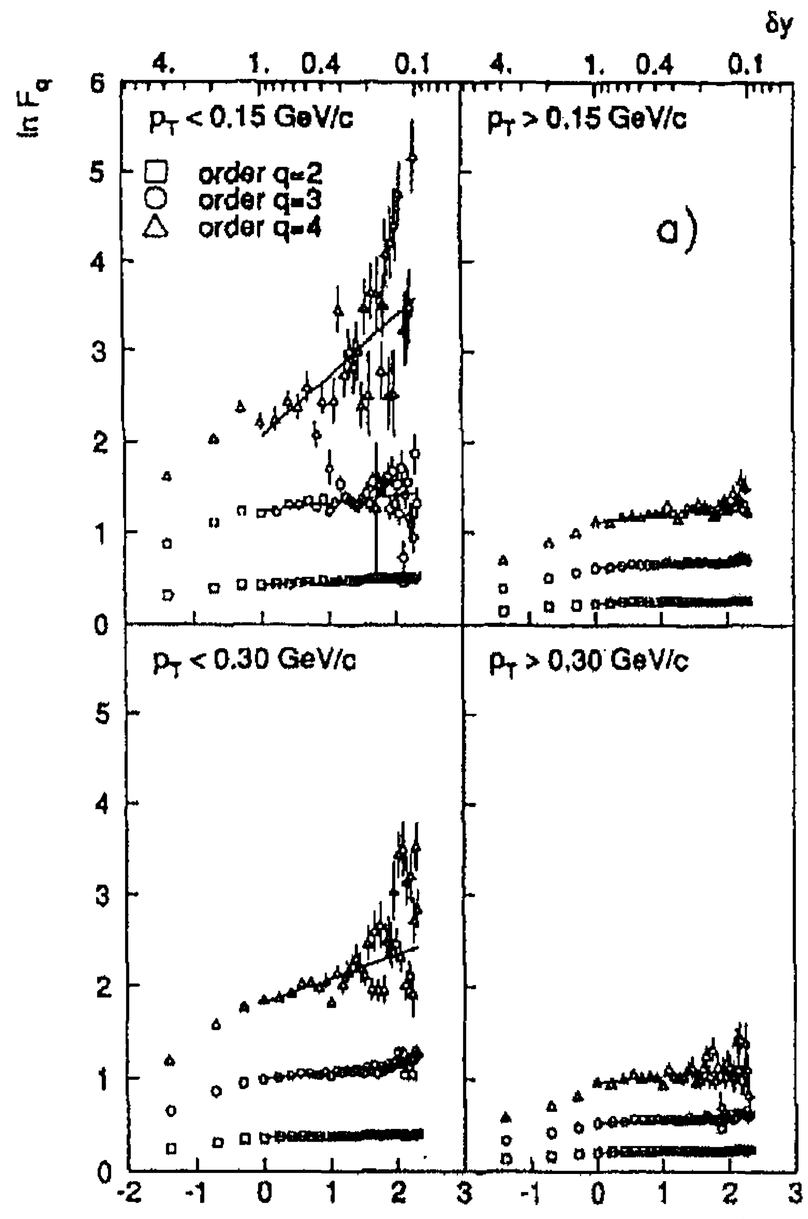

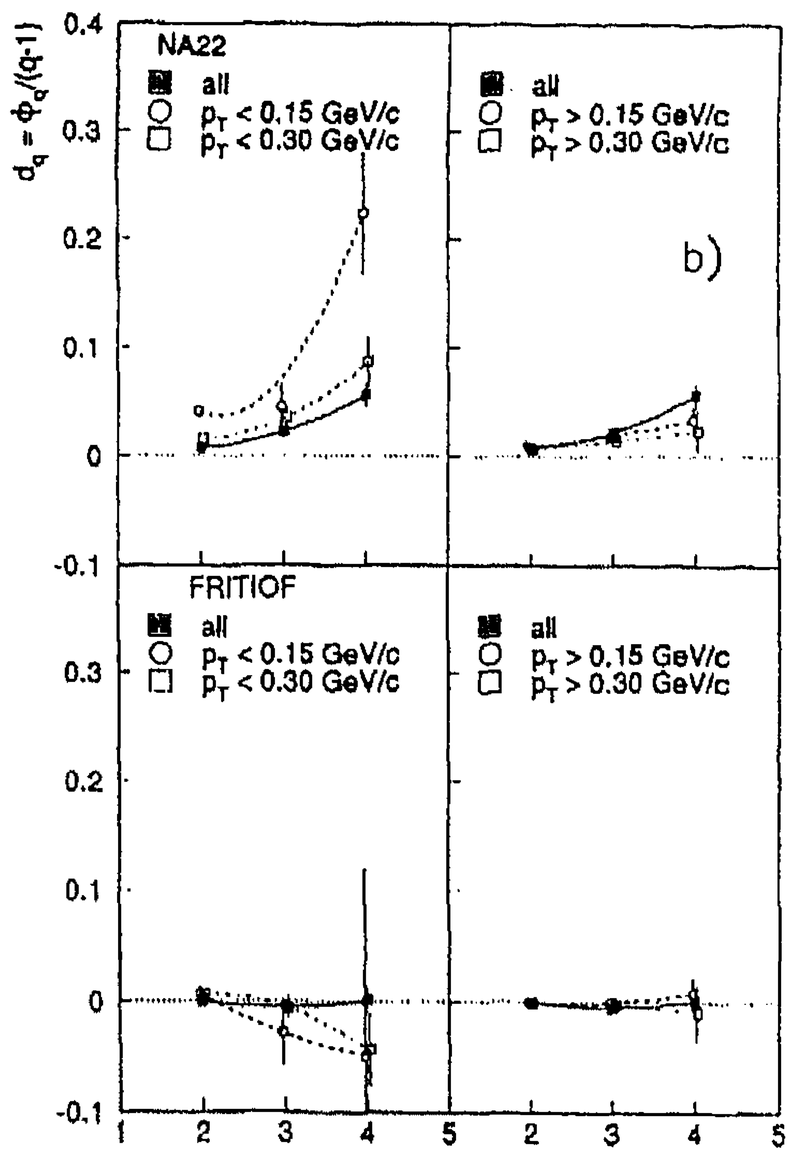

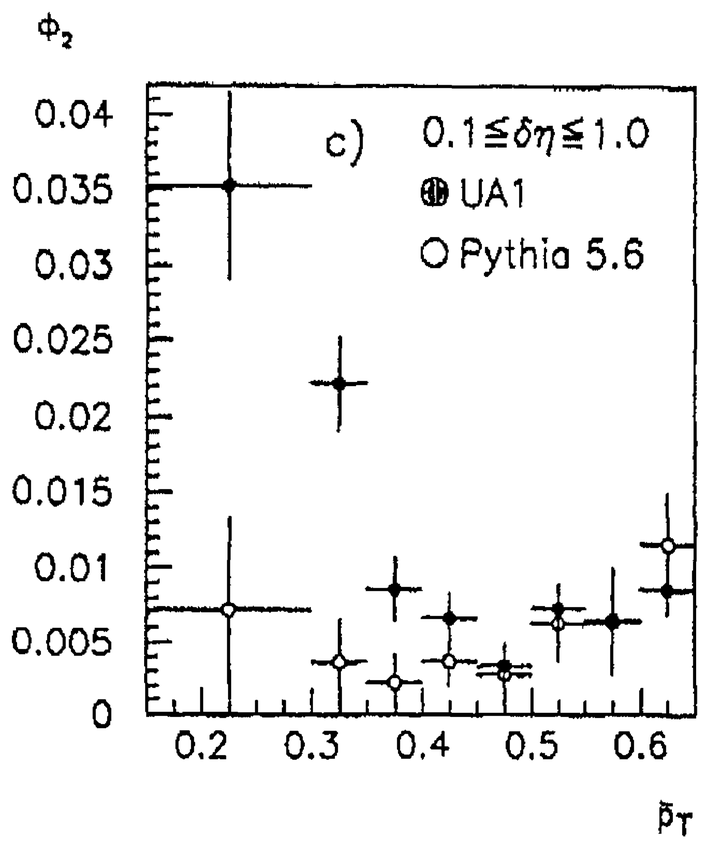

Fig. 4.20. (a) $\ln F_q$ as a function of $-\ln \delta y$ for various p_T cuts as indicated [142], (b) anomalous dimensions d_q as a function of the order q, for various p_T cuts as indicated (lines are to guide the eye) [142], (c) slope ϕ_2 as a function of the average transverse momentum $\bar{p}_T$ in an UA1 event compared to PYTHIA 5.6 [210].

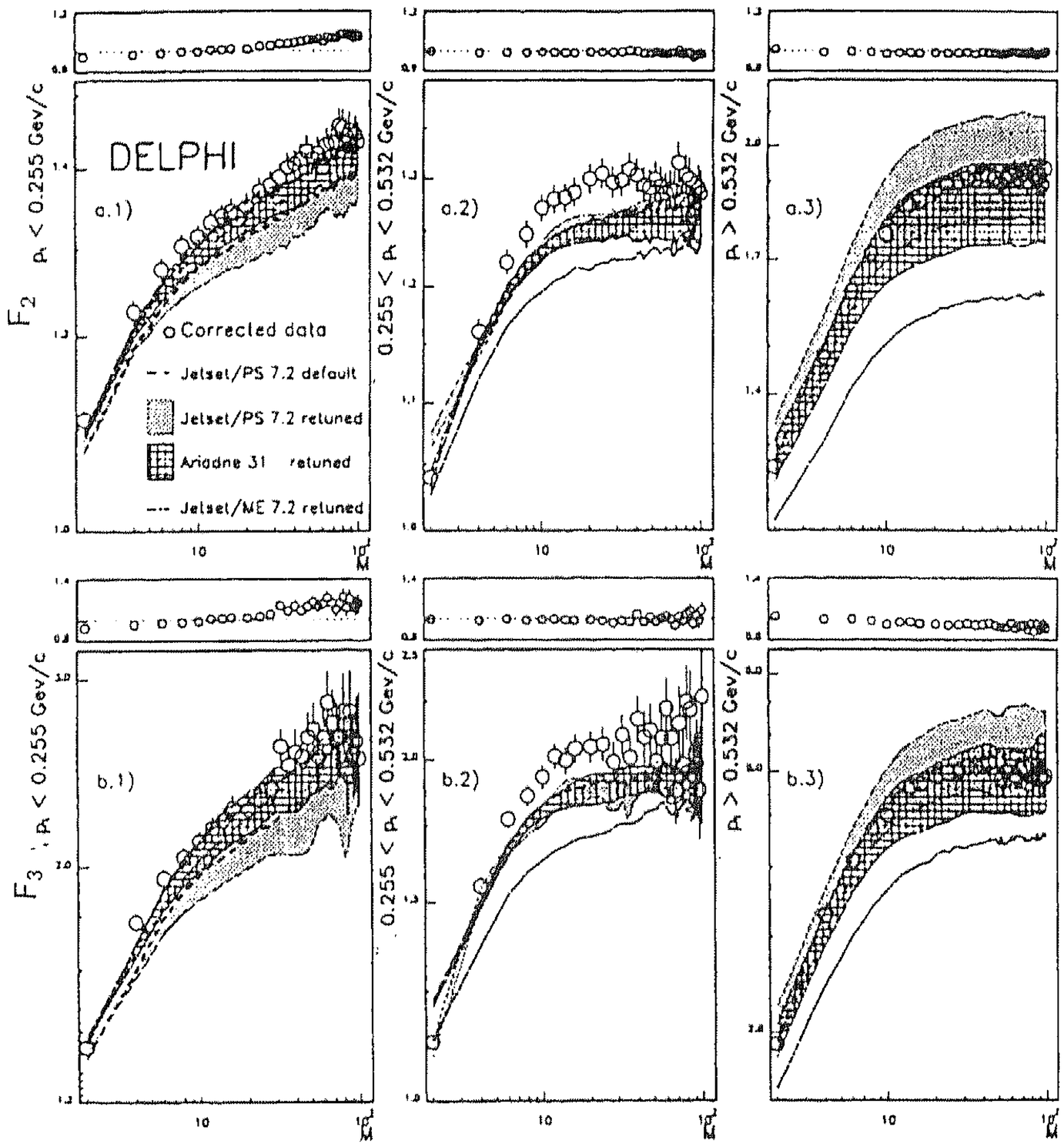

Fig. 4.21. Factorial moment F_2 and F_3 as a function of resolution for three e^+e^- data sets with p_T cuts as indicated [136]. The lines correspond to the models as indicated. Correction factors are given above the corresponding sub-figures.

(ii) A discrepancy between data and models (only indicative in Fig. 4.7(d)) is observed in the interval $0.255 < p_T < 0.532$ GeV/c. This looks surprising at first, but we shall show in Section 4.4.4 that the intermittency effect can be stronger for individual mechanisms than for a mixture.

(iii) The factorial moments are larger for $p_T > 0.532$ GeV/c than for $p_T < 0.255$ GeV/c, opposite to the trend of the NA22 data (Fig. 4.20(a)). Also this seems contradictory, but it should be realized that for NA22 transverse momentum refers to the beam axis, which is usually close to beam and target jet axes. In the e^+e^- analysis, p_T is calculated relative to the global event axis which differs from the direction of individual jets.

4.4.3. Dependence on jet topology

In their recent analysis, DELPHI [136] selects 2-jet and 3-jet events using the JADE/E0 invariant-mass algorithm [212], with resolution parameter values $y_{cut} = 0.04$ and 0.01, and with additional cuts to clean the 2-jet and 3-jet sample. At large bin sizes, factorial moments rise faster

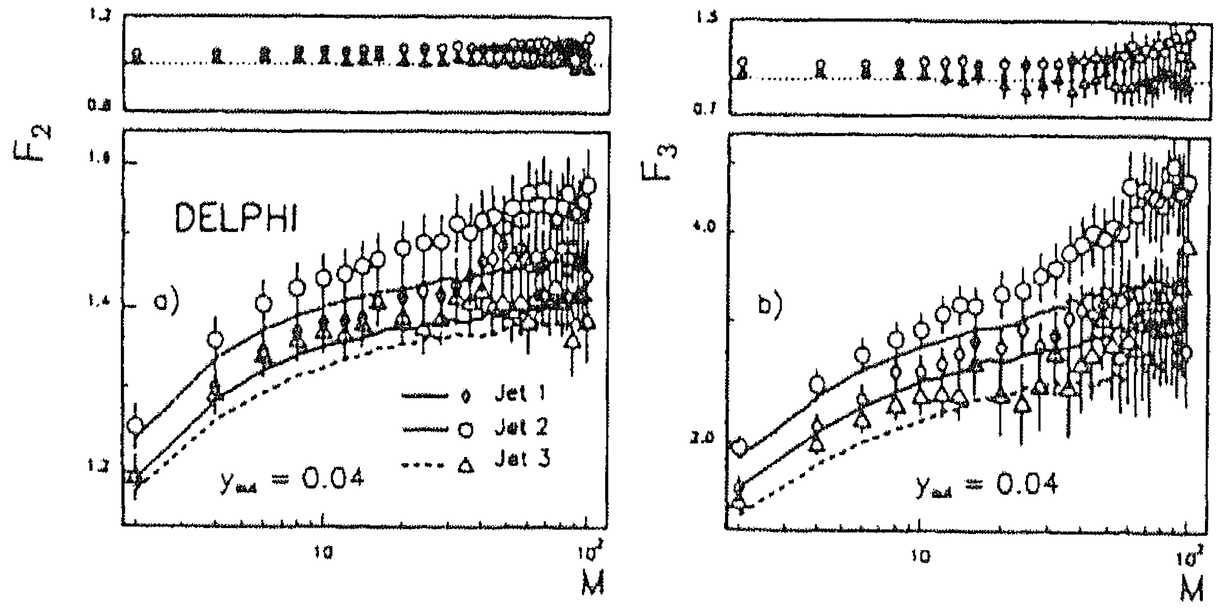

Fig. 4.22. F_2 and F_3 of the first, second and third jet ordered by their energy. DELPHI corrected data (open symbols) are compared with JETSET 7.2 PS Monte-Carlo predictions with re-tuned settings [136].

with decreasing bin size (and are, therefore, larger) in 3-jet than in 2-jet events. This is compatible with the (large bin size) behaviour expected from hard gluons. At small bin sizes the increase is similar for 2-jet and 3-jet events.

In 3-jet events, factorial moments were calculated for tracks belonging to jet 1, jet 2 and jet 3 ordered in energy. The rapidity was defined with respect to the individual jet axis. As seen in Fig. 4.22, intermittency is weakest in jet 3 and strongest in jet 2. The deviation from JETSET is also strongest for jet 2.

4.4.4. Multiplicity (density) dependence

In general, a decrease of the intermittency indices ϕ_q is found with increasing energy, in particular for hh, hA and AA collisions. As seen in Fig. 4.23(a), a strong multiplicity dependence of the intermittency strength is observed for hh collisions by UA1 [143]. The trend is opposite to the predictions of the models used by this collaboration. This decrease of the intermittency strength with increasing multiplicity is usually explained as a consequence of mixing of independent sources of particles [131]. The cross-over of data and FRITIOF at intermediate multiplicity explains the apparent success of FRITIOF in Fig. 3.3, for multiplicities close to 30 as being accidental.

Mixing of emission sources leads to a roughly linear decrease of the slopes ϕ_q with increasing particle density $\langle\rho\rangle$ in rapidity [108, 213, 214]: $\phi_q \propto \langle\rho\rangle^{-1}$. This is indeed observed by UA1 [143]. Multiple emission sources are present in multichain Dual Parton models. The calculated slopes indeed depend linearly on multiplicity but are too small by a factor of two [215]. Similarly, the model studied in [216] with independent emission at fixed impact parameter finds decreasing ϕ_q with increasing multiplicity.

Also here, a study of the multiplicity dependence in e^+e^- data and JETSET allows interesting comparisons. In fact, the LEP results [136] suggest little or no n-dependence, except for the lowest multiplicities, where the slope is largest and also the difference with JETSET PS is the largest.

Fig. 4.23(a) helps in explaining why intermittency is so weak in heavy-ion collisions (cf. Fig. 4.3): the density (and mixing of sources) is particularly high there. In Fig. 4.23(b) EMU01 [155], therefore, compares ϕ_2 for NA22 (hp at 250 GeV) and heavy-ion collisions at similar beam momentum per nucleon, as a function of the particle density. Whereas slopes averaged over

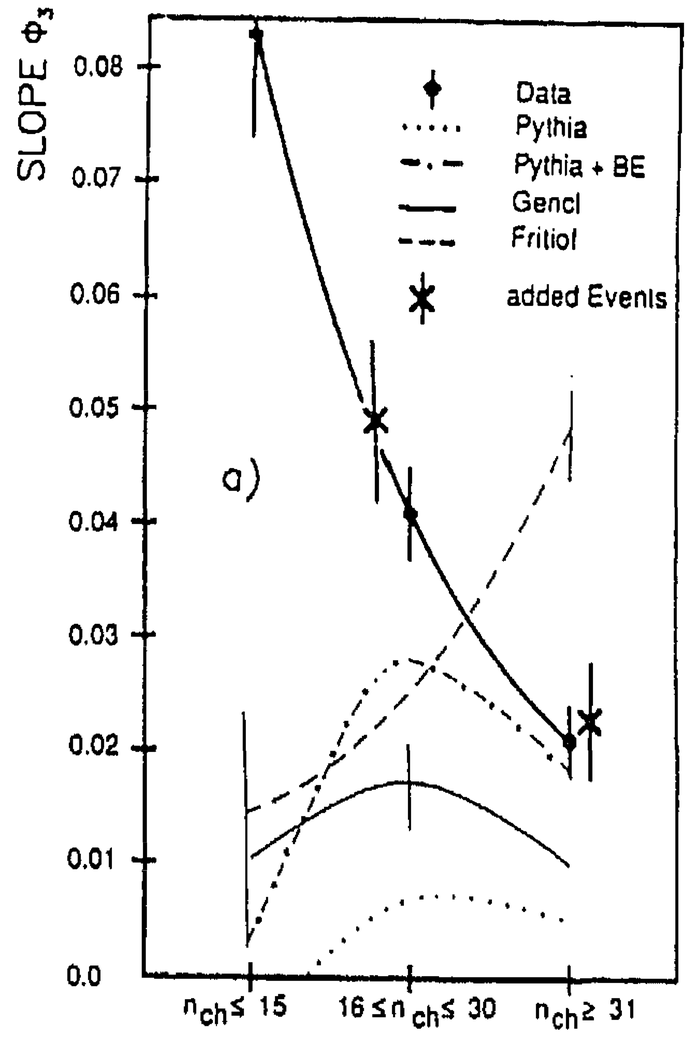

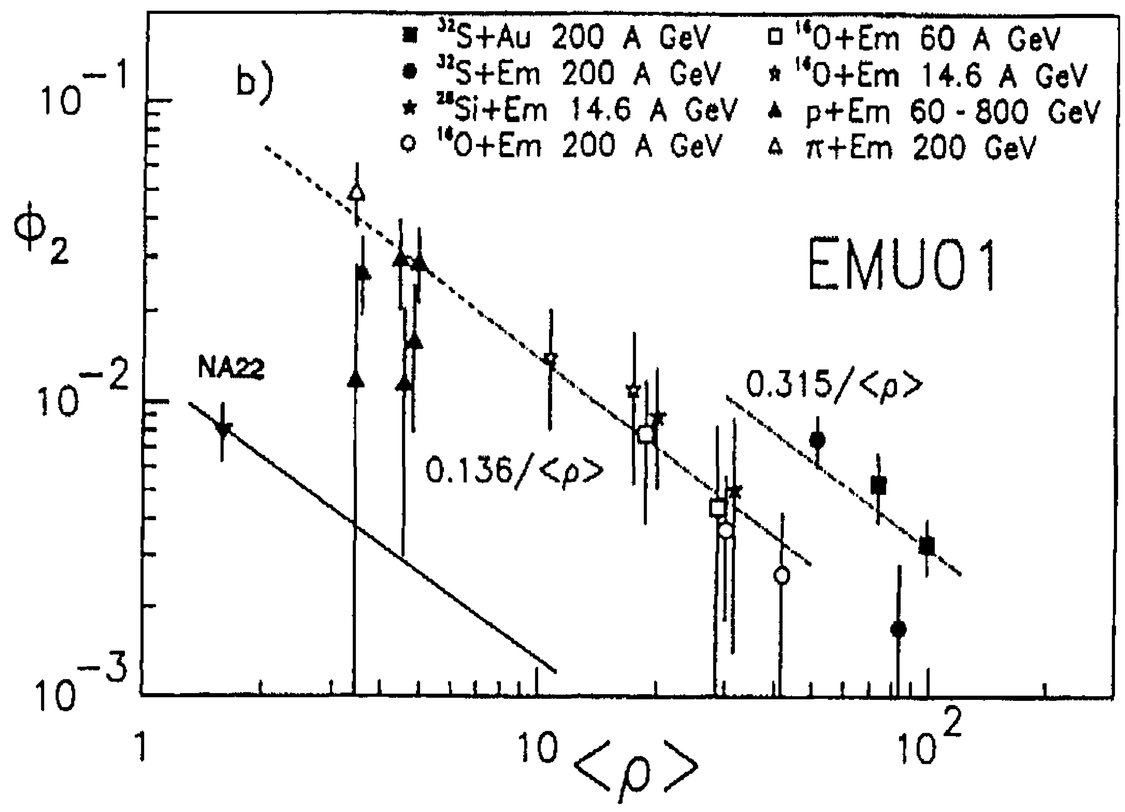

Fig. 4.23. (a) Multiplicity dependence of the slope ϕ_3, compared to that expected from a number of models, the crosses correspond to a combination of independent events [143], (b) slope ϕ_2 as a function of particle density for NA22 (hp at 250 GeV) and heavy-ion collisions as indicated [155]. The full line corresponds to an extrapolation from the NA22 point to higher densities using $\phi_2 \propto 1/\rho$. The dotted lines show fits for the ^{16}O and ^{28}Si samples and for the ^{32}S samples.

multiplicity are smaller for AA collisions than for NA22 in Fig. 4.3, at fixed $\langle\rho\rangle$ they are actually higher than expected from an extrapolation of hh collisions to high density and even grow with increasing size of the nuclei. This may be evidence for re-scattering (see [141]) or another (collective) effect, but, as shown by HELIOS [157] and recently confirmed by EMU-01 [155], one has to be very sure about the exclusion of γ conversions before drawing definite conclusions.

We conclude this section with an additional warning. In Section 4.3.2 we mentioned the Fiałkowski "universality conjecture" and noted that it is incompatible with the "mixing" hypothesis usually invoked to explain the multiplicity dependence of factorial moments and slopes. A different explanation of the multiplicity dependence may therefore be needed, especially since intermittency and Bose–Einstein effects are now known to be closely related.

4.5. Factorial cumulants

Normalized factorial cumulant moments, first introduced in [8] and recently studied in [26], are defined in (2.71) as integrals over the background subtracted correlation functions. They share with factorial moments the property of "noise suppression". The normalized factorial moments F_q can be expanded in terms of normalized cumulant moments K_q as given in (2.72). This expansion has been found to converge rapidly [26]. The terms in the expansion correspond to contributions from genuine $q,(q-1)\ldots,$ 2-particle correlations.

An analysis of factorial cumulant moments is presented in [26]. Roughly, it is estimated that $K_2 \sim 0.6, K_3 \sim 0.7, K_4 \lesssim 1.0, K_5 \lesssim 1.5$ for UA1 data at $\sqrt{s} = 630$ GeV. (The inequalities for K_4 and K_5 are due to the approximation $\overline{AB}$ by $\bar{A}\cdot\bar{B}$ in (2.72) since no direct measurements of these averages exist.) Clearly, the two-particle contribution to factorial moments is large, but higher orders are not negligible. At the energy of the NA22 experiment K_2 is small ($\sim$0.2), but K_3 is significantly larger ($\sim$0.45).

From (2.72) it is seen that the contribution $F_q^{(2)}$ to F_q from two-particle correlations alone can be expressed as

$$F_3^{(2)} = 1 + 3K_2\,, \tag{4.16}$$

$$F_4^{(2)} = 1 + 6K_2 + 3\overline{K_2^2}\,; \tag{4.17}$$

the contribution $F_4^{(3)}$ from two- and three-particle correlations to F_4 as

$$F_4^{(3)} = 1 + 6K_2 + 3\overline{K_2^2} + 4K_3\,. \tag{4.18}$$

The difference $F_q - F_q^{(p)}$ is a measure for the importance of higher-order correlations.

Fig. 4.24(a) shows a cumulant decomposition of F_3 and F_4 in UA1 data [217]. The differences between the curves indeed indicate large contributions from genuine higher-order correlations. Similar results are observed for NA22 [142] in Fig. 4.24(b), for $p = 2$ and 3 and $q = 3$ and 4, in one-, two- and three-dimensional phase space (transformed y, $y - \varphi$ and $y - \varphi - \ln p_T$). In general, the difference increases with increasing $\ln M$ (decreasing bin size). This means that the contribution of higher-order correlations to the factorial moments increases at higher resolution. An exception is

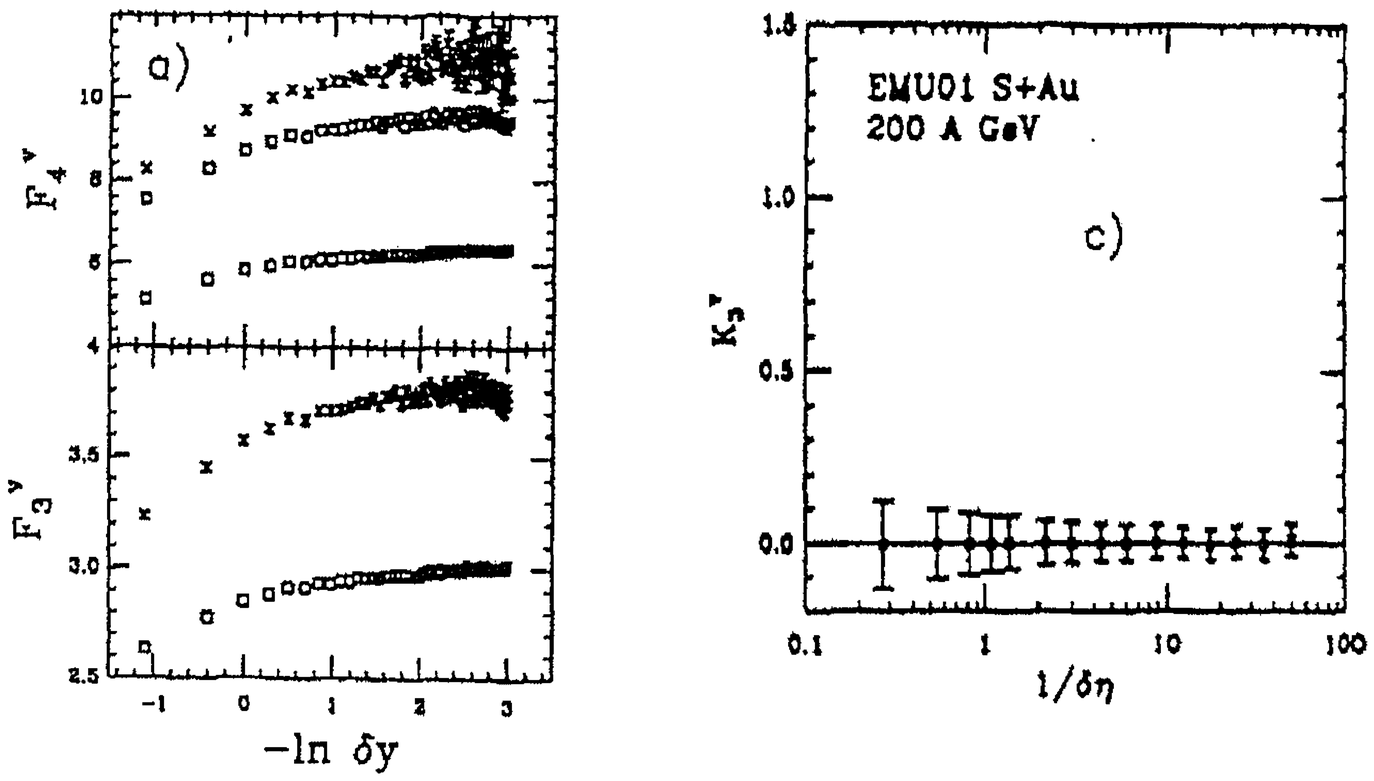

Fig. 4.24. (a) UA1 factorial moments (crosses) decomposed into cumulant contributions: lower squares indicate 2-particle, upper squares 2 + 3-particle contributions [217], (b) Upper row: normalized factorial moments F_q(□) from NA22, together with contributions from two-particle correlations (△), the sum of 2- and 3-particle correlations (○), and the sum of 2-, 3- and 4-particle correlations (◇); lower part: the normalized cumulant moments K_q [142]. (c) K_3 for nuclear collisions [217].

factorial moments in the variable φ, for which only two-particle correlations are found to be non-zero (not shown).[2]

The situation is completely different in heavy-ion collisions where, with present accuracy $K_q \approx 0$ for $q > 2$ (Fig. 4.24(c)). The factorial moments are completely dominated by two-particle correlations [217, 219, 220], implying that higher-order F_q contain little or no further dynamical information for this type of collisions (see Eq. (2.56)).

Using the linked-pair ansatz [26] (see also Section 5.1.1), higher-order cumulant functions can be expressed as products of K_2 (see also [221] for an interpretation in terms of independent superposition of sources)

$$K_q = A_q K_2^{q-1}, \tag{4.19}$$

with free constants A_q.

For a negative-binomial (NB) multiplicity distribution, $K_2 = 1/k$ and the linking parameters are fixed numbers given by $A_q^{\mathrm{NB}} = (q-1)!$ [109]. A necessary condition is stationarity, i.e. constancy of $1/k$. This works well for UA1. For NA22 [142], A_q is observed to increase with decreasing bin size. Approximately constant $A_q \approx (q-1)!$ are found if the data are averaged only over a narrow rapidity region ($-0.75 \leq y \leq 0.75$) and the most prominent spike event is excluded. The linked-pair ansatz may thus be a valid approximation for high-order correlations in small phase-space domains but not for the average over phase space. This would be consistent with the well-documented fact [13] that the negative binomial is often a good parametrization of multiplicity distributions in restricted δy intervals.

We shall come back to cumulants and genuine higher-order correlations in Section 4.10, where they are studied by means of a largely improved methodology.

4.6. Factorial correlators

4.6.1. The method

The moments defined in (2.68)–(2.70) measure local density fluctuations in phase space. Additional information is contained in the correlation between these fluctuations within an event. This correlation can be studied by means of the factorial correlators defined in (2.75). Correlators are typically calculated at a given δy for each combination mm' of bins with size δy, and then averaged over all combinations separated by a given bin distance D. This is illustrated below.

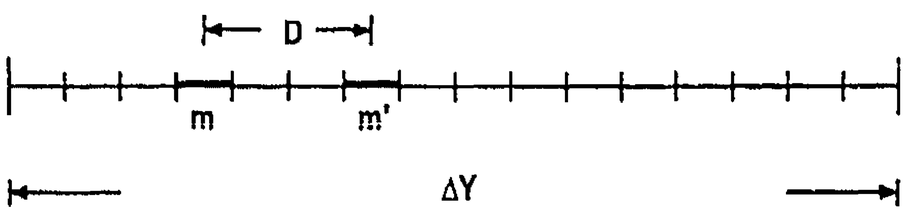

[2] Absence of genuine higher-order correlations has been reported in [218], but at far too low statistics.

In the simple intermittency model (α-model) described in [21,22], F_{pq} depends on D but not on δy and follows the power law

$$F_{pq} \propto (\Delta Y/D)^{\phi_{pq}} . \tag{4.20}$$

The powers ϕ_{pq} (slopes in a log–log plot) obey the relations [21,22]:

$$\phi_{pq} = \phi_{p+q} - \phi_p - \phi_q = pq\phi_2 , \tag{4.21}$$

where the first equality sign is due to the α model proper, the second to the log-normal approximation. According to (4.20) $\phi_{11} = \phi_2$, so that (4.21) can also be written in the form

$$\phi_{pq} = pq\phi_{11} . \tag{4.22}$$

4.6.2. Results

Preliminary results for pseudo-rapidity resolution $\delta\eta \geq 0.2$ have been reported by the HELIOS Collaboration [222]. There, however, multiplicities n_m had to be estimated from the transverse energy $E_{T,m}$ in bin m and the average transverse energy $\langle E_T \rangle$ per particle: $n_m = E_{T,m}/\langle E_T \rangle$ rounded to the nearest integer. The first direct measurement is from NA22 [223]. The $\ln F_{pq}$ are shown as a function of $-\ln D$ in Fig. 4.25(a)–(d), for four values of $\delta y \geq 0.1$ (corresponding to $M = 10, 20, 30$ and 40). Statistical errors (estimated from the dispersion of the F_{pq} distribution) are in general smaller than the size of the symbols. F_{pq} can be measured up to third order in p and q for $\delta y = 0.4$ binning (Fig. 4.25(a)). For $\delta y = 0.1$, the analysis is possible to first and second order only (Fig. 4.25(d)). The smallest possible value for D being equal to the bin size δy, Fig. 4.25(a) extends to $D = 0.4$ and Fig. 4.25(d) to $D = 0.1$. In all cases, an increase of $\ln F_{pq}$ is observed with increasing $-\ln D$. Very similar results have recently been reported by EMC [140], EMU-01 [155] and in [152].

In Fig. 4.26(a), the $\ln F_{pq}$ are compared at fixed $D = 0.4$ for four different values of δy. The dashed lines correspond to a horizontal line fit through the data. In agreement with the α-model, the F_{pq} indeed do not depend on δy. Also this result has been confirmed on EMC data [140] and in [152]. The δy-independence of correlators holds exactly in the α-model. Nevertheless, Fig. 4.26(b) shows that the δy independence is also valid in FRITIOF. For the particular value of $D = 0.4$, this even happens at very similar values of $\ln F_{pq}$ as in the data. In fact, this property is far from unique to the α model, but holds approximately in any model with short-range order [224].

For F_{11}, the δy independence is easily derived from a parametrization of the two-particle density, integrated over two regions of size δy separated by D. Using exponential short-range order [109], this gives

$$F_{11} - 1 \propto (1/a^2)\,\mathrm{e}^{-D/L}/(\mathrm{e}^a - 1)(1 - \mathrm{e}^{-a}) , \tag{4.23}$$

where L is a correlation length and $a = \delta y/L$. According to (4.23), F_{11} becomes independent of δy for $a \ll 1$. Since $\mathrm{e}^{-D/L} \to 1$ as $D \to 0$, this form also leads to the deviations from (4.20) observed as a bending in Fig. 4.25.

Because of the bending, fitted slopes ϕ_{pq} have no meaning, except as an indication for the increase of F_{pq} in a restricted range. The slopes for two values of δy are compared to FRITIOF predictions in Fig. 4.27(a) and (b), respectively. As observed earlier for the case of univariate moments [142], the FRITIOF slopes are too small also for the correlators. This is not surprising

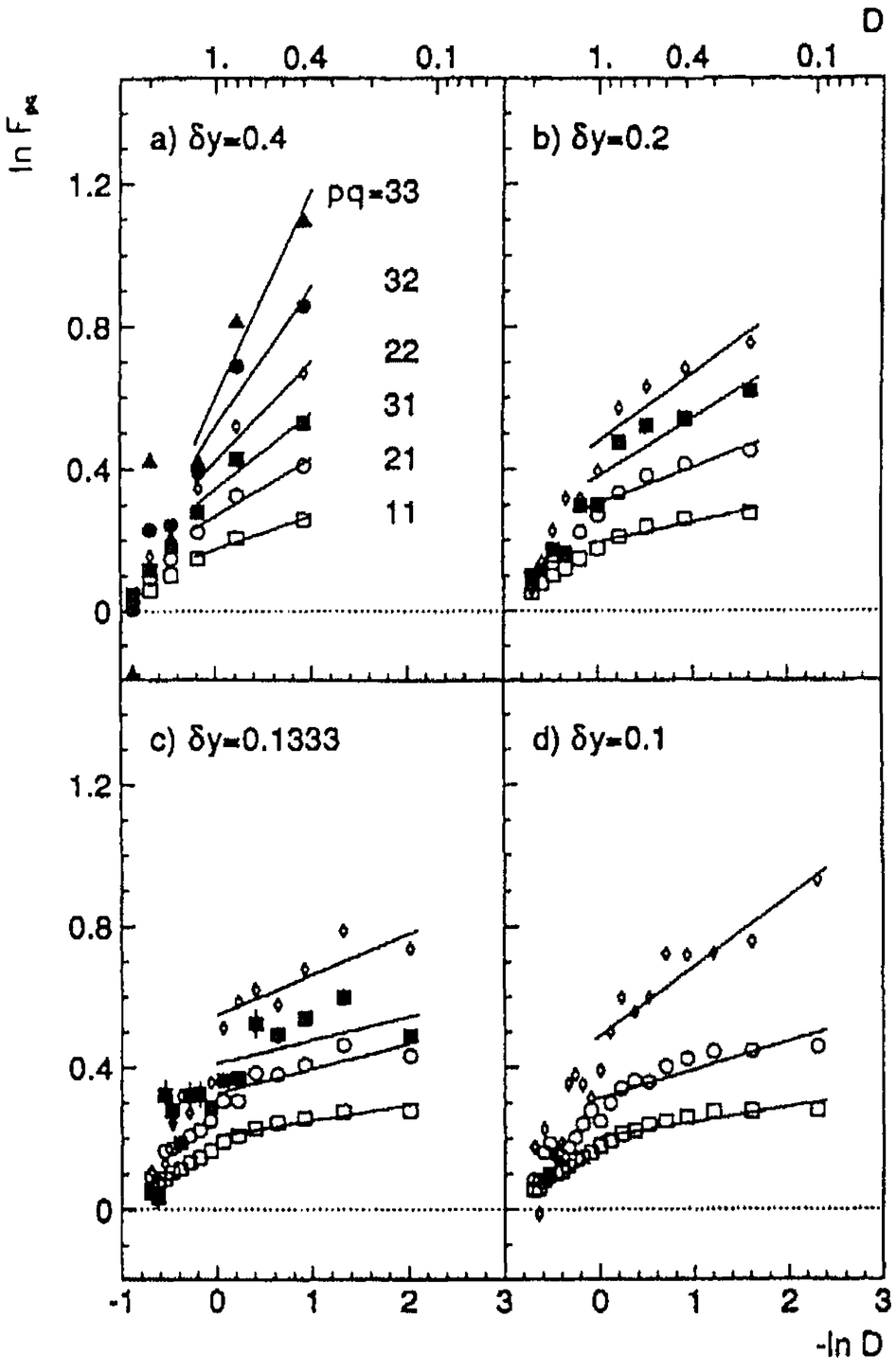

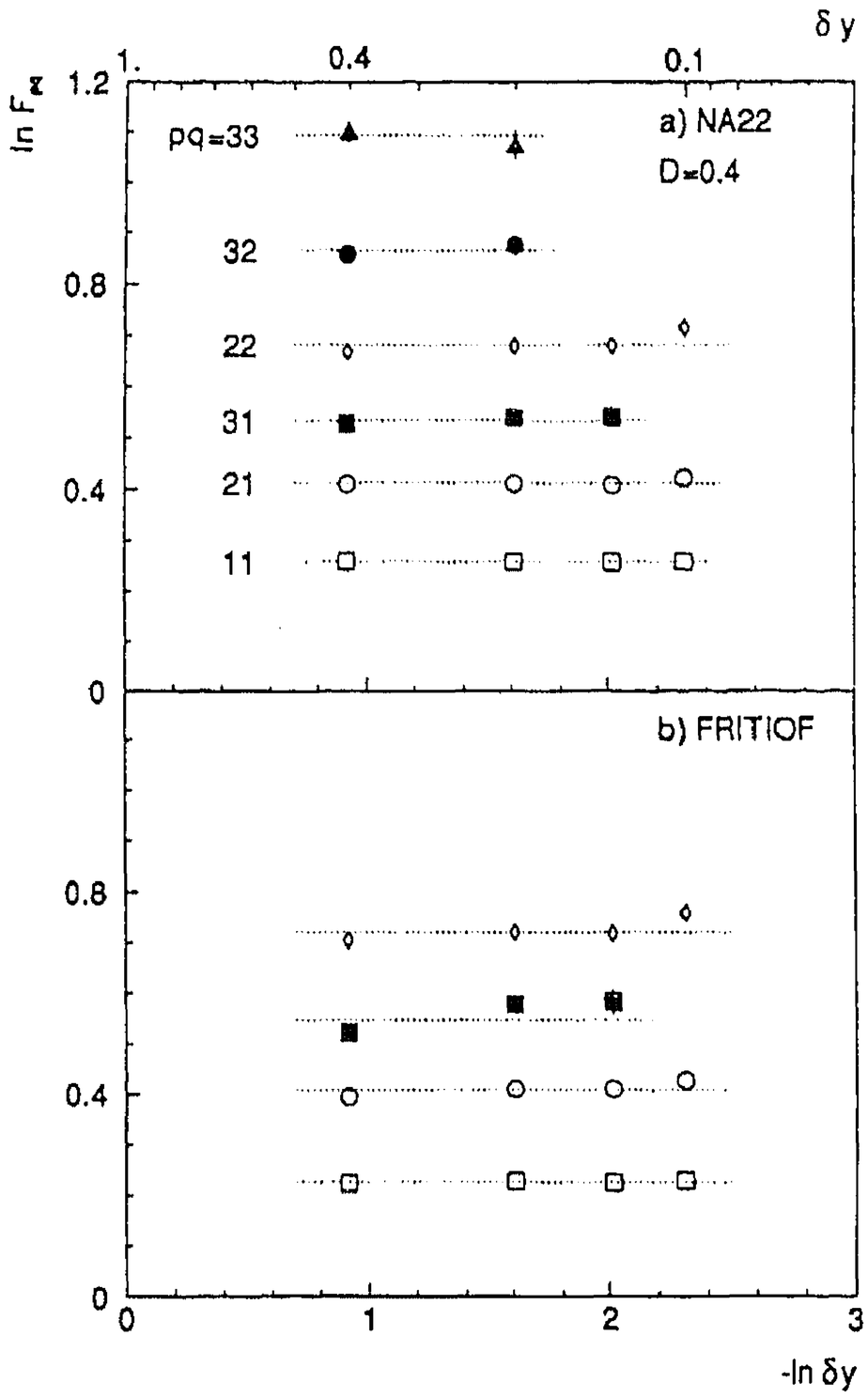

Fig. 4.25. $\ln F_{pq}$ as a function of $-\ln D$ for four values of δy, as indicated [223].

Fig. 4.26. Dependence of $\ln F_{pq}$ on the bin size δy for a correlation distance $D = 0.4$, (a) for NA22 data, (b) for a sample of 60 000 FRITIOF Monte-Carlo events. The dashed lines correspond to horizontal-line fits through the points [223].

since the model does not succeed in reproducing even the lowest-order (i.e. two-particle) rapidity correlation function (Section 3).

4.6.3. Interpretation

Factorial correlators have been analysed in [33] using a suitable parametrization of $K_2(y_1, y_2)$ and the linked-pair ansatz [107] for higher-order correlations. The relations (2.83)–(2.86) of Section 2.1.6 then allow to express all correlators in terms of K_2 for arbitrary (p, q). Note that the expressions for F_{pq} contain many lower-order "combinatorial" terms which effectively dominate and mask the contribution from genuine $(p + q)$-order correlations.

A basically similar analysis is presented in [224], inspired by techniques used in quantum optics. The two analyses have no difficulty in describing basic features of the NA22 data, including the sum

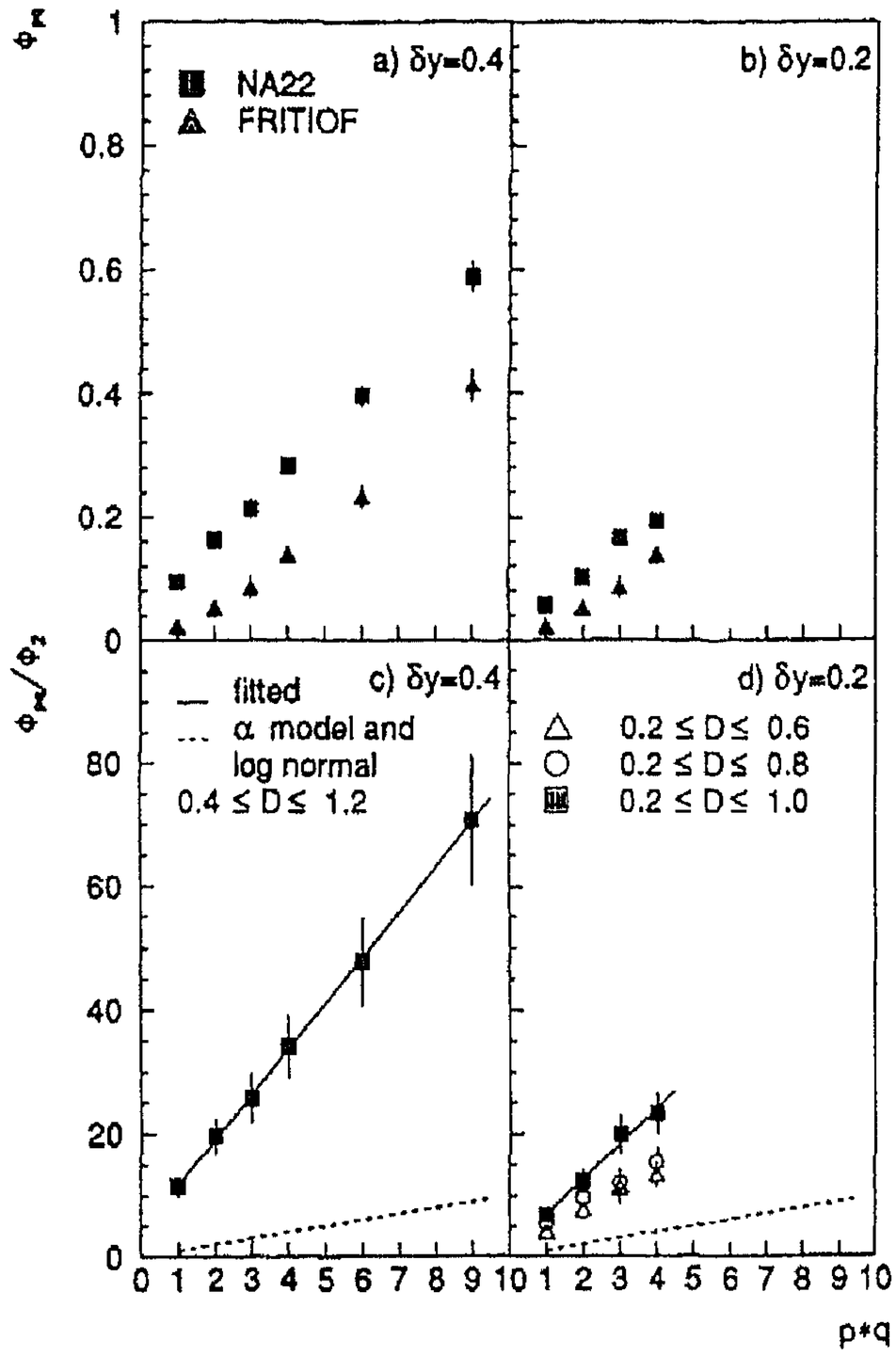

Fig. 4.27. (a),(b) The increase of the slopes ϕ_{pq} with increasing order pq compared to the expectation from FRITIOF, for two values of δy, respectively; (c), (d) the increase of ϕ_{pq}/ϕ_2 with increasing order pq, compared to that expected from the α model (dashed line), for two values of δy, respectively [223].

rules discussed in Section 2.3 which were claimed to be a unique test of random cascade models. Fig. 4.28(a) compares NA22 data on $F_2(\delta y)$ and $F_{11}(D)$ with the calculations from [224]. $F_2(\delta y)$ is used to fix the parameters of $K_2(\delta y)$ (assuming stationarity); $F_{11}(D)$ follows after integration over the appropriate rapidity domains. With the linking ansatz of [109] all other correlators are calculated without further assumptions. An illustrative example is shown in Fig. 4.28(b) which compares $F_{12}(D)$ from NA22 to the prediction. The agreement is excellent in all cases. This observation is confirmed in [152].

According to (4.21), the ratio ϕ_{pq}/ϕ_2 is expected to grow with increasing orders p and q like their product pq. In Figs. 4.27(c) and (d) this is tested for $\delta y = 0.4$ and $\delta y = 0.2$, respectively. In both cases, the experimental results lie far above the dashed line corresponding to the expected $\phi_{pq}/\phi_2 = pq$. Since the dependence of $\ln F_{pq}$ on $-\ln D$ is not strictly linear, this comparison depends on the range of δy and D used to determine ϕ_2 and ϕ_{pq}. In Fig. 4.27(d) one, therefore, compares a number of fits. Slopes are smaller when the upper limit in D is reduced, but do not reach the α-model prediction (dashed line).

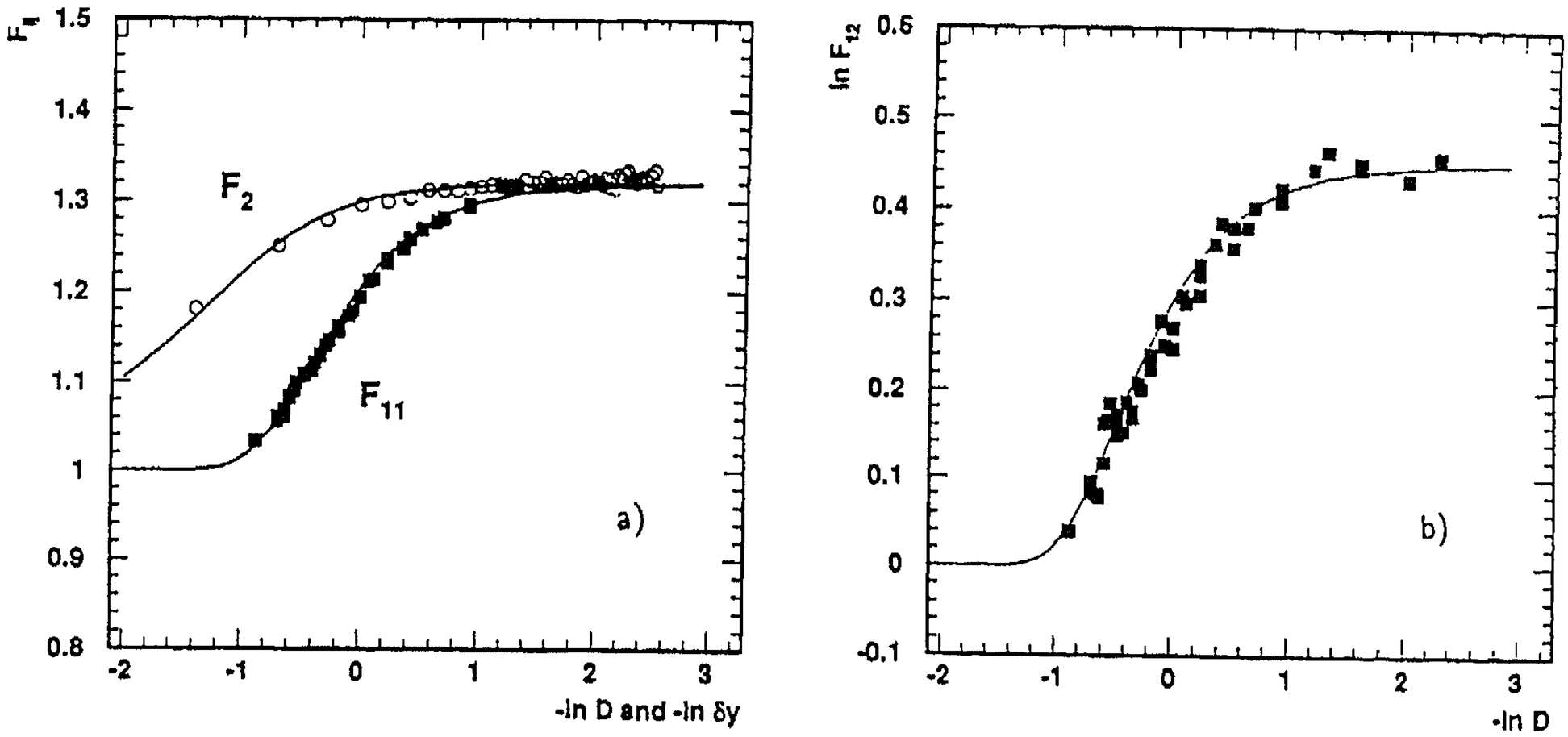

Fig. 4.28. (a) F_{11} versus D ($\delta y = 0.2$) and F_2 versus δy for a Gaussian-shaped two-particle correlation function [224] compared to NA22 data [223]; (b) F_{12} versus $D(\delta y = 0.2)$ as in (a).

It can be verified that, at least for the higher orders, the discrepancy with (4.21) is mainly due to the second equal sign, derived from a log-normal approximation to the density distribution. In a recent paper [180], this approximation has been shown to be valid if the density fluctuations are weak or if the density probability distribution is log-normal. The NA22 data demonstrate that none of these conditions is fulfilled.

We conclude that the correlators F_{pq} increase with decreasing correlation length D, but do not really follow a power law for $D \lesssim 1$. For fixed D, the values of F_{pq} do not depend on the resolution δy, a feature expected from the α-model, but also reproduced by FRITIOF and approximately true in any model with short-range order. When the increase of the correlators is roughly approximated by a straight line in a restricted interval, the powers ϕ_{pq} increase linearly with the product pq of the orders, but are considerably larger than expected from FRITIOF and from the simple α-model.

The extension of single-variate factorial moments to the multivariate case offers better insight into the complicated nature of the correlations. However, the original expectation that correlators would help in clarifying the issue of intermittency is not borne out by present data. Simple but reasonable models for higher-order correlation functions which use the experimental two-particle correlations as input, have no difficulty in reproducing the behaviour of factorial correlators measured e.g. by NA22.

4.7. Multifractal analysis

Power-law dependence of normalized factorial moments on the resolution δ (bin size) is a signature of self-similarity in the fluctuation pattern of particle multiplicity. It suggests that the probability distribution $P(\rho, \delta)$ of the particle density ρ has fractal properties. For simple

Widom–Wilson [225] type scaling, $P(\rho,\delta)$ is of the form

$$P(\rho,\delta) \sim \delta^{-\beta} P^*(\rho/\delta^{\nu}) , \tag{4.24}$$

where β and ν are critical exponents. All qth order moments of ρ ($q = 1, 2, \ldots$) obey power laws in δ with inter-related exponents depending on q and on (β,ν). This characterizes a simple or monofractal. Another possibility is a multifractal behaviour, in which $P(\rho,\delta)$ obeys a relation of the type (cf. [226])

$$\ln P(\rho,\delta)/\ln\delta = f(\alpha) , \quad \alpha = \ln\rho/\ln\delta . \tag{4.25}$$

Multifractals, first introduced in [227] represent infinite sets of exponents – the multifractal spectrum – which describe the power-law scaling of all moments of $P(\rho,\delta)$. In principle, knowledge of the multifractal spectrum is completely equivalent to knowledge of the probability distribution.

Unlike geometrical or statistical systems, multiparticle production processes pose special problems if a multifractal analysis is to be considered. The most obvious one is the finiteness of particle multiplicity in an event at finite energy. Self-similarity, if existent, therefore cannot persist indefinitely to finer and finer scales of resolution.

In multiparticle production $P(\rho,\delta)$ is not directly accessible. At best one can construct, for a single event of multiplicity n and for given δ, a frequency distribution which approaches $P(\rho,\delta)$ only for $n \to \infty$. For any finite (and usually small) n, the frequency distribution and its moments will be subject to statistical fluctuations.

Since the data sample contains a large number of events, it is obviously recommended to consider the event average. This averaging, however, supposes ergodicity. The applicability of the multifractality concept can, therefore, only be justified a posteriori.

4.7.1. The method

A multifractal analysis is based on the properties of G-moments whose definition is given in (2.73). The moments G_q (or more often $\ln G_q$) are obtained for each individual event at a specified resolution $\delta y \sim 1/M$ and then averaged over the event sample.[3]

In the theory of multifractals, the G-moments share with the scaled factorial moments the property that self-similar density fluctuations lead, in principle, to scaling behaviour

$$G_q \propto (\delta y)^{\tau_q} \quad \text{for } \delta y \to 0 . \tag{4.26}$$

In a fractal analysis (see also Section 2.4), one therefore determines the slope

$$\tau(q,M) = -\partial\langle \ln G_q(M)\rangle/\partial \ln M \tag{4.27}$$

on a double-logarithmic plot, after averaging over all events in the sample.

A multifractal spectral function is introduced via a Legendre transform defined as

$$f(\alpha_q) = q\alpha_q - \tau_q , \tag{4.28}$$

with

$$\alpha_q = \partial\tau_q/\partial q \tag{4.29}$$

[3] Note that analyses based on $\langle G_q\rangle$ or on $\langle \ln G_q\rangle$ in general differ and probe different aspects of the system under study [228].

being the Lipschitz–Hölder exponents. The spectral function $f(\alpha_q)$ is a smooth function, concave downward, with its maximum at $q = 0$. It gives a quantitative description of the density fluctuations in the dense and in the sparse regions, corresponding to its left and right wing, respectively. A wide spectrum reveals a non-smooth density distribution.

The generalized (Rényi)-dimensions are given by

$$D_q = [1/(q-1)]\,\tau_q = [1/(q-1)]\,[q\alpha_q - f(\alpha_q)]\,. \tag{4.30}$$

4.7.2. Experimental results

G moments have been studied in a number of experiments [140, 152–154, 156, 158, 159, 229, 238]. As an illustrative example, we show UA1 results [233] in Fig. 4.29(a), where the event average $\langle \ln G_q \rangle$ is plotted as a function of the resolution ($M = 2^\mu$). Starting at a value of 0 for $\mu = 0$ according to definition (2.73), the moments grow for $q < 1$ and fall for $q > 1$ as μ increases. The slopes decrease and $\langle \ln G_q \rangle$ tends to saturate for large μ. The saturation is due to an increasing number of bins with content $n_m = 0$ or 1, as M becomes large,

$$G_q(M) \to n(1/n)^q = n^{1-q} \quad \text{for } M \to \infty. \tag{4.31}$$

Fig. 4.29(b) shows $\langle \tau_q \rangle$ and $\langle \alpha_q \rangle$ for $\mu = 1$ and 2 (small M). The corresponding spectral function $\langle f(\alpha_q) \rangle$ is given in Fig. 4.29(c) as a function of $\langle \alpha_q \rangle$. The fact that $\langle f(\alpha_q) \rangle$ does not degenerate into a single point implies multifractality in hadron production, at least for large bin size $\delta y = \Delta Y/M$ (small μ). However, for smaller bin sizes, the function turns over (i.e. bends upward) and falls into the non-physical region above the dashed line (not shown).

4.7.3. Universality

From Fig. 4.29(c), it is clear that $\langle f(\alpha) \rangle$ depends on μ. It also depends on the cms energy $\sqrt{s}$ (or the multiplicity $n = 2^\nu$). In [30] it is conjectured that G moments (at fixed q) show universality in $\xi = \mu - \nu$, however. The latter quantity is directly related to the average particle multiplicity per bin, $n/M = 2^{\nu-\mu} = 2^{-\xi}$. Using a branching model, the authors of [30] derive the universality relation

$$\Gamma_q(\xi) = \ln G_q(\mu, \nu) - \ln G_q(\nu, \nu)\,. \tag{4.32}$$

It expresses the scaling behaviour of a function of two variables (μ, ν) in terms of a function of one variable only. The function $\Gamma_q(\xi)$ determines the G moments as functions of μ for all values of ν. The validity of (4.32) is claimed to be a strong evidence for self-similarity.

Fig. 4.30(a) shows Γ_q as a function of ξ for $q = \pm 5$. All data points are close to universal lines, thus indeed indicating universal behaviour.

A further prediction is that also $\langle f(\alpha_q) \rangle$ is universal for fixed ξ. Fig. 4.30(b) demonstrates that this is not confirmed by the UA1 data [233]. In the EMC data [140] the left branch shows universality, but not the right one. Besides being more sensitive to universality breaking than $\Gamma_q(\xi)$, the function $\langle f(\alpha_q) \rangle$ also reveals more clearly shortcomings in the models. For PYTHIA and GENCL this is illustrated by Fig. 4.30(b).

4.7.4. Modified G moments

As stated earlier, G moments have the advantage that not only spikes are included in the analysis, but also non-empty valleys (for $q < 0$). Disadvantages are that the moments saturate at

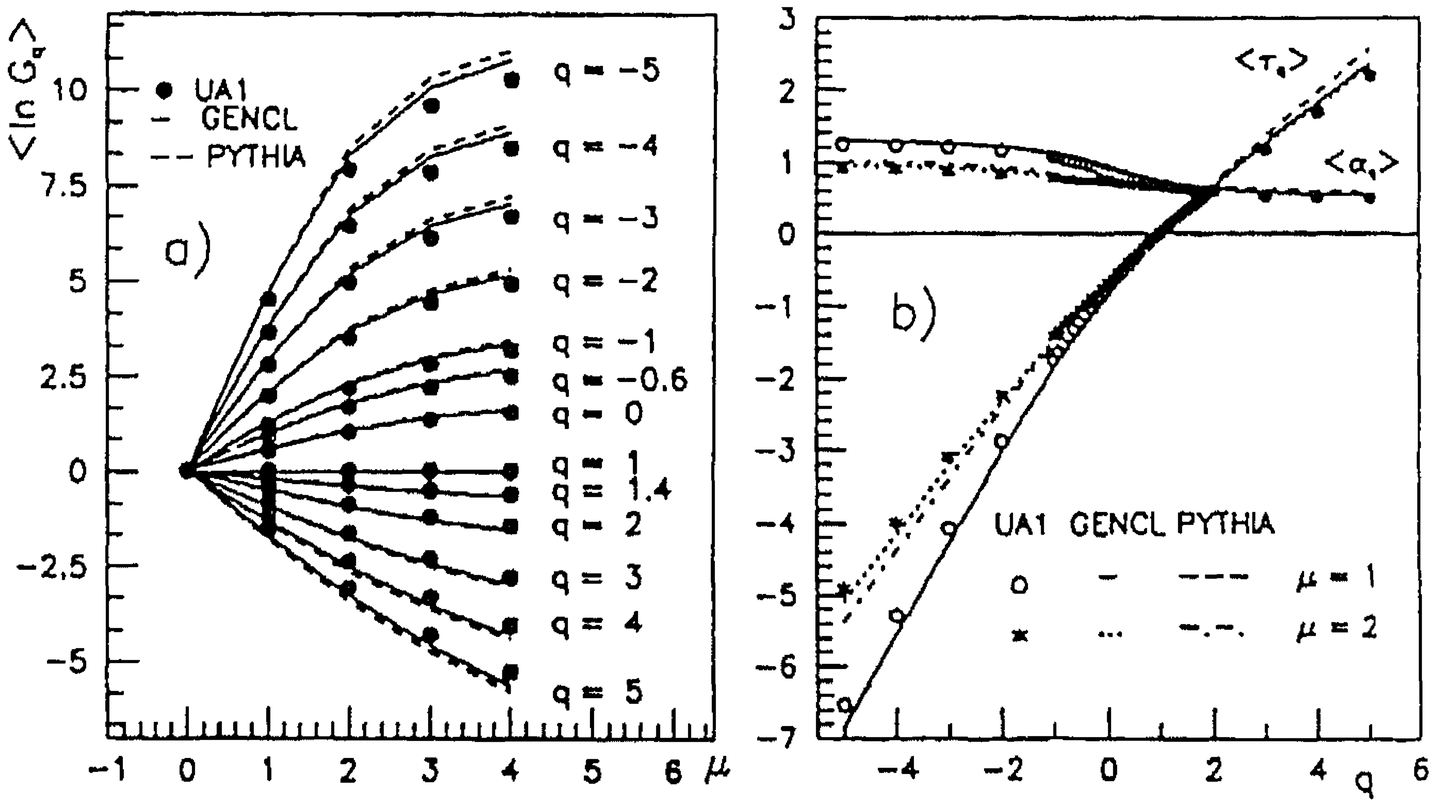

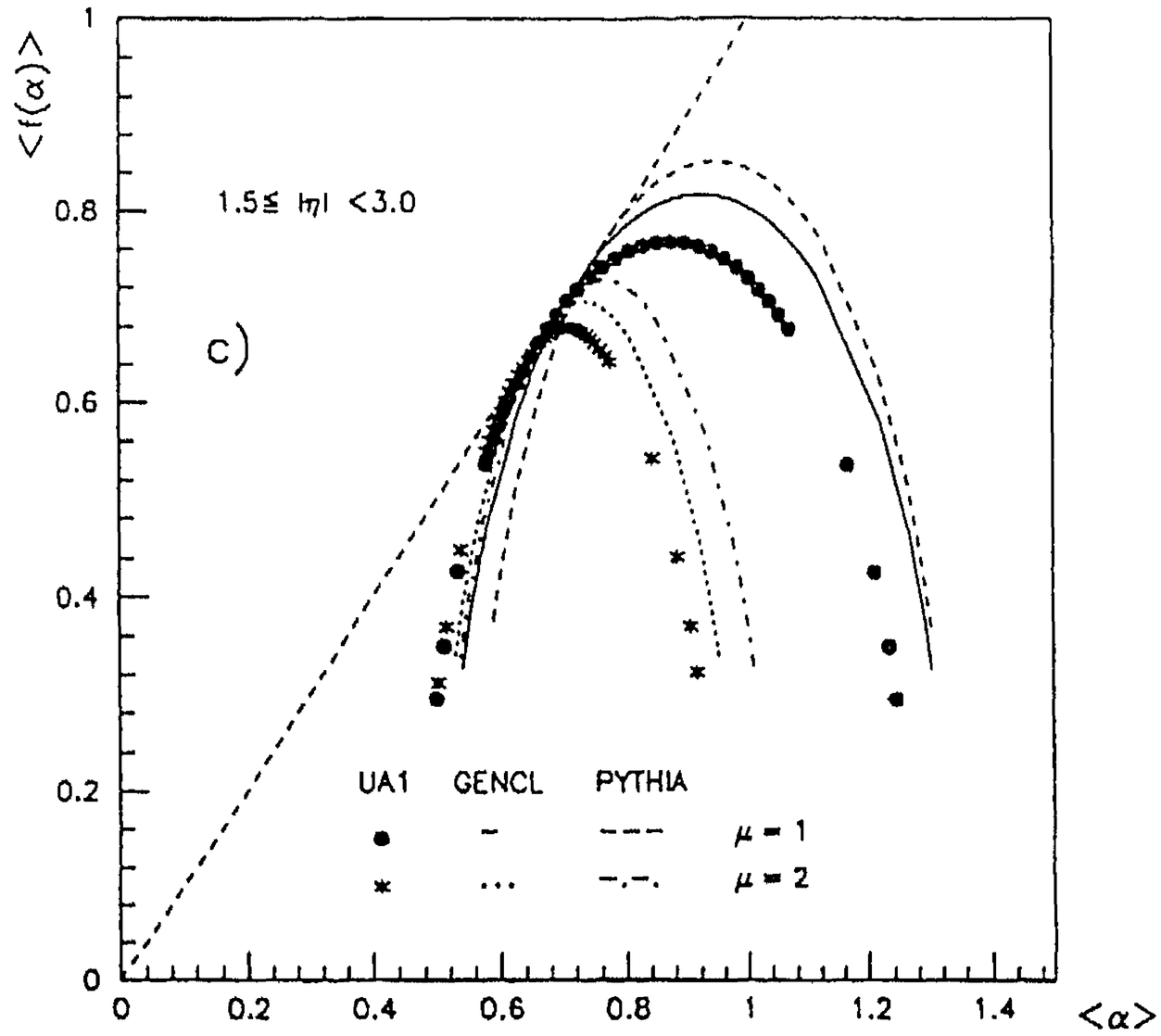

Fig. 4.29. (a) $\langle \ln G_q \rangle$ as a function of resolution ($M = 2^{\mu}$) for UA1 compared to the expectations from the Monte-Carlo models GENCL and PYTHIA, (b) $\langle \alpha_q \rangle$ and $\langle \tau_q \rangle$ as a function of q, (c) the multifractal spectral function $\langle f(\alpha_q) \rangle$ as a function of $\langle \alpha_q \rangle$ [233].

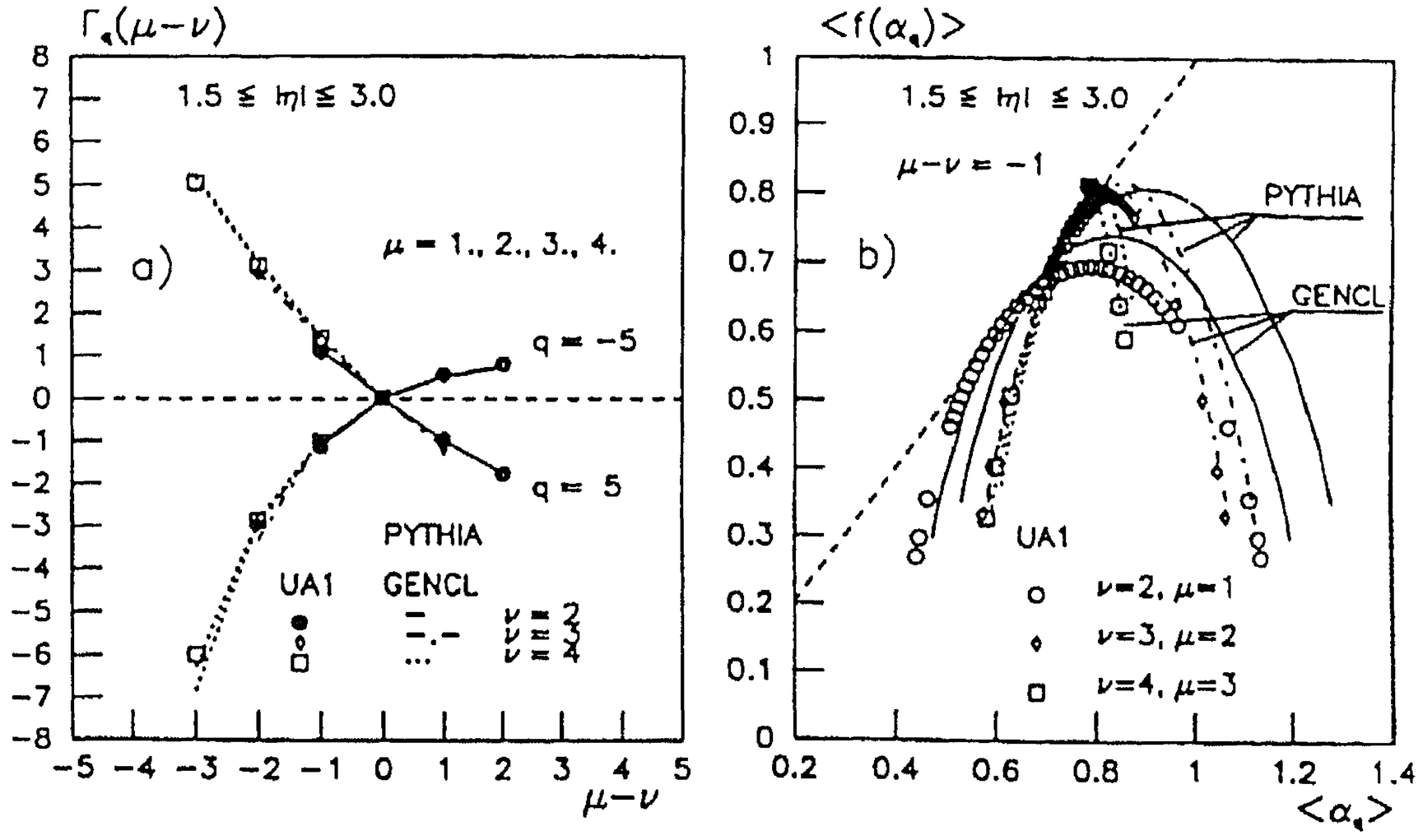

Fig. 4.30. (a) The universality function Γ_q as a function of $\xi = \mu - \nu$ for $q = \pm 5$ for UA1, (b) the spectral function $\langle f(\alpha_q)\rangle$ as a function of $\langle\alpha_q\rangle$ [233].

$\delta y \to 0$ when the content of non-empty bins approaches unity and that statistical fluctuations are not filtered out (see also [239,240]).

In [241] a modified definition of the G moments is proposed in an attempt to circumvent the problem of statistical noise. "Truncated" G moments are defined as

$$G_q = \sum_{m=1}^{M} p_m^q \Theta(n_m - q)\,, \tag{4.33}$$

where Θ is the usual step function equal to 1 for $n_m \geq q$ and zero otherwise. For very large multiplicity n (as in a macroscopic statistical system), $n/M \gg q$ and (4.33) is in practice identical to (2.73). In particle physics, n is a relatively small number and the Θ function exerts a crucial influence on the G moments. It imposes non-analytical cut-offs at positive integer values of q. With the help of a Monte Carlo (ECCO) based on the Geometrical Branching Model, the authors show that $\ln\langle G_q\rangle$ now exhibits a linear dependence on $\ln M$ for $q > 1$, without saturation.

For $q > 1$, the linearity of $\ln\langle G_q\rangle$ with $\ln M$ has been verified on μp, p̄p and e^+e^- data [230,233]. The slopes τ_q turn out to be very similar in all three reactions and roughly equal to $\tau_q = -0.9(q-1)$.

4.7.5. Bernoulli trials and G moments

Before we conclude the discussion of experimental characteristics of G moments, it is of interest to inquire in more detail about the dynamical content revealed in multifractal analyses. This is best done in a comparison to a model without dynamics.

Let $P(n)$ be the probability distribution for observing n particles in an initial wide interval ΔY. Let this interval be subdivided into M smaller intervals of size $\delta y = \Delta Y/M$, each of which contains n_m particles ($n_m = 0, 1, \ldots, n$; $m = 1, 2, \ldots, M$) with $\sum_m n_m = n$. Assume that for every subdivision of ΔY the n particles are independently distributed over the intervals with probability $1/M$. For fixed n, the joint occupation probability in M cells is given by (see also [239])

$$P_n(n_1, \ldots, n_M) = P(n) \frac{n!}{n_1! \ldots n_M!} \left(\frac{1}{M}\right)^n \delta\left(\sum_j n_j - n\right) . \tag{4.34}$$

With (4.34) the G moments (2.73) at fixed n are given by

$$G_q(n, M) = M n^{-q} \sum_{i=1}^{n} i^q B(n, 1/M; i) , \tag{4.35}$$

where $B(n, 1/M; i)$ is the binomial distribution. For integer $q \geq 1$ one obtains

$$G_q(n, M) = M n^{-q} \sum_{j=1}^{q} \mathcal{S}_q^{(j)} n^{[j]} , \tag{4.36}$$

$\mathcal{S}_q^{(j)}$ is a Stirling number of the second kind (cf. (2.67)) and $n^{[j]} = n(n-1)\cdots(n-j+1)$. In the Poisson limit of the binomial (n large and $1/M$ small with n/M fixed), (4.36) simplifies further to

$$G_q(n, M) = M n^{-q} \sum_{j=1}^{q} \mathcal{S}_q^{(j)} (n/M)^j . \tag{4.37}$$

In inclusive analyses the average over $P(n)$ has to be taken in (4.36)–(4.37). This introduces the (inverse) moments $\langle n^{j-q} \rangle$ and $\langle n^{[j]}/n^q \rangle$ of the multiplicity distribution in ΔY.

Numerical studies indicate that (4.35)–(4.37) reproduce and explain many of the multifractal and universality properties seen in the data. Here we can only give a few examples.

With respect to the structure of (4.35) it should be noted that the binomial distribution is in fact a multifractal[4] in the sense of (4.25) [242, 226]. Consequently, "proper", but quite trivial binomial multifractal behaviour will be seen if the data are noise dominated. This is the case in practically all analyses referred to before. This point was recognized in [239], but its full consequences were not further studied.

From (4.37) follows immediately that the function $\Gamma_q(\mu, \nu)$ defined in (4.32) depends only on the ratio $n/M = 2^{-\xi}$. Thus, the parameter-free function $\Gamma_q(\mu, \nu)$ is indeed, but trivially, universal in the Poisson limit. It describes accurately the data in Fig. 4.30(a). Being a purely mathematical property of noise, it is not surprising that the usual Monte-Carlo models also show this type of universality. $\Gamma_q(\mu, \nu)$ ceases to be universal in the (more general) binomial case, although the deviations remain small in cases of practical interest. This probably explains the universality breaking observed in e^+e^- Monte-Carlo simulations at 1–10 TeV in [243].

The above considerations can be extended to the modified G moments defined in (4.33). In particular $\Gamma_q(\mu, \nu)$ remains universal in the Poisson limit. Further numerical properties of modified G moments are illustrated on Fig. 4.31(a)–(c). The results shown are based on (4.37) further

[4] This is easily verified using Stirling's approximation to $n!$ which is notoriously accurate even for quite small n.

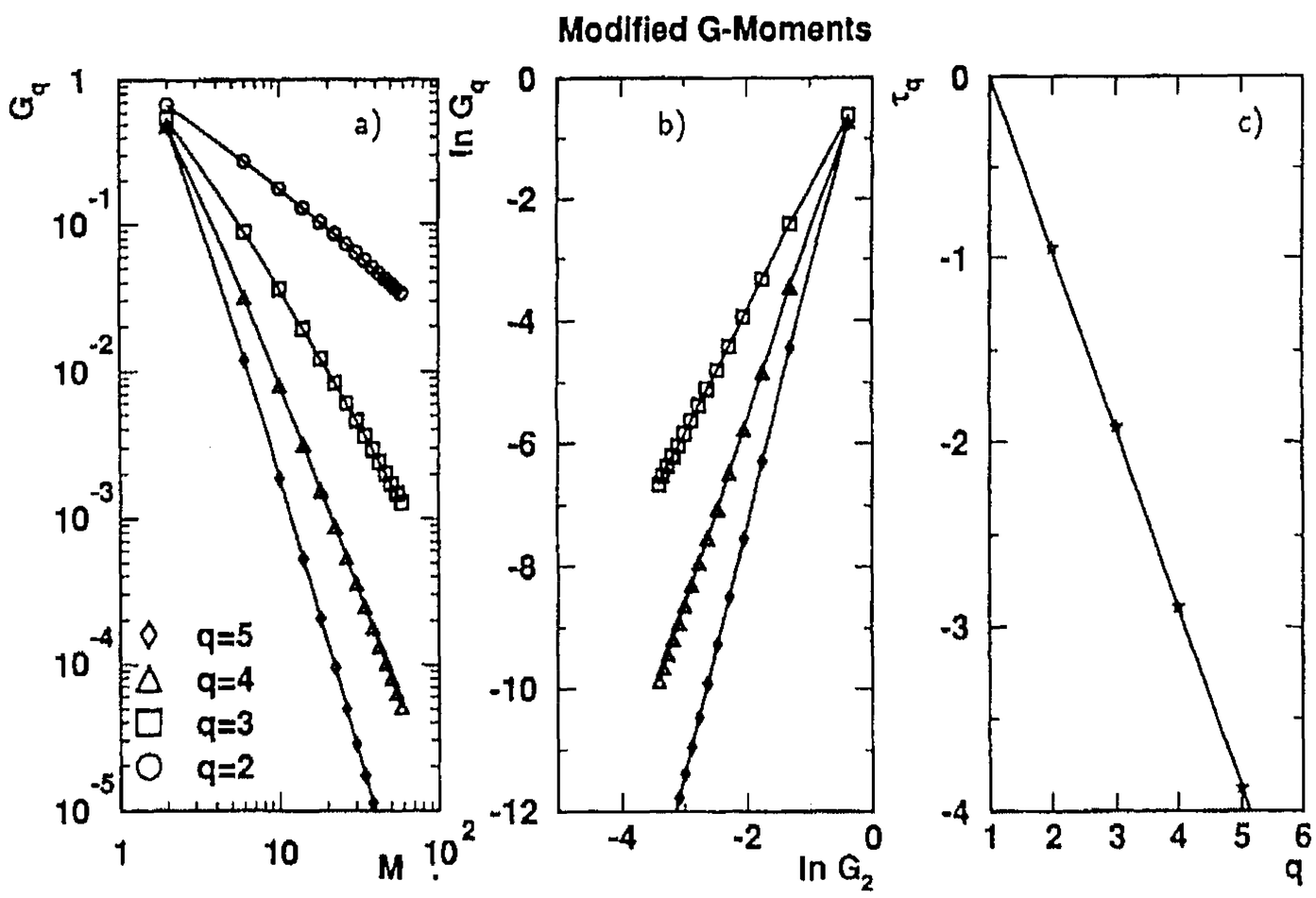

Fig. 4.31. (a)–(c) numerical results based on the Bernoulli-trial model (4.37) averaged with a negative binomial distribution $P(n)$ with $\langle n\rangle = 6.26$ and dispersion 2.94 [230]. The line in (c) is a fit to $\tau_q = -C(q-1)$.

averaged over n with a negative binomial distribution truncated at 0. They depend only on $\langle n\rangle$ in ΔY and on the NBD parameter k.

Fig. 4.31(a) demonstrates that the modified G moments can be well approximated by power laws. The pseudo-linearity extends over a much larger interval in M than for usual G moments obtained from (4.37). The improved linearity is due to negative terms in the expressions of truncated moments of the Poisson (or binomial) distribution. The calculations displayed in this figure coincide (up to an overall normalization factor) nearly exactly with the EMC data for $M \geq 8$ shown in [230]. This proves that the "clear asymptotic power-law behaviour of $\langle G_q\rangle$ characteristic for a self-similar system" [230] is in fact due to Bernoulli noise.

Fig. 4.31(b) shows the "Ochs–Wošiek" plot for modified G moments. Here again, the quasi-perfect linear relation between $\ln G_q$ and $\ln G_2$ is seen to be a characteristic of Bernoulli trials. This linearity property holds in fact for any combination of $\ln G_q$ and $\ln G_{q'}$. The exponents τ_q derived from power-law fits to the "data points" in Fig. 4.31(a) are shown in Fig. 4.31(c). The line is a fit with the form $\tau_q = -C(q-1)$. The slope C is a slowly changing function of the NBD parameter k with a value around 0.9, as experimentally observed in Section 4.7.4 above!.

4.7.6. Evaluation of noise and connection between F_q and G_q

The self-similar property of multiparticle production at high energy can, in principle, be investigated by F moments and by G moments. The power-law behaviour of the scaled F moments provides evidence for a self-similar cascading process of dynamical origin. The G moments, as an ingredient of fractal theory, are designed to describe the multifractality aspect of high multiplicities. In the real environment of high energy collisions, however, the multiplicities are rather low and the G moments are dominated by statistical fluctuations.

The F moments are defined for integer powers $q \geq 1$, the G moments for all real powers q. In order to establish a connection to the F moments, the powers q are restricted to integer values of $q \geq 1$ here also for the G moments.

The number n_m of particles per subdivision $\delta y = \Delta y/M$ has to be equal to, or larger than q ($n_m = q + k$, $k = 0, 1, \ldots$) for the F- and G-moments. Functions

$$B_{q,k}(M) = \left\langle \frac{Q_{q+k}(M,n)}{n^q} \right\rangle \tag{4.38}$$

are defined from the number of bins $Q_{n_m}(M,n)$ containing $n_m = q + k$ particles in an event of multiplicity n in the total phase-space region Δy, normalized by n^q and averaged over all events. They express the basic fractal structure of the data, if they show a power-law behaviour of the form

$$B_{q,k}(M) \propto M^{\lambda_{q,k}(M)} . \tag{4.39}$$

In order to suppress statistical fluctuations, the G moments can be defined as the event average over (4.33), or, equivalently, as

$$\langle G_q(M) \rangle = \sum_{k=0}^{\infty} B_{q,k}(M)(q+k)^q . \tag{4.40}$$

They are proportional to $M^{-\tau_q}$ for large M. The F moments are defined as

$$\langle F_q(M) \rangle = M^{-1} \sum_{m=1}^{M} \langle n_m(n_m - 1) \cdots (n_m - q + 1)/(n/M)^q \rangle \tag{4.41}$$

or, equivalently, as

$$\langle F_q(M) \rangle = M^{q-1} \sum_{k=0}^{\infty} B_{q,k}(M)(q+k)!/k! . \tag{4.42}$$

They are proportional to M^{ϕ_q} for large M (note, however, that (4.41) is different from the form (2.68) of the F moments generally used).

When (4.33) and (4.40)–(4.42) are applied to the data they should show a power-law behaviour for large M, if there are fractal structures present in the data.

The dynamical contribution to the G moments can be expressed by

$$\langle G_q \rangle^{\mathrm{dyn}} = [\langle G_q \rangle / \langle G_q \rangle^{\mathrm{st}}] M^{(1-q)} , \tag{4.43}$$

where $\langle G_q \rangle^{\mathrm{st}}$ can be determined by distributing the n particles of an event randomly in Δy. The randomization procedure destroys short-range particle correlations, but does not alter the Bernoulli nature of the particle repartition in smaller bins discussed in Section 4.7.5. As a result, this method does not eliminate the binomial, noise-induced multifractal behaviour, but just gives its behaviour.

When $\langle G_q \rangle^{\mathrm{st}}$ is equal to $\langle G_q \rangle$, a trivial "dynamical" effect remains: a flat $\mathrm{d}n/\mathrm{d}y$ leads to a probability $1/M$ for a particle to be in a given bin and $\langle G_q \rangle^{\mathrm{dyn}} = M^{1-q}$.

The dynamical contributions to the slope τ_q can be expressed by

$$\tau_q^{\mathrm{dyn}} = \tau_q - \tau_q^{\mathrm{st}} + q - 1 , \tag{4.44}$$

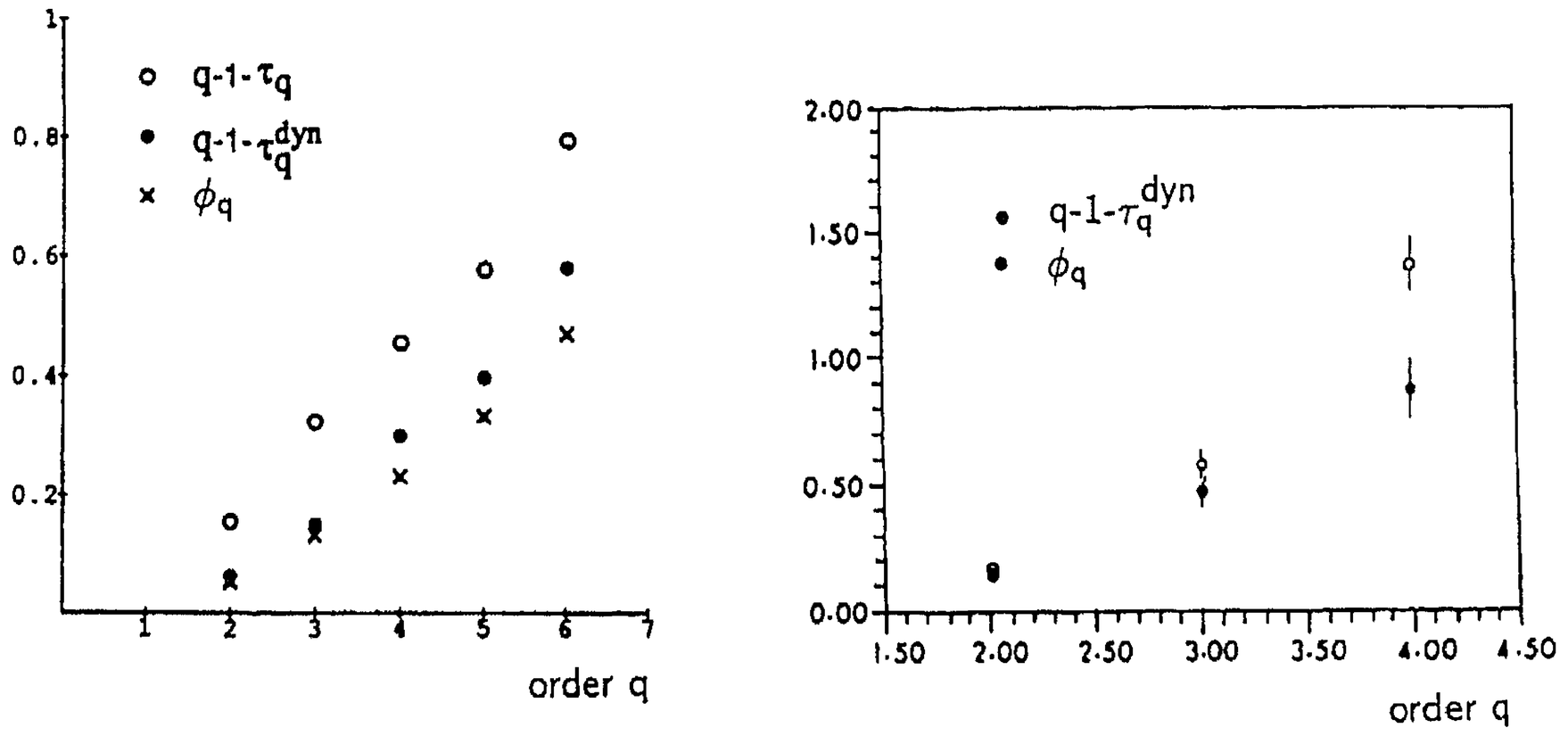

Fig. 4.32. Comparison of the exponents ϕ_q of F_q and $1-q-\tau_q^{dyn}$ (respectively $1-q-\tau_q$) of G_q in (a) ECCO Monte-Carlo simulations [241] and (b) π^-AgBr data at 350 GeV/c [152].

where τ_q^{st} is the statistical part of the slope. Subtracting the statistical contribution from τ_q gives

$$\tau_q - \tau_q^{st} = \tau_q^{dyn} - q + 1 \approx -\phi_q \tag{4.45}$$

which can be directly compared to the slopes ϕ_q obtained from the F moments [241].

Fig. 4.32(a) gives a comparison [241] of ϕ_q (crosses) and $(q-1-\tau_q^{dyn})$ (full circles) from ECCO simulation results and shows that the deviation of τ_q^{dyn} from $q-1$ is indeed close to the deviation of ϕ_q from zero. This observation gains support from the UA1 [233], hA [152] (Fig. 4.32(b)) and AA [156] analysis. The remaining difference can be attributed to the difference in the definition of $\langle F_q\rangle$ and $\langle G_q\rangle$.

Fig. 4.32(a), however, also shows that τ_q^{dyn} cannot be simply replaced by τ_q (open circles) in a quantitative analysis. This is in agreement with the observation of Section 4.7.5, but has not been taken into proper consideration in recent experimental application on lh [230], hA [153] and AA [236] collisions.

To summarize the present experimental findings, the data indicate that the multifractal spectral function $f(\alpha)$ has, at least for large bin sizes, the properties expected from the theory of multifractals. The function $f(\alpha)$ is very sensitive to violations of universality and to details of present Monte-Carlo models. However, with the methods used so far, the multifractality analysis breaks down at finer resolution. The finite multiplicity effect – statistical noise – overwhelms and it is difficult to disentangle it from dynamical features. An advantage is that the $\langle G_q\rangle$ can probe holes in the distribution, not just spikes. A recent extension of the definition of the G moments filtering out high multiplicities can claim some success in extracting the dynamical component. The advantage is that $\langle G_q\rangle^{dyn}$ lends itself more readily to (multi)fractal interpretation and direct extraction of the Rényi dimensions according to (2.114), while $\langle F_q\rangle$ is more closely related to the correlation function. Fig. 4.32 can serve as a rough link between the two. Whereas a higher-dimensional

analysis could be useful also here, the low average multiplicity even in the highest energy experiments presently precludes further progress in this direction.

4.7.7. Universal multifractals

At first sight interesting approaches, recently applied [51] to obtain the degree of multifractality (or Lévy index) μ in multiparticle production, are the methods of Probability Distribution Multiple Scaling (PDMS) and Double Trace Moments (DTM) [50]. In the first method, the fundamental scaling law is written in terms of the probability for the number of particles n_m in bin m at resolution M to be larger than a certain threshold $n_{\text{th}} = M^{\gamma}$,

$$P(n_m(M) > M^{\gamma}) \propto M^{-c(\gamma)} . \tag{4.46}$$

The statistical function $c(\gamma)$ is the codimension function describing the sparseness of large intensities n_m. Like the factorial moments (2.68)–(2.70) or the extended G-moments (4.33), the DPMS method is a straightforward filter for spikes of large n_m.

The PDMS method is closely related to Large Deviation Theory, a topic in probability theory and of much theoretical interest in statistical mechanics [244]. Eq. (4.46) expresses a Level-2 Large Deviation property, describing deviations of the "empirical measure" n_m from the infinite sample probability density; $c(\gamma)$ is related to a generalized entropy.

Fig. 4.33(a) shows data [51] at different charge multiplicity ($n = 6$ and 14 are given as examples) presented in a double-logarithmic plot, for various threshold values $n_{\text{th}} = M^{\gamma}$. In spite of limitations on statistics and on multiplicity n_m, a region of linearity can be seen for all multiplicities and thresholds. This is claimed to be evidence for PDMS.

When $c(\gamma)$ is smaller than the topological dimension D of the embedding space, it is possible to define a function $D(\gamma) = D - c(\gamma)$ corresponding to the classical fractal dimension. If a sample of N_s events is used in the analysis (instead of one event), $c(\gamma)$ can become larger than the topological dimension since different events can contribute to the same bin m. In Fig. 4.33(b) the function $c(\gamma)$ is shown for the same multiplicities. The dotted line corresponds to $c(\gamma_s) = D + D_s$, where D_s is the sample dimension defined as $N_s = M^{D_s}$. For $n = 20$ e.g. this limit is crossed for a threshold of $n_{\text{th}} = 3$ with $N_s = 15$. Singularities of that type are called "wild" singularities (not arising from Poisson-like fluctuations).

A parametrization of $c(\gamma)$ in terms of two parameters is provided by the theory of universal multifractals [50],

$$\begin{aligned} c(\gamma) &= C_1 \left(\frac{\gamma}{\mu' C_1} + \frac{1}{\mu} \right)^{\mu'} \quad \text{for } \mu \neq 1 \\ &= C_1 \exp\left(\frac{\gamma}{C_1} - 1 \right) \quad \text{for } \mu = 1 , \end{aligned} \tag{4.47}$$

with

$$\frac{1}{\mu} + \frac{1}{\mu'} = 1 \quad \text{and} \quad 0 \leq \mu \leq 2;$$

μ is the Lévy index giving the degree of multifractality and C_1 is the codimension of the average field. The two parameters can be obtained from fits to the results given in Fig. 4.33(a), but turn out to be highly correlated.

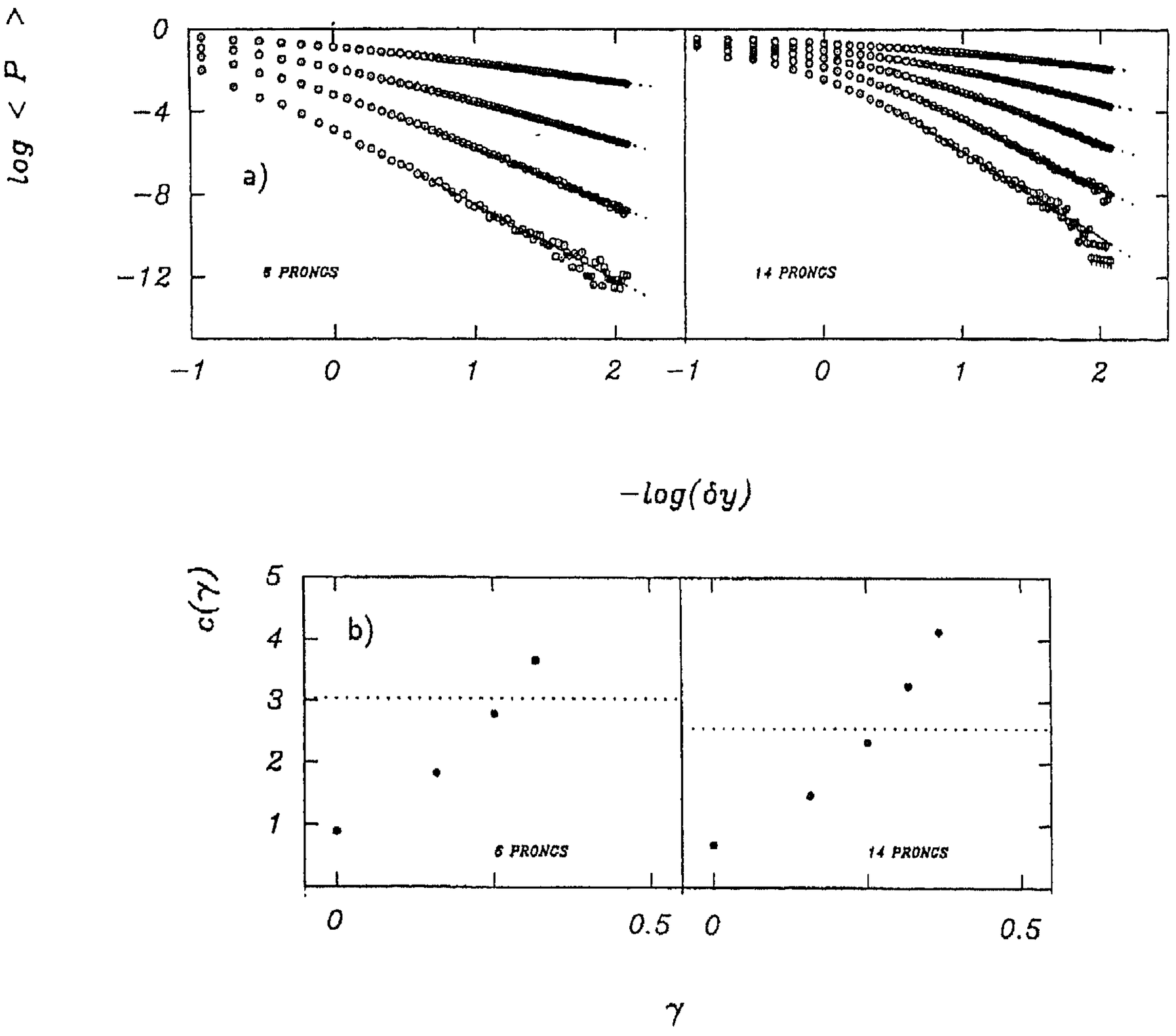

Fig. 4.33. (a) Plot of $\log P$ versus $-\log \delta y$ for $n = 6$ and 14. The data correspond, downwards, to thresholds $n_{\text{th}} \equiv M^{\gamma} = 1, 2, 3, 4, 5$; (b) codimension functions $c(\gamma)$ versus degree of singularity γ for $n = 6$ and 14 [51].

The Lévy index μ can, however, be determined independent of C_1 with the help of the Double Trace Moments [50], a generalization of the G moments. They are defined in (2.126). A DTM analysis of $\sqrt{s} = 16.7$ GeV data [51] yields μ values ranging from 0.4 to about 0.9, increasing with multiplicity n. Such values are far from monofractality ($\mu = 0$), but considerably below $\mu \sim 1.6$ obtained in Section 4.3.3 from factorial moments.

For multifractal theory, it is important to know whether the limit $\mu = 1$ is crossed (signalling "hard unbounded" singularities) or asymptotically approached from below (indicating "soft bounded" singularities). This question cannot be answered at low energies and needs high-energy, high-multiplicity data.

Extension to higher-dimensional space, though difficult in practice, is necessary since singularities can easily be washed out if a particular variable is not sensitive to them.

In spite of the interesting potential of the "Universal Multifractal" idea, one should keep in mind that the method suffers from the same limitations as the multifractal method based on G-moments. This is easily illustrated by considering again the Bernoulli-trials model discussed in Section 4.7.5, above. For the pure binomial noise (4.34), one has

$$P_B(n_m(M) \geq n_{\text{th}}) = I_{1/M}(n_{\text{th}}, n - n_{\text{th}} + 1)\,, \tag{4.48}$$

where $I_x(a,b)$ is the incomplete beta function [16].

The logarithm of (4.48) is approximately linear in $\ln M$ for reasonably large M. Eq. (4.48) not only has all the features of the data plotted in Fig. 4.33(a), but even agrees numerically quite well. The co-dimension function $c(\gamma)$ is, for this simple model, approximately equal to n_{th}, implying constant differences between the slopes for successive values of n_{th}. The data in Fig. 4.33(b) show exactly this property.

Double Trace Moments are easily calculated in the Bernoulli model. We find that the "Lévy index" μ is a smoothly increasing function of the event multiplicity n crossing the "hard unbounded" value $\mu = 1$ near $n = 30$. We conclude that the data in Fig. 4.33 are merely reflecting statistical noise.

Dynamically useful information could possibly be extracted if Double Trace *factorial moments* were used instead of the usual moments. This is easily verified on the simple Bernoulli model and, of course, applies to G-moments as well.

4.8. Density and correlation strip integrals

4.8.1. The method

A fruitful recent development in the study of density fluctuations is the density and correlation strip-integral method [130, 245, 246]. By means of integrals of the inclusive density over a strip domain, rather than a sum of box domains, one not only avoids unwanted side-effects, such as splitting up of density spikes, but also drastically increases the integration volume (and therefore the accuracy) at a given resolution.

Consider first the (vertical) factorial moments F_q defined, for an analysis in one dimension, as

$$F_q(\delta y) \equiv \frac{1}{M}\sum_{m=1}^{M}\frac{\langle n_m^{[q]}\rangle}{\langle n_m\rangle^q} = \frac{1}{M}\sum_{m=1}^{M}\frac{\int_{\Omega_m}\prod_i \mathrm{d}y_i\,\rho_q(y_1\ldots y_q)}{\int_{\Omega_m}\prod_i \mathrm{d}y_i\,\rho_1(y_1)\ldots\rho_1(y_q)}\,. \tag{4.49}$$

The integration domain $\Omega_{\text{B}} = \sum_{m=1}^{M}\Omega_m$ thus consists of M q-dimensional boxes Ω_m of edge length δy. For the case $q = 2$, Ω_{B} is the domain in Fig. 4.34(a). A point in the mth box corresponds to a pair (y_1, y_2) of distance $|y_1 - y_2| < \delta y$ and both particles in the same bin m. Points with $|y_1 - y_2| < \delta y$ which happen *not* to lie in the same but in adjacent bins (e.g. the asterix in Fig. 4.34(a)) are left out. The statistics can be approximately doubled by a change of the integration volume Ω_{B} to the strip domain of Fig. 4.34(b). For $q > 2$, the increase of integration volume (and reduction of squared

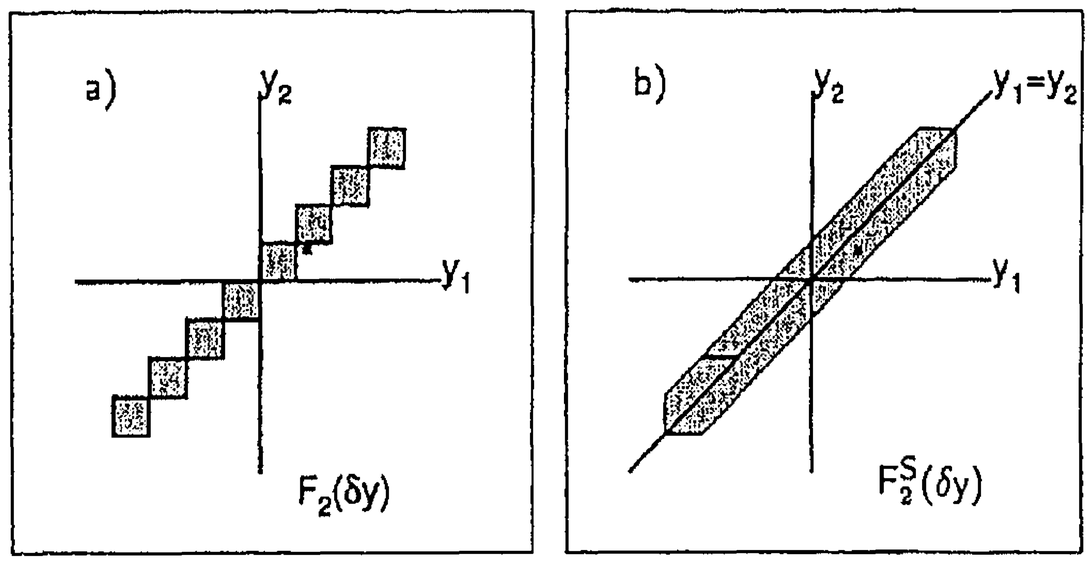

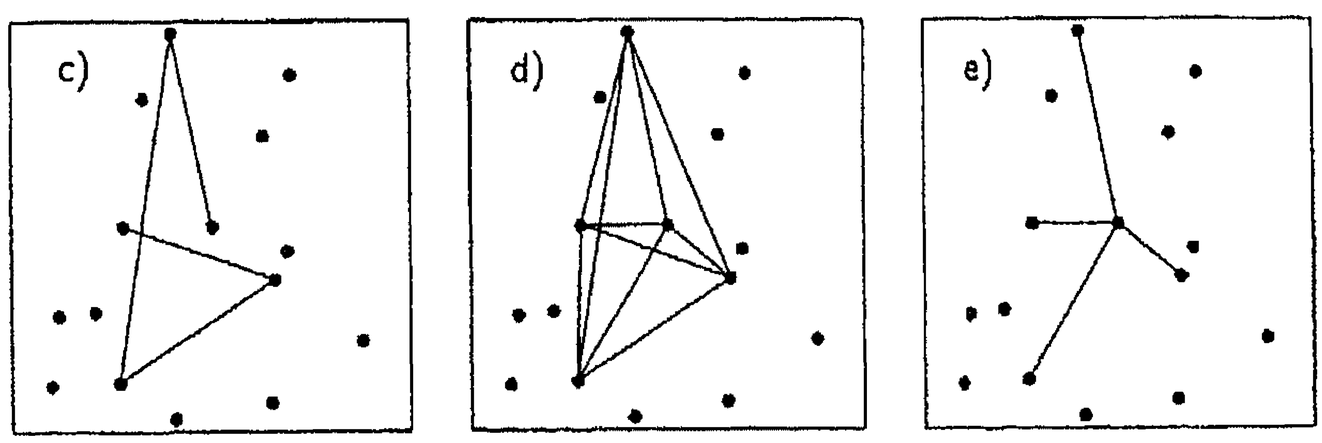

Fig. 4.34. (a) The integration domain $\Omega_B = \sum_m \Omega_m$ of $\rho_2(y_1, y_2)$ for the bin-averaged factorial moments, (b) the corresponding integration domain Ω_S for the density integral [246], (c) illustration of a q-tuple in snake topology, (d) GHP topology, (e) star topology.

statistical error) is in fact roughly proportional to the order of the correlation. The gain is even larger when working in two or three phase-space variables.

In terms of the strips (or hyper-tubes for $q > 2$), we define as (vertical) *density* integrals

$$F_q^S(\delta y) \equiv \frac{\int_{\Omega_s} \prod_i \mathrm{d}y_i \, \rho_q(y_1, \ldots, y_q)}{\int_{\Omega_s} \prod_i \mathrm{d}y_i \, \rho_1(y_1) \ldots \rho_1(y_q)} \tag{4.50}$$

and, similarly, the *correlation* integrals $K_q^S(\delta y)$ by replacing the density $\rho_q(y_1, \ldots, y_q)$ by the correlation function $C_q(y_1, \ldots, y_q)$. (Note that in the literature the term "correlation integral" is often also used for the $F_q^S(\delta y)$.)

These integrals can be evaluated directly from the data, after selection of a proper distance measure $(|y_i - y_j|, [(y_i - y_j)^2 + (\phi_i - \phi_j)^2]^{1/2}$, or better the four-momentum difference $Q_{ij}^2 = -(p_i - p_j)^2)$ and after definition of a proper multiparticle topology, the snake integral [107], the GHP integral [130], or the star integral [247] as shown in Figs. 4.34(c)–(e), respectively.

4.8.2. Results

As an example, $F_4(\delta y)$ is compared to $F_4^S(\delta y)$ (and F_2^S, F_3^S) for the NA22 spike event [119] in Fig. 4.35(a) (no error bars are shown, because it is one event). Depending on whether the prominent spike lies entirely in one bin or is split across two, F_4 shows large fluctuations. These are practically absent in F_4^S (Fig. 4.35(b)). Large improvement in one-dimensional (η) and two-dimensional ($\eta - \varphi$) analysis is also observed in [248].

How much the statistical errors are reduced can be seen on Fig. 4.36(a) where the NA22 data [142] are plotted as a function of $-\ln Q^2$, with all two-particle combinations in an n-tuple having $Q_{ij}^2 < Q^2$ [130]. The following observations can be made:

(i) the errors and fluctuations are indeed largely reduced, as compared e.g. to Fig. 4.20(a),

(ii) with the (one-dimensional) distance measure Q^2, the moments show a similarly steep rise as in the three-dimensional analysis (e.g. Fig. 4.11(c)),

(iii) contrary to the results in rapidity, positives and negatives behave very similarly here (only negatives are shown in Fig. 4.36(a)), but are now much steeper than all-charged,

(iv) F_2^S is flatter for $(+\ -)$ than for all-charged or like-charged combinations.

The first two observations demonstrate the strength of the new method and the advantage of using the proper variable. The second two observations directly demonstrate the large influence of identical particle correlations on the factorial moments. These results agree very well with results from the UA1 collaboration [143] shown in Fig. 4.36(b) and with Ih results [77, 249].

Monte-Carlo simulations with FRITIOF 2 show the following (see Fig. 4.37 for the case of F_2^S). The default "plain" version is unable to describe the all-charged NA22 data, but a "biased" version (including misidentified Dalitz decay + 0.25% undetected γ conversions) comes closer to the data. However, not unexpectedly, both versions fail completely in describing the like-sign data, where the

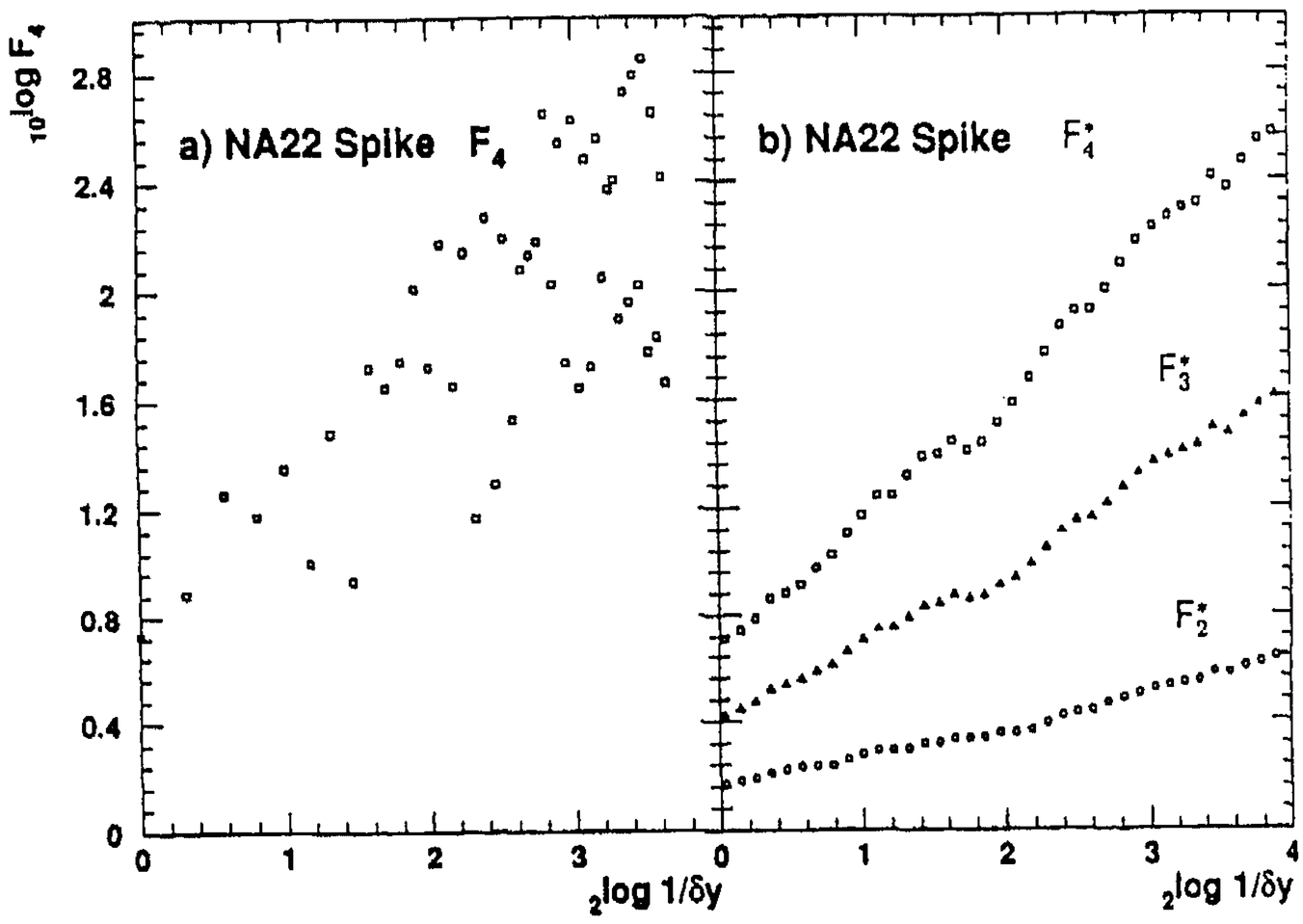

Fig. 4.35. (a) The fourth factorial moment of the NA22 spike event [119], (b) the density strip integrals for $q = 2$–4 [246].

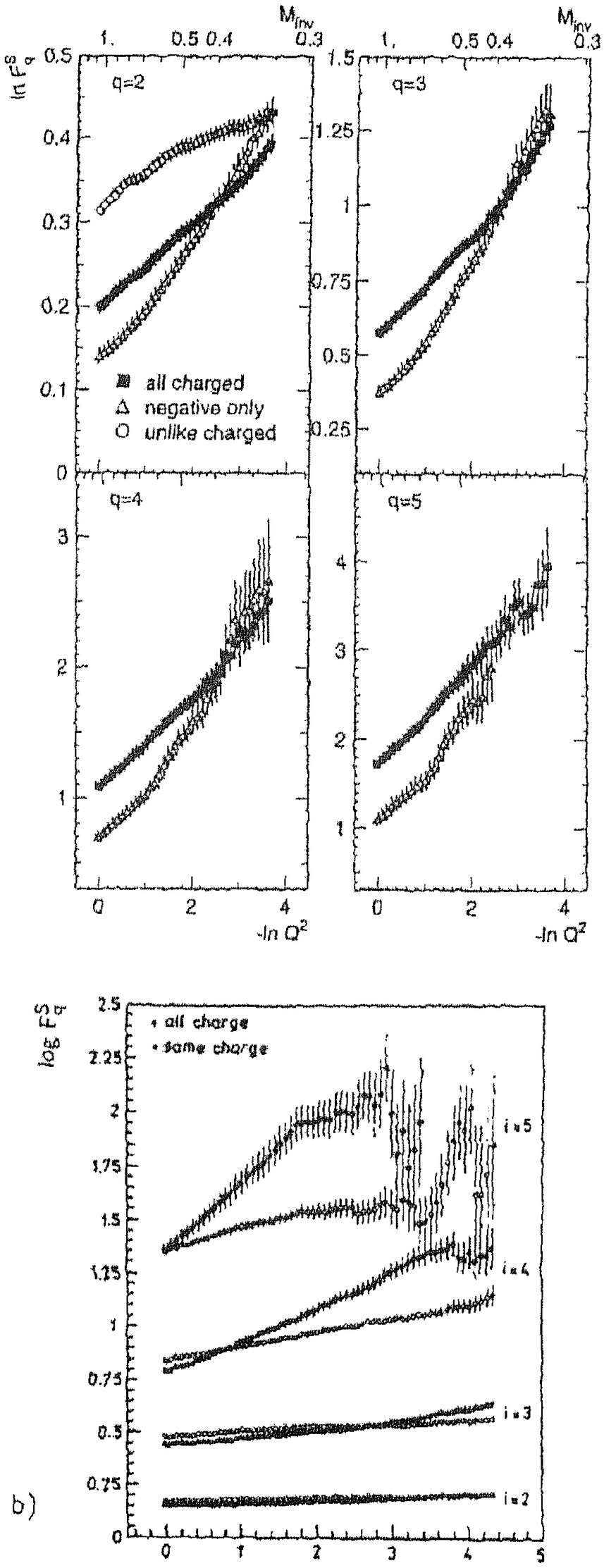

Fig. 4.36. Density strip integrals C_q for $q = 2 - 5$ for (a) all-charged and negatives in $\pi^+ p$ and $K^+ p$ collisions at $\sqrt{s} = 22$ GeV (the integral F_2^5 is also given for $(+\ -)$ combinations) [142], (b) all-charge and same-charge combinations in $p\bar{p}$ collisions at 630 GeV [143].

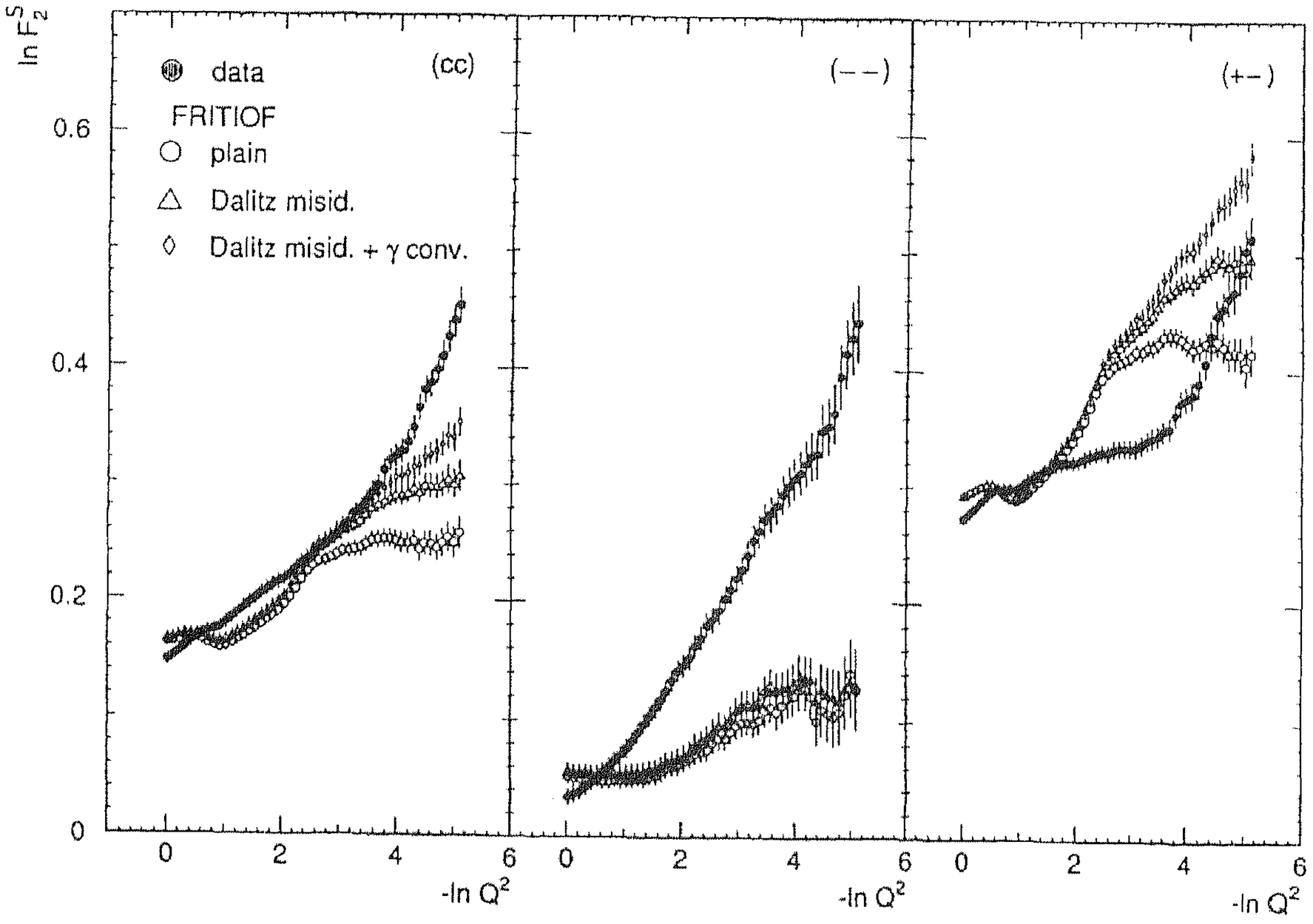

Fig. 4.37. $\ln F_2^S$ in the NA22 data (full circles) compared to FRITIOF2.0, FRITIOF2.0 with Dalitz decay and γ-conversion (open symbols), for (cc), $(--)$ and $(+-)$ combinations, as indicated [142].

model stays way too low. On the other hand, F_2^S for the $(+-)$ combination is largely overestimated when γ-conversions are included, but saturates without.

4.8.3. Transverse-momentum and multiplicity dependence

As in Section 4.4.2 (Fig. 4.20(c)), UA1 [210] has studied the ϕ_2 dependence on the average transverse momentum $\bar{p}_T$ of the event, but now in terms of density integrals in Q^2. In contrast to the strong decrease (and subsequent slight increase of ϕ_2) with increasing $\bar{p}_T$ observed for the one-dimensional analysis in Fig. 4.20(c), a strikingly flat behaviour (and slight increase above 0.6 GeV/c) is observed for the data (full circles) in Fig. 4.38(a). The discrepancy of PYTHIA (open circles) is even stronger here than in Fig. 4.20(c). The slope ϕ_2 starts at even negative values for small $\bar{p}_T$, but increases fast with increasing $\bar{p}_T$ to reach values overestimating ϕ_2 at $\bar{p}_T \gtrsim 0.5$ GeV/c.

A similar disagreement is observed for the multiplicity dependence in Fig. 4.38(b). While the UA1 data (full circles) decrease with increasing n, PYTHIA predicts a strong increase. In Figs. 4.38(c) and (d), it is shown that this violent discrepancy between PYTHIA and data is mainly due to like-sign pairs, so to the way Bose–Einstein correlations are incorporated into the model.

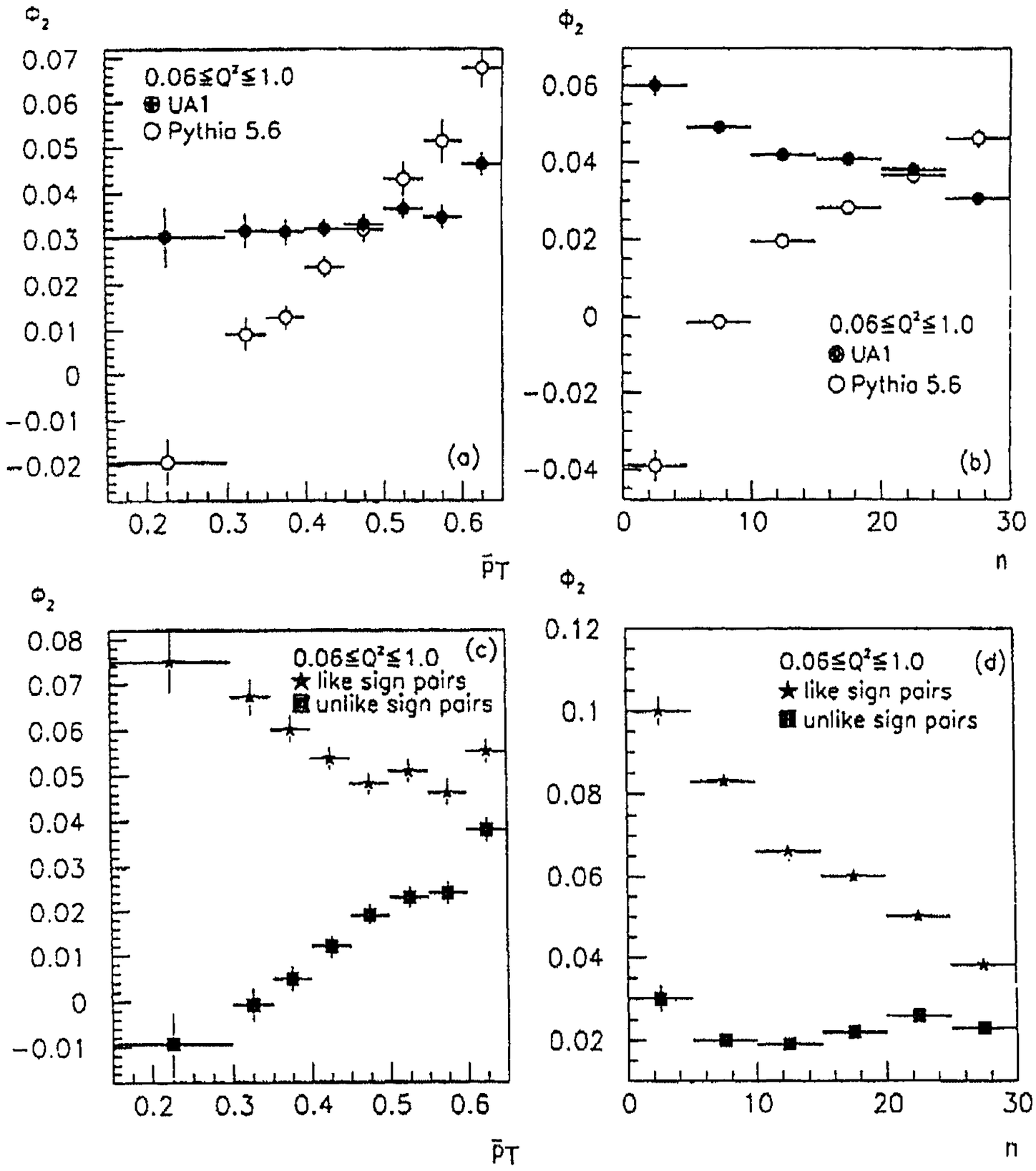

Fig. 4.38. The slope ϕ_2 as a function of average transverse momentum $\bar{p}_T$ and multiplicity n for UA1 data and PYTHIA [210].

4.8.4. *Bose–Einstein correlations versus QCD effects*

Of particular interest is a comparison of hadron–hadron to e^+e^- results in terms of same and opposite charges. This is shown in Fig. 4.40 for $q = 2$ UA1 and DELPHI data in [250] (note that in this figure the derivative of (4.50) is presented in small Q^2 bins). An important difference between UA1 and DELPHI can be observed on both sub-figures: For "large" $Q^2(>0.03\ \mathrm{GeV}^2)$, where Bose–Einstein effects do not play a role, the e^+e^- data increase much faster with increasing $_2\log(1/Q^2)$ than the hadron–hadron results. For e^+e^-, the increase in this Q^2 region is very similar for same and for opposite sign charges. At small Q^2, however, the e^+e^- results approach the hadron–hadron results. The authors conclude that for e^+e^- at least two processes are responsible for the power-law behaviour: Bose–Einstein correlations at small Q^2 following the evolution of jets

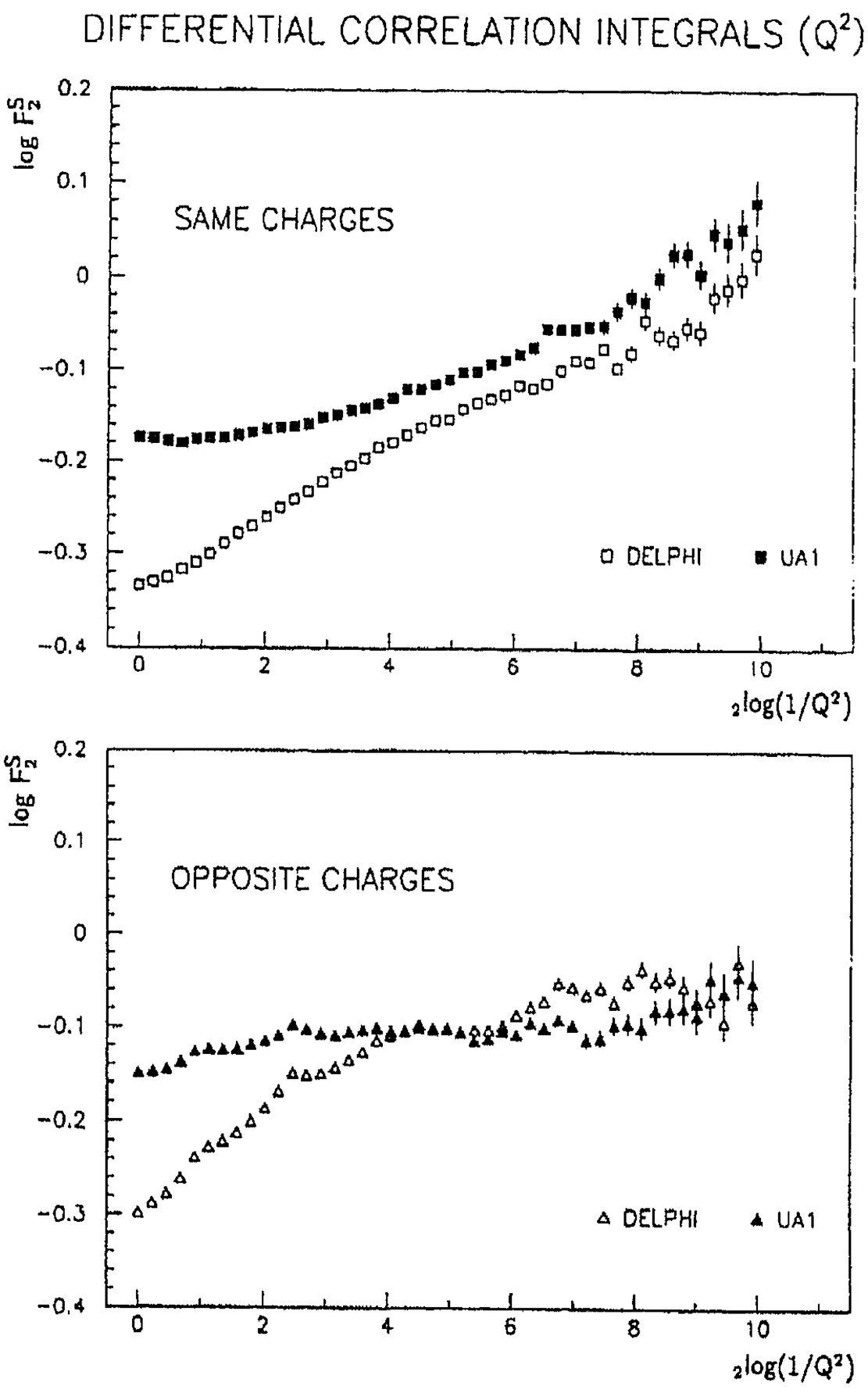

Fig. 4.39. Comparison of density integrals for $q = 2$ in their differential form (in intervals $Q^2, Q^2 + dQ^2$) as a function of $_2\log(1/Q^2)$ for e^+e^- (DELPHI) and hadron–hadron (UA1) collisions [250].

at large Q^2. In hadron–hadron collisions at present collider energies only Bose–Einstein effects seem relevant.

Since string fragmentation causes an anti-correlation between same-charged particles, it is of interest to compare e^+e^- results to JETSET in terms of strip integrals for the different charge combinations, separately. This has been done in [250] and, indeed, the Monte-Carlo results level off at small Q^2 and fall below the data for the same-charge results, while they describe the opposite-charge data perfectly well (not shown here).

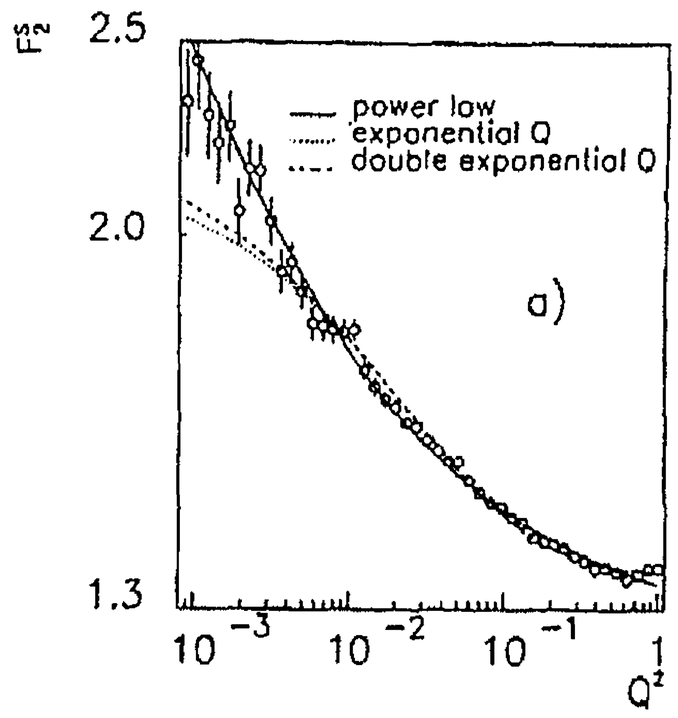

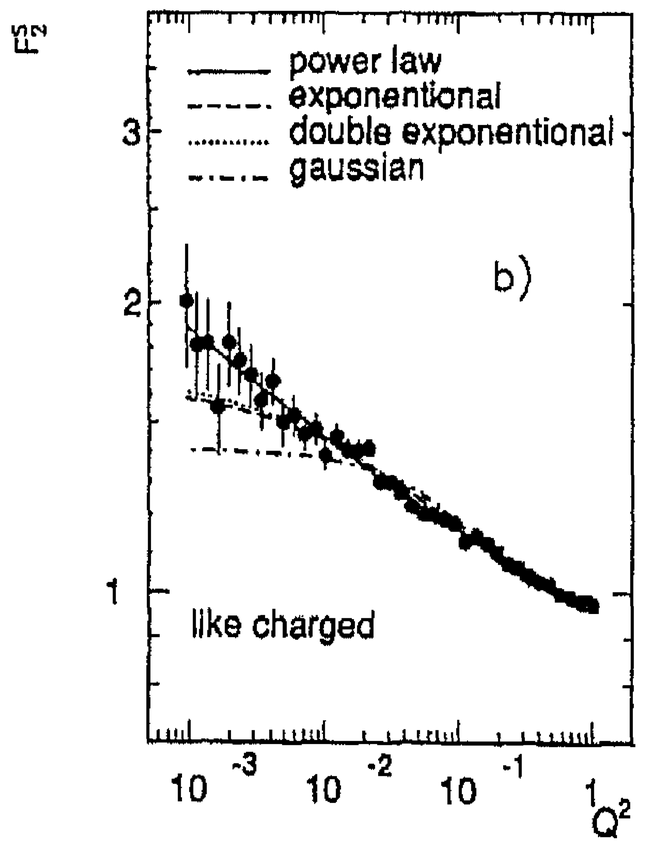

Fig. 4.40. Density integrals F_2^S (in their differential form) as a function of Q^2 for like-charged pairs in UA1 [143] and NA22 [142], compared to power-law, exponential, double-exponential and Gaussian fits, as indicated.

The exact functional form of F_2^S is derived from the data of UA1 [143] and NA22 [142], again in its differential form,[5] in Fig. 4.40. Clearly, the data favour a power law in Q over an exponential, double-exponential or Gaussian law.

If the observed effect is real, it supports a view recently developed in [165]. There, intermittency is explained from Bose–Einstein correlations between (like-sign) pions. As such, Bose–Einstein correlations from a static source are not power behaved. A power law is obtained (i) if the size of the interaction region is allowed to fluctuate, and/or (ii) if the interaction region itself is assumed to be

[5] In fact in this differential form $F_2^S(Q^2)$ is identical to $R(Q^2)$ usually used in Bose–Einstein analysis. The only difference is that it is plotted on a double-logarithmic plot, here.

a self-similar object extending over a large volume. Condition (ii) would be realized if parton avalanches were to arrange themselves into self-organized critical states [251]. Though quite speculative at this moment, it is an interesting new idea with possibly far-reaching implications. We should mention also that in such a scheme intermittency is viewed as a final-state interaction effect and is, therefore, not troubled by hadronization effects.

The effect on the factorial moments of adding Bose–Einstein correlations in FRITIOF is convincingly demonstrated for heavy-ion collisions in [252]. Because of the large number of collision processes, other correlation effects are expected to play a much reduced role for this type of interaction and Bose–Einstein correlations, as a collective effect, can become the dominant source of non-statistical fluctuations. Also from these results it is clear that more than one fixed interaction-volume radius is needed to reproduce the experimental results.

In perturbative QCD, on the other hand, the intermittency indices ϕ_q, are directly related to the anomalous multiplicity dimension $\gamma_0 = (6\alpha_s/\pi)^{1/2}$ [253–257] and, therefore, to the running coupling constant α_s. In the same theoretical context, it has been argued [254–257] that the opening angle χ between particles is a suitable and sensitive variable to analyse and well suited for these first analytical QCD calculations of higher-order correlations. It is, of course, closely related to Q^2.

A first analytical QCD calculation [254,255] is based on the so-called double-log-approximation with angular ordering [99] and on local parton–hadron duality [100]. A preliminary comparison with DELPHI data [258] gives encouraging results, even including an estimate for the running of the strong coupling constant α_s.

4.9. Correlations in invariant mass

The previous section has illustrated the advantages of the correlation integral method with a "distance" measure directly related to the invariant mass of the particle system. The results give additional support to the Fiałkowski conjecture, mentioned in Section 4.3.2, from which could be anticipated that dynamical effects are most clearly revealed if the correlation functions and factorial moments are directly analysed in terms of Lorentz-invariant variables.

Evidently, there are many arguments in favour of invariant mass as a dynamical variable rather than the single-particle variables often used in early intermittency studies. Resonances, the cause of most of the correlations among hadrons, and threshold effects appear at fixed values of mass; Bose–Einstein interference correlations depend on four-momentum differences; multiperipheral-type ladder diagrams are functions of two-particle invariant masses, and so on.

The idea to study correlations as a function of invariant mass was, to our knowledge, first proposed in [259, 260]. The authors introduce a method which is technically a differential version of the correlation integral method. It focusses directly on the correlation functions (cumulants) rather than on the inclusive density as in (4.50). Starting from the definition (2.21), one defines the correlation function

$$C_2(M_{\mathrm{inv}}) = \rho_2(M_{\mathrm{inv}}) - \rho_1 \otimes \rho_1(M_{\mathrm{inv}}) , \tag{4.51}$$

obtained after integration (in a suitable region of phase space) of $C_2(p_1, p_2)$ over all variables except M_{inv}. Here, $\rho_2(M_{\mathrm{inv}})$ is the familiar normalized 2-particle invariant-mass spectrum. The "background term" $\rho_1 \otimes \rho_1(M_{\mathrm{inv}})$ is the integral of $\rho_1(p_1)\rho_1(p_2)$ with M_{inv} fixed. For the data shown below, it is obtained from "uncorrelated" ("mixed") events, built by random selection from a track

pool. The same method is used in evaluating the denominator in (4.50). Higher-order correlations are obtained in a completely analogous manner. We further utilize the function $K_2(M_{\mathrm{inv}}) = C_2(M_{\mathrm{inv}})/\rho_1 \otimes \rho_1(M_{\mathrm{inv}})$, the normalized factorial cumulant of order two.

The analysis in [259], based on low statistics pp data at 205 GeV/c, demonstrates that $K_2^{+-}(M_{\mathrm{inv}})$ and $K_2^{\pm\pm}(M_{\mathrm{inv}})$ follow an approximate power law, written by the authors as

$$K_2(M_{\mathrm{inv}}) = (M_{\mathrm{inv}}^2)^{\alpha_X(0)-1}. \tag{4.52}$$

The notation reminds of the interpretation of (4.52) in terms of the Mueller–Regge formalism (for details see [259]). The power $\alpha_X(0)$ is the appropriate Regge-intercept, X = R for non-exotic pairs and X = E for exotic ones. The ratio K_2^{--}/K_2^{+-} was further seen to fall as M_{inv}^{-2}, consistent with $\alpha_R(0) - \alpha_E(0) = 1$. Not relying on Mueller–Regge theory, the authors argued that most of the correlations at small M_{inv} are due to resonance decays into three or more pions and to interference of amplitudes [260].

The results already obtained in [259] clarify several issues which have troubled the interpretation of intermittency data. Among others, they demonstrate that different charge states should be treated separately since the M_{inv} dependence is very different. This fact, obvious in M_{inv} but much less so in rapidity, was not fully appreciated in early intermittency analysis and the crucial importance of like-sign particle correlations remained hidden in "all-charged" analyses.

The method of [259] has now been applied by NA22 [261] and DELPHI [262]. Fig. 4.41 shows data on $K_2(M_{\mathrm{inv}})$ for a combined sample of non-diffractive π^+/K^+p collisions at 250 GeV/c in the central c.m. rapidity region $-2 < y < 2$. $K_2^{+-}(M_{\mathrm{inv}})$ has a prominent ρ^0 peak, but is quite flat near threshold. The peak in the first bin of Fig. 4.41(a) is attributed to contamination from Dalitz decays and γ conversions. $K_2^{--}(M_{\mathrm{inv}})$ falls much faster. A fit of $K_2 \sim (M_{\mathrm{inv}}^2)^{-\beta}$ yields $\beta^{--} = 1.29 \pm 0.04$, $\beta^{++} = 1.46 \pm 0.03$, $\beta^{+-} = 0.17 \pm 0.02$, in agreement with [259] and consistent with the relation $\alpha_R(0) - \alpha_E(0) = 1$.

NA22 also finds that cuts on transverse momentum or relative azimuthal angle $\delta\varphi$ strongly affect the shape of $K_2^{+-}(M_{\mathrm{inv}})$, but have little effect on $K_2^{--}(M_{\mathrm{inv}})$ for $M_{\mathrm{inv}} < 0.5$ GeV/c^2. This means that $K_2^{--}(M_{\mathrm{inv}})$ at small M_{inv} is essentially a function of M_{inv} (or Q^2) only, illustrating once more the advantage of M_{inv} compared to other variables.

The data in Fig. 4.41 confirm the conclusion of Section 4.8 that the correlations in like-charge systems are at the origin of the strong increase of factorial moments for small invariant masses. Whether Bose–Einstein effects are solely responsible for the differences between $(\pi^{\pm}\pi^{\pm})$ and $(\pi^+\pi^-)$ pairs is not so evident. It suffices to consider [260] the contributions from decays of various resonances to realize that the M_{inv}-dependence near threshold for "exotic" particle systems must be stronger than for "non-exotic" ones. In a dual Regge picture, such differences translate into very different values of the respective Regge intercepts as in (4.52). It remains, therefore, to be verified if the M_{inv}-dependence of the data can be explained as a superposition of a "standard" Regge-type power law and a conventional Bose–Einstein enhancement.

As pointed out in [263], there is a feasible way to test this and even to give access to the relative strength of BE interference and exotic like-charge $\pi\pi$ interaction. The idea is that particle combinations exist which are either (a) exotic, but not identical (e.g. $K^+\pi^+$ or $K^-\pi^-$ pairs) or (b) identical, but not exotic ($I = 0$ $\pi^0\pi^0$ pairs). NA22 [264] and ALEPH [265] data indicate that very short range correlations are indeed absent in the exotic Kπ channel. This supports Bose–Einstein correlations rather than exotic Regge behaviour, but the point deserves further investigation.

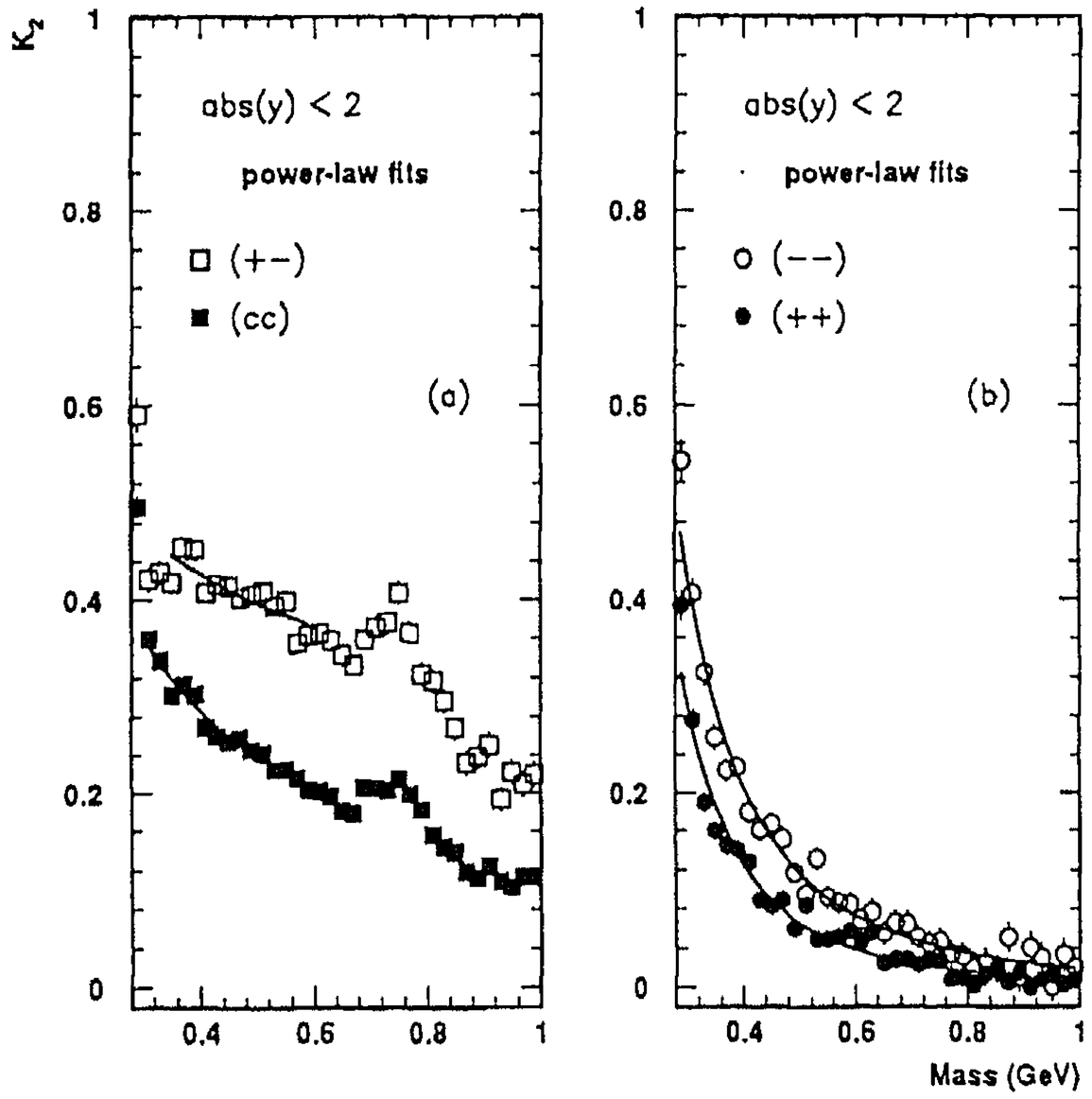

Fig. 4.41. $K_2(M_{\text{inv}})$ for cc, $+-$, $--$, and $++$ pairs of tracks with c.m. rapidity $-2 < y < 2$, in $K^+/\pi^+ p$ collisions at 250 GeV/c [261]. The solid line is a power-law fit (see text).

The possibility that the correlation functions depend mainly on invariant mass has interesting further consequences. These were analysed in [185]. Taking in (4.51)

$$C_2(M_{\text{inv}}) \propto (M_{\text{inv}}^2)^{\alpha-1}\text{BE}(M_{\text{inv}}) , \tag{4.53}$$

with BE a conventional Bose–Einstein factor, exponential in Q, good agreement is obtained with the NA22 second-order correlation integral data of $(--)$-pairs. Integrating the correlation function over all variables except δy gives $F_2^{--}(\delta y)$ which also fits the data. Although C_2 does not explicitly depend on the transverse momentum of the particles, it turns out that $F_2(\delta y, p_{T1}, p_{T2})$ is larger and more steeply increasing than $F_2(\delta y)$ for small δy and small p_T's. The opposite happens for large p_T's. This is the "low-p_T intermittency effect" seen in the NA22 and UA1 data (cf. Fig. 4.20(a) and Section 4.4.2). The explanation is simple: under the stated hypothesis, small p_T for the two particles in a pair means, on the average, smaller invariant mass than for unrestricted transverse momentum and, therefore, larger and shorter-ranged correlations in rapidity. Enhanced intermittency follows as a consequence of kinematical cuts! The influence of the Bose–Einstein factor is easily checked in this simple model. It is found to be necessary in order to reproduce the correlation integral data and F_2 for restricted p_T but has, as expected a priori, very little influence on the p_T-integrated $F_2(\delta y)$. This explains early controversy over the role of Bose–Einstein effects in one-dimensional factorial moment analyses (Section 4.4.1).

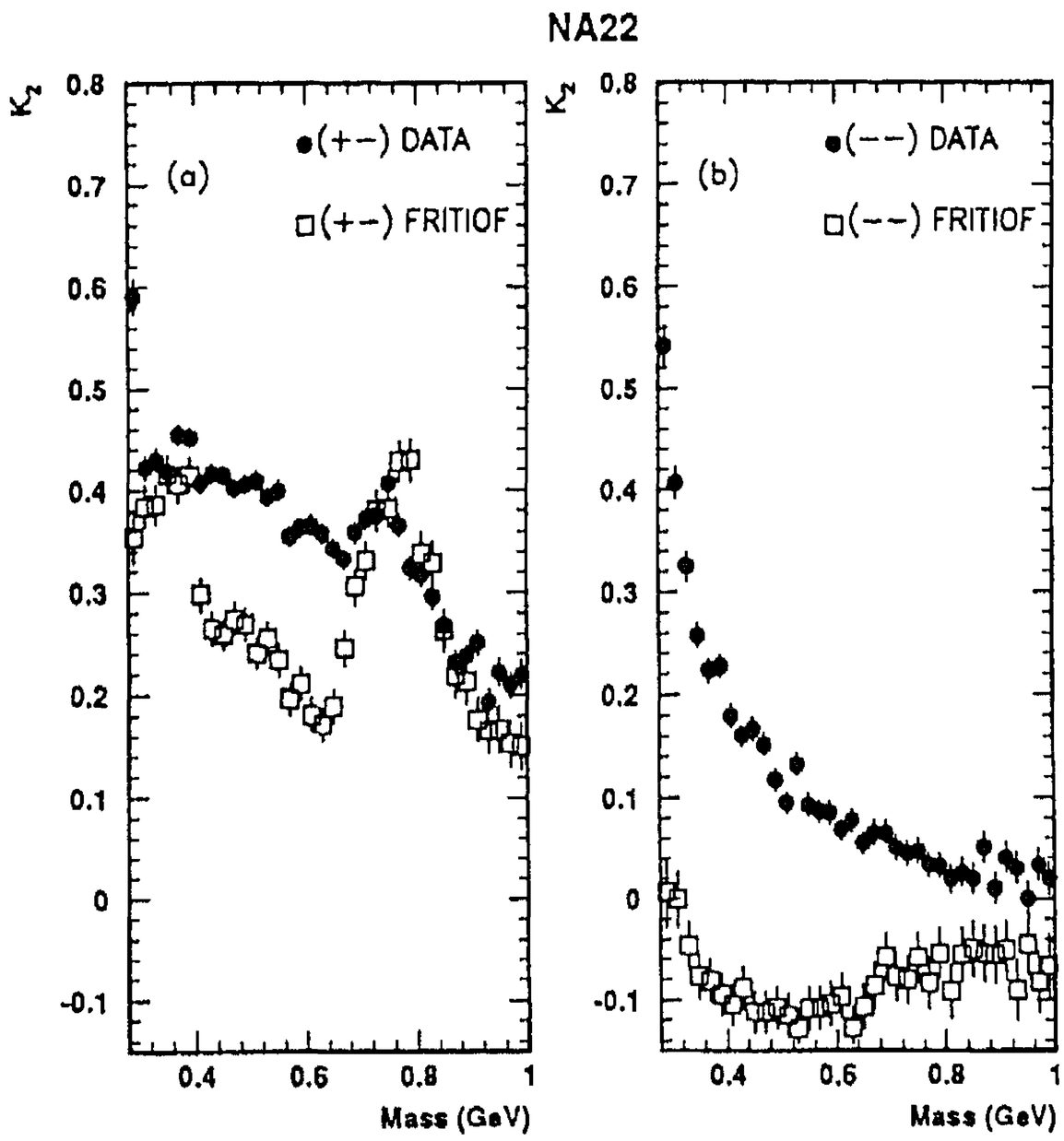

Fig. 4.42. $K_2(M_{\text{inv}})$ for (a) $+-$, (b) $--$ pairs of tracks with c.m. rapidity $-2 < y < 2$, in $K^+/\pi^+ p$ collisions at 250 GeV/c [261], compared to FRITIOF2.

A study of the invariant-mass dependence of the two-particle correlation function has for the first time given clear indications as to why the hadron–hadron Monte-Carlo models fare so badly when confronted with factorial moment data. For example, Fig. 4.42 shows NA22 data for $K_2^{--}(M_{\text{inv}})$ and $K_2^{+-}(M_{\text{inv}})$ compared to FRITIOF. The predicted shape of $K_2^{+-}(M_{\text{inv}})$ is very different from the data, especially in the ρ^0 region. It shows an enhancement at low mass which causes the correlation function to drop much faster than seen in the experiment. In the model, this structure is traced back to reflections from η, η' and ω resonances. The model also fails to describe $K_2^{--}(M_{\text{inv}})$ since correlations are very weak or even negative, except for a threshold enhancement due to η' decays.

These examples suffice to demonstrate that FRITIOF (or rather JETSET) has serious shortcomings and is unable to reproduce two-particle correlations in invariant mass. For correlations in rapidity and azimuthal angle this was seen earlier (Section 3.1), but the reasons remained obscure, mainly because of the insensitivity of these variables to dynamical correlations at small mass.

A study of the correlation function in terms of invariant mass clarifies the situation considerably. For NA22, the model was known to overestimate significantly the production rates of ρ^0 and η mesons [266] and presumably also those of η' and ω for which no direct measurements exist (see also [171] for hA collisions). This is now seen to distort heavily the M_{inv} dependence of K_2. Also Bose–Einstein low-mass enhancements, most likely responsible for the fast drop of $K_2^{--}(M_{\text{inv}})$ in

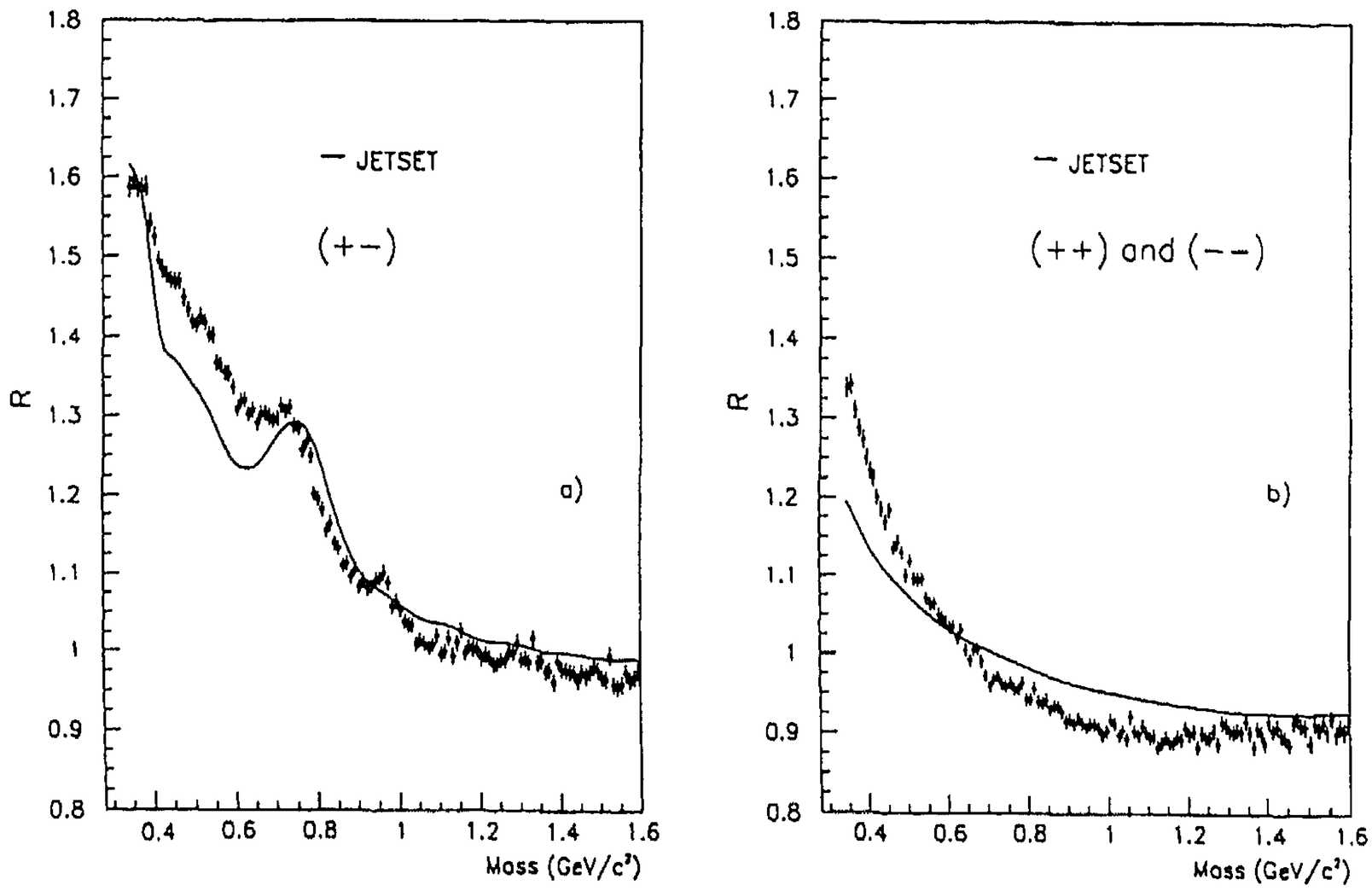

Fig. 4.43. $R = K_2(M_{\text{inv}}) + 1$ for e^+e^- annihilation compared to the JETSET7.3 prediction with parameters tuned to the DELPHI data for (a) unlike-sign and (b) like-sign combinations [262].

the threshold region, are not included in the FRITIOF model commonly used. Finally, we note that the values of K_2 in the considered mass interval are much smaller than the data. This is related to the width of the charged particle multiplicity distribution which is known to be too small in FRITIOF. It affects the global magnitude of factorial moments and cumulants.

In Fig. 4.43(a), the discrepancy is shown to be quite similar for $(+-)$ correlations in e^+e^- collision [262] and JETSET. As in hh collisions, the correlation is underestimated in the mass region below the ρ^0. This discrepancy can be cured by decreasing the η' and ρ^0 production and increasing ω production in JETSET.

Fig. 4.43(b) gives the like-sign correlation for the data and JETSET without BE correlation. For $M_{\text{inv}} < 0.6\ \text{GeV}/c^2$, the experimental data are considerably higher than JETSET. This can be attributed to Bose–Einstein interference. However, it is striking that JETSET also predicts a strong rise towards threshold even without Bose–Einstein correlations. This is the tail of the QCD effect also seen in Fig. 4.39 and mainly due to multijet events. The difference between JETSET and data can indeed be removed by including BE correlations in the model, but the Q^2 cut used ($Q^2 > 0.04^2$) is too high to be able to distinguish a power law from an exponential or Gaussian, as is done in Fig. 4.40.

To summarize, the above proves that the failures of models such as FRITIOF and JETSET with respect to factorial moment and correlator data (Sections 4.2.3 and 4.6.3), are not necessarily due to "novel" dynamics. They are in first instance a consequence of a variety of defects – such as incorrect resonance production rates and absence of identical particle symmetrization – which belong to "standard" hadronization phenomenology. These defects should be eliminated before "new physics" can be claimed.

For e^+e^- annihilation at LEP energies, we have found that models such as JETSET-PS are much more successful than for all other processes. Besides the evident fact that this process is much better understood theoretically, QCD effects dominate and the model parameters are much better tuned to the data. Still, serious, recently observed discrepancies of e.g. JETSET-PS with LEP measurements on particle and resonance production rates are a clear sign that hadronization in e^+e^- is in fact less well understood than commonly stated and needs improvement. It could be rewarding to investigate carefully and differentially the invariant mass dependence of the correlations using the sensitive methods now available.

Originating mainly from the low invariant mass region (typically $<1.5\,\mathrm{GeV}/c^2$), it is not impossible that the observed correlations are quite independent of the process initiating the primary colour separation in the collision, being dominated by strong final-state interactions. This would explain "universality" in the sense discussed earlier.

Many authors argue that "intermittency" is somehow connected to (nearly scale invariant) perturbative QCD cascading. Others strongly contest this view on the argument that QCD cascades have a limited extent even at LEP energies and are dominated by a very small number of "hard" emissions. In the former case, one may expect significant differences in the correlation functions at low mass for e^+e^-, on the one hand, and for hh, hA and AA collisions, on the other. Preliminary e^+e^- data, mentioned in Section 4.8, seem to support the last opinion. Whatever the final outcome, if differences are found, they should be used to clarify the respective roles of perturbative and hadronization phases in the different types of collision processes.

4.10. Genuine higher-order correlations

Multiparticle production in high-energy collisions is one of the rare fields of physics where higher-order correlations are directly accessible in their full multidimensional characteristics, under well-controlled experimental conditions.

Three-particle correlations have been observed in the form of short-range rapidity correlations and higher-order Bose–Einstein correlations, but evidence for *genuine* higher-order correlations (i.e. after subtraction of all lower-order contributions) is very limited. While it was found to be completely absent in heavy-ion collisions, first evidence was given in Section 4.5 for their existence in hh collisions.

The correlation integral method turns out particularly useful for the unambiguous establishment of genuine higher-order correlations in terms of the normalized cumulants $K_q(Q^2)$, when using the star integration [247]

$$K_q^*(Q^2) = \frac{\int \prod_i \mathrm{d}y_i \, \Theta_{12} \cdots \Theta_{1q} C_q(y_1, \ldots, y_q)}{\int \prod_i \mathrm{d}y_i \, \Theta_{12} \cdots \Theta_{1q} \rho_1(y_1) \cdots \rho_1(y_q)}, \tag{4.54}$$

with $\Theta_{1j} = \Theta(Q^2 - Q_{1j}^2)$ restricting all $q-1$ distances Q_{1j}^2 to lie within a distance Q^2 of the position of particle 1. The star-integral method combines the advantage of optimal use of available statistics and minimal use of computer time. Since higher accuracy is obtainable, dynamical structures in the correlations can be studied in greater detail than with conventional methods.

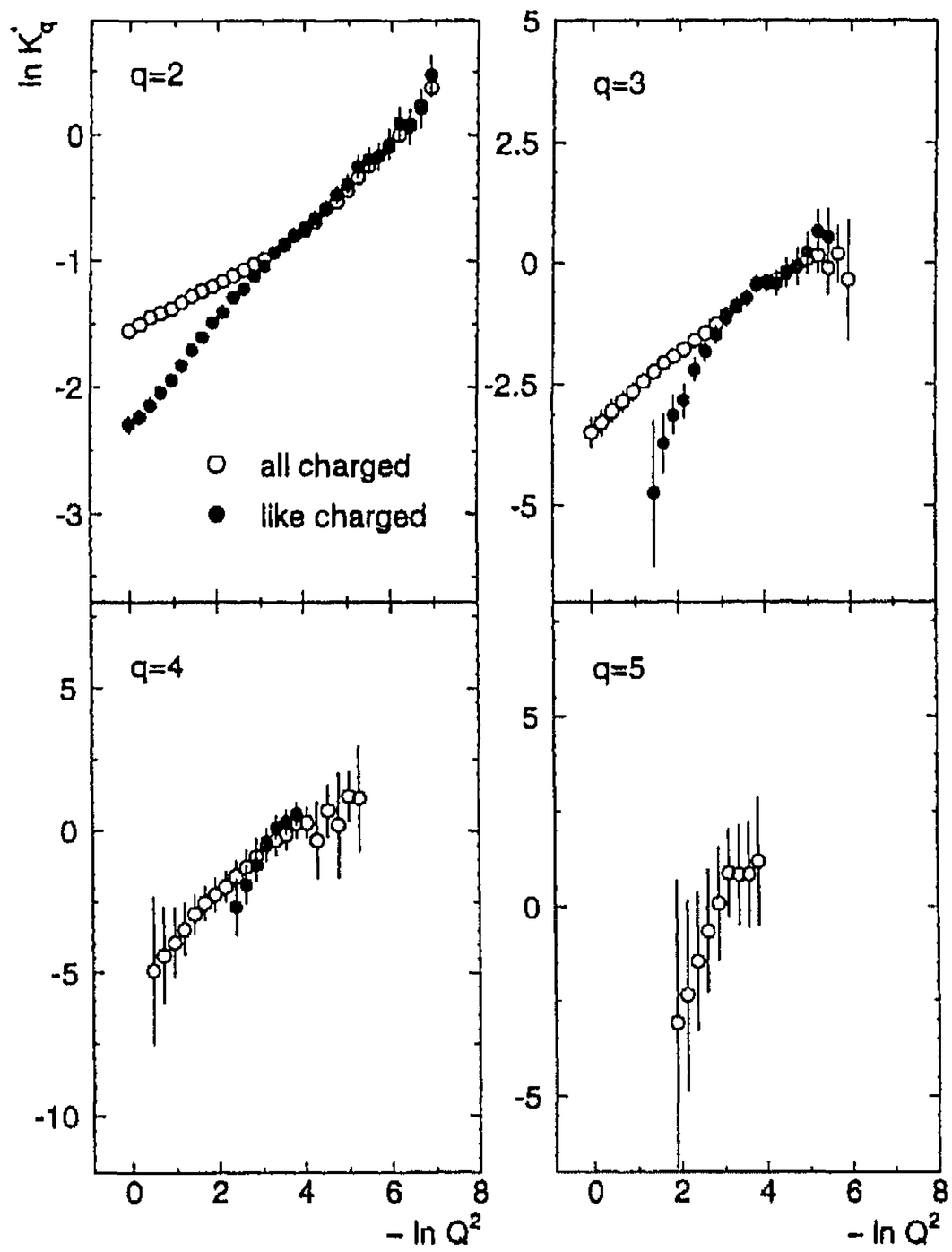

Fig. 4.44. $\ln K_q^*(Q^2)$ as a function of $-\ln Q^2$ for all charged particles as well as for like-charged particles [267].

Non-zero values of $K_q^*(Q^2)$ increasing according to a power law with decreasing Q^2 are indeed observed for E665 for third order [249] and for NA22 up fifth order [267] (see Fig. 4.44 for the latter).

4.11. Summary and conclusions

1. Intermittency, defined as an increase of normalized factorial moments with increasing resolution in phase space, is seen in all types of collision. Intermittency is a 3D phenomenon. The anomalous dimensions are small ($d_q = 0.01$–0.1) in a one-dimensional analysis, but the factorial moments are considerably larger, and their resolution-dependence more power-like, in two- or three-dimensional phase space. Self-similarity in the dynamics of multiparticle production is an attractive but not fully proven explanation.
2. The factorial-moment method is very sensitive to biases in the data. These have to be studied in detail before final conclusions can be drawn. Because of its sensitivity, the method has in fact proven to be very helpful in detecting and tracing such biases.

3. The logarithms of factorial moments satisfy a possibly dimension-independent linear relation which allows to determine directly ratios of anomalous dimensions. The observed order dependence of anomalous dimensions excludes a second-order phase transition (as treated in [183]) as the origin of intermittency. Valid in random cascade models, the Ochs–Wošiek relation shows that correlation functions of different order are inter-related in a specific hierarchical structure. An explanation in terms of dynamics has not yet been found.
4. In hadron–hadron collisions, factorial moments and intermittency indices depend strongly on transverse momentum and are largest for low transverse momentum hadrons. This effect, also seen in rapidity correlations and azimuthal correlations, needs further study in e^+e^- collisions and in parton shower Monte Carlo's. There are serious indications that "low-p_T intermittency" is a reflection of the very strong dependence of correlation functions for identical particles on invariant mass. This has to be examined in more detail.
5. The multiplicity dependence in hh collisions agrees with what is expected from mixing of independent sources. However, the Fiałkowski observation on possible universality casts some doubt on this type of interpretation. For a given density, heavy-ion collisions show more intermittency than hadron–hadron collisions, possibly as a result of Bose–Einstein interference or other collective effects.
6. Factorial cumulants are direct measures of genuine higher-order correlations. These are present in hadron–hadron collisions, in particular for small phase-space domains, but seem to be absent in heavy-ion collisions.
7. Factorial correlators reveal bin–bin correlations. The correlators F_{pq} increase with decreasing correlation length D, but only approximately follow a power law for $D \lesssim 1$. For fixed D, the values of F_{pq} are independent of resolution δy, a property predicted in the α-model, but also shared by models with short-range order such as FRITIOF. The powers ϕ_{pq} increase linearly with the product pq of the orders, but are considerably larger than expected from FRITIOF and from the simple α-model.
8. A recent extension of the definition of G moments filtering out high multiplicities, claims success in extracting the dynamical component. However, under the conditions prevailing in present hadroproduction experiments, multifractal and generalized multifractal methods seem unable to overcome the overwhelming dominance of statistical fluctuations.
9. The correlation (or density) strip integral strongly reduces statistical errors, as well as fluctuations due to splitting of spikes. Using the squared four-momentum difference Q_{ij}^2 as a distance measure, an increase similar to that found in three-dimensional analyses is observed. This increase is caused by correlations among like-charged particles. Bose–Einstein interference must contribute significantly to the intermittency effect but is not power behaved in the conventional approach. Power-law behaviour in Bose–Einstein interferometry would imply a random superposition of "emission centres" with possibly fractal properties. Parton avalanches in a self-organized critical state are an intriguing possibility.
10. The analysis of cumulants in terms of invariant mass, or related variables, reintroduced recently after early work, has helped in clarifying several issues in intermittency. The reasons behind the dramatic failures of models for hadron–hadron collisions are clearly revealed. They are in first instance incorrectly predicted particle and resonance production rates and the near absence of correlations (or even presence of anti-correlations) in identical particle systems with small invariant masses. These defects are not easy to cure in a consistent manner by simple

parameter tuning and "new" physics may be needed to restore internal consistency in e.g. string-fragmentation models.

11. The hadronization mechanism in hadron–hadron collisions is based on identical physical principles and Monte-Carlo algorithms as those applied with apparently great success to "hard" processes, in particular to e^+e^- annihilation. There is now growing experimental evidence that the mentioned discrepancies, first seen in hadron collisions, are also present in such processes. These should first be removed before commonly expressed claims that "No new physics is involved in intermittency" can be accepted.
12. The The relative importance of perturbative and non-perturbative QCD contributions to hadron correlations in e^+e^- remains controversial, also theoretically. This can be studied further with the new techniques now available.

5. Theoretical description

In parallel to the extensive experimental effort in quest for power-law behaviour, intense activity has developed on the theoretical side, to find acceptable explanations of the rapidly accumulating collection of data on factorial moments. The meaning of "intermittency" in multiparticle processes is still the subject of much debate and no definite consensus has as yet emerged. Let us remember once again that we are dealing here with the problem of evolution of particle number distributions (or multiparticle correlations) in ever smaller bins.

A priori, the most direct road of attack starts from quantum chromodynamics (QCD), now firmly established as the theory of strong interactions. Unfortunately, since the problem of confinement is unsolved, QCD can only be used as a guideline to build phenomenological models for soft hadronic phenomena. While successful for e^+e^- annihilation, such models remain at present unsatisfactory for most other processes, and in particular for hh collisions. The model's deficiencies are often invoked in support for claims of "new physics", but also this matter is far from being settled.

From the outset it is clear that phenomena such as "intermittency" are manifestations of dynamics in a, most probably, strongly non-linear regime of QCD. It is, therefore, quite likely that the observed phenomena are not very sensitive to the precise form of the Lagrangian, even though the general properties of the interacting fields (e.g. the vector nature of gluons) surely play a crucial role. Hence, a satisfactory description might be possible on the basis of quite general properties of non-linear systems as revealed by complex systems in many other branches of physics. This idea lies at the origin of various attempts to establish connections with models for turbulence, multiplicative cascade processes, "effective" field theory, the statistical mechanics of disordered systems, fractals, phase transitions of various kinds and others.

A perturbative QCD approach to intermittency would provide a viable explanation if the hadronization of quark and gluon systems possesses the property of "early confinement" such that local parton–hadron duality would hold. Various efforts in this direction have indeed established that parton (quark–gluon) avalanches exhibit (multi)fractal properties. These follow from the (fortunate) fact that the process possesses Markovian properties. Further developments along this line will evidently improve our understanding of perturbative cascades. A direct connection with experimental observations is, however, not yet established.

Numerous other interpretations of "intermittency" have been advanced and will briefly be described further below.

5.1. Simplest approximations

5.1.1. The linked-pair approximation

If the rapidity distribution does not change appreciably within a bin interval (this is justified for small intervals, at least) one can rewrite (2.71), approximating it by

$$K_q(\delta y) \approx \frac{1}{M(\delta y)^q} \sum_{m=1}^{M} \int_{\delta y} \prod_i \mathrm{d}y_i \, K_q(y_1, \ldots, y_q) \,. \tag{5.1}$$

Since there are no statistically independent contributions to the cumulant functions C_q and K_q, their arguments should be somehow linked. Studying the correlation of galaxies [184], it was noted that K_q can be decomposed into sums of products of two-particle correlation functions, K_2 with overlapping arguments, in such a way that all multiparticle correlations are expressible as successive two-particle ones, so that the whole chain of particles becomes correlated. The last condition is necessary since we have learned that q-particle correlations ($q > 2$) are indeed present in the data.

In this scheme, higher-order scaled cumulants [107] are written as

$$K_3(y_1, y_2, y_3) = \frac{A_3}{3} \sum_{\text{perm}} K_2(y_1, y_2) K_2(y_2, y_3) \,, \tag{5.2}$$

$$K_4(y_1, y_2, y_3, y_4) = \frac{A_4}{12} \sum_{\text{perm}} K_2(y_1, y_2) K_2(y_2, y_3) K_2(y_3, y_4) \,, \tag{5.3}$$

etc. Here, all the permutations of indices $1, \ldots, q$ are summed over; the number of terms is equal to the denominator of the factor in front of the sum. The numerator is an a priori arbitrary parameter for each order of correlation.

Even now, the numerical integration in (5.1) is hard to perform. For that reason it was suggested [107] to assume translation invariance of the cumulants K_q, and to use the strip approximation (i.e. instead of integrating over a set of hyper-cubes with linear size δy, one integrates over a strip along the main axis Y and over the differences $\zeta_i = (y_{i+1} - y_i)$). In this way (5.1) reduces to a simple but approximate formula [26]:

$$K_q \approx A_q (K_2)^{q-1} \,. \tag{5.4}$$

Substitution of K_q in (2.72) allows any factorial moment to be expressed in terms of the second moment so that, for example,

$$F_3 = 1 + 3K_2 + A_3 K_2^2 \,. \tag{5.5}$$

As mentioned in Section 4.5, one can describe [26] the UA1 and UA5 data on factorial moments at energies from $\sqrt{s} = 200$ GeV to $\sqrt{s} = 900$ GeV with constant values of A_q for all intervals δy. Still, the intermittency indices derived from the linked-pair approximation remain somewhat below the experimental ones. At the lower energy of the NA22 experiment, one gets a much larger value of A_3 if the above estimate of F_3 is used boldly [142]. However, the assumption of translation

invariance is not really justified there and one can hardly use (5.5) on data which are averaged over a large region of phase space.

Apart from this problem, there are also more basic questions which remain unanswered. For instance, even within the framework of the linked-pair ansatz, one could add to (5.2) a term containing a product of three K_2's (loops or ring graphs), as well as further terms with multiple links among the pairs.

Although a dynamical justification for the linked-pair approximation is lacking at present, it should be remembered that similar approximation methods have proven their utility, e.g. in the theory of liquids. Within the Born–Bogoliubov–Green–Kirkwood–Yvon (BBGKY) hierarchy scheme, they allow to "close" the otherwise infinite sequence of equations relating correlation functions of all orders. That the linked-pair ansatz may have more than accidental relevance is further indicated by the non-trivial fact that (5.4) with $A_q = (q-1)!$ corresponds to a multiplicity distribution in δy which is of Negative Binomial type with k-parameter $k = 1/K_2(\delta y)$ [109]. This two-parameter distribution satisfactorily describes a large variety of (non-averaged) mutliplicity data and also occurs as an approximation to the soft parton multiplicity distribution in QCD-jets [268–270]. Further extensions of the linked-pair approach beyond those of [107, 109] are treated in [271, 272].

The structure of many-particle correlations has also been analysed in partially coherent radiative systems [201]. This approach is closely related to the linked-pair ansatz [109].

Conformal theories, treated in connection with intermittency in [273], provide an alternative [274] to the linked-pair ansatz. In such theories the qth order irreducible Green function is written as a product of two-particle ones to the power $1/(q-1)$. Taking into account the $q(q-1)/2$ permutations of all particle indices, one finds

$$K_q \approx B_q (K_2)^{q/2} , \tag{5.6}$$

instead of (5.4), which also fits the experimental data reasonably well [274].

5.1.2. The singularities of the correlation functions

According to relations (2.68)–(2.72), the singular behaviour of the factorial moments at small rapidity binning implies that the correlation functions are singular for small separation of their arguments. In particular, the leading singularities of the correlation functions ρ_2 and C_2 should coincide with the singularity of the corresponding factorial moment F_2, if the formal mathematical limit $\delta y \to 0$ is considered. For

$$F_2 \sim (\delta y)^{-\phi_2} \quad (\delta y \to 0) \tag{5.7}$$

one should get

$$C_2(y_1, y_2) \sim C_2^{(\mathrm{L})}(y_1, y_2) |y_1 - y_2|^{-\beta} + C_2^{(\mathrm{N})}(y_1, y_2) \tag{5.8}$$

with $\beta = \phi_2$, $C_2^{(\mathrm{L})}$ is a regular function of $(y_1 - y_2)$, while $C_2^{(\mathrm{N})}$ can contain non-leading singularities (less singular than the first term).

A two-component model of this kind has been used in [275], where $C_2^{(\mathrm{N})}$ (and similarly for the higher-order correlations) is chosen to be a regular function which results in a constant additive term of F_2. The origin of the singular term has been ascribed in [275] to a phase transition. For

a singular term to be dominant, it must overwhelm F_2 even numerically. However, the experimental data discussed above indicate that this is not the case. Linear dependence in a double-log plot is observed over quite a large background in the available region of δy. This implies that in this region the integral contribution $F_2^{(L)}$ of the singular terms in (5.8) to F_2 is rather small so that

$$F_2^{(L)} \ll F_2 \,. \tag{5.9}$$

Such a situation provides [275,178] new possibilities with β different from ϕ_2, since in that case one gets

$$\ln F_2 \approx \ln(1 + F_2^{(N)}) + F_2^{(L)}/(1 + F_2^{(N)}) \,. \tag{5.10}$$

It could even suggest a logarithmic dependence of $F_2^{(L)}$ on δy: $F_2^{(L)} \sim \log \delta y$, i.e. a logarithmic singularity of the correlation function for coinciding rapidities. However, such a behaviour is indistinguishable from a power-like one for small exponents β and the rather restricted range of rapidity intervals (e.g. $0.1 < \delta y < 1$) in which one usually looks for this dependence. Actually, if $\beta \log \delta y \ll 1$ one gets [178]

$$\ln F_2 \approx \ln(1 + F_2^{(N)}) + \frac{\bar{C}_2^{(L)}}{\rho_1^2} (\delta y)^{-\beta} \approx \alpha_2 - \phi_2 \ln \delta y \tag{5.11}$$

where

$$\alpha_2 = \ln(1 + F_2^{(N)}) + \bar{C}_2^{(L)}/\rho_1^2 \quad \text{and} \quad \phi_2 = \beta \bar{C}_2^{(L)}/\rho_1^2 \,. \tag{5.12}$$

Herefrom, one would expect the intermittency exponent to be much smaller than the corresponding strength of the singularity of the correlation function, i.e. $\phi_2 \ll \beta$.

The difference between logarithmic and power-like singularities may become observable for higher moments at small δy as an upward curvature appearing on log–log plots for power-law dependence. This would be more noticeable for smaller δy, for higher q and for larger values of β. Still, one should not enter into the region of extremely small δy, where the empty-bin effect may dominate and turn down all the curves.

The existing experimental data on factorial moments are not in contradiction with the above, although no clear signal of an upward curvature of higher moments is seen because of large irregularities appearing at small δy and large q. These irregularities are suppressed if the method of correlation integrals [130,245,107,143] is used, where the binning procedure is not fixed but naturally follows the event structure. This has been discussed in Section 3.8. In fact, the singularities are still better exposed if factorial cumulants (2.71) are used instead of factorial moments [177].

5.1.3. Intermittency and Bose–Einstein correlations

One of the possible sources of increase of factorial moments at small bin sizes is the well-known attraction of identical Bose-particles (pions) when their momenta are very close. Therefore, one is tempted [202] to the extreme supposition that "intermittency" is governed by Bose–Einstein correlations, i.e. by symmetry properties of fields but not by their dynamics. As was shown in Section 4, the experimental data do indeed give some indications on the relevant contribution of such an effect. In general, the introduction of BE correlations tends to reduce the disagreement between experimental data and Monte-Carlo models. However, it was also shown there that the dynamical part is non-negligible and, consequently, is of main concern to us.

Referring the reader to the more specialized review of the subject in [276], we would like just to point out that the same physics effects can become more (or less) pronounced depending on the corresponding choice of the variable in which it is displayed. In particular, it is shown in [276] that the rapidity variable is suitable to reveal the dynamical intermittency and to suppress the Bose–Einstein contribution to factorial moments. At the same time, when analysed as functions of squared 4-momentum transferred between pions, the factorial moments get the power-like increasing share of BE correlations which shadows the true (dynamical) intermittency. Therefore, the power-like behaviour in that variable neither proves nor disproves dynamical intermittency. One should keep this in mind when looking at the corresponding experimental data. Surely, for quantitative estimates Monte-Carlo calculations are necessary with full account of the indefiniteness in the description of the BE effect itself.

5.2. Dynamical approaches

5.2.1. Various theoretical models

From a theoretical point of view, experimental results are best approached via quantum chromodynamics (QCD). Attempts in that direction are further described in Section 5.2.6. Unfortunately, the application of QCD to soft processes involving small momentum transfers is quite limited since strong non-perturbative effects are involved (unless we use additional assumptions, as the local parton–hadron duality hypothesis generalized to correlations of any order). Hence, we are compelled either to construct general relations like those of Section 2 and the previous section, or to develop phenomenological models that fit experimental distributions by adjusting a number of free parameters.

By now, many phenomenological models have been proposed. Ideas inspired by QCD have been used in parton shower models and in their phenomenological counterparts: the dual topological model and quark–gluon string models [73, 74, 76, 277–279]; in coherent gluon jet emission (Cherenkov gluons, in particular) [280]; in the cold quark–gluon plasma model [192]. Models of a still more phenomenological nature have been tried, such as cluster models [67, 281–283], clan models [284] and narrow hadron jet emission [179]. Whereas in all these models definite dynamical mechanisms are proposed for the origin of the fluctuations in multiparticle production, they still suffer from one important deficiency: they do not reveal the nature of the scaling laws observed for factorial moments at small bin sizes.

From that point of view, one would prefer the random cascade models [21, 22, 285] and/or the general approach of phase transitions [275, 193, 286, 287]. While the cascade models rely on analogies with turbulence theories and lead to phase transitions, general considerations of the transition from parton to hadron phases of the process are based on important properties of strong coupling field theories reminding of QCD lattice computations and the conformal group symmetry. Both approaches lead in quite a natural way to scaling behaviour of factorial moments and are preferred as heuristic tools. However, to date they cannot compete with phenomenological Monte-Carlo models in providing computational results comparable with experimental data at the same level of precision. We shall discuss them separately at some length later, together with important ideas of intermittency and fractality, but first we shall describe a variety of phenomenological models applied to the fluctuation problem.

First of all, we should mention the furthest developed Monte-Carlo versions of QCD inspired models [73, 74, 76, 83, 85, 277–279] of parton showers or quark–gluon strings. Qualitatively, these models describe the behaviour of the two-particle correlation function $C_2(y_1, y_2)$ observed experimentally, showing the signature of short-range correlations. However, they cannot pretend to fit them quantitatively in hh collisions for all topologies and cut-offs. All the models predict noticeably smaller values of intermittency indices than the experimental data. Such models also fail to describe the probability distribution of maximum particle number per event at a given resolution δy [288, 289].

As discussed in Section 4.2.3, for e^+e^--annihilation the situation is still controversial. Initially, the DELPHI collaboration, working at the Z^0 peak, claimed agreement with the LUND parton shower model. Later, increasing statistics tenfold, it finds that the agreement only holds at the level of 10–20% (see Fig. 4.7(d)) [136]. However, in general the situation is better here than in hadronic reactions. In nucleus–nucleus reactions, these models fail to describe the damping of spectator particles observed in experiment [290]. Further, more detailed studies are needed.

Thus, we see that fluctuations appear to be a stumbling block for phenomenological models. They meet with difficulties when confronted with measured factorial moments, in particular in hadron–hadron collisions.

In earlier days, no data existed on factorial moments for small bins and information on strong fluctuations in the number of particles inside such bins existed only for individual events. A distinctive feature of the fluctuations was the azimuthal symmetry of particles belonging to the spike. The whole event showed a noticeable ring of particles in the plane perpendicular to the collision axis. Precisely for this reason, the very first attempt to explain such fluctuations was based on an analogy with Cherenkov photon radiation.

The hypothesis of coherent emission of gluon jets [280] (involving, in particular, the Vavilov–Cherenkov mechanism) predicted that these jets should be emitted in a narrow pseudo-rapidity bin at rather large angles in the center-of-mass system of the colliding hadrons. All subsequent models did not predict any particular polar angle dependence for the dense groups of produced particles. This specific feature was experimentally verified in pp-interactions at 205 and 360 GeV energies [291]. It turned out that the distribution of centres of dense particle groups on the pseudo-rapidity axis contained several peaks superimposed on a fairly strong background. Consequently, the proposed mechanism of coherent jet emission in hadron interactions probably does exist but is not dominant. It could provide the only distinction [291] between pp and $p\bar{p}$ data available from ISR, but no analysis of that kind has yet been performed. The ring-like events were observed in earlier cosmic-ray experiments [114–117] and in recent studies of nucleus–nucleus collisions [292]. Nevertheless, other mechanisms must be involved since intermittency is also observed in e^+e^--annihilation, where the conditions for coherence seem unlikely to be satisfied.

Large fluctuations may arise in an extended blob of a cold quark–gluon plasma [192]. The appealing feature of such a model is the relationship between this phenomenon and the production of soft and low-p_T hadrons, lepton pairs and photons. However, this model faces problems in explaining the large values of intermittency indices in electron–positron annihilation compared to hadronic and nuclear processes, since, contrary to present experimental results, it leads one to expect that the effect is largest in nucleus–nucleus collisions.

Models based on clusters [282, 283] or clans [284] are more flexible in fitting factorial moments, since they involve several free parameters. It has been demonstrated [192, 293] that the existence of

clans leads to a power-law increase of factorial moments for smaller bin sizes. No quantitative comparison with experiment has been attempted, however. As to cluster models, in some cases they succeeded in describing the multiplicity distribution in symmetric rapidity bins of various sizes [67, 281] and of the two-particle correlation function. The data available at that time were limited to rather large rapidity interval sizes ($\delta y \geq 0.5$). In smaller regions, however, simple cluster model fail completely (see Figs. 4.4(b), 4.20(c) and 4.23(a)).

Multiparticle production is described somewhat differently in [294, 201], where particle emission is explained by two types of sources – chaotic and coherent.

Some of the above approaches attempt to describe multiplicity distributions in varying rapidity bins in terms of the negative binomial distribution (or modifications thereof). In the cluster model, this is accomplished by varying the cluster parameters. In the clan model, the negative binomial distribution is obtained by compounding a Poisson distribution for the number of clans with a logarithmic distribution for their decay. In the statistical model with two types of sources, the negative binomial distribution naturally describes the chaotic sources, while the coherent sources contribute a Poisson component.

Even though the negative binomial distribution can be phenomenologically used to fit experimental data in the very first approximation, there are definite distinctions from it in experiment. Besides, the asymptotic QCD predictions disfavour it revealing new features [295] of multiplicity distributions. In particular, the NBD cumulants are always positive, while perturbative QCD predicts negative values (and oscillations) of the higher-order cumulants. The pQCD prediction is supported by experiment for the case of the total rapidity range.

5.2.2. Intermittency and fractality

In most cases, the models considered above need to have their parameters adjusted to be able to fit (if at all) the data on factorial moments. Power-law behaviour of factorial moments is most naturally obtained for cascading mechanisms and in phase transitions, as we shall see later.

The concept of intermittency has been borrowed from the theory of turbulence. There, it represents the following property of a turbulent fluid: vortices of different size alternate in such a manner as to form a self-similar structure. They do not fill in the whole volume, but form an intermittent pattern alternating with regions of laminar flow. Mathematically, this property is described by a power-law dependence of the vortex distribution moments on the vortex size. This is the reason why the exponents ϕ_q in the power-law dependence of factorial moments $F_q(\delta y) \propto (\delta y)^{-\phi_q}$ in (2.110) are called "intermittency indices".

As mentioned in Section 2.4, the self-similar nature of vortices directly implies a connection between intermittency and fractality. Fractals are self-similar objects of a non-integral dimension. The fractal dimension is a generalization of ordinary topological dimensionality to non-integers.

More complicated self-similar objects exist, consisting of differently weighted fractals with different non-integer dimensions. They are called multifractals and are characterized by generalized (or Rényi) dimensions D_q which depend on the rank q of the moment of the probability distribution over such objects. The analysis of multifractals according to the Lévy indices goes beyond the simple definition of intermittency.

The formal definitions are given in Section 2.4. For more details, we refer to the review papers [44, 45, 47] and references therein. In connection with multiparticle production, fractals were first mentioned in [124, 126–128].

Somehow, the concept of fractality goes beyond a purely formal definition of intermittency, by connecting the observed dimensionality with the geometrical and thermodynamical properties of an object, as well as with the properties of the distributions over this object [44,130]. The power-law behaviour of factorial moments reveals the fractal structure of rapidity distributions as decomposed in individual events. Its relation to geometrical and thermodynamical properties is discussed below. In string models [270], the self-similar behaviour of fluctuations is ascribed to the fractal nature of the phase space available for subsequent branchings that is formulated in [296] as a "plumber view" of multiparticle processes.

Sometimes, intermittency is ascribed [297] to the fluctuations of the geometrical sizes of emitting sources.

Some caution is necessary when applying these concepts to multiparticle production. As discussed in Section 4, finite statistics, the rather small number of particles produced in an event and, especially, in a given cell, the method of bin splitting, the rather restricted range of bin widths over which the power-law behaviour is observed, all influence the final conclusion. This is described in more detail in [45,298].

5.2.3. Random cascade models

In turbulence, intermittency was first demonstrated in cascade models [299]. Modifications of these, as applied to multiparticle processes, are rather popular nowadays [21,22].

In such models, one considers a series of self-similar steps in partitioning phase space. Let us denote by M the number of bins obtained by breaking up the total phase space into λ parts at each of the ν iterations of the self-similar cascade. Thus $M = \lambda^{\nu}$ ($\equiv \Delta Y/\delta y$ for a total rapidity range ΔY divided into bins of width δy). Random cascade models involve a probability distribution $r(W)$ with corresponding moments

$$\langle W^q \rangle = \int \mathrm{d}W\, r(W) W^q\,, \quad \langle W \rangle = 1\,. \tag{5.13}$$

The function $r\langle W \rangle$ induces density fluctuations as the rapidity window is broken up into ever smaller bins. The density P_m in the mth bin is given by the product

$$P_m = \frac{1}{M} \prod_{n=1}^{\nu} W_n \equiv \frac{1}{M} \frac{\rho_{(m)}}{\langle \rho_{(m)} \rangle}\,, \tag{5.14}$$

where the sequence of indices n defines a path leading to a given bin m with density $\rho_{(m)}$. One assumes that there exists a range of scales inside of which the weights W are constant, i.e. they do not depend on the scale at which they operate.

Herefrom, the intermittent character of the models follows as:

$$F_q = \langle (MP_m)^q \rangle = \left\langle \prod_{n=1}^{\nu} W_n^q \right\rangle = (\Delta Y/\delta y)^{\ln \langle W^q \rangle / \ln \lambda}\,. \tag{5.15}$$

The intermittency indices are equal to

$$\phi_q = \ln \langle W^q \rangle / \ln \lambda\,, \tag{5.16}$$

i.e. random cascade models possess a multifractal spectrum [44].

The simplest type of distribution $r(W)$ is the subclass of so-called α-models [300] given by the two-level probability distribution:

$$r(W) = p\delta(W - W_-) + (1-p)\delta(W - W_+)\,, \tag{5.17}$$

where $0 \leq W_- < 1 < W_+$ and $pW_- + (1-p)W_+ = 1$ because of the normalization condition (5.13). The density enhancement $W_+ > 1$ occurs with probability $(1-p)$ at each step of the cascade, while a depletion $W_- < 1$ is present with a probability p. Combined, they create "spikes" and "holes" in the rapidity distribution. The intermittency indices are given by

$$\phi_q = \ln[pW_-^q + (1-p)W_+^q]/\ln\lambda\,. \tag{5.18}$$

The study of moments and multifractal analysis reveal new interesting features. (Let us mention that the α model is reduced to the β model for $W_- = 0$ and describes a monofractal in that case). As the parameters p and λ are changed, the model predicts various phase transitions [45, 301, 194]. The moments of factorial moments are useful to reveal these transitions due to the fact that the distributions of factorial moments are extremely irregular by themselves [302]. Introducing the normalized moments of moments and ascribing to these a power-law behaviour at small bins of the form

$$\langle Z_q^p\rangle = \frac{\langle F_q^p(\delta y)\rangle}{\langle F_q(\delta y)\rangle^p} \propto (\delta y)^{p\phi_q}\langle F_q^p(\delta y)\rangle \propto (\delta y)^{\varepsilon_{p,q}}\,, \tag{5.19}$$

one can analyse, in the framework of α-models, the dependence of the indices $\varepsilon_{p,q}$ on the parameters of the model. As discovered in [301], this dependence defines four regions in the parameter space, which are reminiscent of four different phases. The indices $\varepsilon_{p,q}$ act as order parameters.

The same conclusions have been obtained when studying [194] the normalized factorial correlators F_{pq}/F_pF_q. Another important property of these correlators is their independence of the bin width [21, 22]. This property has been confirmed by experiments (see Section 4.6). However, the α model does not predict the correct dependence on the distance between bins. It predicts power-law behaviour with an exponent

$$\phi_{pq} = \phi_{p+q} - \phi_p - \phi_q \tag{5.20}$$

related to the usual intermittency indices. The experimental values do not follow a straight line on a double-log plot. Moreover, there are no finite intervals where they satisfy the above relation. When roughly approximated by a straight-line fit, the experimental values of ϕ_{pq} are larger than those of the α-model.

However, one should keep in mind that this is a toy-model, which could pretend to be valid for asymptotically long cascades, i.e. for extremely high energies and multiplicities. Otherwise, one should develop Monte-Carlo programs [298] losing the beauty of analytical formulae. In fact, it has been clearly shown for such a well-known mathematical model as the Cantor set [303], that it is not an easy task to reveal its fractal dimension (known a priori) using factorial moments, if the number of iterations is finite.

Nevertheless, the heuristic value of α models in describing qualitative features of the process is rather high since, in particular, they suggest the possibility of phase transitions. The nature of the transitions and their relation to the quark–hadron transformation are not clear yet. An interesting

observation is the existence of "non-thermal" transitions similar to those in spin-glass systems. They differ from the usual "order–disorder" transitions by producing "different order" in different regions of phase space, so that one may call them "clustered order–disorder" transitions. In that case, the intermittency indices increase with increasing rank faster than linear. Analogies to statistical-mechanics systems [193, 194] provide further insight into the nature of the transitions.

5.2.4. Field-theoretical approach and phase transitions

Besides the scenario of a self-similar cascade, as another extreme, a higher-order quark–hadron phase transition has been proposed to explain strong fluctuations leading to intermittency patterns [275, 287]. Evidently, the statistical mechanics description is most useful here. Hadronization of a quark–gluon plasma becomes the origin of exceptional events with large fluctuations observed above a strong background of conventional events. Such a point of view is supported by studies of a two-dimensional lattice of Ising spins [304, 182], which shows that intermittency appears at the critical temperature. The intermittency indices are directly related to critical exponents of the system. Similar features have been found for the q-state Potts model on the Bethe lattice [305] at the phase transition but without long-distance correlation. Clear fractal structure is also observed for $SU(2)$ gluodynamics near the phase-transition point in lattice calculations [306].

The scenarios of cascading and of phase transitions need not contradict each other, if one accepts the point of view that the role of a quark–hadron transition is to fix the fractal pattern formed by cascading. The fluctuations are "frozen" at the transition point and can be computed by just considering this point.

A well-defined field-theoretical procedure exists to treat fluctuations and phase transitions in common media [307]. It requires, first of all, the definition of an order parameter and its treatment as an effective fluctuation field. In case of multiparticle production, one could choose the rapidity density distribution of particles in individual events $\rho_{(e)}(y)$ (or a function of it) as an order parameter which fluctuates about its inclusive average $\rho(y)$ at each rapidity value y. Its function as an order parameter is clarified by the local parton–hadron duality hypothesis, which has been successful in describing the experimental data for electron–positron annihilation processes. This hypothesis states that the average values of $\rho_{(e)}(y)$ at partonic $\rho_{(p)}$ and hadronic $\rho_{(h)}$ levels differ by a (for all rapidities) common numerical factor. In particular, if one defines [287] the fluctuation field as

$$\varepsilon(y) = [\rho_{(e)}(y)/\rho_{(h)}(y)] - 1 \,, \tag{5.21}$$

then its average in the hadronic phase is equal to zero, while it differs from zero at the partonic level: $\langle \varepsilon(y) \rangle_{(p)} = \rho_{(p)}(y)/\rho_{(h)}(y) - 1 = \text{const}$. Other possible choices for the fluctuation field exist (for example, $\rho^{1/2}(y)$ [275, 286, 308] or $\rho - \rho_{(h)}$ [273]). They have advantages and disadvantages which we shall not discuss here.

The probability of a fluctuation is given by

$$W(\varepsilon) = Z^{-1} \exp[-F(\varepsilon)] \,, \tag{5.22}$$

$$Z = \int D\varepsilon \exp[-F(\varepsilon)] \tag{5.23}$$

where $D\varepsilon$ refers to the functional differential, $F(\varepsilon)$ is the free energy and Z is the partition function. Adding to $F(\varepsilon)$ a term $J(y)\varepsilon(y)$ with an external current $J(y)$, one obtains the irreducible Green functions:

$$\langle \varepsilon_1 \ldots \varepsilon_q \rangle = \delta^q \ln Z / \delta J(y_1) \ldots \delta J(y_q)|_{J=0} , \tag{5.24}$$

which are related to correlation functions, so that, for example (we omit the index h),

$$\langle \varepsilon_1 \varepsilon_2 \rangle = \frac{\rho_2(y_1, y_2)}{\rho(y_1)\rho(y_2)} - 1 \equiv K_2(y_1, y_2) . \tag{5.25}$$

The factorial moments are easily obtained as

$$F_q(\delta y) = (\delta y)^{1-q} \int_0^{\delta y} \mathrm{d}\zeta_1 \ldots \int_0^{\delta y} \delta\zeta_{q-1}\, r_q(\zeta_1, \ldots, \zeta_{q-1}) \tag{5.26}$$

where

$$\zeta_i = y_{i+1} - y_i \quad \text{and} \quad r_q = \rho_q(y_1, \ldots, y_q)/\rho(y_1) \ldots \rho(y_q) . \tag{5.27}$$

At first sight, the fluctuation field theory is not directly related to the underlying QCD. Yet, these theories are connected through the fluctuation pattern of individual events $\rho_{(e)}(y)$, which should be described by both of them if they pretend to be valid. Thus, our guesses on the fluctuation field $\varepsilon(y)$ reflect special features of cascading and confinement in QCD.

For small fluctuations, one can represent $F(\varepsilon)$ by a Taylor series

$$F(\varepsilon) = F_0 + \int \mathrm{d}y \left[\frac{b}{2} \left[\frac{\mathrm{d}\varepsilon}{\mathrm{d}y} \right]^2 + \frac{a}{2}\varepsilon^2 + c\varepsilon^3 + \mathrm{d}\varepsilon^4 + \cdots \right] , \tag{5.28}$$

which corresponds to the Ginzburg–Landau Hamiltonian when $c = 0$, $d \neq 0$ and all higher terms are equal to zero. It has been found [188] that some scaling indices (but not the critical exponents) have universality properties in this approach.

For free fields, i.e. $c = d = \cdots = 0$, one gets

$$\langle \varepsilon_1 \varepsilon_2 \rangle_f = \gamma \exp[-|y_1 - y_2|/\xi] , \tag{5.29}$$

$$\gamma = \pi\xi/b; \quad \xi = (b/a)^{1/2} . \tag{5.30}$$

This exponential form fits the two-particle correlation function qualitatively (and is often used, in particular, for nucleus–nucleus collisions [217]), but it does not provide intermittency at small δy. One should remember that it is related to the free-field Lagrangian but not to the Ginzburg–Landau potential and, therefore, describes usual short-range correlations without any phase transitions. One should also note that the approach is formulated in momentum space and not in configuration space.

One is tempted to conclude that fluctuations are strong at small rapidity intervals and that the perturbative approach fails. The phenomenon of intermittency should be described by a strong coupling field theory, where perturbative methods do not work. In particular, the renormalization group approach and conformal theories have been tried [287, 273] and have provided power-law behaviour of Green functions and factorial moments at small bin widths. So, it seems rather

reasonable to fit the correlation function by an expression

$$C_2(y_1, y_2) \propto \frac{1}{|y_1 - y_2|^{\kappa}} \exp[-|y_1 - y_2|/\xi] \quad (\kappa < 1) \tag{5.31}$$

for all rapidity separations. For rapidity separations smaller than the correlation length ξ one gets pure power-law dependence of the correlation function due to a phase transition phenomenon. The associated singularity should soften energy and transverse momentum spectra. In the simplest approximation, intermittency indices increase linearly with their rank.

Let us stress an important difference of the above consideration with the previous treatment of phase transitions. The correlation length ξ does not tend to infinity and the exponential law is not replaced by a power law at large δy, as one is accustomed to. Instead, the power law appears at small $\delta y (\delta y \ll \xi)$, and does not influence the dependence at large rapidity. This happens, because rapidities play now the role of coordinates in the usual treatment, so that one has to deal with the ultraviolet (not infrared) stable point of the Gell–Mann–Low function. One can speculate that particles lying far apart on the rapidity scale reveal the dynamics of the process with a finite correlation length related to a particular form of the Lagrangian, while those at nearer points remind of the self-organizing critical processes with a scaling law not tightly connected to a particular form of the Lagrangian (sandpile phenomenon). Thus, correlations appear as "*frozen* (due to hadronization) *sounds*" of cascading.

Similar problems have been discussed in the framework of Feynman–Wilson fluid models [275, 286]. One should introduce the notion of temperature, additional assumptions on thermal equilibrium, on Kadanoff scaling at the critical temperature, on the relative role of conventional and stochastic (or quark–gluon plasma) components, and so on. Imposing special boundary conditions [309] on the grand canonical partition function, one can relate Kadanoff scaling in the fluid to KNO scaling in multiparticle processes and describe the fractal properties of the fluid in a wide range of scales. Formula (5.31) appears to be valid for correlation functions of the conventional hadronic system, but for a system at the critical point, pure power-like behaviour with a different exponent is restored. One is therefore lead to consider the whole process in the framework of a two-component (conventional + critical) model.

The same approach has been extended [310] to a multidimensional analysis of intermittency using, however, the assumption that the correlation functions factorize in rapidity and transverse momentum. The predictions for factorial moments differ from QCD predictions. The factorization hypothesis allows to proceed analytically and to relate intermittency to fractal properties of the system in original space–time (this problem has been addressed also in [128, 311, 165]) but looks rather artificial for any field theory (QCD included). For instance, if one assumes that conformal symmetry is responsible for intermittency [287, 273], one obtains non-factorizable Green functions and the predictions differ from the above-mentioned ones due to the mixing of longitudinal and transverse momentum components, inherent in field theories. We shall see, however, that conformal theory and QCD also differ.

Numerical values of intermittency indices can be calculated in the conformal scheme and agree qualitatively with experimental findings. Again, the phase transition plays a crucial role.

Studies of the role of phase transitions in multiparticle production are still in their infancy and have, until now, provided qualitative results only. Also the relation between hadronization

and phase transitions in the simple cascade models treated in the previous sub-section is not yet clear.

The relative role of parton cascading and hadronization is another matter of debate. The problem would be solved if extreme proposals were valid. Indeed, parton cascading with an "infinite" number of steps would provide intermittency indices quadratically increasing with their rank (this corresponds to "wild" or "hard" singularities). Phase transitions, on the other hand, yield monofractal behaviour with a linear increase of the indices. In reality, the two extremes must be modified so that finite cascading would lead to a slower increase, while the next operator-product expansion terms for a phase transition would induce a faster than linear rise of the intermittency exponent. Such problems have as yet not been treated.

5.2.5. The statistical mechanics formalism

Statistical analogy is a powerful way to analyse properties of chaotic dynamical systems [312], in general, and of multifractals and cascade models, in particular [313, 193, 45]. It rests on the possibility to define a partition function $Z(q)$ of the system in the following way:

$$Z(q) = \sum_{m=1}^{M} p_m^q \,, \tag{5.32}$$

where

$$p_m = \rho_{(m)} / M \langle \rho_{(m)} \rangle \tag{5.33}$$

is a normalized probability weight on the ensemble of bins (m) and $\rho_{(m)}$ is a random (rapidity) density registered in each bin m.

The relation to multifractal (or intermittent) properties of a system is established if one considers systems for which the probability inside a box m is proportional to a power α_m of the box size and the number of degenerate boxes (with the same value of α_m) follows a power law as well. Then, assuming a continuous limit, one finds as in (2.118)

$$Z(q) \simeq \int_{a_-}^{a_+} M^{f(\alpha) - q\alpha} \, \mathrm{d}\alpha \,, \tag{5.34}$$

(integration running between maximum and minimum zeros of $f(\alpha)$), wherefrom one easily obtains the multifractal spectrum of the system $f(\alpha)$ (see, for example, [44, 47, 129]).

Remembering the definition of the intermittency indices ϕ_q, one relates them to the spectrum $f(\alpha)$ via the relation

$$f(\bar{\alpha}) = -q^2 \frac{\mathrm{d}}{\mathrm{d}q}\left[\frac{\phi_q + 1}{q}\right], \tag{5.35}$$

where $\bar{\alpha}$ is defined as

$$\bar{\alpha}(q) = 1 - \mathrm{d}\phi_q / \mathrm{d}q \,. \tag{5.36}$$

The interpretation of $f(\alpha)$ is transparent since it weights the number of degenerate boxes. It, therefore, corresponds to the entropy in statistical mechanics. In a similar way, the rank q may be interpreted as an inverse "temperature" $\beta = 1/T$ and the relation (5.35) corresponds to the usual

thermodynamical formula

$$S = -\mathrm{d}F/\mathrm{d}T\ , \tag{5.37}$$

where S is the entropy and F is the free energy, whose "temperature" dependence is provided now by

$$\lambda(q) = (\phi_q + 1)/q = 1 - F\ . \tag{5.38}$$

Two features of this analogy are particularly useful. On the one hand, application of the thermodynamical formalism allows for coverage of multifractals by boxes of different sizes, i.e. for a more precise description of individual events. This has been used in proposals of correlation measures with non-uniform coverage [130, 245, 143]. On the other hand, the multifractal treatment admits an extension of the thermodynamical formalism to non-equilibrium systems. It has been used to classify the phase transitions in α models and to demonstrate that, in multiparticle processes, phases could exist similar to spin-glass states [193, 45].

It is important to note that the minimum of the $\lambda(q)$ (5.38) corresponds, according to (5.35), to zeros of the fractal spectrum. This is a signal for a phase transition in thermodynamical systems. One should stress, however, that the similarity of the distributions is in itself not sufficient to justify use of statistical physics terminology in its original meaning for the quantum field systems we are interested in here. Besides, the analogy breaks down completely for values of q exceeding the multiplicities effectively contributing to the moments. Nevertheless, this analogy is used in [314, 315] to derive the dependence of the pressure in a Feynman–Wilson liquid on its chemical potential and some peculiar features are found in hadron–hadron reactions (see also the review paper [316]).

It is evident that further explorations of statistical mechanics approaches to multiparticle production are needed. In particular, analytical properties of a partition function, often useful in connection with phase transitions, have not been much analysed.

The location of the (complex) roots (zeros) Z_ν of the multiplicity generating function (2.43) has recently been studied in [317, 318] after earlier suggestions by Biebl and Wolf [2]. This work is based on the analogy with the famous Lee-Yang zeros [319], whose location fully characterizes the thermodynamic properties of the physical system.

For multiplicity distributions, the strength of the fluctuations of the multiplicity in an event is directly related to the location of the zeros in the complex z plane: the magnitude of the factorial cumulants, and thus the strength of the correlations, is determined by the roots closest to the origin.

In the discrete version of QCD, developed in LUND, it was demonstrated that the zeros of (2.43) belong to a fractal Julia set [320] with intruiging properties. Detailed studies of this set, and various connections with standard phenomenology, such as KNO scaling, remain to be worked out.

5.2.6. Intermittency, evolution equations and QCD

In the previous section we considered two rather extreme possibilities, simple cascade models and phase transitions, as possible mechanisms leading to scale invariance in particle production processes.

Further interesting results have been derived from studies of simplified kinetic branching evolution equations for "birth–death" (or "gain–loss") processes. Many of these are treated in textbooks [322, 323] and were applied to multiparticle production [324–328]. In general, the

time-evolution of the number of "clusters" (partons, resonances, etc.) is described by forward or backward (retrospective) Kolmogorov equations, which relate the time derivative of the generating function to some combinations of that function. A particular example is the Smoluchowski equation treated in [329]. The terms "forward" and "backward" imply, that each tree graph may be viewed either as a splitting to ever "thinner" branches, or as a convolution to ever "thicker" branches.

For linear evolution equations, the solutions depend directly on the initial conditions [205]. Non-linear equations often have solutions asymptotically independent of pre-history [327, 329]. Stationary regimes may appear if the annihilation of clusters is stronger than the "birth rate". In that case, the dispersion is proportional to the average multiplicity and intermittent behaviour can be obtained, if the proportionality factor is larger than one and the mean multiplicity decreases correspondingly for smaller bins. This can easily be proven by means of the definition of the second-order factorial moment. Let us note that systems obeying non-linear evolution could exhibit quite general properties, independent of the detailed form of the equations, such as period doubling. Some ideas along this line of thought, using properties of stochastic systems and Feigenbaum attractors, have been formulated in [330, 331].

More detailed analysis of intermittency in the framework of the Smoluchowski equation [329] reveals various regimes of time-evolution and cascading, depending on the parameters of the model. The Smoluchowski equation is of the backward type. It contains terms linear and quadratic in the generating function G with opposite signs. Formally it looks like

$$\mathrm{d}G/\mathrm{d}t = G*G - G*G_1 \,, \tag{5.39}$$

where $G(u,t) = \sum_{n\geq 1} N(n,t)u^n$, $G_1 = G(1,t)$ with $N(n,t)$ representing the number of clusters of (integer) mass n at time t and the convolution $*$ is defined through the aggregation coefficients of clusters. The fractal properties of aggregates and the occurrence of phase transitions have been analysed in [329].

Obviously, it would be desirable if an explanation of scaling phenomena in multiparticle production could be derived from, so to say, first principles, i.e. in the framework of QCD. Multiparticle production in QCD is the result of quark–gluon branching and the subsequent transition to hadrons. As such, the self-similar multiplicative branching (or cascade) process could give rise to a scaling regime. The perturbative QCD parton shower picture is justified for interactions with large transferred momenta (or virtualities), but in hadronic reactions one mostly has to deal with soft processes. Perturbative QCD is valid in the initial stages of high-energy cascades in electron–positron annihilation and could, therefore, be used as an explanation for intermittency.

It is well known that the perturbative QCD cascade gives rise [332] to a mean multiplicity of partons increasing rapidly with energy. Equations for higher moments of parton multiplicity distributions are rather complicated [333, 98], but reveal in any case that the parton number distributions are much wider than a Poissonian. The infrared limit becomes very important and one should consider infrared-safe properties. Assuming that the singularity is avoided in a way similar as in an electromagnetic cascade in a medium, one can estimate the fractal dimension of internal motion of partons in a jet and it turns out to be quite low for a single jet in e^+e^--annihilation [128].

The simplest theoretical models, such as the tree diagrams of the ϕ^3 model, simplified QCD [334,335,29] also based on tree diagrams, the Schwinger tunnelling transition [336] or the effective Lagrangian approach [308], indicate that the totality of all produced partons exhibits intermittency.

It is not yet clear what modifications of QCD equations going beyond the tree graphs (so-called Double Logarithmic Approximation – DLA) would fit this region best. An approach to that problem has been proposed [337] in deep inelastic processes where the transition from the Bjorken limit to the Regge domain proceeds through some intermediate region in which quadratic terms (in the fields) appear and cause some recombination of partons at high densities. Here, the evolution equation for the number of gluons $xG(x,q^2)$ in a hadron with a transverse size q^{-1} and for small values of the Bjorken x-variable is taken to be

$$\frac{\partial^2 xG(x,q^2)}{\partial \ln(1/x)\,\partial \ln q^2} = \alpha_s\, xG(x,q^2) - \frac{C\alpha_s^2}{q^2}[xG(x,q^2)]^2\,, \tag{5.40}$$

where α_s is the QCD coupling strength and C is a constant. It is inspired by QCD ideas and Regge phenomenology, but has not been derived rigorously. No analysis of the intermittency property has been attempted so far. One should note, however, that the general effect of such a quadratic damping is to narrow the multiplicity distribution (see, for example [338]), which leads to decreasing factorial moments.

One should, however, not rely on the similarity of Eqs. (5.39) and (5.40), since this could be misleading. As is well known [333,339,98], the equations for the generating functionals for gluon and quark jets in QCD are non-linear, while the corresponding equations for the structure functions in DLA are just linear GLAP equations. The generating functional for a parton p is given by

$$G_{\mathrm{p}}(u,v,x,Y) = \sum_{n_{\mathrm{q}},n_{\mathrm{g}}} \frac{1}{n_{\mathrm{q}}!\,n_{\mathrm{g}}!} \prod \int \mathrm{d}x_{\mathrm{q},i}\,\mathrm{d}x_{\mathrm{g},j}\,u(x_i)v(x_j)W^{\mathrm{p}}_{n_{\mathrm{q}}n_{\mathrm{g}}}(x,x_i,x_j,Y) \tag{5.41}$$

where W is a differential probability to create n_{q} quarks and n_{g} gluons with an evolution parameter $Y \sim \ln\ln Q^2$ in a p jet. The equations for the generating functionals are

$$\frac{\partial G_{\mathrm{q}}(x,Y)}{\partial Y} = \int_0^1 \mathrm{d}x'\, P_{\mathrm{qq}}(x',x)[G_{\mathrm{q}}(x',Y)G_{\mathrm{g}}(1-x',Y) - G_{\mathrm{q}}(x,Y)]\,, \tag{5.42}$$

$$\frac{\partial G_{\mathrm{g}}(x,Y)}{\partial Y} = \int_0^1 \mathrm{d}x'\,[P_{\mathrm{gg}}(x',x)G_{\mathrm{g}}(x',Y)G_{\mathrm{g}}(1-x',Y) - G_{\mathrm{g}}(x,Y)) + n_{\mathrm{f}}P_{\mathrm{qg}}(x',x)(G_{\mathrm{q}}(x',Y)G_{\mathrm{q}}(1-x',Y) - G_{\mathrm{g}}(x,Y))]\,, \tag{5.43}$$

where the P's are the corresponding GLAP kernels, n is the number of flavours and the initial conditions are such that at $Y=0$, $G_{\mathrm{q}} = u$ and $G_{\mathrm{g}} = v$ for a single jet.

The status of the equations for generating functionals is not completely clear up to now. They are able to reproduce the higher-order graphs of the perturbation theory far beyond the tree level [98]. Their success in predicting the tiny features of multiplicity distributions in total phase space (for a review see [295]) encourages speculations about their quite general status, with some confinement properties taken into account already at that stage.

A simplified version of (5.43) with the quark term omitted (gluodynamics) has been studied in [339]. Intermittency for the factorial moments of the gluon cascade is claimed to be in qualitative agreement with experimental data, as well as evidence for a structural phase transition. However, the formula for the intermittency indices contradicts other QCD results. This is not surprising, since the generating function technique should here be applied to the subjet hitting the bin under investigation, not to the whole jet as done in [339].

The treatment of QCD cascades has been taken further in [253] within the framework of the dipole formalism including coherence effects. The multifractal dimension of the parton cascade for high order q is found to be equal to the QCD anomalous dimension $\gamma_0 = (6\alpha_s/\pi)^{1/2}$ and a first pre-asymptotic correction has been calculated. Moreover, a geometrical interpretation of the anomalous dimension of QCD is proposed.

A direct solution of QCD evolution equations has been attempted for the second correlator in [254]. The behaviour of factorial moments of any rank (as well as of double trace moments – see below) in small phase-space windows for e^+e^- collisions is treated both in DLA and in the next Modified Leading Logarithmic Approximation (MLLA) of QCD in [256]. Similar results for factorial moments in DLA are obtained in [255,257]. They are closely related to the previously derived formulae of [340].

In the approach described above, one considers three stages of the process:

1. the initial quark emits a hard gluon,
2. the gluon evolves into a jet consisting of several subjets,
3. one of the subjets hits the phase-space window chosen.

Integrating over all the stages one gets the final multiplicity distribution (for details see [256]). For comparatively large windows one can use the fixed coupling constant, while for smaller bins its running should be taken into account.

Fixed coupling QCD factorial moments reveal [254,256] the intermittency phenomenon with intermittency indices equal to

$$\phi_{\mathrm{QCD}}(q) = (q-1)\left(D - \frac{q+1}{q}\gamma_0\right), \tag{5.44}$$

in DLA. This formula is valid if, for the D-dimensional analysis with M bins along each axis, one defines $F_q \propto M^{\phi(q)}$. For large q the indices increase linearly. The term with negative sign in the second bracket is proportional to the QCD multiplicity anomalous dimension γ_0. From (5.44), one would conclude that QCD prescribes fractal behaviour with codimension

$$d_q|_{\mathrm{QCD}} = D - [(q+1)/q]\,\gamma_0\,. \tag{5.45}$$

The phase space term D is obviously non-fractal. The γ_0 term in (5.45) is due to the energy dependence of multiplicity and gives monofractal behaviour. The gluon energy spectrum contribution, represented by γ_0/q, gives multifractal behaviour. The next-to-leading corrections to γ_0 also provide q-dependent terms.

The calculated values should be compared to the slopes in the region $\delta y > 1$ (which are rather large) since (5.45) is derived in fixed-coupling QCD (the intermittent behaviour in that region was discussed first in [341]). In smaller bins, the QCD running coupling becomes important and modifies the above relations [256]. The factorial moments now behave in a semi-power-like manner so that there is no strict intermittency even though an approximate one can still be claimed.

The second term becomes very close to 1 for the low-rank moments and the low-rank intermittency indices turn out to be very small for one-dimensional analyses, in accordance with experiment. Corrections to γ_0 of the order of γ_0^2 can be taken into account [256]. The influence of confinement seems negligible. Thus small as well as large δy intervals may be described in a unified treatment, at least at a qualitative level. The transition point from "large" to "small" bins depends on the rank of the moment in QCD, in full accordance with experimental findings.

We should further mention that the ratio d_q/d_2 depends explicitly on D, contrary to experimental claims (see Section 4.3.3).

The "free energy" $F(q)$ is related to $\lambda(q)$ given by (5.38) as

$$F(q) = 1 - \lambda(q) \approx \gamma_0 - \gamma_0/q^2 \ . \tag{5.46}$$

In DLA, it is a steadily increasing function of q. However, with corrections to γ_0 taken into account [256] $F(q)$ becomes non-monotonic. This happens for rather large values of q, with the result, that the distinction between factorial and usual moments becomes crucial and statistical analogies inapplicable. These findings show the limitations of perturbative QCD and provide further insight into the properties of multiplicity distributions, such as KNO scaling, in full phase space [342, 343].

In particular, QCD gives rise to the prediction [343, 295] of a negative value of the cumulant of rank 5 confirmed by experiment and to the general conclusion of a non-infinitely-divisible nature of total multiplicity distributions in QCD (that prohibits e.g. the one-ladder multiperipheral cluster models).

The increasing branch of the multifractal spectrum $f(\alpha)$ may be easily calculated using (5.35) and (5.36) giving

$$f(\alpha) = 2\gamma_0^{1/2}(\alpha - \gamma_0)^{1/2} \ . \tag{5.47}$$

The double trace moments (DTM), redefined in analogy with factorial moments as

$$F_{q,\nu} \equiv \frac{1}{\Delta}\left(\sum_{\Theta_m \in \Delta} \frac{n_m(n_m-1)\cdots(n_m-\nu+1)}{n^\nu}\right)^q , \tag{5.48}$$

behave [256] in QCD as

$$F_{\nu,q}(\Delta) \propto \Delta^{\gamma_0(q^2-1)/q\nu} \propto \Delta^{q\phi_\nu - \phi_{q\nu} + q - 1} \equiv \Delta^{-\phi(q,\nu)+q-1} , \tag{5.49}$$

wherefrom one finds

$$\phi(q,\nu) = \phi(q\nu) - q\phi(\nu) = (q-1)\left(1 - \frac{q+1}{q}\cdot\frac{\gamma_0}{\nu}\right) . \tag{5.50}$$

The second factor in (5.50) may be called "double codimension". It is not symmetric in q and ν and shows that increasing ν one decreases effectively the anomalous dimension. For $\nu = 1$, as required, the double codimension becomes equal to the usual codimension. The scaling exponent (5.50) is not factorizable in ν and q. The above redefinition of DTM is aimed at reducing the Poissonian noise and the role of phase-space factors, otherwise very important.

In fact, it is surprising that the above expression describes qualitatively the general trends and even the absolute normalization of the functions $K(q,\nu)$ shown in [50, 51]. For large ν, the ratio $K(q,\nu)/(q-1)$ is completely determined by the phase-space factor and should tend to 1. This is seen in the experimental data. In the region of small $q \sim 1$ and $\nu \sim 1$ the strong compensation in (5.50) prevents its use, but even there it gives quite reasonable values of $K(q,\nu)$. This probably

indicates that DTM defined as powers of multiplicities are not sensitive enough to dynamics, a suspicion raised earlier (Section 4.7).

On the other hand, the parton cascading picture employed in [256] may be applied, strictly speaking, only to hard processes at extremely high energies and one should not rely much on the asymptotic estimates of QCD when considering experimental data. Also, the difference between usual and factorial moments becomes extremely important at large values of q or at sufficiently small bins with low multiplicities. One may suspect that relation (5.50) and, especially its first part, has a much wider range of applicability than just for e^+e^- collisions and some universal relation could be valid for other reactions. If so, it will be important to understand whether these common features are due to common dynamics or to insufficient sensitivity of the proposed measures.

The large fluctuations, e.g. those observed by the NA22 collaboration, have raised the suspicion that at small bins one is dealing with unusually wide distributions, which could have infinite moments. This has led one to consider Lévy-stable probability distributions. The Lévy indices derived from QCD factorial moment indices or DTM exponents show [256] no sign of "wild" singularities.

The DTM technique has been first applied to experimental data from hadron–hadron reactions (described in Section 4.7.7) where direct QCD arguments are invalid. For e^+e^- collisions, however, it may be worthwhile to analyse the data with this method.

Let us further note that there is a difference between predictions of QCD and those of variants of conformal theories considered in [273], or of multiplicative models [310]. For example, the intermittency indices derived in a rapidity or azimuthal angle analysis should be equal in QCD. This is a consequence of the symmetrical form (in pseudorapidity η and azimuthal angle φ) of the gluon propagator, which can be written as

$$k^2 = (p_{T,1} + p_{T,2})^2 = 4p_{T,1}p_{T,2}(\sinh^2\eta_{12}/2 + \sin^2\varphi_{12}/2)\,, \tag{5.51}$$

where $p_{T,i}$ is the transverse momentum of ith parton. In a conformal theory, the intermittency indices for the second factorial moment are given by

$$\phi_2(\delta y) = 2\eta\,, \qquad \phi_2(\delta\varphi) = 0\,, \tag{5.52}$$

respectively. Here, η is the conformal anomalous dimension estimated to be $\eta \approx 0.07$–0.1. For multiplicative models, one finds

$$\phi_2(\delta y) = 1 - D_y\,, \qquad \phi_2(\delta\varphi) = D_\varphi - 1 \tag{5.53}$$

with $0 < D_y < 1, 1 < D_\varphi < 2$.

The emergence of intermittent behaviour in solutions of non-linear equations and in perturbative QCD encourages further studies along these directions. At the least, they hold a promise of further theoretical insight. One should keep in mind, however, that a direct comparison of QCD-based asymptotic results with present-day experiments is not justified. Some effects revealed by the data seem to be of a different, as yet unsatisfactorily explained, origin.

6. Conclusions

Developments in physics – and in science in general – over the last decade, have brought exciting new discoveries and deeper insight into the dynamics of complex systems. Studies of classical and

quantum chaos, non-equilibrium dissipative processes, random media, growth phenomena and many more have all contributed to reveal the pervasive importance of self-similarity, of power laws and of fractals in nature. Research in these fields is still in full evolution and continues to uncover intriguingly simple and often surprisingly universal behaviour in complex, non-linear systems.

The suggestion of Białas and Peschanski to look for scaling in particle fluctuations was one of the first attempts to apply modern ideas and techniques from complex-system research to multihadron-production processes. In preceding pages, we have presented a critical overview of the impressive amount of experimental and theoretical work this proposal has generated since its formulation in 1986. The continuing interest in the field testifies of the growing conviction that new avenues need to be explored for progress in strong-interaction physics.

Impressive as it may be, this work has not yet led to final answers concerning the fundamental issues. Approximate power-law scaling of particle density and correlation functions is now indeed observed, especially in two- or three-dimensional phase space. However, so far it can be explained from an interplay between jet formation and more or less "conventional" correlations among identical particles due to quantum interference.

Nevertheless, as often happens, the detailed scrutiny of data (and detectors) on the full variety of collision processes in the search for power behaviour has led to many new observations of interest in their own right. It has helped to recognize the importance of detailed studies of correlation phenomena at large and small distances in momentum space and new sensitive and general techniques have been developed for their analysis.

Standard hadronization models, all too often accepted as satisfactory, have been exposed to severe and sometimes even painful tests. Intermittency analysis has revealed deficiencies in our understanding of the hadronization process. These defects are not easy to cure in a consistent manner by simple parameter-tuning and "new" physics may well be needed to restore internal consistency in e.g. fragmentation models of the LUND type. Present work on this subject starts to provide hints that purely probabilistic treatment of the break-up of colour fields has to be supplemented with effects deeply connected with the structure of the non-perturbative QCD vacuum. Progress in this direction would in itself be ample compensation for the efforts spent on attempting to establish fractality in multihadron production.

Data obtained in the last years have shown the overwhelming importance of correlations among identical particles in the "intermittent" regions of phase space. This quantum mechanical phenomenon, discovered in particle physics in 1959, still awaits satisfactory incorporation into present hadronization phenomenology, if it is to be used as a reliable interferometric tool e.g. in studies of quark–gluon plasma formation.

Theoretical work has developed along a large variety of directions. Fractal properties have been discovered in string-fragmentation models. Within the realm of perturbative QCD, parton correlations and emergence of power behaviour are now studied with increasing sophistication. The relevance for present-day phenomenology remains doubtful, however.

The powerful methods of statistical mechanics have been intensively exploited in studies of random cascades as well as in equilibrium and non-equilibrium critical phenomena. Results of real intrinsic value have been obtained, with potentially interesting applications in other fields.

In search for an explanation of "unusually large" density fluctuations, "intermittency", in analogy with fluid turbulence, has progressively led to appreciate the importance and often spectacular manifestation of non-linear strong-coupling dynamics.

Experiments in deep-inelastic scattering are now starting to probe hadron structure in a regime where the perturbative parton-cascade picture becomes blurred. Non-linear perturbative evolution and confinement play an increasingly important role in the very low Bjorken-x region now accessible in HERA. Present attempts to understand this region invoke QCD Reggeon theory.

It is intriguing to speculate that a power-law dependence of the low-x parton correlation functions could manifest itself as "gluonic" intermittency in virtual parton cascades, with the occasional creation of regions with very large, or very small gluon density.

Acknowledgements

It is a great pleasure to thank the many physicists who have contributed enthusiastically to this new field with experimental data, theoretical or methodical ideas or constructive criticism. Among those from which we have gained most considerably are B. Andersson, I.V. Andreev, A. De Angelis, A. Białas, J. Bjorken, F. Botterweck, B. Buschbeck, P. Carruthers, A. Capella, M. Charlet, S. Chekanov, H. Dibon, I. Derado, H. Eggers, E.L. Feinberg, K. Fiałkowski, A. Giovannini, E. Grinbaum–Sarkisyan, G. Gustafson, R. Hwa, G. Jancso, V. Kuvshinov, A.V. Leonidov, P. Lipa, F. Mandl, M. Markytan, W. Metzger, J.-L. Meunier, W. Ochs, R. Peschanski, O. Podobrin, S. Ratti, I. Sarcevic, H. Satz, N. Schmitz, J. Seixas, E. Stenlund, A. Syed, F. Verbeure, R. Weiner, B. Wošiek, J. Wošiek, Y.F. Wu, K. Zalewski, and many others to be found in the references. It is a great favour to be able to work with these scientists and to share their pioneering spirit in difficult territory.

References

[1] N.N. Bogoliubov, Problems of Dynamical Theory in Statistical Physics (Gosizdat, USSR, 1946).
[2] L.S. Brown, Phys. Rev. D 3 (1972) 748;
K.J. Biebl and J. Wolf, Nucl. Phys. B 44 (1972) 301.
[3] T.N. Thiele, Ann. Math. Stat. 2 (1931) 165.
[4] R. Kubo, J. Phys. Soc. Japan 17 (1962) 1100.
[5] R.F. Chang, V. Korenman, C.O. Alley and R.W. Detenbeck, Phys. Rev. 178 (1969) 612.
[6] B. Kahn and G.E. Uhlenbeck, Physica 5 (1938) 399.
[7] K. Huang, Statistical Mechanics (Wiley, New York, 1963).
[8] A.H. Mueller, Phys. Rev. D 4 (1971) 150.
[9] M.G. Kendall and A. Stuart, The Advanced Theory of Statistics, Vol. 1 (C. Griffin, London, 1969).
[10] Z. Koba, Acta Phys. Pol. B 4 (1973) 95.
[11] B.R. Webber, Nucl. Phys. B 43 (1972) 541.
[12] H.C. Eggers, Ph.D. Thesis, University of Arizona, 1991.
[13] A. Giovannini and L. Van Hove, Z. Phys. C 30 (1986) 391.
[14] P. Carruthers, Phys. Rev. A 43 (1991) 2632.
[15] W.I. Weisberger, Phys. Rev. D 8 (1973) 1387.
[16] M. Abramowitz and I. Stegun, Handbook of Mathematical Functions (Dover, New York, 1964).
[17] H. Cramér, Mathematical Methods of Statistics (Princeton, NJ, 1946).
[18] D. Weingarten, Nucl. Phys. B 70 (1974) 501.
[19] Z. Koba and D. Weingarten, Nucl. Phys. B 70 (1974) 534.
[20] M. Koutras, Discrete Math. 42 (1982) 73.
[21] A. Białas and R. Peschanski, Nucl. Phys. B 273 (1986) 703.

[22] A. Białas and R. Peschanski, Nucl. Phys. B 308 (1988) 857.
[23] K. Fiałkowski, B. Wošiek and J. Wošiek, Acta Phys. Pol. B 20 (1989) 639.
[24] W. Ochs, Phys. Lett. B 247 (1990) 101; Z. Phys. C 50 (1991) 339.
[25] A. Białas and M. Gazdzicki, Phys. Lett. B 252 (1990) 483.
[26] P. Carruthers, H.C. Eggers and I. Sarcevic, Phys. Lett. B 254 (1991) 258.
[27] J. Feder, Fractals (Plenum, New York, 1988).
[28] R.C. Hwa, Phys. Rev. D 41 (1990) 1456.
[29] C.B. Chiu and R.C. Hwa, Phys. Rev. D 43 (1991) 100.
[30] W. Florkowski and R.C. Hwa, Phys. Rev. D 43 (1991) 1548.
[31] B. Saleh, Photoelectron Statistics (Springer, Berlin, 1978).
[32] D. Cantrell, Phys. Rev. A 1 (1970) 672.
[33] H.C. Eggers, P. Carruthers, P. Lipa and I. Sarcevic, Phys. Rev. D 44 (1991) 1975.
[34] L. Mandel, Proc. Phys. Soc. 72 (1958) 1037.
[35] L. Mandel, Proc. Phys. Soc. (London) 74 (1959) 233.
[36] E. Wolf and C.L. Mehta, Phys. Rev. Lett. 13 (1964) 705.
[37] G. Bédard, Proc. Phys. Soc. 90 (1967) 131.
[38] J.N. Fry, Astrophys. J. 289 (1985) 10.
[39] R. Peschanski and J. Seixas, preprint CERN-TH-5903/90.
[40] C.D. Cantrell and J.R. Fields, Phys. Rev. A 7 (1973) 2063.
[41] J. Bures, Can. J. Phys. 50 (1972) 706.
[42] B. Mandelbrot, The Fractal Geometry of Nature (Freeman, New York, 1982).
[43] Ya.B. Zeldovitch, Sov. Phys. Usp. 152 (1987) 3.
[44] G. Paladin and A. Vulpiani, Phys. Rep. 156 (1987) 147.
[45] R. Peschanski, Int. J. Mod. Phys. A 6 (1991) 3681.
[46] A. Rényi, Probability Theory (North-Holland, Amsterdam, 1970).
[47] I.M. Dremin, Sov. Phys. Usp. 160 (1990) 647.
[48] D. Schertzer and S. Lovejoy, J. Geophys. Res. 92 (1987) 9693.
[49] J.P. Bouchaud and A. Georges, Phys. Rep. 195 (1990) 127;
A.Y. Khintchine and P. Lévy, C.R. Acad. Sci. (Paris) 202 (1936) 374.
[50] S.P. Ratti et al., Z. Phys. C 61 (1994) 229.
[51] S.P. Ratti et al. (IHSC), in: Proc. XXI Int. Symp. Multiparticle Dynamics, Wuhan, China, 1991, eds. Y.F. Wu and L.S. Liu (World Scientific, Singapore, 1992) p. 409;
V. Arena et al. (IHSC), Nuovo Cimento 108A (1995) 417.
[52] S.V. Chekanov and V.I. Kuvshinov, Acta Phys. Pol. B 25 (1994) 1189.
[53] S.V. Chekanov and V.I. Kuvshinov, in: Proc. 4th Int. Seminar on Nonlinear Phenomena in Complex Systems, Minsk, Belarus, to be published.
[54] S.V. Chekanov and V.I. Kuvshinov, J. of Phys. A: Math. and Gener., to be published.
[55] H. Abarbanel, F. Dyson et al., Report on Wavelets, Cornell Mathematics, 1994.
[56] M. Greiner, P. Lipa and P. Carruthers, Phys. Rev. E 51 (1995) 1948;
M. Greiner, J. Giesemann, P. Lipa and P. Carruthers, preprint HEPHY-PUB 618/95, AZPH-TH/95-03 (1995).
[57] I. Daubechies, Ten Lectures on Wavelets (Society for Industrial and Applied Mathematics (SIAM), Philadelphia, 1992).
Y. Meyer, Wavelets: Algorithms and Operators (Cambridge University Press, New York, 1992).
G. Kaiser, A Friendly Guide to Wavelets (Birkhauser, Boston, 1994).
[58] N. Suzuki et al., preprint SULDP-1995-4, HEP-PH/9503402, Prog. Theor. Phys. in press.
[59] P. Carruthers and C.C. Shih, Int. J. Mod. Phys. A 2 (1987) 1447.
[60] Z. Koba, H.B. Nielsen and P. Olesen, Nucl. Phys. B 40 (1972) 317.
[61] K.G. Wilson, Cornell Report No. CLNS-131/1970 reprinted in: Proc. 14th Scottisch Universities Summer School Conf. (1973), eds. R.L. Crawford and R. Jennings (Academic Press, New York, 1974);
R.P. Feynman in: Proc. Int. Conf. Neutrino 72, Baltonfured, 1972, eds. A. Frenkel and G. Marx (Budapest, 1973).
[62] L. Foá, Phys. Rep. 22 C (1975) 1.

[63] J. Whitmore, Phys. Rep. 27 C (1976) 187.
[64] F.C. Winkelman et al., Phys. Lett. 56 B (1975) 101.
[65] R.E. Ansorge et al. (UA5), Z. Phys. C 37 (1988) 191.
[66] S.R. Amendolia et al., Nuovo Cimento A 31 (1976) 19.
[67] Ch. Fuglesang, Ph.D. Thesis, University of Stockholm (1987).
[68] G.J. Alner et al. (UA5), Nucl. Phys. B 291 (1987) 445.
[69] B. Andersson, G. Gustafson and B. Nilsson-Almqvist, Nucl. Phys. B 281 (1987) 289; Lund preprint LUTP 87-6.
[70] H.U. Bengtsson and T. Sjöstrand, Comput. Phys. Commun. 46 (1987) 43.
[71] J.L. Bailly et al. (NA23), Z. Phys. C 40 (1988) 13.
[72] A. Breakstone et al., Phys. Lett. 114 B (1982) 383.
[73] B. Andersson, G. Gustafson, I. Holgersson and O. Månsson, Nucl. Phys. B 178 (1981) 242; T. Sjöstrand, Comput. Phys. Commun. 39 (1986) 347; T. Sjöstrand and M. Bengtsson, Comput. Phys. Commun. 43 (1987) 367.
[74] A. Capella, Proc. Europ. Study Conf. on Protons and Soft Hadronic Int., Erice, R.T. Van de Walle (ed.) (World Scientific, Singapore, 1982) p. 199;
E.A. De Wolf, Proc. XV Int. Symp. on Multiparticle Dynamics, Lund, Sweden 1984, eds. G. Gustafson and C. Peterson (World Scientific, Singapore, 1984) p. 1.
[75] V.V. Aivazyan et al. (NA22), Z. Phys. C 51 (1991) 167.
[76] A.B. Kaidalov and K.A. Ter-Martirosyan, Sov. J. Nucl. Phys. 39 (1984) 979; ibid 40 (1984) 135;
N.S. Amelin et al., Sov. J. Nucl. Phys. 51 (1990) 133; ibid 51 (1990) 535;
N.S. Amelin, L.V. Bravina and L.N. Smirnova, Sov. J. Nucl. Phys. 52 (1990) 362.
[77] I. Derado, G. Jancso and N. Schmitz (EMC), Z. Phys. C 56 (1992) 553;
M. Arneodo et al., Z. Phys. C 31 (1986) 333; ibid. 40 (1988) 347.
[78] P. Malecki, Festschrift L. Van Hove, eds. A Giovannini and W. Kittel (World Scientific, Singapore, 1990) p. 159;
J. Figiel, Krakow preprint IFJ 1398/Ph (1988).
[79] M. Althoff et al., Z. Phys. C 29 (1985) 347;
J. Chwastowski, Ph.D. thesis, DESY, Hamburg, 1988.
[80] O. Podobrin, preprint DESY 91-111; Ph.D. Thesis, DESY FCE-92-03, 1992.
[81] P.D. Acton et al. (OPAL), Phys. Lett. B 287 (1992) 401.
[82] C.P. Fong and B.R. Webber, Nucl. Phys. B 355 (1991) 54;
C.P. Fong, Ph.D. Thesis, University of Cambridge (1991).
[83] G. Marchesini and B.P. Webber, Nucl. Phys. B 310 (1988) 461;
G. Marchesini et al., Comput. Phys. Commun. 67 (1992) 465.
[84] U. Pettersson, preprint LU TP 88-15 (1988);
L. Lönnblad and U. Pettersson, preprint LU TP 88-15 (1988);
L. Lönnblad, preprint LU TP 89-10 (1988).
[85] R. Odorico, Comput. Phys. Commun. 32 (1984) 139; ibid. 59 (1990) 527;
P. Mazzanti and R. Odorico, Nucl. Phys. B 370 (1992) 23.
[86] K. Eggert et al., Nucl. Phys. B 86 (1975) 201.
[87] N.N. Biswas et al., Phys. Rev. Lett. 37 (1976) 175.
[88] I.V. Ajinenko et al. (NA22), Z. Phys. C 58 (1993) 357.
[89] H. Aihara et al., Phys. Rev. Lett. 53 (1984) 2199.
[90] M. Asai et al. (NA23), Z. Phys. C 34 (1987) 429.
[91] B.Y. Oh et al., Phys. Lett. 56B (1975) 201.
[92] C. de la Vaissière et al., Phys. Rev. Lett. 54 (1985) 2071.
[93] W.G. Ma et al., Z. Phys. C 30 (1986) 191.
[94] M. Aguilar-Benitez et al. (NA27), Phys. Lett. B 164 (1985) 404.
[95] M. Adamovich et al. (BEATRICE Coll.), Phys. Lett. B 348 (1995) 256.
[96] S. Frixione, M.L. Mangano, P. Nason and G. Ridolfi, Nucl. Phys. B 43 (1994) 543.
[97] P.C. Acton et al. (OPAL), Z. Phys. C 58 (1993) 207.
[98] Yu.L. Dokshitzer, V.A. Khoze, A.H. Mueller and S.I. Troyan, Basics of Perturbative QCD (Editions Frontières, 1991).

[99] B.I. Ermolaev and V.S. Fadin, JETP Lett. 33 (1981) 269; A.H. Mueller, Phys. Lett. B 104 (1981) 161; A. Bassetto, M. Ciafaloni, G. Marchesini and A.H. Mueller, Nucl. Phys. B 207 (1982) 189; G. Marchesini and B.R. Webber, Nucl. Phys. B 238 (1984) 1.
[100] Ya.I. Azimov, Yu.L. Dokshitzer, V.A. Khoze and S.I. Troyan, Z. Phys. C 27 (1985) 65.
[101] M.A. Chmeissani, ALEPH internal note 93-097, unpublished.
[102] M. Acciarri et al. (L3), Phys. Lett. B 353 (1995) 145.
[103] C.L. Basham et al., Phys. Rev. Lett. 41 (1978) 1585.
[104] V.A. Bumazhnov et al., Serpukhov preprint IHEP 79-181 (1979);
V.A. Bumazhnov et al., Sov. J. Nucl. Phys. 46 (1987) 289 and 40 (1984) 96.
[105] S.A. Azimov et al., Dokl. AN Uzbekh SSR 9 (1980) 31.
[106] A. Breakstone et al., Mod. Phys. Lett. A 6 (1991) 2785.
[107] P. Carruthers and I. Sarcevic, Phys. Rev. Lett. 63 (1989) 1562.
[108] A. Capella, K. Fiałkowski and A. Krzywicki, Phys. Lett. B230 (1989) 149.
[109] E.A. De Wolf, Acta. Phys. Pol. B 21 (1990) 611.
[110] I.V. Ajinenko et al. (NA22), Phys. Lett. B197 (1987) 457.
[111] T. Ludlam and R. Slansky, Phys. Rev. D 8 (1973) 1408;
J. Hanlon et al., Phys. Lett. 46 B (1973) 415.
[112] R. Slansky, Phys. Rep. 11C (1974) 99.
[113] V.A. Abramovskii, V.N. Gribov and O.V. Kancheli, Yad. Fiz. 18 (1973) 595; Sov. J. Nucl. Phys. 118 (1974) 308.
[114] K.I. Aleksejava et al., J. Phys. Soc. Japan 17 (1962) A-III, 409
D.H. Perkins and P.H. Fowler, Proc. R. Soc. A 273 (1964) 401
J. Iwai et al., Nuovo Cimento 69 A (1982) 295.
[115] N. Arata, Nuovo Cimento 43 A (1978) 455.
[116] A.V. Apanasenko et al., JETP Lett. 30 (1979) 145;
I.M. Dremin and M.I. Tretyakova, paper presented at the XVIII Int. Cosmic Ray Conf., Paris (1981);
S.A. Slavatinskii et al., paper presented at XVIII Int. Cosmic Ray Conf., Paris (1981);
S.A. Azimov et al., paper presented at XVIII Int. Cosmic Ray Conf., Paris (1981).
[117] N.A. Marutjan et al., Sov. J. Nucl. Phys. 29 (1979) 804.
[118] T.H. Burnett et al. (JACEE), Phys. Rev. Lett. 50 (1983) 2062.
[119] M. Adamus et al. (NA22), Phys. Lett. B 185 (1987) 200.
[120] P. Carlson (UA5), Proc. 4th Topical Workshop on $p\bar{p}$ Collider Physics, Bern, March 1984, CERN Yellow Report 84-09 (1984) 286 and G.J. Alner et al. (UA5), Phys. Rep. 154 (1987) 247.
[121] M.I. Adamovich et al. (EMU01), Phys. Lett. B 201 (1988) 397.
[122] F. Takagi, Phys. Rev. Lett. 53 (1984) 427; idem Phys. Rev. D 32 (1985) 1799.
[123] R.P. Feynman, Proc. 3rd Workshop on Current Problems in High Energy Particle Theory, Florence 1979, eds. R. Casalbuoni et al. (Johns Hopkins University Press, Baltimore, 1979).
[124] G. Veneziano, in: Proc. 3rd Workshop on Current Problems in High Energy Particle Theory, Florence, 1979, eds. R. Casalbuoni et al. (Johns Hopkins University Press, Baltimore, 1979) p. 45.
[125] K. Konishi, A. Ukawa and G. Veneziano, Phys. Lett. 78 B (1978) 243; Nucl. Phys. B 157 (1979) 45.
[126] A. Giovannini, in: Proc. Xth Int. Symp. Multiparticle Dynamics, Goa, 1979, eds. S.N. Ganguli, P.K. Malhotra and A. Subramanian (Tata Inst.) p. 364.
[127] P. Carruthers and Minh Duong-Van, Los Alamos preprint LA-UR-83-2419 (1983).
[128] I.M. Dremin, JETP Lett. 45 (1987) 643.
[129] I.M. Dremin, Festschrift L. Van Hove, eds. A. Giovannini and W. Kittel (World Scientific, Singapore, 1990) p. 455.
[130] H.G.E. Hentschel and I. Procaccia, Physica 8 D (1983) 435;
P. Grassberger, Phys. Lett. 97A (1983) 227.
[131] P. Lipa and B. Buschbeck, Phys. Lett. B 223 (1989) 465.
[132] Ya.B. Zeldovich, A.A. Ruzmaikin and D.D. Sokoloff, The Almighty Chance, World Scientific Lecture Notes in Physics, Vol. 20 (World Scientific, Singapore, 1990).
[133] B. Buschbeck, P. Lipa and R. Peschanski, Phys. Lett. B 215 (1988) 788;
S. Abachi et al. (HRS), preprint ANK-HEP-CP-90-50, unpublished.

[134] W. Braunschweig et al. (TASSO), Phys. Lett. B 231 (1989) 548.
[135] H.-J. Behrend et al. (CELLO), Phys. Lett. B 256 (1991) 97;
P. Podobrin (CELLO), Proc. 26th Rencontre de Moriond, Les Arcs, 1991, ed. J. Tran Thanh Van (Editions Frontières 1991) p. 311.
[136] P. Abreu et al. (DELPHI), Phys. Lett. B 247 (1990) 137;
A. De Angelis, Mod. Phys. Lett. A 5 (1990) 2395;
A. De Angelis and N. Demaria, in: Proc. Ringberg Workshop on Multiparticle Production, Ringberg Castle, Germany, 1991, eds. R.C. Hwa, W. Ochs and N. Schmitz (World Scientific, Singapore, 1992) p. 1.
P. Abreu et al. (DELPHI), Nucl. Phys. B 386 (1992) 471.
[137] M.Z. Akrawy et al. (OPAL), Phys. Lett. B 262 (1991) 351;
N. Geddes, in Proc. Ringberg Workshop on Multiparticle Production, Ringberg Castle, Germany 1991, eds. R.C. Hwa, W. Ochs and N. Schmitz (World Scientific, Singapore, 1992) p. 16.
[138] D. Decamp et al. (ALEPH), Z. Phys. C 53 (1992) 21;
N. Lieske, in Proc. Ringberg Workshop on Multiparticle Production, Ringberg Castle, Germany, 1991, eds. R.C. Hwa, W. Ochs and N. Schmitz (World Scientific, Singapore, 1992) p. 32;
V. Raab, idem, p. 46.
[139] W.N. Murray, R.E. Frey and H.O. Ogren (Mark II), Oregon preprint OREXP-93-16, subm. to PRL
[140] I. Derado, G. Jancso, N. Schmitz and P. Stopa (EMC), Z. Phys. C 47 (1990) 23;
I. Derado et al. (EMC), Z. Phys. C 54 (1992) 357.
[141] L. Verluyten et al. (WA59 and E180), Phys. Lett. B 260 (1991) 456.
[142] I.V. Ajinenko et al. (NA22), Phys. Lett. B 222 (1989) 306, B 235 (1990) 373;
N.M. Agababyan et al. (NA22), Phys. Lett. B 261 (1991) 165;
F. Botterweck et al. (NA22), in: Proc. Ringberg Workshop on Multiparticle Production, Ringberg Castle, Germany, 1991, eds. R.C. Hwa, W. Ochs and N. Schmitz (World Scientific, Singapore, 1992) p. 125;
M. Charlet (NA22), idem, p. 140;
N. Agababyan et al. (NA22), Z. Phys. C 59 (1993) 405.
[143] C. Albajar et al. (UA1), Nucl. Phys. B 345 (1990) 1;
B. Buschbeck, Festschrift L. Van Hove, eds. A. Giovannini and W. Kittel (World Scientific, Singapore, 1990) p. 211;
P. Lipa, Ph.D. Thesis, University of Vienna, 1990;
P. Lipa et al. (UA1), in: Proc. Ringberg Workshop on Multiparticle Production, Ringberg Castle, Germany, 1991, eds. R.C. Hwa, W. Ochs and N. Schmitz (World Scientific, Singapore, 1992) p. 111;
N. Neumeister et al. (UA1-MB): Z. Phys. C 60 (1993) 633.
[144] J.B. Singh and J.N. Kohli (NA23), Phys. Lett. B 261 (1991) 160.
[145] V. Arena et al. (IHSC), Nuovo Cimento A 105 (1992) 883.
[146] L.V. Bravina et al. (Mirabelle), Moscow preprint 92-37/286 (1992).
[147] F. Rimondi (CDF), in: Proc. XXI Int. Symp. on Multiparticle Dynamics, Wuhan, China, 1991, eds. Y.F. Wu and L.S. Liu (World Scientific, Singapore, 1992) p. 476.
[148] S.S. Wang et al. (NA27), Phys. Rev. D 49 (1994) 5785.
[149] R. Hołynski et al. (KLM), Phys. Rev. Lett. 62 (1989) 733 and Phys. Rev. C 40 (1989) R2449.
[150] I. Derado (NA35), Festschrift L. Van Hove, eds. A Giovannini and W. Kittel (World Scientific, Singapore, 1990) p. 257;
I. Derado (NA35) in: Proc. Ringberg Workshop on Multiparticle Production, Ringberg Castle, Germany, 1991, eds. R.C. Hwa, W. Ochs and N. Schmitz (World Scientific, Singapore, 1992) p. 184;
J. Bächler et al. (NA35), Z. Phys. C 56 (1992) 347; ibid. C 61 (1994) 551.
[151] F. Botterweck et al. (NA22), Z. Phys. C 51 (1991) 37.
[152] D. Ghosh et al. Phys. Rev. D 46 (1992) 3712; ibid. D 47 (1993) 1235; ibid. D 49 (1994) 3113; ibid. D 51 (1995) 3298; Europhys. Lett. 29 (1995) 521.
[153] R.K. Shivpuri and V.K. Verma, Phys. Rev. D 47 (1993) 123; R.K. Shivpuri and Vandana Anand, Z. Phys. C 59 (1993) 47 and Phys. Rev. D 50 (1994) 287.
[154] R.K. Shivpuri and N. Parashar, Phys. Rev. D 49 (1994) 219.

[155] M.I. Adamovich et al. (EMU-01), Phys. Rev. Lett. 65 (1990) 412;
M.I. Adamovich et al. (EMU-01), Phys. Lett. B 263 (1991) 539;
M.I. Adamovich et al. (EMU-01), Z. Phys. C 49 (1991) 395;
M.I. Adamovich et al. (EMU-01), Nucl. Phys. B. 388 (1992) 3.
[156] K. Sengupta, P.L. Jain, G. Singh and S.N. Kim (EMU-08), Phys. Lett. B. 236 (1990) 219;
P.L. Jain and G. Singh, Phys. Rev. C 44 (1991) 854; Z. Phys. C53 (1992) 355; P.L. Jain, G. Singh and A. Mukhopadhysay, Phys. Rev. C 48 (1993) R517.
[157] T. Åkesson et al. (HELIOS), Phys. Lett. B 252 (1990) 303.
[158] D. Ghosh et al., Phys. Lett. B 272 (1991) 5.
[159] E.K. Sarkisyan and G.G. Taran, Phys. Lett. B 279 (1992) 177; E.K. Sarkisyan, L.K. Gelovani, G.G. Taran and G.I. Sakharov, Phys. Lett. B 318 (1993) 568; E.K. Sarkisyan, L.K. Gelovani, G.L. Gogiberidze and G.G. Taran, Phys. Lett. B 347 (1995) 439.
[160] T. Abbott et al. (E-802), Phys. Lett. B 337 (1994) 254.
[161] R. Albrecht et al. (WA80), Phys. Rev. C 50 (1994) 1048.
[162] A. Białas, Nucl. Phys. A 525 (1991) 345c.
[163] F.W. Bopp, A. Capella, J. Ranft and J. Tran Thanh Van, Z. Phys. C 51 (1991) 99.
[164] R.C. Hwa and J.C Pan, Phys. Rev. D 45 (1992) 106;
J.C. Pan and R.C. Hwa, Phys. Rev. D 46 (1992) 4890.
[165] A. Białas, Nucl. Phys. A 545 (1992) 285;
A. Białas, Acta Phys. Pol. B 23 (1992) 561.
[166] F. Botterweck, private communication;
B. Buschbeck and P. Lipa, private communication.
[167] M. Jędrzejczak, Phys. Lett. B 228 (1989) 259;
I. Sarcevic, private communication.
[168] P. Dahlqvist, G. Gustafson and B. Andersson, Nucl. Phys. B 328 (1989) 76;
B. Andersson, G. Gustafson, A. Nilsson and C. Sjögren, Z. Phys. C 49 (1991) 79;
G. Gustafson and A. Nilsson, Nucl. Phys. B 355 (1991) 106;
G. Gustafson and C. Sjögren, Phys. Lett. B 248 (1990) 430.
[169] N.M. Agababyan et al. (NA22), Z. Phys. C 46 (1990) 387.
[170] M. Arneodo et al. (EMC), Z. Phys. C 33 (1986) 167.
[171] W.D. Walker et al., Phys. Lett. B 255 (1991) 155.
[172] B. Andersson, G. Gustafson and J. Samuelsson, Z. Phys. C 64 (1994) 653.
[173] B. Wošiek, Krakow preprint INP 1496/PH (1990);
G. Ekspong, R. Peschanski and J. Wošiek, Phys. Lett. B 251 (1990) 455;
D. Seibert, preprint (1990).
[174] E.M. Friedlander, Mod. Phys. Lett. A 4 (1989) 2457;
P. Lipa, H.C. Eggers, F. Botterweck and M. Charlet, Z. Phys. C 54 (1992) 115.
[175] A. Białas and J. Seixas, Phys. Lett. B 250 (1990) 161.
[176] F. Botterweck, Ph.D. Thesis, University of Nijmegen, 1992.
[177] K. Fiałkowski, Phys. Lett. B 272 (1991) 139.
[178] K. Fiałkowski, Z. Phys. C 61 (1994) 313.
[179] W. Ochs and J. Wošiek, Phys. Lett. B 214 (1988) 617; B 232 (1989) 271.
[180] J. Alberty and A. Białas, Z. Phys. C 50 (1991) 315.
[181] Ph. Brax and R. Peschanski, Phys. Lett. B 253 (1991) 225.
[182] H. Satz, Nucl. Phys. B 326 (1989) 613; B. Bambah, J. Fingberg and H. Satz, Nucl. Phys. B 332 (1990) 629.
[183] A. Białas and R. Hwa, Phys. Lett. B 253 (1991) 436.
[184] P.J.F. Peebles, The Large Scale Structure of the Universe (Princeton, NJ, 1980).
[185] E.A. De Wolf, in: Proc. XXII Int. Symp. on Multiparticle Dynamics, Santiago de Compostela, Spain, 1992, ed. C. Pajares (World Scientific, Singapore, 1993) p. 263.
[186] L.E. Reichl, A Modern Course in Statistical Physics (University of Texas Press, Austin, 1980).
[187] J. Wošiek, Acta Phys. Pol. B 19 (1988) 863.

[188] R.C. Hwa and M.T. Nazirov, Phys. Rev. Lett. 69 (1992) 741.
[189] M.R. Young, Y. Qu, S. Singh and R.C. Hwa, Opt. Commun. 105 (1994) 325.
[190] M. Charlet, private communication.
[191] L.F. Babichev, D.V. Klenitsky and V.I. Kuvshinov, Phys. Lett. B 345 (1995) 269.
[192] L. Van Hove, Ann. Phys. 192 (1989) 66.
[193] R. Peschanski, Nucl. Phys. B 327 (1989) 144.
[194] Ph. Brax and R. Peschanski, Nucl. Phys. B 346 (1990) 65 and Int. J. Mod. Phys. A 7 (1993) 709.
[195] A. Białas and K. Zalewski, Phys. Lett. B 238 (1990) 413.
[196] Y.F. Wu and L.S. Liu, Phys. Rev. Lett. 70 (1993) 3197; Y.F. Wu, Y. Zhang and L.S. Liu, Phys. Rev. D 51 (1995) 6576.
[197] J. Wošiek, in: Proc. XXIV Int. Symp. on Multiparticle Dynamics, eds. A. Giovannini et al. (World Scientific, Singapore, 1995) p. 99.
[198] L. Van Hove, Phys. Lett. B 28 (1969) 429; Nucl. Phys. B 9 (1969) 331.
[199] B.B. Mandelbrot, in: Dynamics of Fractal Surfaces, eds. E. Family and T. Vicsek (World Scientific, Singapore, 1991).
[200] Y. Zhang, L.S. Liu and Y.F. Wu, Wuhan preprint (1995).
[201] P. Carruthers, E.M. Friedlander, C.C. Shih and R.M. Weiner, Phys. Lett. B 222 (1989) 487.
[202] M. Gyulassy, Festschrift L. Van Hove, eds. A. Giovannini and W. Kittel (World Scientific, Singapore, 1990) p. 479.
[203] W.A. Zajc, in: Proc. Particle Production in Highly Excited Matter, eds. H.H. Gutbrod and J. Rafelski (Plenum Press, New York, 1993) p. 435.
[204] E.A. De Wolf, in: Proc. XXVII Int. Conf. on High Energy Physics, Glasgow, 1994, eds. P.J. Bussey and I.G. Knowles (Institute of Physics Publishing, Bristol and Philadelphia, 1995) p. 1281.
[205] M. Biyajima et al., Prog. Theor. Phys. 84 (1990) 931.
[206] N. Neumeister et al. (UA1), Phys. Lett. B 275 (1992) 186.
[207] N.M. Agababyan et al. (NA22), Phys. C 68 (1995) 229.
[208] P. Abreu et al. (DELPHI), Phys. Lett. B 355 (1995) 415.
[209] A. Białas et al., Phys. Lett. B 229 (1989) 398.
[210] Y.F. Wu et al. (UA1), Acta Phys. Slov. 44 (1994) 141.
[211] Y.F. Wu and L.S. Liu, Z. Phys. C 53 (1992) 273.
[212] W. Bartel et al. (JADE), Z. Phys. C 33 (1986) 23;
S. Bethke et al., Phys. Lett. B 213 (1988) 235.
[213] A. Białas, Festschrift L. Van Hove, eds. A. Giovannini and W. Kittel (World Scientific, Singapore, 1990) p. 75.
[214] D. Seibert, Phys. Lett. B 240 (1990) 215.
[215] P. Aurenche et al., Phys. Rev. D 45 (1992) 92;
F.W. Bopp et al., in: Proc. Ringberg Workshop on Multiparticle Production, Ringberg Castle, Germany, 1991, eds. R.C. Hwa, W. Ochs and N. Schmitz (World Scientific, Singapore, 1992) p. 313.
[216] S. Barshay, Z. Phys. C 47 (1990) 199.
[217] H.C. Eggers, Ph.D. Thesis, University of Arizona, 1991;
T. Elze and I. Sarcevic, Phys. Rev. Lett. 68 (1992) 1988;
I. Sarcevic, in: Proc. Ringberg Workshop on Multiparticle Production, Ringberg Castle, Germany 1991, eds. R.C. Hwa, W. Ochs and N. Schmitz (World Scientific, Singapore, 1992) p. 206.
[218] S.S. Wang et al. (NA27), Phys. Lett. B 321 (1994) 431.
[219] P.L. Jain, A. Mukhopadhyay and G. Singh, Z. Phys. C 58 (1993) 1.
[220] M.I. Adamovich et al. (EMU-01), Phys. Rev. D 47 (1993) 3726.
[221] J. Dias de Deus, Phys. Lett. B 240 (1990) 481; Phys. Lett. B 278 (1992) 377.
[222] HELIOS, paper submitted to the EPS Conf. on High Energy Physics, Madrid, 1989.
[223] V.V. Aivazyan et al. (NA22), Phys. Lett. B 258 (1991) 487.
[224] E.A. De Wolf, in: Proc. Ringberg Workshop on Multiparticle Production, Ringberg Castle, Germany, 1991, eds. R.C. Hwa, W. Ochs and N. Schmitz (World Scientific, Singapore, 1992) p. 222.
[225] B. Widom, J. Chem. Phys. 43 (1965) 3892, 3898;
K.G. Wilson, Phys. Rev. 179 (1969) 1499.

[226] L. Kadanoff, Physica D 38 (1989) 213.
[227] B. Mandelbrot, J. Fluid Mech. 62 (1974) 331.
[228] A. Aharony, Physica D 38 (1989) 1.
[229] K. Sugano (HRS), in: Proc. Santa Fé Workshop Intermittency in High Energy Collisions, 1990, eds. F. Cooper, R.C. Hwa and I. Sarcevic (World Scientific, Singapore, 1991) p. 1;
in: Proc. Int. Workshop on Correlations and Multiparticle Production, Marburg, eds. M. Plümer, S. Raha and R.M. Weiner (World Scientific, Singapore, 1991) p. 240.
[230] I. Derado, R.C. Hwa, G. Jancso and N. Schmitz (EMC), Phys. Lett. B 283 (1992) 151.
[231] G. Boca et al. (IHSC), Nuovo Cimento A 105 (1992) 865.
[232] F. Botterweck and M. Charlet, private communication.
[233] C. Albajar et al. (UA1), Z. Phys. C 56 (1992) 37;
H. Dibon (UA1), paper submitted to the XXVI Int. Conf. on High Energy Physics, Dallas (USA) 1992.
[234] F. Rimondi (CDF), in: Proc. Int. Workshop on Correlations and Multiparticle Production, Marburg, eds. M. Plümer, S. Raha and R.M. Weiner (World Scientific, Singapore, 1991) p. 276.
[235] S.S. Wang et al. (NA27), Phys. Lett. B 344 (1995) 447.
[236] E.K. Sarkisyan, L.K. Gelovani and G.G. Taran, Phys. Lett. B 302 (1993) 331.
[237] R.K. Shivpuri and V.K. Verma, Z. Phys. C 58 (1993) 7.
[238] P.L. Jain, K. Sengupta and G. Singh, Phys. Lett. B 241 (1990) 273; P.L. Jain, G. Singh and A. Mukhopadhyay, Phys. Rev. C 46 (1992) 721; K. Sengupta et al., Phys. Rev. D 48 (1993) 3174.
[239] C.B. Chiu, K. Fiałkowski and R.C. Hwa, Mod. Phys. Lett. A 5 (1990) 2651.
[240] D. Seibert, Phys. Lett. B 254 (1991) 253.
[241] R.C. Hwa and J.C. Pan, Phys. Rev. D 45 (1992) 1476.
[242] P. Billingsley, Ergodic Theory and Information (Wiley, New York, 1965) p. 139.
[243] C.B. Chiu and R.C. Hwa, Phys. Rev. D 45 (1992) 2276.
[244] R.S. Ellis, Entropy, Large Deviations and Statistical Mechanics (Springer, New York, 1985);
D.W. Stroock, An Introduction to the Theory of Large Deviations (Springer, New York, 1984);
J. Seixas and R. Vilela Mendes, Nucl. Phys. B 383 (1992) 622.
[245] I.M. Dremin, Mod. Phys. Lett. A 3 (1988) 1333.
[246] P. Carruthers, Ap. J. 380 (1991) 24;
P. Lipa, P. Carruthers, H.C. Eggers and B. Buschbeck, Phys. Lett. B 285 (1992) 300.
[247] H.C. Eggers et al., Phys. Rev. D 48 (1993) 2040; M. Charlet, in: Proc. XXIIIrd Int. Symp. on Multiparticle Dynamics, Aspen, 1993, eds. M.M. Block and A.R. White (World Scientific, Singapore, 1994) p. 302.
[248] Zhang Jie, Phys. Lett. B 352 (1995) 169.
[249] M.R. Adams et al. (E665), Phys. Lett. B335 (1994) 535.
[250] F. Mandl and B. Buschbeck (DELPHI/UA1), in: Proc. XXII Int. Symp. on Multiparticle Dynamics, Santiago de Compostela, Spain, 1992, ed. C. Pajares (World Scientific, Singapore, 1993), p. 561.
[251] P. Bak, C. Tang and K. Wiesenfeld, Phys. Rev. Lett. 59 (1087) 381;
P. Bak and K. Chen, Scientific American 264 (1991) 46.
[252] K. Kadija and P. Seyboth, Phys. Lett. B 287 (1992) 363.
[253] G. Gustafson and A. Nilsson, Z. Phys. C 52 (1991) 533.
[254] W. Ochs and J. Wošiek, Phys. Lett. B 289 (1992) 159.
[255] W. Ochs and J. Wošiek, Phys. Lett. B 305 (1993) 144; Z. Phys. C 68 (1995) 269.
[256] Yu.L. Dokshitzer and I.M. Dremin, Nucl. Phys. B402 (1993) 139.
[257] Ph. Brax, J.L. Meunier and R. Peschanski, Z. Phys. C 62 (1994) 649.
[258] F. Mandl and B. Buschbeck, Vienna preprint HEPHY-PUB 614/94 (December 94).
[259] E.L. Berger, R. Singer, G.H. Thomas and T. Kafka, Phys. Rev. D 15 (1977) 206.
[260] G.H. Thomas, Phys. Rev. D 15 (1977) 2636.
[261] I.V. Ajinenko et al. (NA22), Z. Phys. C 61 (1994) 567.
[262] P. Abreu et al. (DELPHI), Z. Phys. C 63 (1994) 17.
[263] A. Białas and R. Peschanski, Phys. Rev. D 50 (1994) 6003.
[264] M. Adamus et al. (NA22), Z. Phys. C 37 (1988) 347.

[265] D. Decamp et al. (ALEPH), Z. Phys. C 54 (1992) 75.
[266] M.R. Atayan et al. (NA22), Z. Phys. C 54 (1992) 247.
[267] N.M. Agababyan et al. (NA22), Phys. Lett. B 332 (1994) 458.
[268] E.D. Malaza and B.R. Webber, Nucl. Phys. B 267 (1986) 702.
[269] A. Giovannini, in: Proc. XXI Int. Symp. on Multiparticle Dynamics, Wuhan, China, 1991, eds. Y.F. Wu and L.S. Liu (World Scientific, Singapore, 1992) p. 285.
[270] B. Andersson, Nucl. Phys. B 360 (1991) 109.
[271] L. Van Hove, Phys. Lett. B 242 (1990) 485.
[272] P. Bozek and M. Płoszajczak, Phys. Lett. B 254 (1991) 161.
[273] I.M. Dremin and M.T. Nazirov, Z. Phys. C 59 (1993) 647.
[274] I.M. Dremin, JETP Lett. 57 (1993) 626.
[275] N.G. Antoniou, A.P. Contogouris, C.G. Papadopoulos and S.D.P. Vlassopulos, Phys. Lett. B 245 (1990) 619.
[276] I.V. Andreev, M. Biyajima, I.M. Dremin and N. Suzuki, Int. J. Mod. Phys. A 10 (1995) 3951.
[277] A. Capella and J. Tran Thanh Van, Z. Phys. C 38 (1988) 177.
[278] B. Andersson et al., Nucl. Phys. B 281 (1987) 289.
[279] A.B. Kaidalov, Phys. Lett. B 116 (1982) 459.
[280] I.M. Dremin, JETP Lett. 30 (1980) 140; Sov. J. Part. Nucl. 18 (1987) 31.
[281] C. Fugelsang, in: Proc. 19th Int. Symp. on Multiparticle Dynamics, Arles, 1988, eds. D. Schiff and J. Tran Thanh Van (Editions Frontières, France and World Scientific, Singapore, 1988) p. 257.
[282] I.M. Dremin and A.M. Dunaevskii, Phys. Rep. 18 (1975) 159.
[283] L.S. Liu and T.C. Meng, Phys. Rev. D 27 (1984) 2640.
[284] A. Giovannini and L. Van Hove, Acta Phys. Pol. B 19 (1988) 495, 917, 931.
[285] A. Białas and R. Peschanski, Phys. Lett. B 207 (1988) 59.
[286] P. Carruthers and I. Sarcevic, Phys. Lett. B 189 (1987) 442.
[287] I.M. Dremin and M.T. Nazirov, in: Proc. 26th Moriond Meeting, ed. J. Tran Thanh Van (Editions Frontiers, 1991) p. 341; Sov. J. Nucl. Phys. 55 (1992) 197; 55 (1992) 2546.
[288] R. Peschanski and J. Tran Thanh Van, in: Proc. XVIII Int. Symp. on Mutiparticle Dynamics, Tashkent, USSR, 1987, eds. I. Dremin and K. Gulamov (World Scientific, Singapore, 1988) p. 149.
[289] B. Andersson et al., in Proc. 19th Int. Symp. on Multiparticle Dynamics, Arles, 1988, eds. D. Schiff and J. Tran Thanh Van (Editions Frontières, France and World Scientific, Singapore, 1988) p. 347.
[290] E. Stenlund (EMU 01), in: Proc. of Quark Matter-95 conference, to be published.
[291] I.M. Dremin et al., Sov. J. Nucl. Phys. 52 (1990) 840.
[292] O.D. Chernavskaya et al., in: Proc. Int. Cosmic Ray conference, 1995, to be published.
[293] D. Seibert, Phys. Rev. Lett. 63 (1989) 136.
[294] F.N. Fowler and R.M. Weiner, Phys. Rev. D 17 (1978) 3117.
[295] I.M. Dremin, Physics-Uspekhi 37 (1994) 715.
[296] J.D. Bjorken, Phys. Rev. D 45 (1992) 4077.
[297] A. Białas and B. Ziaja, Acta Phys. Pol. B 24 (1993) 1509.
[298] A.V. Leonidov and M.M. Tsypin, Mod. Phys. Lett. A 6 (1991) 1203.
[299] A.N. Kolmogorov, Docl. Akad. Sci. USSR 30 (1941) 301; E.A. Novikov and R.W. Stewart, Izv. Acad. Sci. USSR. Ser. Geofiz. 3 (1964) 408.
[300] D. Schertzer and S. Lovejoy, in: Turbulent Shear Flows 4 (Springer, Berlin, 1984); U. Frish et al., J. Fluid Mech. 87 (1978) 719.
[301] A. Białas, A. Szczerba and K. Zalewski, Z. Phys. C 46 (1990) 163.
[302] I.M. Dremin, in: Proc. XX Int. Symp. on Multiparticle Dynamics, Gut Holmecke, Germany, 1990, eds. R. Baier and D. Wegener (World Scientific, Singapore, 1991) p. 459.
[303] B.B. Levtchenko, preprint MPI-PAE/Exp. El. 219, 1990, unpublished.
[304] J. Wošiek, Nucl. Phys. B Suppl. 9 (1989) 640.
[305] D. Hajduković, preprint CERN-TH.6474/92, 1992, unpublished.
[306] M.I. Polikarpov, Phys. Lett. B 236 (1990) 61; Physics-Uspekhi, 165 (1995) 627.
[307] A.Z. Patashinky and V.L. Pokrovsky, Fluctuation Theory of Phase Transitions (Nauka, Moscow, 1982).

[308] D.J. Scalapino and R.L. Sugar, Phys. Rev. D 8 (1973) 2284.
[309] N.G. Antoniou, A.P. Contogouris, C.G. Papadopoulos and S.D.P. Vlassopulos, Phys. Rev. D 45 (1992) 4034.
[310] N.G. Antoniou, F.K. Diakonos and I.S. Mistakidis, Phys. Lett. B 293 (1992) 187; N.G. Antoniou, F.K. Diakonos, I.S. Mistakidis and C.G. Papadopoulos, Phys. Rev. D 49 (1994) 5789.
[311] I.M. Dremin and B.B. Levtchenko, Phys. Lett. B 292 (1992) 155.
[312] Y. Sinai, Russ. Math. Surv. 166 (1972) 21.
[313] T. Tel, Z. Naturforsch. 43a (1988) 1154.
[314] M. Bander, Phys. Lett. D 7 (1973) 2256.
[315] S. Hegyi and S. Krasznovszky, Phys. Lett. B 251 (1990) 197.
[316] I.M. Dremin and A.V. Leonidov, Physics-Uspekhi, 165 (1995) 644.
[317] E.A. De Wolf, in: Proc. XXIV Int. Symp. on Multiparticle Dynamics, eds. A. Giovannini et al. (World Scientific, Singapore, 1995) p. 15.
[318] I.M. Dremin, JETP Lett. 60 (1994) 764.
[319] C.N. Yang and T.D. Lee, Phys. Rev. 87 (1952) 404 and 410.
[320] B. Andersson, in: Proc. XXIV Int. Symp. on Multiparticle Dynamics, eds. A. Giovannini et al. (World Scientific, Singapore, 1995) p. 263.
[321] I.M. Dremin, Phys. Lett. B 341 (1994) 95.
[322] M.S. Bartlett, An Introduction to Stochastic Processes with Special Reference to Methods and Applications (Camb. University Press, Cambridge, 1955).
[323] B.A. Sevastianov, Branching Processes (Nauka, Moscow, 1971).
[324] A. Giovannini, Nucl. Phys. B 161 (1979) 429.
[325] C.S. Lam and M.A. Walton, Phys. Lett. B 140 (1984) 246.
[326] C.C. Shih, Phys. Rev. D33 (1986) 3391; D 34 (1986) 2710.
[327] A.V. Batunin, Phys. Lett. B212 (1988) 495.
[328] P.V. Chliapnikov and O.G. Tchikilev, Phys. Lett. B 242 (1990) 275.
[329] J.L. Meunier and R. Peschanski, Nucl. Phys. B 374 (1992) 327.
[330] J. Dias de Deus, Phys. Lett. B 194 (1987) 297.
[331] A.V. Batunin, Sov. J. Nucl. Phys. 55 (1992) 1407; Physics-Uspekhi, June 1995.
[332] G. Altarelli and G. Parisi, Nucl. Phys. B 126 (1977) 298.
[333] I.V. Andreev, Chromodynamics and Hard Processes at High Energies (Nauka, Moscow, 1981).
[334] R.C. Hwa, Nucl. Phys. B 328 (1989) 59.
[335] C.B. Chiu and R.C. Hwa, Phys. Rev. D 43 (1991) 100.
[336] A. Białas et al., Phys. Lett. B 229 (1989) 398.
[337] L.V. Gribov, E.M. Levin and M.G. Ryskin, Phys. Rep. 100 (1983) 1.
[338] A.V. Batunin, Mod. Phys. Lett. B 3 (1989) 543.
[339] Ph. Brax and R. Peschanski, preprint SPht/92-005, 1992, unpublished.
[340] Yu.L. Dokshitzer, G. Marchesini and G. Oriani, Nucl. Phys. B 387 (1992) 675.
[341] I. Sarcevic and H. Satz, Phys. Lett. B 233 (1989) 251.
[342] Yu.L. Dokshitzer, Phys. Lett. B 305 (1993) 295.
[343] I.M. Dremin, Phys. Lett. B 313 (1993) 209.
[344] I.M. Dremin et al., Phys. Lett. B 336 (1994) 119.